Halide Removal from Water by Novel Bismuth Materials

by

Author: Elham Nariyan

Supervisors:

Prof. Qin Li

Dr. Jimmy Yu

A thesis submitted in fulfillment of the requirement for the degree of Doctor of Philosophy

in the

Queensland Micro- and Nanotechnology Centre

Environmental Engineering School

Griffith University

Declaration of Authorship

I, Elham Nariyan, declare that this thesis titled, ` Halide Removal from Water by Novel Bismuth Materials ' and the work presented in it are my own.

 I confirm that:

- This work was not published before anywhere and was done in Griffith University for the PhD degree candidature.
- The other works in the thesis were cited.
- I have acknowledged all the assistance and sources for this work.

Signed:

Date: 2020.03.17

Acknowledgment

Thank you to all the people who have contributed to this work and supported me in achieving my PhD. Special thank you to Professor Qin Li for her support and advice. A grateful thank you to Dr Jimmy Yu for his advice and Nikhil Aravindakshan for helping me with the analysis and characterisation of my samples. Mr Alan White from Griffith Chemistry Lab for his help and suggestions for water analysis and helping me with various struggles during the PhD. From the University of Queensland, I would like to thank Dr Barry Wood who helped me analyze and characterize my samples. Thank you to my colleagues Mostafa Esmaeili, Georgina Wu, Fan Yang and Zhengfen Wan for their help and motivation during the journey. For their generous scholarship provision and opportunity to work as a PhD student I thank Griffith University. I dedicate this work to my Mother, Father and brothers and Wade Hart who have offered great support along the way.

Table of contents

Contents

List of figures

List of tables

Abbreviations

Abbreviations	Description
THMs	Trihalomethanes
HAAs	Haloacetic acids
DBAN	Dibromoacetonitrile
HAN$_4$	Trichloroacetonitrile
DCAN	Dichloroacetonitrile
DBAN	Dibromoacetonitrile
DBPs	Disinfection By-Products
ESP	Electrostatic Precipitator Catch or Dust
TFT-LCD	Thin-film-transistor liquid-crystal display
TDS	Total Dissolved Solids
NOM	Natural Organic Material
RO	Reverse Osmosis
FO	Forward Osmosis
FDFO	Fertilizer Drawn Forward Osmosis
NF	Nano Filtration
MED	Multiple-effect distillation
MD	Membrane Distillation
DCMD	Direct Contact Membrane Distillation
MEH	Multi-Effect Humidification
VMD	Vacuum Membrane Distillation
ED	Electrodialysis
EDR	Electrodialysis Reversal
Solar PV/EDR	Solar Photovoltaic/ Electrodialysis Reversal
AD	Adsorption Desalination
VC	Vapour Compression
TVC	Thermal Vapor Compression
MVC	Mechanical Vapor Compression
ME	multiple-effect evaporation
CAPEX	Capital expenditures
OPEX	Operating expense

MSF	Multi-stage flash distillation
ZDL	Zero Liquid Discharge
UHLA	Ultra-high lime aluminium
PCD	Permeation and Chemical Desorption
EC	Electrocoagulation
LDH	Layered Double Hydroxide
SIAC	Silver Impregnated Activated Carbon
Rpm	Round Per Minute
PFO	Pseudo First Order
PSO	Pseudo second Order
XPS	X-ray Photoelectron Spectroscopy
SEM	Scanning Electron Microscope
DLS	Dynamic Light Scattering
S-2-200	Hydrothermally treated sucrose for 2h at 200 °C
S-4-200	Hydrothermally treated sucrose for 4h at 200 °C
CNS	CNS (carbon nanosheets)
BS-2-200	Bismuth particles mixture with hydrothermally treated sucrose for 2h at 200 °C
BS-4-200	Bismuth particles mixture with hydrothermally treated sucrose for 4h at 200 °C
BCNS	Bismuth particles mixture with CNS
BS-2-200-450	Bismuth particles composite with hydrothermally treated sucrose at 200 °C for 2h and then calcined at 450 °C with heating rate of 5 °C/min
BS-2-200-600	Bismuth particles composite with hydrothermally treated sucrose at 200 °C for 2h and then calcined at 600 °C with heating rate of 5 °C/min
BS-4-200-450	Bismuth particles composite with hydrothermally treated sucrose at 200 °C for 4h and then calcined at 450 °C with heating rate of 5 °C/min

BS-4-200-600	Bismuth particles composite with hydrothermally treated sucrose at 200 °C for 4h and then calcined at 600 °C with heating rate of 5 °C/min
BCNS-450	Bismuth particles composite with CNS and then calcined at 450 °C with heating rate of 5 °C/min
BCNS-600	Bismuth particles composite with CNS and then calcined at 600 °C with heating rate of 5 °C/min

Abstract

Water is scarce and there is a high demand for water usage at different parts of domestic usage (9%), agriculture (70%) and industries (21%). The halides in natural and sea waters are typically of a ration of Cl: Br: I is 100-200:10:1, which means chloride is 10-20 times more than bromide and bromide is 10 times of iodide. Excessive halides-release into the water could be as a result of natural or human activities, for example, mining and produced waters from oil and gas industries could release a high level of halides in water.

Removal of excessive amount of halides is crucial for human and living creatures. High chloride concentration could lead to destruction to aquatic lives (as indicated by *A. maculatum* and *R. sylvatica*), phytotoxicity, crop damage, corrosion of pipes, and other infrastructures (such as reduced electrode lifetime in hydrometallurgy). Iodide/iodine has some radioactive isotopes and contributed to the environmental disasters during the Chernobyl and Fukushima catastrophes. However, iodide and bromide even at very low concentrations also could bring up problems in health issues such as producing disinfection by-products (DBPs) during water treatment.

More than 600 species of DBPs could be produced in the chlorination disinfections process, and some of the DBPs are known to be very toxic and their levels in water are so restricted. For example, Environmental Protection Agency (EPA) has set limitations for chloroform and bromodichloromethane at 80 and 60 ppb, respectively. The best way to avoid DBPs production is to remove the excessive amount of halides before application of any kind of oxidation for water treatment.

This thesis is focused on removal of Cl⁻, Br⁻ and I⁻ ions in water. F⁻ is excluded because F⁻ is much easier to precipitate out in comparison to the other three halide anions. Two types of novel bismuth-based materials have been developed for removal of halides at high concentrations (> 1000 mg/L) and low concentrations (< 10 mg/L), respectively. The high concentration halide removal addresses issues in mining industry, whilst the low concentration removal addresses the issue of drinking water quality.

1. Introduction

Excessive chloride release in water can be a result of de-icing of roads with chloride-containing salts [1-4], aluminium chloride coagulants as water treatment agents, oil-gas and mining industries, incineration of wastes [4-7], and landfill leaching [8-11]. Mining activities could release 70-140 g/L of chloride in water [12]. Oil and gas extraction would release salt into the water known as produced water [8]. For example, chloride concentration can reach 14-41 g/L in the produced waters [4].

Anthropogenic activities which would lead to iodine/iodide release into water include LCD production [13], nuclear fission [14-16], mining activities and oil-gas extractions [17-19]. Bromide at high concentrations in water is also a result of mining activities and oil-gas extractions, desalinations, and chemical productions which involves using bromide [20]. Nature would also lead to halide release into the water, such as seawater intrusion, leaching of geological rocks which contain halides [20].

Different regulations have been set for halide concentrations based on the water application. For example, agricultural water has set more restrict regulations for chloride levels than drinking water (105 mg/L vs. 250 mg/L). Regulations set by Australia for chloride and iodine are 250 mg/L and 0.5 mg/L, respectively [21, 22]. For bromide, there is no regulatory enforcement, but a recommended upper limit, which is currently set at 0.1 mg/L [23]. Research on safe bromide concentrations for avoiding potent brominated-DBPs production recommends a concentration for Br- of less than 50-60 µg/L [24, 25].

1.1. Background and research scope

Despite the importance of halide removal from water as mentioned before, halide removal is a challenging task because of their high solubility, high stability and less selectivity compared to the other anions. This thesis is focused on removal of Cl-, Br- and I- ions in water. F- is excluded because F- is much easier to precipitate out in comparison to the other three halide anions.

Selecting a technology which addresses the halide removal depends on various parameters such as investment, halide concentration, and the scale that is going to be used. Chloride removal technologies mostly are in reverse osmosis (RO), multi-stage flash distillation (MSF), multiple-effect distillation (MED) and electrodialysis (ED) based on

their respective capacity. MED and then MSF has the highest capital expenditures (CAPEX), followed by RO. MSF and MED are used for very high chloride concentrations like seawater desalination or brine management. However, RO and ED are used for high and medium concentrations of chloride. Merely solar technologies such as solar still and multi-Effect Humidification (MEH) showed low capacity at low cost as well. Therefore, solar technologies are more useful for small scale applications. While the application of membrane with thermal technology (MD) has enhanced the capacity significantly and makes them the most commonly used technologies for chloride removal at very high concentrations.

All of the membrane technologies are challenged by fouling and scaling problems in brine management. Concentrated brine disposal would comprise 5-33% of desalination process cost [26]. Brine management cost depends on the method of its dispose and treatment, the quality of brine and its volume. For example, as it was mentioned before, MED brine disposal has a lower cost for disposal than RO. Especially, RO produces a considerable amount of brine (10-25% of feed water), which should be considered in the decision making and designing phases.   Till now, discharge to the surface water and sewer is the cheapest way but not environmentally friendly way to deal with brine management from desalination plants (chloride removal).

On the other hand, adsorption and resins are also available options for halide removal with a cheaper cost and a lower capacity compared to RO and MSF. One option of chloride adsorption is precipitate it as Freidel salt which was obtained via coagulation and electrocoagulation, which is called ultra-high lime aluminium (UHLA) [27, 28]. But UHLA is not applicable for bromide and iodide removal, and other disadvantage of this technology is that it would be affected by the existence of other anions. For example, sulfate competes with chloride in UHLA precipitation.   Other option which is applicable to chloride, iodide and bromide removal is using of silver containing adsorbents or silver impregnated activated carbon (SIAC), but silver could leach into water and their removal efficacy would decrease [25].

Therefore, a gap has been identified in which an affordable and effective removal of halides (Cl^-, Br^- and I^-) at different concentrations. Therefore, this research is focused on finding an ion exchanger or adsorbent to tackle with high (mining water) and low halide concentrations (drinking/surface water), respectively.

1.2. Objective

The PhD project is aimed at finding cost-effective removal methods for removing Cl^-, Br^- and I^- of high concentrations (> 1000 ppm) as in mining and produced waters, and of low concentrations (< 10 ppm) in the context of drinking water treatment. This involves identifying a new type of material that preferably incorporates Cl^-, Br^- and I^-. The specific aims of the thesis include:

- To identify and synthesis a material for cost-effect removal of high concentration halide ions from mining waters;
- To characterize the produced material and evaluate the effect of other parameters on halide removal;
- To design, synthesize and characterize micro-nano bismuth compounds and test them for removing halides at trace concentrations;

1.3. Outline of the Report

Outline of this thesis is as below:

Chapter 1: Introduction

The aim and importance of this PhD thesis would be depicted.

Chapter 2: Literature Review

The importance of halide removal and the reasons for having halide in waters by nature or anthropogenic impacts to release halides in water would be discussed. Furthermore, various halides concentrations by mining and produced water would be shown. Finally, the limits set for halide concentrations in aqueous solutions would be presented and the removal technologies that are being used for halide removal and their cost and challenges would be discussed.

Chapter 3: Synthesis, characterization, and mechanism of a novel bismuth hydroxide sulphate adsorption material for halide removal at high concentrations

A novel bismuth material synthesis and characterizations would be presented. Subsequently, it would be used for halide removal at high concentrations and different parameters would be tested on its removal efficacy. Finally, the material conversion to other material (BiOX, X=Cl, I, Br) after halide removal would be shown by characterizations. Eventually, isotherms and kinetics relevant for the removal have been calculated.

Chapter 4: Synthesis of various nano-micro sized bismuth composites: effect of various substrates and temperature

Synthesis of bismuth materials at smaller scales than the previous material (nano-micro sized). For this aim, different substrates were being synthesized and being used as sacrificial substrates which were removed later by calcination at different temperatures. As functional groups of substrates are varied from each other, this would have an effect on the final product. Then the final products being tested for iodide removal as an example for halide removal and the best one would be chosen for the halide removal at trace concentrations**.**

Chapter 5: Removal of iodide and bromide at low/trace concentrations with novel bismuth composite material

Testing of the best-performed material for iodide and bromide removal at trace concentrations and then checking the effect of parameters such as initial concentrations and pH, and etc. finally, calculations for isotherm and kinetics for this material.

Chapter 6: Conclusion and future scope

Conclusion and the limitations of this work would be presented, and the final suggestions for future works would be presented.

1. Corsi, S.R., et al., *A fresh look at road salt: aquatic toxicity and water-quality impacts on local, regional, and national scales.* Environ. Sci. Technol., 2010. **44**(19): p. 7376-7382.

2. Chapra, S.C., A. Dove, and D.C. Rockwell, *Great lakes chloride trends: long-term mass balance and loading analysis.* J. Great Lakes Res., 2009. **35**(2): p. 272-284.

3. Dugan, H.A., et al., *Salting our freshwater lakes.* PNAS, 2017. **114**(17): p. 4453-4458.

4. Maciel, R., G.L. Sant'Anna, and M. Dezotti, *Phenol removal from high salinity effluents using Fenton's reagent and photo-Fenton reactions.* Chemosphere, 2004. **57**(7): p. 711-719.

5. Rogora, M., et al., *Recent trends in chloride and sodium concentrations in the deep subalpine lakes (Northern Italy).* Environ. Sci. Pollut. Res. Int., 2015. **22**(23): p. 19013-26.

6. Silva, T.L.S., et al., *An overview on exploration and environmental impact of unconventional gas sources and treatment options for produced water.* J. Environ. Manage., 2017. **200**: p. 511-529.

7. Kameda, T., et al., *The simultaneous removal of calcium and chloride ions from calcium chloride solution using magnesium–aluminum oxide.* Water Res., 2003. **37**(16): p. 4045-4050.

8. Envitech, C. *Saline water management (or brine treatment) in industry.* 2017; Available from: https://blog-en.condorchem.com/saline-water-management/#.WzQ8p4oRVhE.

9. Lv, L., et al., *Uptake of chloride ion from aqueous solution by calcined layered double hydroxides: Equilibrium and kinetic studies.* Water Res., 2006. **40**(4): p. 735-743.

10. Kinnarinen, T., et al., *Removal of chloride from fly ash produced in hazardous waste incineration by leaching and displacement washing in a vertical filter press.* Waste Manage. Res., 2013. **31**(2): p. 178-186.

11. Chen, W.-S., et al., *Removal of chloride from MSWI fly ash.* Journal Hazard. Mater., 2012. **237-238**: p. 116-120.

12. Turek, M., *Recovery of NaCl from saline mine water in an electrodialysis-evaporation system.* Chem. Pap., 2003. **1**: p. 50-52.

13. Kentjono, L., et al., *Removal of boron and iodine from optoelectronic wastewater using Mg–Al (NO₃) layered double hydroxide.* Desalination, 2010. **262**(1): p. 280-283.

14. Madrakian, T., et al., *Application of Modified Silica Coated Magnetite Nanoparticles for Removal of Iodine from Water Samples.* Nano-Micro Lett., 2012. **4**(1): p. 57-63.

15. Theiss, F.L., G.A. Ayoko, and R.L. Frost, *Iodide removal using LDH technology.* Chem. Eng. J., 2016. **296**: p. 300-309.

16. Li, D., et al., *Removal capacity and chemical speciation of groundwater iodide (I^-) and iodate (IO_3^-) sequestered by organoclays and granular activated carbon.* J. Environmen. Radioactiv., 2018. **192**: p. 505-512.

17. Fruit, J.T., et al., *Recovery of Iodine from Produced Water Through Anion Resin Exchange*, in *2011 Research Experiences for Undergraduates posters and presentations.* 2011, Advanced Water Technology Center (AQWATEC) Colorado School of Mines, 1500 Illinois street, Golden, CO 80401.

18. Kim, H.I., et al., *A process to recover high purity iodine in wastewater from liquid crystal display (LCD) manufacturing industry.* Hydrometallurgy, 2018. **181**: p. 91-96.

19. Ordóñez, J.I., et al., *Use of discharged brine from reverse osmosis plant in heap leaching: Opportunity for caliche mining industry.* Hydrometallurgy, 2015. **155**: p. 61-68.

20. Watson, K., M.J. Farré, and N. Knight, *Strategies for the removal of halides from drinking water sources, and their applicability in disinfection by-product minimisation: A critical review.* J. Environ. Manage., 2012. **110**: p. 276-298.

21. NHMRC and NRMMC, *Australian Drinking Water Guidelines Paper 6 National Water Quality Management Strategy.* 2011: National Health and Medical Research Council, National Resource Management Ministerial Council, Commonwealth of Australia, Canberra.

22. Shaffer, D.L., et al., *Seawater desalination for agriculture by integrated forward and reverse osmosis: Improved product water quality for potentially less energy.* J. Membr. Sci., 2012. **415**(Supplement C): p. 1-8.

23. José Farré, M., et al., *Assessment of Regulated and Emerging Disinfection By-Products in South East Queensland Drinking Water.* 2012: Urban Water Security Research Alliance.

24.   Gruchlik, Y., et al., *Impact of bromide and iodide during drinking water disinfection and potential treatment processes for their removal or mitigation.* Water, 2014. **41**(8): p. 38-43.

25.   Rajaeian, B., *Removal of Bromide from Drinking Water Sources using Silver impregnated activated carbon (SIAC) understanding Br-SIAC interactions*, in *Department of Civil Engineering.* 2017, Curtin University: Curtin University.

26.   Morillo, J., et al., *Comparative study of brine management technologies for desalination plants.* Desalination, 2014. **336**: p. 32-49.

27.   Abdel-Wahab, A.I.A., *The ultra-high lime with aluminum process for removing chloride from recirculating cooling water*, in *Civil engineering.* 2003, Texas A&M University.

28.   Abdel-Wahab, A. and B. Batchelor, *Effects of pH, temperature, and water quality on chloride removal with ultra-high lime with aluminum process.* Water Environ. Res., 2006. **78**(9): p. 930-937.

2. Halide Removal in Water Treatment: the Whys and the Hows

Elham Nariyan[1,2], Jimmy (Qiming) Yu[2] and Qin Li[1,2]*

1. Queensland Micro- and Nanotechnology Centre, Griffith University, Nathan, QLD 4111, Australia
2. School of Engineering and Built Environment, Griffith University, Nathan, QLD 4111, Australia

2.1. Abstract

Halide management in water is important for various reasons ranging from disinfection by-products in drinking water, infrastructure corrosion to soil salination issues. For example, excess chloride in water could damage crops and endangering aquatic lives, corroding the infrastructures; Iodide could be radioactive, therefore, the importance of iodide removal is essential in radioactive disasters. This review discusses the toxicity and safe regulations for Cl^-, Br^- and I^-, and the sources for excessive quantity of these ions in waterways and the current technologies in place for their removal. It's highlighted that halide removal is challenging because of the high solubility and less selectivity compared to other anions, which makes halide removal expensive. There is a need for developing cost-effective methods for halide removal.

2.2. Introduction

2.2.1. Why halide removal is important

2.2.1.1. Chloride

59% and 22% of the total water on the earth are seawater and brackish water, respectively [1]. Desalination of seawater for agricultural purposes has been applied in various arid and semi-arid countries such as Israel [2], Spain, Middle Eastern [3], and Australia [3]. The desalination of seawater for irrigation purposes is mainly related to chloride removal because chloride constitutes more than half of seawater salts. The other ions in seawater such as Ca^{2+}, Mg^{2+} and SO_4^{2-} are desirable ionic species for agriculture purposes [3]. Excessive chloride has negative impacts on a wide range of applications such as damaging agricultural crops, corrode the infrastructures and reduce their lifetime such as electrodes' life-time in the electro-winning electroextraction of metals from ores,

corrodes metallic pipes, concrete, heat exchangers, kraft recovery furnace [4-10], which could cause significant operation disruption and finanicial damage to industries and communities [4, 11-13]. For example, bridge corrosion by chloride has cost $ 275.7 billion/year, in USA in 1998 [11]. Infrastructures in contact with seawater or de-icing brines are more prone to be corroded [14].

2.2.1.2.Iodide

Different isotopes of iodine are being produced within the plutonium and uranium fission reactions. The exposure to these iodine isotopes can lead to thyroid illness such as thyromegaly, leukemia, thyroid cancer and metabolic disorders [15-18]. Moreover, in the context of nuclear energy systems, it is critical to ensure safe handling and storage of radioiodine, such as ^{129}I and ^{131}I. Because of the long half-life of iodine (half-life of ^{129} I: 15.7 million years), it is very crucial to control its presence in waterways [16, 19]. Radioactive iodine could enter easily to human and animal organs, environment (water and air), and plants [17, 18]. The most common chemical forms of I in the nuclear wastes which can leak to the water are iodide (I^-) and iodate (IO_3^-) [20].

Till 1998, 2360 kg of ^{129}I was released into seawater by Sellafield (UK) and La Hague (France). In addition, from 1944-1972, plutonium production at the Hanford Site (Washington) released 266 kg of ^{129}I into the air [19]. The worst-case was the radioactive disaster of Chernobyl - Ukraine and Fukushima- Japan, it made clear for the human that it is dangerous, especially in high amounts [21]. Fukushima disaster lead to a release of 6.9-52 % ^{131}I into water pools. More iodide and cesium (CsI) were released than strontium and barium released into the fuel. The Chernobyl disaster was even harsher than Fukushima. In the Chernobyl disaster, 1,760 Petabecquerel (PBq) ^{131}I was released, along with other isotopes of iodine as enlisted in Table 2-1 [22].

Other health problems related to iodine (I), is that if a human is exposed to larger amounts of iodine than what is suggested, it would result in the itches, bronchitis, sleep disorders, rashes in the long run. In addition, inhaling and contacts with iodine fumes would result in lung and eye irritation, respectively [21].

Table 2-1. various radio-iodine released in the Chernobyl disaster [22].

Nuclide	PBq	Inventory (%)
^{131}I	1760	42
$^{132}Te/^{132}I$	1040	25
^{133}I	910	19
^{134}I	25	1.2
^{135}I	250	8.6

Considering the risks of mine flooding, uncontrolled discharges (such as tailing entrance to the marine environments) and collapses of mine wastes impoundments from an abandoned mine/ closed mine, the potential disastrous effect of high concentration of iodide/iodine to the adjacent urban and residential areas is clear [23]. Also, the contaminated mining water could enter the other waterways and spread the contamination [23].

The presence of iodide in water during chloramination would possibly produce disinfection by products (DBPs) in drinking water supplies. Iodinated DBPs are 10^5 times more genotoxic and cytotoxic than chlorinated DBPs. Therefore, in the interest of public health, it is important to remove iodide before any oxidations and to set restrict regulations [24].

2.2.1.3.Bromide

Although bromide is not toxic, it will cause odour and taste change of water [25]. Moreover, when it reacts to the natural organic matters (NOM) and disinfectant, it would produce DBPs such as brominated trihalomethane (THM), bromate and haloacetic acid (HAA) [24, 25]. The cyto- and genotoxicity results showed that the toxicity index of brominated DBPs is $>10^4$ times their chlorinated counterparts. Also, brominated DBPs are more reactive than the chlorinated counterparts, which make the situation aggravated [24, 26]. At elevated bromide concentration (500 µg/L), high amount of broform will be formed (70-174 µg/L) [27]. The studies showed that when bromide concentration in water increases the brominated DBP products, whose increase is considerably higher than the chlorinated DBPs. Brominated THMs and brominated haloacetic acids (HAAs) would increase by 50% proportional to the increase of bromide ion concentration. For illustration, when bromide concentration was 60-110 µg/L the

HAA concentration reached to 16-36 µg/L. However, when the bromide concentration reached to 500 µg/L, the HAA concentration reached to 39-76 µg/L. Specifically, when bromide concentration increased almost 5 times the HAA formation increased 2.5 times, approximately [27].

For avoiding the DBP formation, the best strategy is the removal of bromide and iodide prior to the reaction with disinfectant, which would result in not only less toxic DBPs formation, but also reduction in disinfectant loss. Furthermore, the absence of bromide and iodide makes the application of other kinds of disinfectant feasible because the oxidation of the iodide/bromide would not be a problem [25]. In addition, the capital and operational cost of water treatment would decrease [26].

2.3. Sources of halides

2.3.1. Chloride

Seawater (3-3.8% NaCl) and de-icing of roads (20-30% NaCl/$CaCl_2$ de-icing brines) are the main sources of chloride release into water and damaging the infrastructures by their corrosion [14]. Other sources of chloride are the kraft pulping process which turns wood into wood pulp. Chloride comes from electrostatic precipitator catch or dust (ESP dust), which consists of 1-10% wt chloride [28]. Chloride would be released from ESP because chlorine is one of the process elements which enters in the kraft pulping process with wood and other chemicals and will accumulate [29]. The boiler burns the black liquor, which contains organic and inorganic materials such as chloride [30]. Chloride concentration from the inland mill is 0.1-0.8% of the liquor dry solid, while for the coastal mill chloride concentration could be as high as 3-5%, and in the closed process, chloride concentration could be even higher [30]. Mining water also could contain high concentrations of chloride, depending on the geological location, dissolved metals and deposits characterizations that are in contact with water. The mines which release large quantity of chloride into water are typically radio-nucleolus uranium and coal mines [31]. However, they have different chemistry from each other. In particular, coal mine water is usually neutral, having an elevated TDS with high electrical conductivity, with high chloride concentration, which will turn into saline mine water [31]. Other than that if the water would be in contact with the tailings containing chloride, called tailing water, would have high chloride concentrations due to leaching of chloride into water [31]. For example, Polish mine water drainage contributed 6,500 tonnes chloride in the Wisla and

Odra rivers, which disqualified the water from being suitable for drinking nor for agriculture. Also, this lead to increased corrosion of pipes [32]. Most of Upper Hunter Valley's open-pit have saline mine water (chloride concentration from 3100-6580 mg/L), which is used mostly for the coal washing and dust suppression [33]. In Kent Coalfield (UK), chloride concentration was 318,000 tonnes (up to 5000 mg/L) in mine drainage water [34]. This degree of salination caused by mine water if not being addressed would result in heavy penalties for the mining industries [32]. The produced water (the resultant water after the oil and gas activities) also contains high concentrations of chloride [35-37]. Chloride concentration in produced water could reach 250,000 mg/L [36]. For example, chloride concentration in the water produced from Louisiana and Texas platforms were reported to have 37,000-110,000 and 28,000-73,000 mg/L, respectively [38]. The produced water from the extraction of shale gas (SG) and tight gas (TG) or conventional natural gas is saline (>30 g/L chloride) and hypersaline (> 40 g/L chloride), respectively. However, coalbed methane (CBM) produced waters have less than 30 mg/L chloride ions [35]. Chloride concentration in the produced water from oil field, gas field, steam gravity drainage (SAGD), coal gas steam (CGS) reaches to 152,750 mg/L, 2,300 mg/L,4,800 mg/L, and 3,100 mg/L, respectively [39]. The coal seam water has a high concentration of sodium, chloride and bicarbonate (salinity 1,500-10,000 mg/L) [40, 41]. Australian (QLD) coal seam water contains more chloride (500-2000 mg/L) than bicarbonate [40, 42]. The coal seam water in Queensland, Australia has < 5910 mg/L chloride [43], whereas in New Zealand and USA chloride concentration is lower, in the range of 49.3-146 mg/L [43]. Chloride concentrations in produced water and some coal seam gas water are presented in Table 2-2. Salt concentration becomes more important when the oil/gas operations take place onshore [36]. At a higher certain amount of chloride, corrosion and fracture in reactors and vessels will happen. Therefore, keeping chloride concentration as low as possible is necessary for feeding oil [44]. The offshore generated produced water will be released into the sea, which might endanger the aquatic lives [36]. If produced water leaks to surface water could damage the ecosystem drastically [42].

Table 2-2. Chloride concentration in produced water and seam gas water [35, 43, 45].

Cl (mg/L)	Coalbed Methane	Shale Gas
Produced water	0.7-70100	48.9-212700
	Tight Gas	Conventional Natural Gas
	52-216000	1400-190000
	Flowback water (Marcellus Shale)	
	32000-148000	
seam gas water	Southern tenements (Surat) –WB – 56 wells	Moranbah area (Bowen) –WB – Blackwater Group coal formation – 58 wells
	28-5870	1151-4500
Coal seam gas, Surat Basin, Queensland	Field A, (54 wells)	Field B (73 wells)
	471 – 4390 (1595)	875 – 2930 (1579)
	Field C (23 wells)	
	823 – 5910 (2938)	

2.3.2. Iodide

Iodine exists in the natural waters, and its average concentration in seawater and rivers are 60 ppb and almost 5 ppb, respectively [21]. Iodide in the natural waters probably would be with bromide with the ratio of 1:10 (I^-: Br^-) [24]. Iodine in water would be as a result of the raining and also weathering with the rocks which contain iodine or as a result of volcanic activity [21]. Also, iodine could be present in some minerals (which contains Fe, Cu, Ag, Hg, Pb, As, Sb and S), soils and hydroxides [17, 21]. In the case of soil, IO_3^- is better sorbed than I^- in soil. [129]I is present in the surface soil, which could be released into the atmosphere. [131]I is less present in soils and sands, as illustrated by the study performed on the Germany sands [17]. Brown algae accumulate up to 0.45% (dry mass) of iodine. Corals, sea sponges, shells and fishes accumulate high iodine concentrations, usually in the form of thyroxin or tri-iodine thyroxin [21]. The concentration of iodine in the natural materials are being shown in Table 2-3.

Table 2-3. Iodine concentration in natural materials [17].

Occurrence	Concentration-ppb
seawater	60
Atlantic Ocean water	54-59
Ocean waters	52 (11-70)
Sea sediments	1630-2473
River water, mean	2
Japan river water, mean	2.2
German lakes	3,5 (2.5-4.9)
Swiss rivers	0.56 (0.4-1.3)
Groundwater	0-500
New Zealand groundwaters	0.7-14.8
Intrusive rocks (including carbonatites)	140-2000
Marls	1200
Shales	200-2200
Limestones	1300-4200
Clays and argillites	600-1700
Sedimentary rocks	300
British soils	2700-36900
Air, mean	2.3 (ng/m^3)-5.0 (ng/m^3)
Cereals (wet wt.)	100 ± 20
Corn (wet wt.)	69
Vegetables (Cabbage, egg plant, lettuce, turnips, carrots, potatoes, etc ...wet wt.)	<11-48
Human muscle	34
Milk	120
Marine fish (wet wt.)	833 (163-3180)
Freshwater fish (wet wt.)	30 (17-40)
Marine red algae, mean	382500

Human activities also can lead to iodine in the water such as liquid crystal display (LCD) polarizing films industry, which could release very high amount of iodine/iodide in their wastewater such as 10.2 g/L or (1-1.5 wt%) of I$^-$ [18, 46, 47], with the flow rate of 100-300 m^3/day [48]. The wastewater produced by TFT-LCD industry is not possible to be treated by the normal wastewater treatment plants due to possibility of biocidal effect towards microorganisms [46, 47]. The other ways that iodine (mostly iodide and iodate)

enters into water is as a result of nuclear fission [20, 47, 49]. Moreover, mining activities and produced water from gas production could also cause release of iodine into waterways [46, 50, 51]. Iodine was found in Oko uranium deposit in Gabon. As a result of the fission reaction, the heavy elements (Kr, Xe, Rb, Cs, Sr, Ba, Mo) and I are very mobile. The migration of ^{129}I in four uranium ore deposits of the Alligator Rovers region, Northern Territory, Australia was reported by Fabryka-Martin et. al. Basically, the weathering of the deposits contains the iodine, and in the case of Alligator Rovers region deposits, the -FeOH groups in ores such as goethite FeO(OH), were likely the groups where iodide sorption occurred. The weathering of deposits resulted in a strong partitioning of ^{129}I in the groundwater, which is dependent on the distance to the ore place [17]. These iodine extractions lead to water contamination for the people who live near the mining site, which urged the local population to use the desalination plant treatment [51]. Another example is Southeastern Nigeria abandoned mine sites where iodide concentrations were found 0.013-0.05 mg/L [52].

The last but not least way of entering iodine into waterways by human activity is the chemical wastes of x-ray, disinfection, and medical (nuclear medicine) dumps , because of iodine application in these industries [20, 21, 49].

2.3.3. Bromide

Bromide concentration in water could vary because it depends on the different geochemical materials which are in contact with water [26]. Generally speaking, bromide would be found with sodium chloride due to the same chemical and physical properties. However, bromide concentration compared to the chloride is significantly smaller. For example, in the seawater, bromide concentration is between 65-80 mg/L, but the chloride concentration is between 18,980 mg/L to over 23,000 mg/L [53, 54]. Bromide in the natural waters such as groundwater and rivers would be between 0.1-3 mg/L [24]. Bromide concentration in the desalinated water is reported 1 mg/L, while this concentration would be less in the freshwater and would range about 0.5 mg/L [53]. Bromide in drinking water should be less than 1 mg/L [26]. Although there is no information about bromide concentration in the brackish water, it is presumed that the concentration would be between 1-10 mg/L in one study [55]. The summary of bromide concentration in various water substrates has been presented (Table 2-4) [55].

Bromide concentration in the Western Australia groundwater is between 0.4 to 8.4 mg/L [26], which may be associated with the high concentration of bromide in the drinking water in Perth, though the town water source is from dams [25, 26]. However, the water has less dissolved organic carbon (DOC) compared to the other waters in Australia [25]. In Brisbane drinking water tests, it showed that bromide concentration is moderate from 0.053 to 0.140 mg/L, varying from site to site [56]. At Mt Crosby water treatment plant in the western side of Brisbane, the high bromide concentration lead to a high amount of Br-DBP, because this water treatment plant uses chlorination. However, at the Molendinar water treatment plant site in Gold Coast area, the relatively lower bromide concentrations compared to other water treatment plant results in lower DBP formation (Table 2-5) [57]. When bromide concentration is less than 0.1 mg/L, it was shown that the amount of DBPs produced would be considerably lower [57]. Nonetheless, even bromide concentration from 50-100 µg/L would lead to the formation of hazardous DBP [55].

Table 2-4. Bromide concentration in various water substrates.

Substrate	Bromide concentration	Additional information	ref
natural waters	100–3000 µg/L	Br:I 10:1 Cl:Br 100-200	[24]
Brackish water (study)	1, 5, 10 mg/L		[55]
Freshwater	0.5 mg/L		[53]
Sea water	65-85 mg/L	Cl: 18980 mg/L to over 23000 mg/L	[53]
Desalinated water	1 mg/L		[53]
Moderate bromide concentration	0.5-1.2 mg/L		[26]
Drinking water standard	<1 mg/L		[26]

Table 2-5. Bromide, iodide and DOC concentration in various Australian states and the USA [24, 25, 57].

Qld				
Sample site	Br⁻ (µg/L)	I⁻ (µg/L)	DOC (mg/L)	Reference
Capalaba WTP	74-97	1.4	10.21-10.23	[57]
Mt Crosby WTP	238-388	3.3-3.7	3.90-4.01	
Molendinar WTP	33-43	<0.5	3.88-3.98	
WA				
North- West Coastal groundwater	8455	594	0.8	[25]
Great Southern surface water 1	847	17	10.2	
South-East groundwater	754	72	1.2	
North West surface water	448	31	4.3	
South West surface water	400	90	3.5	
Perth Metro groundwater treatment plant raw water	743	31	7.6	
Mid –west eastern ground water bore	1460	<LOD*	0.6	
Goldfields groundwater bore 1	977	<LOD	0.8	
Goldfields groundwater bore 2	1385	26	1.2	
Goldfields groundwater bore 3	817	<LOD	0.7	
Goldfields groundwater bore 4	868	<LOD	0.9	
Goldfields groundwater bore 5	717	<LOD	0.9	

Perth south coastal groundwater bore 1	1483	23	1.0	
Perth south coastal groundwater bore 2	479	<LOD	2.6	
Perth south coastal groundwater bore 3	1307	25	1.2	
Great southern surface water 2	561	6	16.2	
Mid- west western groundwater bore 1	2249	215	0.5	
Mid- west western groundwater bore 2	1908	128	0.4	
Mid- west western groundwater bore 3	2807	493	0.6	
Perth Northern groundwater bore	567	36	2.2	
Perth metro artesian groundwater	2261	37	1	
USA				
Groundwater	2000	100	0.78	[24]
CH-TPH (Influents of drinking water treatment plants in Charleston, south Carolina)	1050	100	<LOD	
Limit of detection (LOD)= 5 µg/L				

2.4. Pourbiax diagrams and chemistry of halides

For the understanding of chemistry and solubility of halides, one method is using the E_h-pH diagram. Various databases for Eh-pH diagrams were used, FACT/FACTSAGE, SUPCRT/FLASK-AQ, LLNL/GW, JNC-TDB/GW [58].

Iodine to iodide conversion requires +0.54 V (standard reduction potential), while Cl_2/Cl^- standard reduction is +1.36 V and Br_2/Br^- has the standard reduction potential of 1.09 V.

Also, the first ionization energy for Cl, Br, and I are 1251, 1140 kJ, and 1008 kJ/mol, respectively. This depicts that oxidizing power is as follows $Cl_2>Br_2>I_2$ [59].

Chloride E_h-pH (Figure 2-1) indicates that chloride is highly soluble under all pH and E_h values unless high voltage is being applied to oxidize chloride to ClO_4^-, even in the case of ClO_4^- would be still soluble. Therefore, it shows the removal of chloride would be a challenge due to its high solubility.
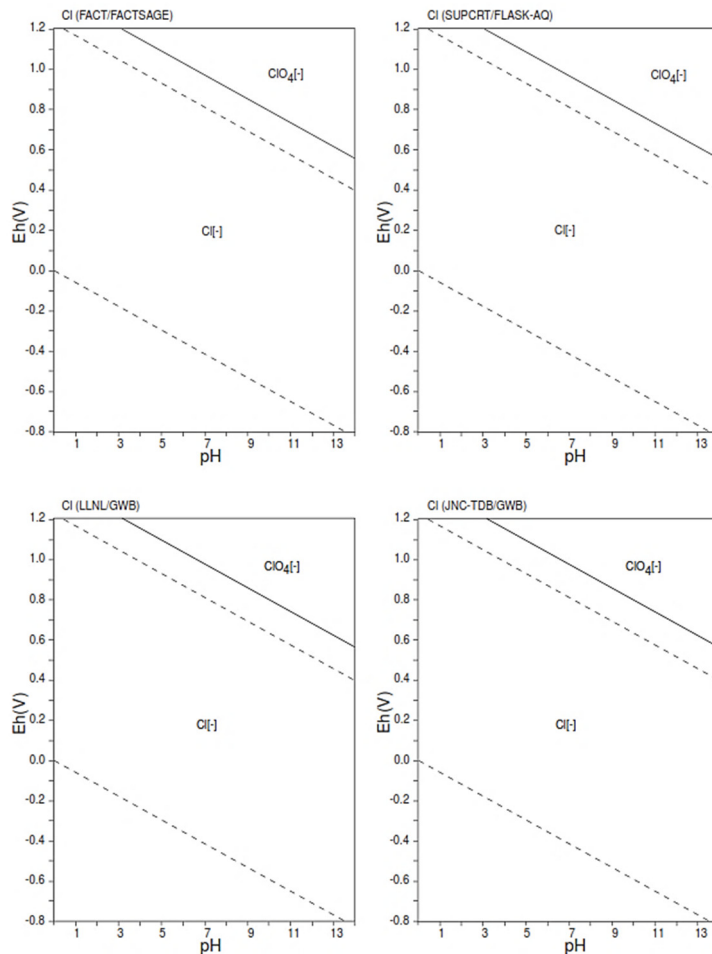
Figure 2-1. E_h-pH diagrams of Cl-O-H with various database and considerations of activity I= 10^{-10} and within 10^5 Pa and T= 298.15 K [58].

Iodide in very acidic and very oxidizing condition would be transformed into other species of iodate (IO_3^-) and a little bit of iodine (I_2). Other than that it is very stable and occurs in the form of iodide (I^-) (Figure 2-2) [60]. However, iodine in water will react and produce iodide and hypoiodite (OI^-) [47]. The possible reactions of iodine in water are as follows (Equation 2-1 - Equation 2-4) [47].

$$I_2 + H_2O(l) \rightarrow OI^-(aq) + 2H^+ + I^-(aq) \qquad K=2.0\times10^{-13} \qquad \text{Equation 2-1}$$

$$I_2 + 2OH^- \rightarrow I^- + H_2O \qquad k=30 \qquad \text{Equation 2-2}$$

$$3OI^- \rightarrow 2I^- + IO_3^- \qquad k=10^{20} \qquad \text{Equation 2-3}$$

$$I_2 + I^- \rightarrow I_3^- \qquad \text{Equation 2-4}$$
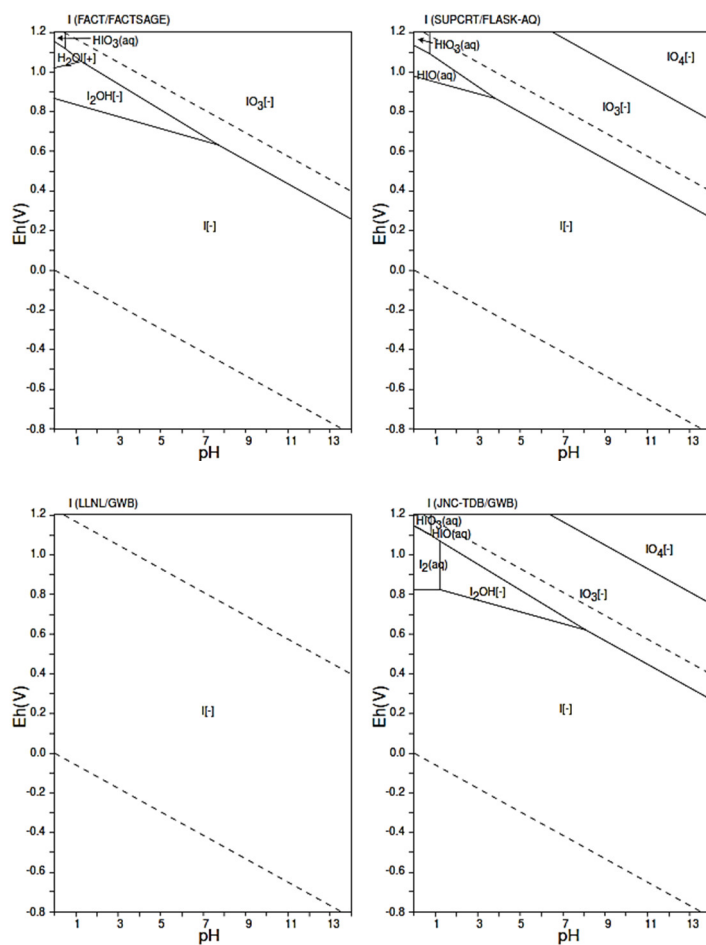
Figure 2-2. E_h-pH diagrams of I-O-H with various database and considerations of activity I= 10^{-10} and within 10^5 Pa and T= 298.15 K [58].

Likewise of chloride, bromide is also very soluble in various conditions, however, JNC-TDB/GW database shows that bromide oxidizes to $Br_2(l)$ at voltages (E_h) higher than 0.3

mV (Figure 2-3). Therefore, bromide removal is also challenging because of its high solubility.
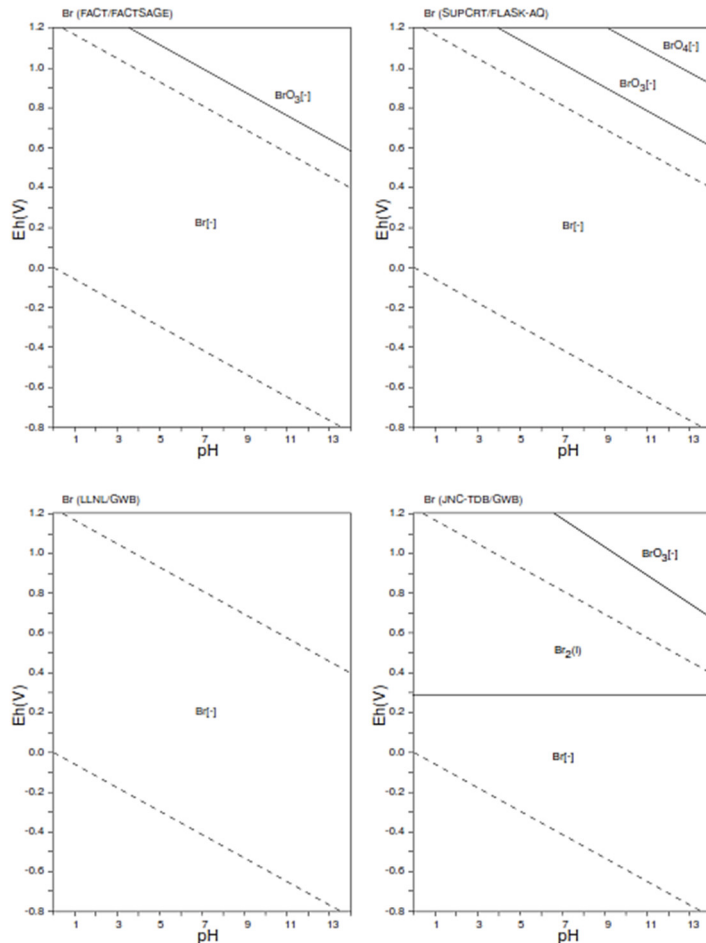
Figure 2-3. E_h-pH diagrams of the system Br-O-OH. $\Sigma Br= 10^{-10}$, 298.15 k, 10^5 Pa [58].

2.5. Limitations and regulations

2.5.1. Chloride

Various limitation for chloride concentration in water has been introduced. European regulations, Australian drinking water guidelines and WHO have set 250 mg/L as the limit for drinking water [61-63]. International environmental protection agency (IEPA) set the limitation of 500 mg/L for chloride concentration for surface water [64]. 94 mg/L of chloride is considered as below risk limits for the ecosystem [65]. Chloride concentration for agricultural purposes has more stringent regulation than portable

water and should be below 105 mg/L [2]. Chloride concentrations below 140 mg/L, 140-350 mg/L and above 350 mg/L are considered as low, moderate and high risk for irrigation, respectively [3]. This is for prevention of soil salination (accumulation of sodium chloride), which otherwise would reduce soil productivity , and exhibit toxicity to crops, known as phytotoxicity [3]. Sensitive and tolerant crops can tolerate different salinities of 650 μS/cm and 8100 μS/cm, respectively. Sensitive, moderately sensitive, moderately tolerant and tolerant crops can tolerate chloride with concentrations of <175, 175-350, 350-700, >700 mg/L, respectively [41]. In Queensland, the chloride concentration set for livestock consumption is 2000 mg/L [43]. In Europe and North America, reinforced concretes the chloride concentration is not allowed to be higher than 0.4% by mass of cement in acid-soluble and 0.15% by mass of cement in and water-soluble environments [6].

2.5.2. Iodide

Iodine concentrations in seawater and freshwater are typically 60 and 2 μg/L, respectively. Iodine in seawater is comprised of 60% I^-, 6% IO_3^- and 10% as organic compounds [17]. USA drinking water iodine level is set at 4-18 μg/L [66]. However, Australian drinking water guideline has set much higher allowance at 0.5 mg/L for iodide regulation, which might be revised in the future [63].

2.5.3. Bromide

The safe concentration of bromide in water by various studies has been indicated (Table 2-6). Australian water regulation suggested having bromide concentration below 0.1 mg/L, because of the formation of bromate in the oxidation process. Specifically, they suggested that if bromide is less than 0.1 mg/L in water, then the water would contain less than 0.02 mg/L bromate which is with Australian regulation alignment. However, they did not set any direct regulations for bromide itself [63].

In one study from south-east Queensland drinking water, it showed that above 0.1 mg/L of bromide, dibromoacetonitrile (DBAN) and trichloroacetonitrile (HAN4) could be produced more considerably compared to that under lower concentrations of bromide. However, when bromide and chloride co-exist in water, the dichloroacetonitrile (DCAN) would form more than DBAN, if bromide concentration is lower [57].

Based on different geochemistry of materials which are in contact in water, the bromide concentration would vary in water. Bromide concentration could be in different categories of risks (Table 2-6) [26].

Table 2-6. Various levels of bromide and DOC risks in water [25-27].

	Concentration, µg/L	Level of risk	Ref
Bromide	Less than 60	Low	[26]
	60-500	Moderate	
	More than 500	high	
	Less than 50	low	[25]
	110	moderate	
	76-540	Moderate to high	
	~700	Very high	
	More than 100	Will cause bromate	[63]
	Concentration, mg/L		
Dissolved organic carbon (DOC)	10 mg/L-13 mg/L	high	[25]
	5 mg/L	moderate	

2.6. Challenges of halide removal

2.6.1. Chloride

Chloride removal is a great challenge because of its high solubility and stability [58]. Conversion of chloride to hydrochloric acid is not a good long-term option as it would be only changing chloride form [9]. Also, oxidation of chloride to chlorine gas by various oxidants such as potassium permanganate is very dangerous for the workplace, also could form DBPs [67]. Due to the high mobility of chloride in water, it would not be influenced by the chemical reactions. Interestingly, chloride is considered as an inert chemical which would not be removed by bioremediation techniques and could not be easily precipitated [68]. Another challenge of chloride removal is that it is usually the less preferred species by the substrate in adsorption and ion exchange processes. Generally,

the selectivity of an ion would get higher, if its charge is much higher than its hydration radius (i.e. smaller ions with more charges are has more selectivity than the bigger ions with smaller charge) [69]. For example, fluoride has smaller hydrated radius with same charge as chloride, therefore, fluoride would have more preference to be adsorbed than chloride. However, nitrate has bigger hydrated radius with same charge as chloride, therefore, chloride has more preferences for being adsorbed than nitrate [70]. Sulphate, carbonate, phosphate have stronger affinity compared to chloride due to their electronegativity. Another example is preferences of chloride over bromide and iodide for being removed first due to the hydration radius as they have the same charge affinity [70, 71].

2.6.2. Iodide

Normally, expensive synthetic materials are shown to have the capability of iodide removal, however, some natural minerals and sediments also have been shown with iodide/iodine removal capacity, but their removal rates were not sufficient [18, 20].

Technologies which have been routinely employed to remove iodide (RO, NF, ED/EDR, electrolysis, CDI, resins) are expensive, and adsorption which is cheaper (except silver contained adsorbents) is not effective all the time such as activated carbon [24, 72]. Another challenge of iodide removal is that most of the adsorbents for iodide removal possess slow reaction kinetic. It's not difficult to imagine that, if there was any disastrous leaking of iodide from the nuclear system, the fast reaction kinetic would be highly desirable [15].

2.6.3. Bromide

Bromide removal is challenging and being less effective with common water treatment technologies (coagulation/flocculation) and is expensive to be removed by membrane assisted technologies such as RO and NF [24, 26, 72]. Bromide oxidation is also not a good strategy to remove bromide from water, especially if there is any NOM in water then brominated DBPs would be produced [24]. Another challenge of bromide removal is that adsorption of bromide on adsorbents or resins in the presence of NOM or alkalinity would be decreased. NOM could block the adsorption sites and bromide removal would decrease [26, 57]. For example, MIEX® showed removal of 49% and 20% for the alkalinity presence in water 11 mg/L and 95 mg/L, respectively [57].

2.7. Technologies for removing halides

2.7.1. Chloride

Most of papers and researches were conducted on desalination rather than chloride removal. However, desalination technologies could be used as merely chloride removal, too. Therefore, here we report the information about desalination plants which is useful for chloride removal, too.

There are various technologies for removing chloride (desalination). Selection of a suitable process for chloride removal is highly dependent on the ease of operation, its effect on the environment, amount of investment, cost of maintenance and operations [9]. Various methods have been employed for chloride removal such as chemical precipitation, electrochemical remediation technology, membrane technologies (non-thermal like RO and thermal like MD), adsorption, ion exchange. Chemical precipitation and electrochemical precipitation with UHLA [73-75], layered double hydroxide (LDH) productions such as Friedel salt, however, other anions such as sulphate would decrease their removal efficacies.

Chemical precipitation with silver nitrate is another option which is expensive as silver lost in this process is inevitable [76]. Produced waters with high chloride concentrations will use RO, and thermally driven technologies such as MD for chloride removal [35], and ZDL would be used for the recovery of brine for zero discharge pollutants [36].

On the other hand, major desalination treatments are happening with RO systems with 58.65%, followed by MSF and MED with 26.95% and 9.51%, respectively (Figure 2-4). Maximum capacity of desalination technologies in Figure 2-4 and Figure 2-5. The capacity and cost of other technologies, which we call them here as non-major technologies are presented (Figure 2-5 and Figure 2-7). As can be seen, these technologies which can be a hybrid of other technologies are having less capacity compared to the major technologies which are being used for desalination plants. Therefore, their applications are less compared to the major ones. However, they can be used in the small-scale applications and they have comparatively less cost compared to the major technologies.

Due to the high importance of the main desalination technologies (RO, MSF, MED and ED), the amount of their energy consumptions is presented in Table 2-7. Some of these technologies just work with electrical energy and some need both electrical and thermal

energy. For example, RO and ED are just working with electrical energy, while, MSF and MED work with both electrical and thermal energy (more thermal basis than electrical basis energy consumer) (Table 2-7).
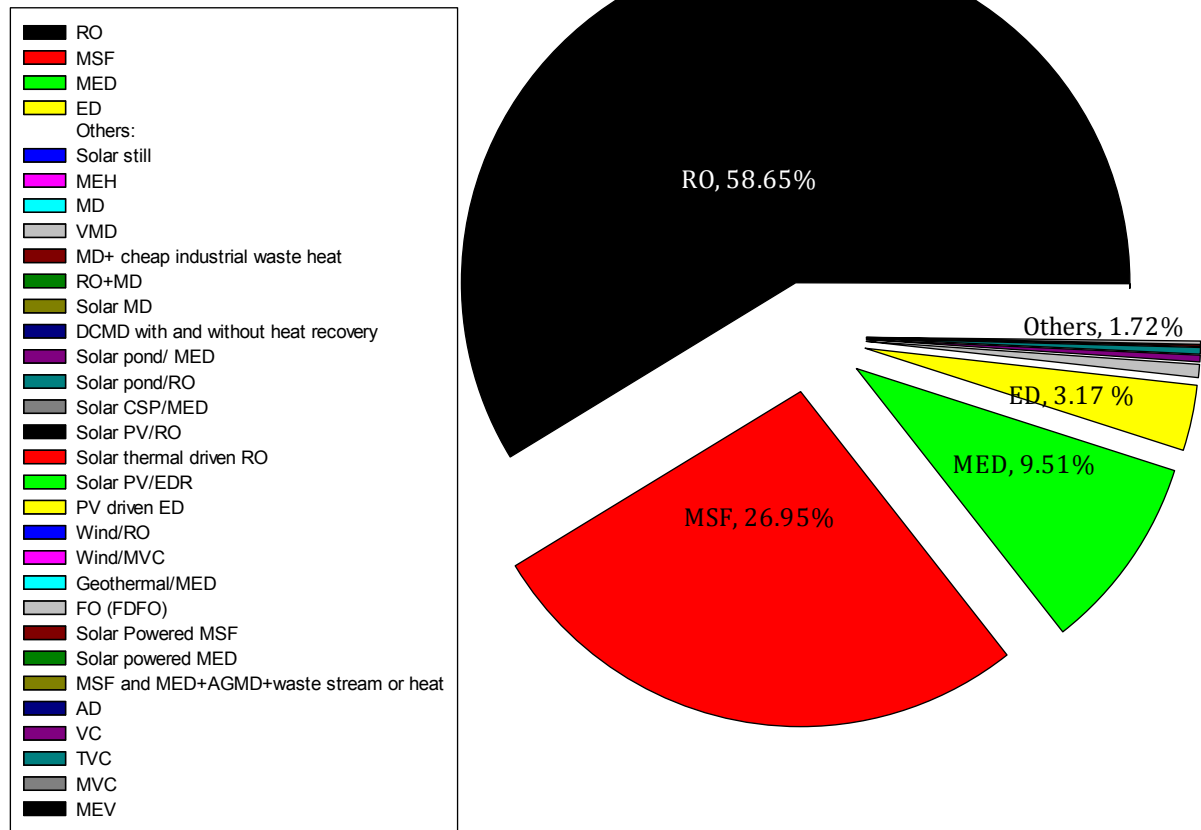
Figure 2-4. Maximum capacity of desalination plants (RO: 37 million m³/day [77], MSF: 17 million m³/day [77] , MED: 6 million m³/day [77] , ED: 2 million m³/day [77], Solar still, 100 m³/day[78], MEH: 100 m³/day [78] , MD: 24000 m³/day [79], VMD: 400,000 m³/day [80] , MD+ cheap industrial waste heat: 48 m³/day [81], RO+MD: 0.065 m³/day [82] , Solar MD: 31 m³/day [83], DCMD with and without heat recovery: 24000 m³/day [79], Solar pond/ MED: 200,000 m³/day [78], Solar pond/RO: 200,000 m³/day [78], Solar CSP/MED: 5000 m³/day [78], Solar PV/RO: 200 m³/day [83], Solar thermal driven RO: 50,000 m³/day [83], Solar PV/EDR: 100 m³/day [78], PV driven ED: 1.14 m³/day [83] , Wind/RO: 2000 m³/day [78], Wind/MVC: 100 m³/day [78], Geothermal/MED: 80 m³/day [78], FO (FDFO): 100,000 m³/day [84], Solar Powered MSF: 5000 m³/day [83], Solar powered MED: 36,112 m³/day [83], MSF and MED +AGMD+ low grade waste stream or heat: 48 m³/day [81], AD: 12.5 m³/day [77], VC: 3000 m³/day [78], TVC: 30,000 m³/day [78], MVC: 3000 m³/day, ME: 6343 m³/day [85]).
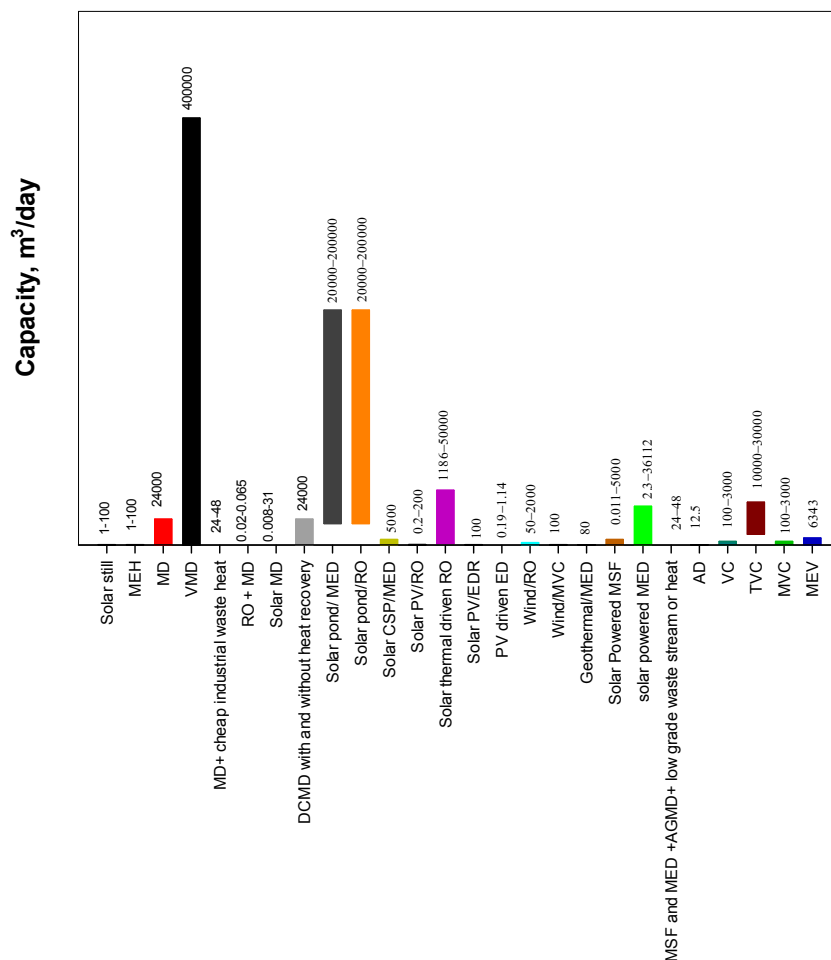
Figure 2-5. Capacities of other technologies (non- major technologies) for desalination/ chloride removal [77-83, 85].

As can be seen, RO has highest OPEX and lowest CAPEX. Nonetheless, MED and MSF have higher CAPEX and lower cost (OPEX). Therefore, selecting of the technology should be based on the preference and considering which one outweigh, the OPEX or CAPEX. Unfortunately, information about ED CAPEX was not found. On the other hand, CAPEX of those technologies (MSF and MED) are higher than RO. CAPEX of RO is 1313, MSF is 1598, MED is 1,860 US $/m³/day (Table 2-7a).

RO Cost could be varied from 0.2-12.99 US$/m³, while other technologies costs are less comparatively. For example, MSF 0.2-1.75, MED 1.36-1.6, ED 0.015-1.05 US $/m³ (Table 2-7b).

Table 2-7. Main technologies used for desalination and their energy consumptions.

technology	Electrical energy needed (kWh/m^3)	thermal energy needed (kWh/m^3)
RO	0.5-10	0
MSF	2.5-5	78.3
MED	2-21.5	63.9
ED	0.7-8	0

(a)

(b)
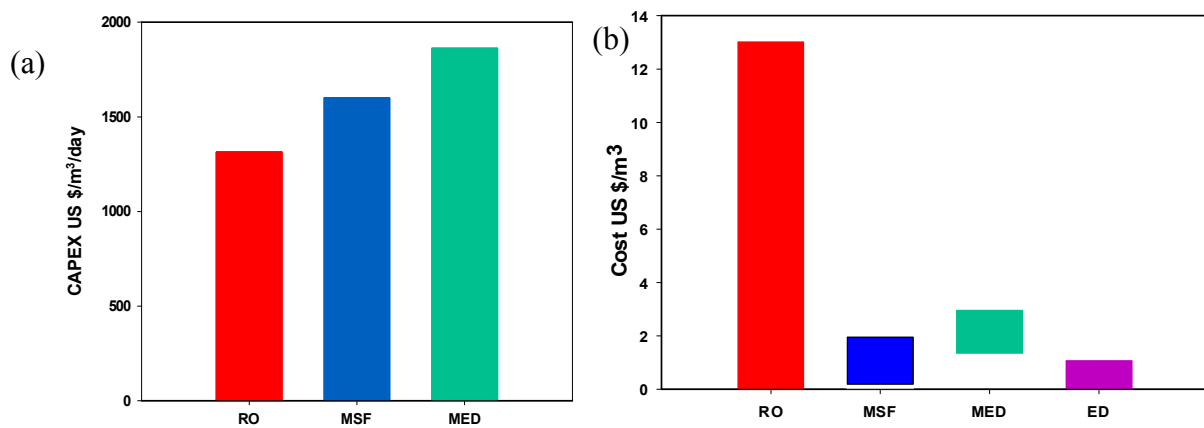
Figure 2-6. Main technologies for desalination (chloride removal); (a) CAPEX and (b) cost (OPEX) (for capacity of 37850 m^3/day) [77-80, 84-93].
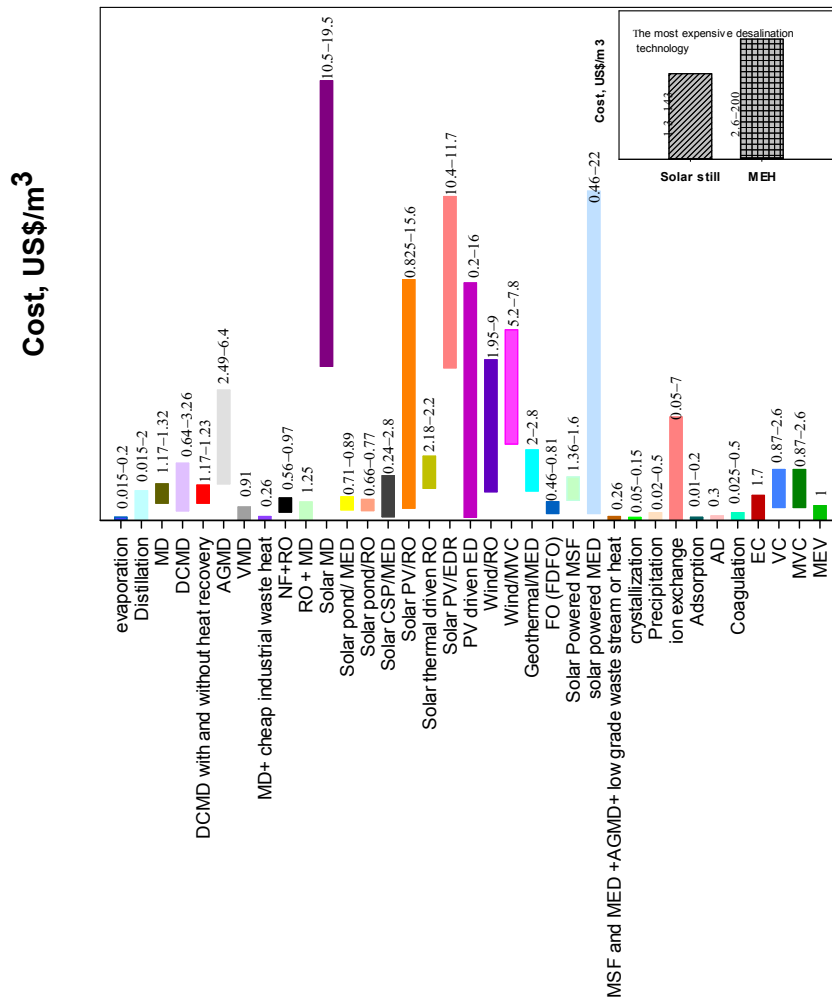
Figure 2-7. Cost of other technologies (non-main technologies) for desalination/chloride removal [77-79, 81, 83-85, 88, 94-98].

Other technologies, which have been specifically being used for chloride removal (selective-technologies) are coagulation and electrocoagulation (UHLA-ultra-high lime aluminium technology), chemical precipitation, ion exchange, adsorption desalination (AD), and adsorption, which their pros and cons are presented in Table 2-8.

Table 2-8. Summary of selective technologies for chloride removal.

Technology		Advantage	Disadvantage	Remarks	reference
Coagulation and electrocoagulation (UHLA)	sludge	Chemical precipitation processes such as (UHLA) can be used on an industrial scale.	In UHLA, chloride removal would be less with the existence of other anions such as silica and sulphate and it is suitable for chloride concentrations higher than 100mM. Finally, aluminium in the feed should be monitored.	UHLA is suitable for [Cl⁻] >100mM.	[42, 74, 75, 99-103]
	Chemical coagulation	compact instrumentation, simplicity, automation and versatility. Chloride removal efficiency with UHLA 84%.	Coagulation alone would not be sufficient and need a calcium salt, too.	Needs Ca:Al: Cl ratio of 10:0:4: 1 (for Freidel's salt). Till now the best way to remove chloride at high concentrations and with the lowest price is chemical precipitation such as (UHLA).	
	Electrocoagulation (EC)	EC produces less sludge over chemical coagulation, has smaller footprints because of no need of adding chemicals.	Same as chemical coagulation, electrocoagulation alone is not efficient enough to remove chloride. However, it can be effective to remove chloride after chemical softening with calcium salts. Aluminium electrodes are costly.	Cathode passivation due to calcium salts precipitation on the cathode is possible, which can be avoided by application of stainless steel.	
Chemical precipitation	Silver nitrate	Can be used in industrial scale	Precipitation with silver nitrate is expensive and mainly is used in hydrometallurgy processes. Silver nitrate is considered		[76]

			suitable for hydrometallurgy processes.		
	Copper slag	Can be used in industrial scale	Copper slag is toxic (due to application of zinc) and is suitable for hydrometallurgy and it needs high acidity and high sulphate. Copper slag is limited for hydrometallurgy processes		[76]
Adsorption		It is a cheap, universal, fast and flexible technology, with low maintenance and is easy to design and operate. The adsorption capacity could be high, depending on the adsorbent type.	Removal of chloride with adsorbents (like C-S-H) in existence of other anions (such as nitrate, carbonate, bromate, sulphate) would be in favour of other anions. Also, this technology depends on the pH and isoelectric of the adsorbent. Chloride leaching after adsorption is possible. The cost of whole process with consideration of continuous dosing adsorbent, due to finite adsorbent capacity, could be high.		[70, 102, 104-110]
Adsorption desalination (AD)		It consumes a small amount of energy. It can also work with a low-temperature heat source or solar heat. It has low maintenance and low evaporative temperature, low fouling and scaling	The data available for this technology is only known at the pilot or demonstration scale. Its economical aspect is questionable if it is not using the heat from cheap sources, such as renewable energies or heat waste. Finally, the robustness of silica gel adsorber beds is not known.		[77, 111]

| Ion exchange | This method is good for the low concentration of chloride. It would be cheap because of lower power consumption and minimal brine production and low capital cost. Therefore, in low and high salinity it is still cheaper, even if we consider the chemicals needed for regeneration of resins. Generally, if salinity is targeted rather than other pollutants to be removed, it is a better option than filtration processes such as RO. It is selective towards chloride. The capacity of the anion resins is 1-1.3 g/L for the strong base anion resins. | Weak base resins need acidic condition for removing chloride. ion exchangers are made out of toxic materials such as 2,4,6-trimethylbenzylamine and styrene, and it is suggested for lower chloride concentration. I^-, NO_3^-, Br^-, ClO_4^-, SO_4^{2-}, HPO_4^{2-}, CO_3^{2-} have preference for sorption more than chloride in SBA, and in WBA OH^- has the most preference for sorption CO_3^{2-}, SO_4^{2-}, OH^-, F^- have more preference for sorption than chloride in LDH and CLDH Regeneration of IX columns are costly. | Regeneration cost of resins could be decreased by the application of core-shell arrangement in the resins. Specifically, shallow shell ion exchange, which are the ones that provide core-shell arrangements have the advantage of regenerating more easily than the normal ones. These resins also reduce the volumes of rinsing and increasing running times. | [42, 70, 97, 102, 112-115] |

(Row above, continued from previous page:) in the evaporators. Finally, it is cheap (low payable cost), if it uses the waste heat of renewable energies.

2.7.2. Iodide

Generally speaking, iodide can be removed via various methods such as ion exchange [60], adsorption [16, 20, 66, 116-134], membrane separation [135, 136], and chemical precipitation [72, 137]. Membrane-assisted technologies, electrochemical and adsorption as the main technologies for removal of iodide and bromide from water, has shown their removal efficacies and costs are presented (Table 2-9).

Iodides (I^-) have been shown to be able co-precipitate with some hydroxides such as Zr, U, Th at pH 4, pH 8 and pH 7. In addition, iodide has shown a high affinity towards $Bi(OH)_3$ [17]. However, U, Th are not good options for iodide removal. Other adsorbents for iodide are iron zero-valent, illite, activated aerogels impregnated with silver ions, Mg-Al LDH/Mg-Al (NO_3) LDH [47] [48]. Alternative technologies for iodine removal are ion exchanges of Amberlite 400 and DOW 21K XLT [50], permeation and chemical desorption (PCD) [46]. Some ion exchanges need iodide oxidation and form iodate and then passing through the resin. It is clear that this process also deals with the oxidating agent which is not very environmentally friendly [46].

2.7.3. Bromide

Membrane desalination and electrochemical methods are not economically viable for bromide removal, because they are energy extensive and the membrane is prone to fouling and scaling. Electrochemical technologies such as electrolysis can oxidize bromide to HBrO, BRO^- and Br_2, which would limit their application in large scale, due to possibility of formation of brominated DBPs [26]. Adsorption is another technology which is being used for bromide removal such as xerogels and hydrogels with a removal efficiency of 9-80%. Nonetheless, xerogels and hydrogels are not effective in the presence of NOM for bromide removal. Because they have more affinity towards the organic than inorganic species [26]. Other adsorbents such as aluminium chloride, LDH, but these adsorbents have limited application due to their efficiency decrease in the presence of other inorganic anions and organic species. Silver integrated to the adsorbent has its own disadvantages of silver leaching to water and is expensive [26].

Table 2-9. Technologies for iodide and bromide removal and their comparison has gotten from [138].

	Technology	I⁻ Removal, %	Br⁻ removal, %	Cost
Membrane assisted	RO	80–92	90–99.8	High
	NF	55–91	93–97	High
	ED/EDR	92–97	72–80	High
Electrochemical	Electrolysis	-	79–99	High
	CDI	69.7–77	50–86.1	High
Adsorption	LDH	14–96	27–94	Low
	Sol-gel double Hydrous oxide	-	9–80	Medium/low
	Coal and Activated carbon	13–46	-	Low
	AgAC			Moderate
	Silver doped Carbon aerogels	1.98–5.03 µmol/g adsorbent	3.01–5.78 µmol/g adsorbent	Medium/high
	MIEX	-	2–83	Medium/high
	Other resins			Medium/high
	Aluminium coagulation	-	34–98	Low
	Soils	11–99	-	Low

2.8. Conclusion

Halide removal is important in providing safe and healthy water to human, living beings. Agriculture and various infrastructure-intensive industries. Chloride would corrode the infrastructure and iodide and bromide would lead to the formation of toxicity-potent DBPs in the water treatment process, and some isotopes of iodide are radioactive with very long half life span. Despite their importance of removal from aquatic solutions, still, a proper removal technology which is cheap with high selectivity towards halides is not found yet. Membrane assisted technologies are being used extensively for halide removal, however, their cost is high, especially for the small-scale applications. Furthermore, the membrane related problems such as fouling and scaling are common problems which should be dealt with. Electrochemical technologies and their hybridization with other technologies would raise a question mark of whether DBPs would form, due to oxidation of halides. Also, chloride oxidation is very dangerous for the workforce and environment.

Adsorption and ion exchange incur lower costs, but their applicability is limited to small scale so far and needs more studies to be done for larger scale. Also, silver-containing adsorbents which are mainly focused on as the adsorbents for halide removal are more expensive compared to the other adsorbents and silver might leach into the water, which would result in decrease the adsorbent efficacy after a while. Overall, there is a need to develop cost-effective methods for halide ions removal in municipal, agriculture and industrial water treatment, which seems to be often overlooked.

References

1.   Burn, S., et al., *Desalination techniques — A review of the opportunities for desalination in agriculture.* Desalination, 2015. **364**(Supplement C): p. 2-16.

2.   Shaffer, D.L., et al., *Seawater desalination for agriculture by integrated forward and reverse osmosis: Improved product water quality for potentially less energy.* J. Membr. Sci., 2012. **415**(Supplement C): p. 1-8.

3.   Martínez-Alvarez, V., B. Martin-Gorriz, and M. Soto-García, *Seawater desalination for crop irrigation — A review of current experiences and revealed key issues.* Desalination, 2016. **381**(Supplement C): p. 58-70.

4.   Tsutsumi, Y., A. Nishikata, and T. Tsuru, *Pitting corrosion mechanism of Type 304 stainless steel under a droplet of chloride solutions.* Corros. Sci., 2007. **49**(3): p. 1394-1407.

5.   Jang, S.-Y., S. Karthick, and S.-J. Kwon, *Investigation on durability performance in early aged high-performance concrete containing GGBFS and FA.* Adv. Mater. Sci. Eng., 2017. **2017**: p. 1-11.

6.   Yodsudjai, W. and W. Saelim, *Influences of electric potential and electrolyte on electrochemical chloride removal in reinforced concrete.* J. Mater. Civ. Eng., 2014. **26**(1): p. 83-89.

7.   Kameda, T., et al., *Removal of chloride from ethylene glycol solution using alumina/zeolite membrane as a physical boundary between the organic and aqueous phases.* J. Mater. Cycles Waste Manage., 2013. **15**(3): p. 404-408.

8. Lito, P.F., J.P.S. Aniceto, and C.M. Silva, *Removal of anionic pollutants from waters and wastewaters and materials perspective for their selective sorption.* Water Air Soil Pollut., 2012. **223**(9): p. 6133-6155.

9. Pfromm, P.H., *Low effluent processing in the pulp and paper industry: electrodialysis for continuous selective chloride removal.* Sep. Sci. Technol., 1997. **32**(18): p. 2913-2926.

10. Şahin, F.Ç., B. Derin, and O. Yücel, *Chloride removal from zinc ash.* Scand. J. Metall., 2000. **29**(5): p. 224-230.

11. Cramer, S.D., et al., *Prevention of Chloride-induced Corrosion Damage to Bridges.* ISIJ Int., 2002. **42**(12): p. 1376-1385.

12. Jiao, L., et al., *Study on Corrosion Performance of Cu-Te-Se Alloys in a 3.5% Sodium Chloride Solution.* J. Mater. Eng. Perform., 2015. **24**(11): p. 4333-4339.

13. Blagojevic, A., S. Fennis, and J.C. Walraven, *Impact of cracks on chloride-induced corrosion and durability of reinforced concrete structures - a literature review.* VTT Technol., 2012. **65**: p. 80-91.

14. Marcos-Meson, V., et al., *Corrosion resistance of steel fibre reinforced concrete - A literature review.* Cem. Concr. Res., 2018. **103**: p. 1-20.

15. Liu, Y., et al., *An investigation into the use of cuprous chloride for the removal of radioactive iodide from aqueous solutions.* J. Hazard. Mater., 2016. **302**: p. 82-89.

16. Rong, J., et al., *High-specific surface area hierarchical Al_2O_3 carbon fiber based on a waste paper fiber template: preparation and adsorption for iodide ions.* J. Wood Chem. Technol., 2017. **37**(6): p. 485-492.

17. Liu, Y. and H.R.v. Guten, *migration chemistry and behaviour of iodine relevant to geological disposal of radioactive wastes-a literature review with a compilation of sorption data*, in *Technischer Bericht 88-29*. 1998. p. 183.

18. Majidnia, Z. and A. Idris, *Photocatalytic reduction of iodine in radioactive waste water using maghemite and titania nanoparticles in PVA-alginate beads.* J. Taiwan Inst. Chem. E., 2015. **54**: p. 137-144.

19. Hu, Q., J.E. Moran, and V. Blackwood, *Geochemical Cycling of Iodine Species in Soils*. 2007: The Comprehensive Handbook on Iodine, Geochemical Cycling of Iodine Species in Soils, Academic Press, New York, NY 2009, pp. 95-107; Lawrence Livermore National Lab. (LLNL), Livermore, CA (United States). Medium: ED; Size: PDF-file: 41 pages; size: 0.2 Mbytes.

20.   Li, D., et al., *Removal capacity and chemical speciation of groundwater iodide (I^-) and iodate (IO_3^-) sequestered by organoclays and granular activated carbon.* J. Environmen. Radioactiv., 2018. **192**: p. 505-512.

21.   LENNTECH. *Iodine and water: reaction mechanisms, environmental impact and health effects*. Available from: https://www.lenntech.com/periodic/water/iodine/iodine-and-water.htm.

22.   Foreman, M.R.S.J., *An introduction to serious nuclear accident chemistry.* Cogent Chem., 2015. **1**(1): p. 1049111.

23.   Northey, S.A., et al., *Water footprinting and mining: Where are the limitations and opportunities?* J. Cleaner Prod., 2016. **135**: p. 1098-1116.

24.   Ateia, M., et al., *Selective removal of bromide and iodide from natural waters using a novel AgCl-SPAC composite at environmentally relevant conditions.* Water Res., 2019. **156**: p. 168-178.

25.   Gruchlik, Y., et al., *Impact of bromide and iodide during drinking water disinfection and potential treatment processes for their removal or mitigation.* Water, 2014. **41**(8): p. 38-43.

26.   Rajaeian, B., *Removal of Bromide from Drinking Water Sources using Silver impregnated activated carbon (SIAC) understanding Br-SIAC interactions*, in *Department of Civil Engineering*. 2017, Curtin University: Curtin University.

27.   Ates, N., U. Yetis, and M. Kitis, *Effects of Bromide Ion and Natural Organic Matter Fractions on the Formation and Speciation of Chlorination By-Products.* J. Environ. Eng., 2007. **133**(10): p. 947-954.

28.   Rapp, H.-J. and P.H. Pfromm, *Electrodialysis for chloride removal in low effluent Kraft pulp production.* Membr. Technol., 1997. **1997**(89): p. 7-11.

29.   Rapp, H.-J. and P.H. Pfromm, *Electrodialysis Field Test for Selective Chloride Removal from the Chemical Recovery Cycle of a Kraft Pulp Mill.* Ind. Eng. Chem. Res., 1998. **37**(12): p. 4761-4767.

30.   Ferreira, L.M.G.A., L. Amaral, and L. Machado, *Removal of Chloride in the Kraft Chemical Recovery Cycle of Pulp Mills Using the Ion-Exchange Process.* Ind. Eng. Chem. Res., 2004. **43**(22): p. 7121-7128.

31.   Lottermoser, B., *Mine Water*, in *Mine Wastes: Characterization, Treatment and Environmental Impacts*. 2003, Springer Berlin Heidelberg: Berlin, Heidelberg. p. 83-141.

32. Ericsson, B. and B. Hallmans, *Treatment of saline wastewater for zero discharge at the Debiensko coal mines in Poland.* Desalination, 1996. **105**(1): p. 115-123.

33. Mercuri, A.M., J.A. Duggin, and C.D. Grant, *The use of saline mine water and municipal wastes to establish plantations on rehabilitated open-cut coal mines, Upper Hunter Valley NSW, Australia.* Forest Ecol. Manag., 2005. **204**(2): p. 195-207.

34. Banks, D., et al., *Mine-water chemistry: the good, the bad and the ugly.* Environ. Geol., 1997. **32**(3): p. 157-174.

35. Silva, T.L.S., et al., *An overview on exploration and environmental impact of unconventional gas sources and treatment options for produced water.* J. Environ. Manage., 2017. **200**: p. 511-529.

36. Jiménez, S., et al., *State of the art of produced water treatment.* Chemosphere, 2018. **192**: p. 186-208.

37. Booth, D.W. and T.L. Anderson, *Method and system for removing NaCl from production water or fracking water produced in an oil well operation, or other wastewater, using CaCl₂.* 2017, Clean Water LLC, USA . p. 14pp.

38. Middleditch, B.S., *Ecological effects of produced water effluents from offshore oil and gas production platforms.* Ocean Manage., 1984. **9**(3): p. 191-316.

39. Adham, S., et al., *Membrane applications and opportunities for water management in the oil & gas industry.* Desalination, 2018. **440**: p. 2-17.

40. Millar, G.J., S.J. Couperthwaite, and S. Papworth, *Ion exchange of sodium chloride and sodium bicarbonate solutions using strong acid cation resins in relation to coal seam water treatment.* J. Water Process. Eng., 2016. **11**: p. 60-67.

41. Vedelago, R. and G.J. Millar, *Process evaluation of treatment options for high alkalinity coal seam gas associated water.* J. Water Process. Eng., 2018. **23**: p. 195-206.

42. Millar, G.J., S.J. Couperthwaite, and C.D. Moodliar, *Strategies for the management and treatment of coal seam gas associated water.* Renewable Sustainable Energy Rev., 2016. **57**: p. 669-691.

43. Rebello, C.A., et al., *Coal seam water quality and the impact upon management strategies.* J. Petrol. Sci. Eng., 2017. **150**: p. 323-333.

44. Ikura, M. and M. Stanciulescu *Process for removing chlorides from crude oil.* 1995, Canada Minister of Energy Mines and Resources

45. Mallants, D., et al., *Review of plausible chemical migration pathways in Australian coal seam gas basins.* Int. J. Coal Geol., 2018. **195**: p. 280-303.

46. Kim, H.I., et al., *A process to recover high purity iodine in wastewater from liquid crystal display (LCD) manufacturing industry.* Hydrometallurgy, 2018. **181**: p. 91-96.

47. Madrakian, T., et al., *Application of Modified Silica Coated Magnetite Nanoparticles for Removal of Iodine from Water Samples.* Nano-Micro Lett., 2012. **4**(1): p. 57-63.

48. Kentjono, L., et al., *Removal of boron and iodine from optoelectronic wastewater using Mg–Al (NO₃) layered double hydroxide.* Desalination, 2010. **262**(1): p. 280-283.

49. Theiss, F.L., G.A. Ayoko, and R.L. Frost, *Iodide removal using LDH technology.* Chem. Eng. J., 2016. **296**: p. 300-309.

50. Fruit, J.T., et al., *Recovery of Iodine from Produced Water Through Anion Resin Exchange*, in *2011 Research Experiences for Undergraduates posters and presentations.* 2011, Advanced Water Technology Center (AQWATEC) Colorado School of Mines, 1500 Illinois street, Golden, CO 80401.

51. Ordóñez, J.I., et al., *Use of discharged brine from reverse osmosis plant in heap leaching: Opportunity for caliche mining industry.* Hydrometallurgy, 2015. **155**: p. 61-68.

52. Okogbue, C.O. and S.N. Ukpai, *Evaluation of trace element contents in groundwater in Abakaliki metropolis and around the abandoned mine sites in the southern part, Southeastern Nigeria.* Environmen. Earth Sci., 2013. **70**(7): p. 3351-3362.

53. WHO, *Bromide in drinking-water. Background document for development of WHO Guidelines for Drinking-water Quality*. 2009.

54. Al-Mutaz, I., *Water desalination in the Arabian Gulf region.* Water Purification, 2000. **2**: p. 245-265.

55. Dorji, P., et al., *Membrane capacitive deionisation as an alternative to the 2nd pass for seawater reverse osmosis desalination plant for bromide removal.* Desalination, 2018. **433**: p. 113-119.

56. UrbanUtilities, Q., *Queensland Urban Utilities SEQ Water Grid Brisbane Drinking Water Quality July 2010-June 2011*. 2011: Queensland UrbanUtilities.

57. José Farré, M., et al., *Assessment of Regulated and Emerging Disinfection By-Products in South East Queensland Drinking Water*. 2012: Urban Water Security Research Alliance.

58. Takeno, N., *Atlas Eh-pH Diagrams Intercomparison of thermodynamic databases Geological Survey of Japan Open File Report No.419*. 2005, National Institute of Advanced Industrial Science and Technology, Research Centerfor Deep Geological Environments: Geological Survey of Japan, AIST. p. 285.

59. Kaiho, T., *Iodine Chemistry and Applications*. Iodine Chemistry and Applications. 2014. 1-636.

60. Decamp, C. and S. Happel, *Utilization of a mixed-bed column for the removal of iodine from radioactive process waste solutions.* J. Radioanal. Nucl. Chem., 2013. **298**(2): p. 763-767.

61. The council of the European Union, *Council Directive 98/83/EC of 3 November 1998 on the quality of water intended for human consumption* OJEC, 1998: p. L 330/32-L 330/54.

62. WHO, *Guidlines for drinking water quality*. 4 ed. 2011, Gutenberg, Switzerland.

63. NHMRC and NRMMC, *Australian Drinking Water Guidelines Paper 6 National Water Quality Management Strategy*. 2011: National Health and Medical Research Council, National Resource Management Ministerial Council, Commonwealth of Australia, Canberra.

64. Kelly, W.R., S.V. Panno, and K. Hackley, *The sources, distribution, and trends of chloride in the waters of Illinois*. 2012, Illinois State Water Survey Prairie Research Institute University of Illinois at Urbana-Champaign: Champaign, Illinois

65. Verbruggen, E.M.J., et al., *Derivation of environmental risk limits for chloride in surface water, groundwater, soil and sediment.* RIVM rapport 711701075, 2008: p. 76.

66. Yu, F., et al., *Enhanced removal of iodide from aqueous solution by ozonation and subsequent adsorption on Ag-Ag$_2$O modified on Carbon Spheres.* Appl. Surf. Sci., 2018. **427**: p. 753-762.

67. Wu, X., Z. Liu, and X. Liu, *Chloride ion removal from Zinc sulfate aqueous solution by electrochemical method.* Hydrometallurgy, 2013. **134–135**: p. 62-65.

68.   Canadian Council of Ministers of the Environment, *Canadian water quality guidelines for the protection of aquatic life*. 2011. p. 1-16.

69.   Mossad, M. and L. Zou, *A study of the capacitive deionisation performance under various operational conditions.* J. Hazard. Mater., 2012. **213–214**: p. 491-497.

70.   Kumar, E., et al., *Interaction of inorganic anions with iron-mineral adsorbents in aqueous media--a review.* Adv. Colloid Interface Sci., 2014. **203**: p. 11-21.

71.   Ying, T.-Y., et al., *Electrosorption of ions from aqueous solutions by nanostructured carbon aerogel.* J. Colloid Interface Sci., 2002. **250**(1): p. 18-27.

72.   A.M.S, P., et al., *Halide removal from aqueous solution by novel silver-polymeric materials.* Sci. Total Environ., 2016. **573**: p. 1125-1131.

73.   Duan, J. and J. Gregory, *Coagulation by hydrolysing metal salts.* Adv. Colloid Interface Sci., 2003. **100–102**: p. 475-502.

74.   Abdel-Wahab, A.I.A., *The ultra-high lime with aluminum process for removing chloride from recirculating cooling water*, in *Civil engineering*. 2003, Texas A&M University.

75.   Abdel-Wahab, A. and B. Batchelor, *Effects of pH, temperature, and water quality on chloride removal with ultra-high lime with aluminum process.* Water Environ. Res., 2006. **78**(9): p. 930-937.

76.   Bodson, F.J.J., *Process for the elimination of chloride from zinc sulphate solutions*. 1977, Jacques, Fernand; Bodson, Joseph USA.

77.   Ng, K.C., et al., *Adsorption desalination: An emerging low-cost thermal desalination method.* Desalination, 2013. **308**: p. 161-179.

78.   Al-Karaghouli, A. and L.L. Kazmerski, *Energy consumption and water production cost of conventional and renewable-energy-powered desalination processes.* Renew. Sust. Energ. Rev., 2013. **24**: p. 343-356.

79.   Al-Obaidani, S., et al., *Potential of membrane distillation in seawater desalination: Thermal efficiency, sensitivity study and cost estimation.* J. Memb. Sci., 2008. **323**(1): p. 85-98.

80.   Morillo, J., et al., *Comparative study of brine management technologies for desalination plants.* Desalination, 2014. **336**: p. 32-49.

81.   Hanemaaijer, J.H., et al., *Memstill membrane distillation - a future desalination technology.* Desalination, 2006. **199**(1-3): p. 175-176.

82. Kubota, S., et al., *Experiments on seawater desalination by membrane distillation.* Desalination, 1988. **69**(1): p. 19-26.

83. Zhang, Y., et al., *Application of solar energy in water treatment processes: A review.* Desalination, 2018. **428**: p. 116-145.

84. Kim, J.E., et al., *Environmental and economic impacts of fertilizer drawn forward osmosis and nanofiltration hybrid system.* Desalination, 2017. **416**: p. 76-85.

85. Zhou, Y. and S.J. Tol Richard, *Evaluating the costs of desalination and water transport.* Water Resour. Res., 2005. **41**(3).

86. Avlonitis, S.A., *Operational water cost and productivity improvements for small-size RO desalination plants.* Desalination, 2002. **142**(3): p. 295-304.

87. Shahzad, M.W., et al., *Multi effect desalination and adsorption desalination (MEDAD): A hybrid desalination method.* Appl. Therm. Eng., 2014. **72**(2): p. 289-297.

88. Gupta, V.K., et al., *Chemical treatment technologies for waste-water recycling—an overview.* RSC Adv., 2012. **2**(16): p. 6380.

89. Sarai Atab, M., A.J. Smallbone, and A.P. Roskilly, *An operational and economic study of a reverse osmosis desalination system for potable water and land irrigation.* Desalination, 2016. **397**: p. 174-184.

90. Malaeb, L. and G.M. Ayoub, *Reverse osmosis technology for water treatment: State of the art review.* Desalination, 2011. **267**(1): p. 1-8.

91. Glater, J. and Y. Cohen *Brine disposal from land based membrane desalination plants: a critical assessment.* 2003.

92. Fritzmann, C., et al., *State-of-the-art of reverse osmosis desalination.* Desalination, 2007. **216**(1): p. 1-76.

93. Kesieme, U.K., et al., *Economic analysis of desalination technologies in the context of carbon pricing, and opportunities for membrane distillation.* Desalination, 2013. **323**: p. 66-74.

94. González, D., J. Amigo, and F. Suárez, *Membrane distillation: Perspectives for sustainable and improved desalination.* Renewable Sustainable Energy Rev., 2017. **80**: p. 238-259.

95. Macedonio, F., E. Curcio, and E. Drioli, *Integrated membrane systems for seawater desalination: energetic and exergetic analysis, economic evaluation, experimental study.* Desalination, 2007. **203**(1-3): p. 260-276.

96.   Moussa, D.T., et al., *A comprehensive review of electrocoagulation for water treatment: Potentials and challenges.* J. Environ. Manage., 2017. **186**: p. 24-41.

97.   Strathmann, H., *Electrodialytic membrane processes and their practical application.* Stud. Environ. Sci., 1994. **59**: p. 495-533.

98.   Ali, I. and V.K. Gupta, *Advances in water treatment by adsorption technology.* Nat. Protoc., 2007. **1**: p. 2661.

99.   Abdel-Wahab;, A. and B. Batchelor, *Chloride removal from recycled cooling water using ultra-high lime with aluminum process.* Water Environ. Res., 2002. **74**(3): p. 256-263.

100.   Wang, L.P., et al., *Removal of Chloride Ions from an Aqueous Solution Containing a High Chloride Concentration through the Chemical Precipitation of Friedel's Salt.* Mater. Trans., 2018. **59**(2): p. 297-302.

101.   Fang, P., et al., *Chloride Ion Removal from the Wet Flue Gas Desulfurization and Denitrification Wastewater Using Friedel's Salt Precipitation Method.* J. Chem-Ny, 2018. **2018**: p. 9.

102.   Semblante, G.U., et al., *Brine pre-treatment technologies for zero liquid discharge systems.* Desalination, 2018. **441**: p. 96-111.

103.   Subramani, A., et al., *Impact of intermediate concentrate softening on feed water recovery of reverse osmosis process during treatment of mining contaminated groundwater.* Sep. Purif. Technol., 2012. **88**: p. 138-145.

104.   Hirao, H., et al., *Chloride binding of cement estimated by binding isotherms of hydrates.* J. Adv. Concr. Technol., 2005. **3**(1): p. 77-84.

105.   Al-Rawajfeh, A., et al., *Pre-treatment of desalination feed seawater by Jordanian Tripoli, Pozzolana, and Feldspar: batch experiments.* Chem. Ind. Chem. Eng. Q., 2011. **17**(2): p. 163-171.

106.   Frau, F., et al., *Influence of major anions on As(V) adsorption by synthetic 2-line ferrihydrite. kinetic investigation and XPS study of the competitive effect of bicarbonate.* Water Air Soil Pollut., 2010. **205**(1): p. 25-41.

107.   Sumner, M.E. and N.G. Reeve, *The effect of iron oxide impurities on the positive and negative adsorption of chloride by kaolinites* J. Soil Sci., 1966. **17**(2): p. 274-279.

108.   Elakneswaran, Y., T. Nawa, and K. Kurumisawa, *Electrokinetic potential of hydrated cement in relation to adsorption of chlorides.* Cem. Concr. Res., 2009. **39**(4): p. 340-344.

109.   Mohapatra, M., et al., *Facile synthesis of additive-assisted nano goethite powder and its application for fluoride remediation.* J. Nanopart. Res., 2010. **12**(2): p. 681-686.

110.   Acelas, N.Y. and E. Flórez, *Chloride adsorption on Fe- and Al-(hydr)oxide: estimation of Gibbs free energies.* Adsorption, 2018. **24**(3): p. 243-248.

111.   Subramani, A. and J.G. Jacangelo, *Emerging desalination technologies for water treatment: a critical review.* Water Res., 2015. **75**: p. 164-87.

112.   Wang, Z., et al., *Effect of surface oxygen/nitrogen groups on hydrogen chloride removal using modified viscose-based activated carbon fibers.* RSC Adv., 2015. **5**(105): p. 86006-86012.

113.   Gärtner, R.S. and G.J. Witkamp, *Regeneration of mixed solvent by ion exchange resin: selective removal of chloride and sulfate.* Sep. Sci. Technol., 2005. **40**(12): p. 2391-2410.

114.   Yun, G., *Colour and chloride removal from pulp mill effluent using ion-exchange*, in *Civil and Environmental Engineering*. 2001, University of Alberta (Canada): Edmonton, Alberta. p. 100.

115.   Kameda, T., et al., *The simultaneous removal of calcium and chloride ions from calcium chloride solution using magnesium–aluminum oxide.* Water Res., 2003. **37**(16): p. 4045-4050.

116.   Ma, X.-X. and Z.-S. Li, *The effect of oxygen molecule adsorption on lead iodide perovskite surface by first-principles calculation.* Appl. Surf. Sci., 2018. **428**: p. 140-147.

117.   Zhang, A., et al., *Adsorption of iodide and iodate on colloidal silver surface.* Appl. Surf. Sci., 2008. **255**(5): p. 3184-3187.

118.   Kubota, T., et al., *Removal of radioactive cesium, strontium, and iodine from natural waters using bentonite, zeolite, and activated carbon.* J. Radioanal. Nucl. Chem., 2013. **296**(2): p. 981-984.

119.   Osmanlioglu, A.E., *Treatment of radioactive liquid waste by sorption on natural zeolite in Turkey.* J. Hazard. Mater., 2006. **137**(1): p. 332-335.

120.   Zhao, X., et al., *Enhanced removal of iodide from water induced by a metal-incorporated porous metal–organic framework.* Appl. Surf. Sci., 2015. **351**: p. 760-764.

121. Liu, S., et al., *Efficient removal of radioactive iodide ions from water by three-dimensional Ag$_2$O–Ag/TiO$_2$ composites under visible light irradiation.* J. Hazard. Mater., 2015. **284**: p. 171-181.

122. Choung, S., et al., *Effects of radiation and temperature on iodide sorption by surfactant-modified bentonite.* Environ. Sci. Technol., 2014. **48**(16): p. 9684-91.

123. Warchoł, J., et al., *Preparation and application of organo-modified zeolitic material in the removal of chromates and iodides.* J. Hazard. Mater., 2006. **137**(3): p. 1410-1416.

124. Choung, S., et al., *Uptake Mechanism for Iodine Species to Black Carbon.* Environ. Sci. Technol., 2013. **47**: p. 10349–10355.

125. Zhang, C., et al., *Adsorption of anionic surfactants from aqueous solution by high content of primary amino crosslinked chitosan microspheres.* Int. J. Biol. Macromol., 2017. **97**: p. 635-641.

126. Mao, P., et al., *Enhanced uptake of iodide on Ag@Cu$_2$O nanoparticles.* Chemosphere, 2016. **164**: p. 396-403.

127. Faghihian, H., M. Ghannadi Maragheh, and A. Malekpour, *Adsorption of radioactive iodide by natural zeolites.* J. Radioanal. Nucl. Ch., 2002. **254**(3): p. 545-550.

128. Ikeda, Y., et al., *Adsorption of I$^-$ Ions on Cinnabar for ^{129}I Waste Management.* Radiochim. Acta, 1994. **65**(3): p. 195-198.

129. Theiss, F.L., G.A. Ayoko, and R.L. Frost, *Leaching of iodide (I$^-$) and iodate (IO$_3^-$) anions from synthetic layered double hydroxide materials.* J. Colloid Interface Sci., 2016. **478**: p. 311-5.

130. Bors, J., S. Dultz, and A. Gorny, *Sorption of Iodide, Cesium and Strontium on Organophilic Bentonite.* Radiochim. Acta, 1998. **82**(1): p. 269-274.

131. Zhang, H., et al., *Adsorption of iodide ions on a calcium alginate–silver chloride composite adsorbent.* Colloids Surf. A Physicochem. Eng. Asp., 2011. **386**(1-3): p. 166-171.

132. Hoskins, J.S., T. Karanfil, and S.M. Serkiz, *Removal and Sequestration of Iodide Using Silver-Impregnated Activated Carbon.* Environ. Sci. Technol., 2002. **36**(4): p. 784-789.

133. Sadasivam, S. and S.M. Rao, *Characterization of silver–kaolinite (AgK): an adsorbent for long-lived 129I species.* SpringerPlus, 2016. **5**(1): p. 142.

134. Sánchez-Polo, M., et al., *Removal of bromide and iodide anions from drinking water by silver-activated carbon aerogels.* J. Colloid Interface Sci., 2006. **300**(1): p. 437-441.

135. Ensafi, A.A. and H. Eskandari, *Efficient and selective extraction of iodide through a liquid membrane.* Microchem. J., 2001. **69**(1): p. 45-50.

136. Liu, Y., et al., *Removal of radioactive iodide from simulated liquid waste in an integrated precipitation reactor and membrane separator (PR-MS) system.* Sep. Purif. Technol., 2016. **171**: p. 221-228.

137. Mao, P., et al., *Synthesis of Cu/Cu$_2$O hydrides for enhanced removal of iodide from water.* J. Hazard. Mater., 2017. **328**: p. 21-28.

138. Watson, K., M.J. Farré, and N. Knight, *Strategies for the removal of halides from drinking water sources, and their applicability in disinfection by-product minimisation: A critical review.* J. Environ. Manage., 2012. **110**: p. 276-298.

3. Synthesis, characterization and mechanism of a novel bismuth hydroxide sulphate adsorption material for halide removal at high concentrations

Inventors: Elham Nariyan[1,2], Qin Li[1,2] and Jimmy Yu[1]

[1.] *School of Engineering and Built Environment, Griffith University, Nathan, QLD 4111, Australia*
[2.] *Queensland Micro- and Nanotechnology Centre, Griffith University, Nathan, QLD 4111, Australia*

Corresponding author: qin.li@griffith.edu.au

3.1. Abstract

High concentrations of halides in water have negative effects on fresh water living organisms and industries such as mining. In this paper, a new material of bismuth hydroxide sulphate was synthesised and characterised for halide removal at high concentrations. The material has high halide adsorption capacities and fast removal kinetics (within 20 min). The removal capacities were not significantly affected by solution pH (except Cl at alkaline conditions) and other anions present in water. Effects of various parameters such as dosage of bismuth hydroxide sulphate, initial halide concentration, pH, and effect of other anions on the halides' removal efficiencies were investigated. With increasing halide initial concentration, the removal efficiency decreased, more significantly for chloride than iodide and bromide. Bismuth hydroxide sulphate was characterized by XRD, XPS, BET, FTIR, and SEM. This material showed the same XRD peaks as $Bi(OH)SO_4.H_2O$ (mineral Riomarinate), while after adsorption with 3000 mg/L of halides (Cl, I, Br) XRD pattern changed to $BiOX$ (X=Cl, I, Br) SEM images showed changes morphology after halide adsorption. The adsorption capacities for chloride, iodide and bromide are 81, 148, 148 mg/g, respectively, at 1500 mg/L initial concentration.

3.2. Introduction

High concentrations of halide ions including Cl^-, Br^- and I^- in water and wastewater can have major environmental issues such as breaking the eco-equilibrium, DBP formation, radioactive presence (in case of iodide). Halide removal is challenging because of their high mobility and solubility, and the removal selectivity is significant lower compared to other anions removals. So far various technologies have been used for halide removal which are not that effective and selective, yet expensive, such as reverse osmosis.

High chloride level is a major problem for many industries such as hydrometallurgy and mining industries because it is corrosive [1, 2]. Also, chloride has negative effects on living organisms and could endanger their health if the conductivity is beyond 3000 µS [3-5]. Mining water could contain a few thousands mg/L of chloride. For example, the chloride concentration in Hunter Valley's open-pit is in the range of 3,100-6,580 mg/L of chloride, and that in the mining drainage at Kent Coalfield (UK) reached to 5,000 mg/L [6]. In oil and gas industries the chloride concentration could be high as 40,000 mg/L, known as produced water [7]. Some of the remediations they used was rehabilitation of the salinity from land was via some plants, membrane assisted technologies [6, 7]. But these technologies have their own pros and cons. In addition, there are other anthropogenic factors that would lead to the release of chloride into waterways such as chlorination of kraft pulping process (1-10% wt. chloride) [8] and de-icing of roads [4].

Iodide concentrations in LCD industries can reach very high levels of 10200 mg/L [9-11]. Other sources of iodide released into environment are nuclear power plants and nuclear medications, oil and gas and mining industries [12-14]. For example, high radioactive iodide release into the environment was a major problem in Fukushima and Chernobyl disaster [12, 15]. Iodide in water is a precursor for the formation of potent hazardous disinfectant by-products (DBPs) [16]. Hence, removing iodide before oxidation process in water treatment is a better option to avoid iodine-contained DBPs formation. USA drinking water standard has set to 4-18 µg/L for iodine [17], while Australian standard is 0.5 mg/L for iodide [18].

Bromide normally is not found at high concentrations, but there are several exceptions. Anthropogenic activities can enter excessive bromide into water such as agricultural activities, industrial discharges, oil and gas industries, mining (especially coal mining) and coal-fired power plants effluents, roadway de-icing materials [19, 20]. Treated

produced water from oil and gas industry released into water can increase bromide concentrations, such as the case of Allegheny and Monongahela rivers in Western Pennsylvania [20]. Another example is the Dead Sea which has a very high concentration of bromide of 5.2 g/L as a result of intrusion of high bromine groundwater and surface water into the Dead sea [21]. Like iodide, bromide can produce highly toxic DBPs, therefore, it is important to maintain its concentration within the safe range [22, 23]. Although currently there is no regulation or guidelines for bromide concentration or discharge in water, it is highly likely to be set in future in many countries. For example, EPA has intended to set regulations for bromide level in steam electric power generating point source category in 2015 [19].

Various methods are used in industrial-scale for removal of chloride such as reverse osmosis [24], membrane distillation [25], nanofiltration [26], ultra-high lime aluminium (UHLA) [27, 28], adsorption [29] and ion exchange [30-32]. Watson et.al [33] has reviewed the technologies for bromide and iodide removal with their pros and cons. Specifically, bromide and iodide also can be removed via membrane technologies (Reverse Osmosis, Nano Filtration, Electrodialysis, and electrodialysis reversal), electrochemical technologies (electrolysis, capacitive deionization, membrane capacitive deionization), adsorption (such as LDH and silver impregnated carbon), ion exchange resins (MIEX) [33].

Ion exchange is a relatively cost-effective technology for halide removal [34]. Ion exchangers are categorized into different groups of organic and inorganic exchangers. Organic ion exchangers are made from organic materials and hard to synthesize, which is a disadvantage [35]. Recently, inorganic groups of ion exchanger are introduced as layered double hydroxides and calcined double hydroxides [36]. Nonetheless, all of the ion exchanges have the disadvantage of low selectivity for halides over other anions such as sulphate and bicarbonate [37, 38].

Bismuth is an abundant element and it is considered nontoxic [39, 40], cheap and with excellent stability [41], with various excellent electrical and optical properties [42]. Therefore, bismuth materials have wide applications such as pharmaceutical, luminance, catalysis [41], and organic degradation [42]. Bismuth oxide phases have tetrahedral crystalline structures that can combine with various anions such as sulphate [43]. Bismuth oxide combination with sulphate could be used as a conductor [43]. Because

bismuth can have flexible coordination numbers from 3 to 10, therefore, it can produce unusual network topologies [41]. For example, if the ratio of bismuth to sulphate is 0.33:1-7:1, the structure could be related to fluorite [43]. Bismuth hydroxide was used as an ion exchanger for various anion removals such as nitrate and fluoride, but not chloride, iodide and bromide [44-47].

In this study, we synthesized a novel bismuth adsorption material and characterized it with FTIR, BET, XRD, XPS, and SEM. The material was tested for halide removal (Cl^-, Br^-, I^-) at high concentrations (1500-4000 mg/L). Furthermore, the capability of this material for halide removals at various conditions (pH, concentrations and other anions presence) were tested. Kinetics and isotherms of halide removal were also obtained. To our knowledge, there has been no study reported on bismuth hydroxide sulphate as an ion exchange for halide (Cl, I, Br) removal.

3.3. Material and methods

3.3.1. Sample preparation

All chemicals were of analytical grade. Bismuth oxide (Bi_2O_3 with 99% purity) was purchased from Alfa Aesar and other chemicals (sodium hydroxide pellets, sodium chloride, sodium iodide, sodium bromide, acid sulphuric 98%, sodium carbonate, sodium nitrate, potassium sulphate) were purchased from Chem-Supply Australia. Glassware and plasticware were cleaned before each usage. pH of solutions was adjusted by adding 0.1 normality (N) NaOH and 0.1N H_2SO_4.

Bismuth hydroxide sulphate was synthesized by chemical precipitation. 7 g of Bi_2O_3 and 70 g/L of sulphuric acid were mixed at 60 °C for an hour to produce a precipitation of bismuth hydroxide sulphate. The precipitates were filtered, washed and dried at 80 °C for 12 hours.

3.3.2. Halide removal experiments

Halide solutions were made from sodium halide (sodium chloride, sodium iodide, and sodium bromide). Halide solutions (20 mL) were put in the beakers and were constantly agitated with a stirrer and magnet (500 rpm). The concentration of the halide was monitored and recorded continuously at every 1 min intervals by halide ion-selective electrodes, and experiments were carried out within 20 min.

For the dosage optimization, halide solutions with an initial concentration of 1500 mg/L and various dosage of bismuth hydroxide sulphate (5, 10, 15 g/L) were added to the adsorption beakers. Then, in the following experiments the optimal dosage was used. The released sulphate concentration after reaction were measured by gravimetric method. The removal efficiency and adsorption capacity, q_e (mg/g) of bismuth hydroxide sulphate, were calculated by Equation 3-1 and Equation 3-2, respectively, where C_i and C_e are the initial and equilibrium concentrations of halide (mg/L) and m is the mass of bismuth hydroxide sulphate which was added to each experiment [46]. Isotherm and kinetic fittings and calculations were done by Sigmaplot version 12.0.

$$Halide\ removal, \% = \left(\frac{C_i - C_e}{C_i}\right) \times 100\% \qquad \text{Equation 3-1}$$

$$q_e = \frac{(C_i - C_e) \times V}{m} \qquad \text{Equation 3-2}$$

3.3.3. Methods of chemical analysis and characterization

All pH values were measured by using a pH electrode (TPS) and the electrode was connected to the smartCHEM-Ion3 and was calibrated. Chloride was measured by a chloride ion-selective electrode (CL-BTA, Vernier), iodide and bromide were measured by iodide and bromide ion-selective electrodes (TPS) and were connected to the smartCHEM-Ion3. The ion-selective electrodes were calibrated each time.

The surface chemistry of bismuth sulphate hydroxide was characterized with a Kratos Axis ULTRA Xray Photoelectron Spectrometer incorporating a 165 mm hemispherical electron energy analyzer. The XPS was equipped with a monochromated Al-Kα (1486.6 eV). X-ray source operated at 150 W (15 kV, 10 mA) with a base pressure 1.0×10^{-9} torr and pressure during analysis of 1.0×10^{-8} torr, to detect the element compositions. Atomic concentrations were calculated using the CasaXPS version 2.3.14 software and a Shirley baseline with Kratos library Relative Sensitivity Factors (RSFs). Peak fitting of the high-resolution data was also carried out using the CasaXPS software. A Fourier transform infrared spectroscopy (Perkin Elmer 'Spectrum Two FT-IR Spectrometer' with an ATR accessory) was used for characterization of samples. The vacuum-dried samples were

pressed into a pellet. The structural properties of samples were evaluated through X-ray diffraction (Powder X-ray diffractometer, X'pert Pro) with Cu-Kα radiation, 40 kV anodic voltage and a 50 mA current. A scanning electron microscope (SEM, JEOL 7001) operated at 15 kV, was employed to examine the morphologies of samples. The samples for SEM observation were prepared by coating onto a silicon wafer. The nitrogen adsorption and desorption isotherms were measured at the liquid nitrogen temperature (77 K) using a TriStar II 3020 automated surface area analyzer.

3.4. Results and discussion

3.4.1. Characteristics and analysis of bismuth hydroxide sulphate

The FTIR spectrum of the bismuth hydroxide sulphate is presented in Figure *3-1*a. Some of the FTIR peaks were related to SO_4/HSO_4^- in the material. Specifically, bismuth hydroxide sulphate has absorption bands at 1166.67, 1095.26, 998.78, 961.62, 633.37, 622.1 and 582.18 cm^{-1} , which are related to S=O (outer bound-symmetric), S=O, S=O (inner sphere sulphate bound), S=O (inner sphere sulphate bound), SO_4^{2-} or HSO_4^-, SO_4^{2-} or HSO_4^-, O-S-O symmetric vibrations, respectively [48-51]. Hydroxide has two peaks in the FTIR at 3276.03 and 1607.27 cm^{-1}, which are related to the OH stretch (H-bond) and OH flexural [39, 48, 52, 53]. A Bi-O bond, with a A2u-type vibrations at 518.32 cm^{-1} was found in the material [39, 45, 53].

Bismuth sulphate hydroxide XRD has been shown Figure 3-12S and its XRD pattern is in agreement with XRD pattern with Riomarinaitre with chemical formula $Bi(SO_4)(OH) \cdot H_2O$, JCPDS-ICDD file 01-076-1103 (Figure 3-12S) [54-56]. Riomarinaite has the cell parameter of a = 6.0118 □, b = 13.3355 □, c = 6.4854 □, and β = 112.906° [57, 58]. Also, the XRD depicts the structure is $Bi(SO_4)OH.H_2O$, with inclination towards (-121) due to the highest peak is at 2theta of 21 degrees.

(a)

Absorbance (a.u)

S=O

HSO$_4^-$/SO$_4^{2-}$

Bi-O

O-S-O

OH

OH

Wavenumber (cm^{-1})

Survey/1

(b)

Name	Pos.	At%
O 1s-BiO	530.18	2.30
O 1s-OH	531.90	41.70
C 1s	284.80	12.13
S 2s	233.03	8.95
S 2p- Sulphate	169.15	8.51
Bi 4f 7/2-Bi2(SO4)3.H2O	160.22	13.70
Bi 4f 5/2	165.53	12.72

CPS

Bi 2p

C 1s

Binding Energy (eV)

O 1s/2

(c)

x 10^3

CPS

O 1s

O 1s-BiO

Binding Energy (eV)

C 1s/3

(d)

x 10^2

CPS

C 1s

Binding Energy (eV)

S 2s/4

(e)

x 10^2

CPS

S 2s

Binding Energy (eV)

54

(f)
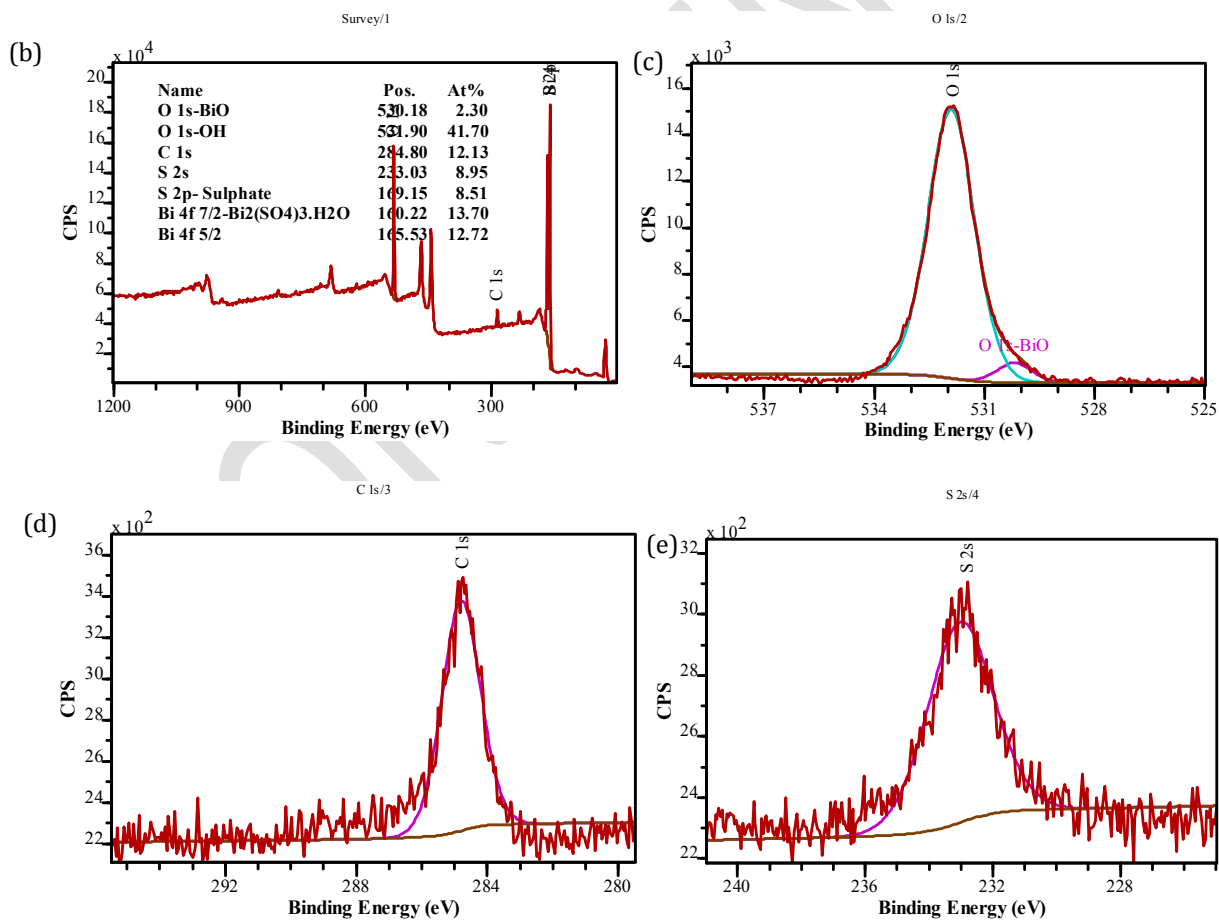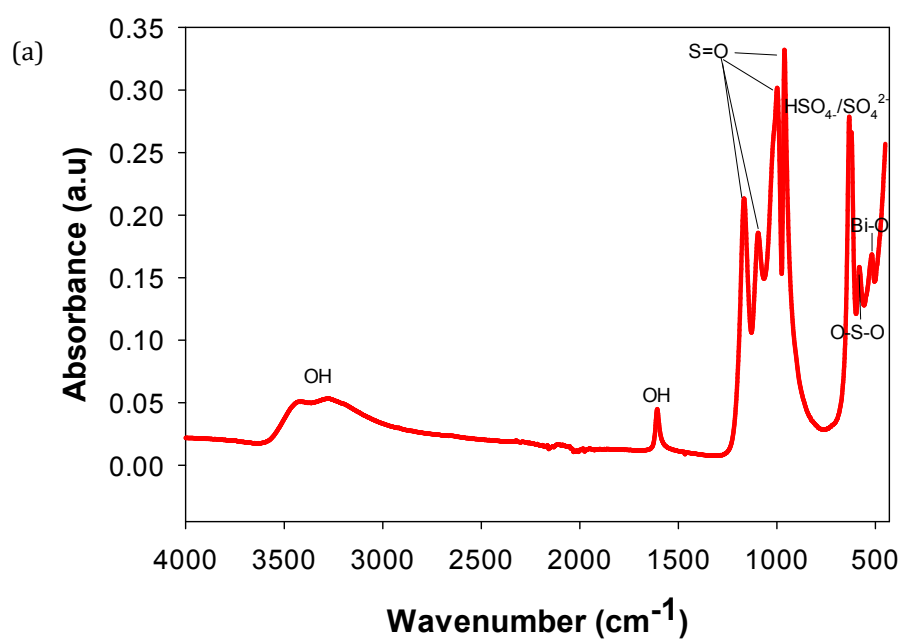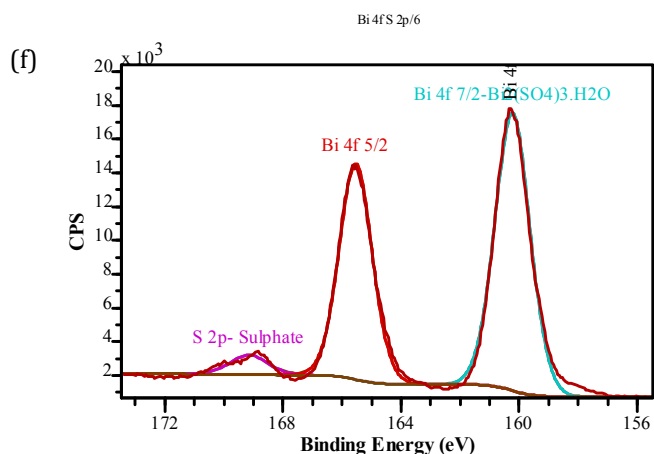
Figure 3-1. Characterization of synthesised material: (a) FTIR of bismuth hydroxide sulphate, and (b-f) Survey XPS patterns of bismuth hydroxide sulphate (b) whole spectrum, (c) O 1s, (d) C 1s, (e) S 2s (f) Bi 4f, and S2p.

The specific surface area and porosity of bismuth hydroxide sulphate were investigated by employing nitrogen adsorption and desorption isotherms. It illustrates the nitrogen adsorption and desorption isotherms and distribution of pore diameter for bismuth hydroxide sulphate. BET surface area and cumulative pore volume were obtained 3.67 m^2/g and 0.0136cm^3/g for bismuth hydroxide sulphate at 77 K, respectively (Figure 3-13S).

X-ray photoelectron spectroscopy (XPS) has been used for chemical analysis and mapping binding energies (Figure *3-1*) [39]. The peak positions of different atoms were determined by internally referencing the carbon at a binding energy of 284.8 eV. As shown in the high-resolution XPS spectrum in Figure *3-1*d, the C1s peak located at a binding energy of 284.8 eV is attributed to the signal from contaminant carbon. Peaks located at 530.18 eV and 531.90 eV in O1s region, are attributed to Bi-O and OH, respectively. 169.15 eV is attributed to sulphate in S2p region. Finally, 160.22 eV and 165.53 eV are related to the $Bi_2(SO_4)_3.H_2O$ in the regions of Bi 4f7/2 and Bi 4f5/2, respectively (Δ= 5.31 eV) [59].

Morphology of bismuth hydroxide sulphate before and after adsorption with halides was investigated by SEM and shown in Figure 3-2. The images show that the morphology is rod, and the size is in the μm and morphology would after reaction with halides the morphology is still rod form consisting of small plates (Figure 3-2).
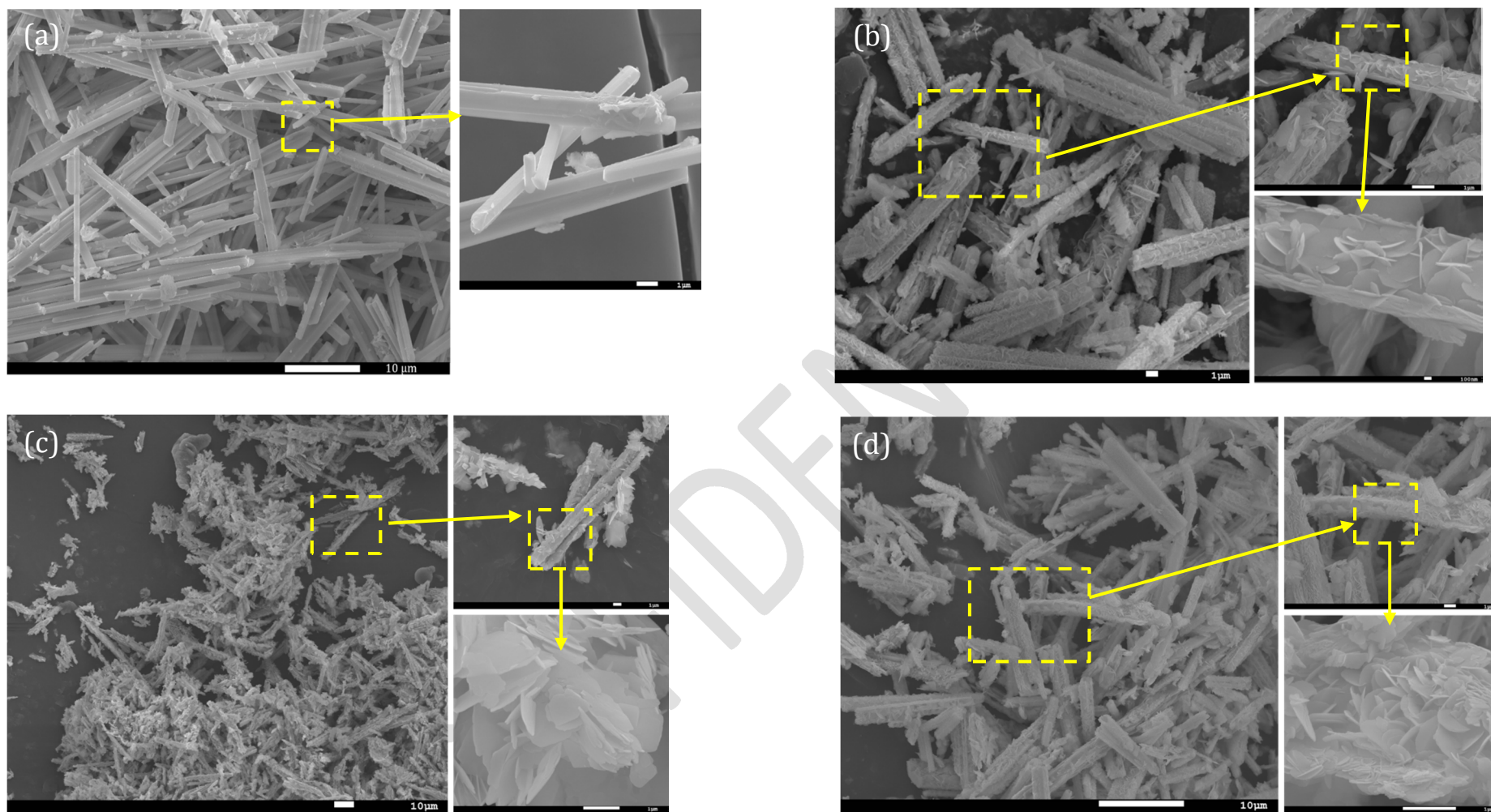
Figure 3-2. SEM images of (a) bismuth hydroxyl sulphate; (b, c, and d) bismuth hydroxide sulphate before, and after adsorption with halide with (chloride, iodide, and bromide) different magnifications, respectively.

3.4.2. Performance of bismuth hydroxide sulphate for halide removal

3.4.2.1.Optimization of bismuth hydroxide sulphate dosage for halide removal

Based on the adsorption capacity q_e and removal efficiency calculations, it was concluded that the optimal dosages of bismuth sulphate hydroxide for chloride, iodide, and bromide are 15 g/L, 10 g/L, and 10 g/L, respectively. Iodide and bromide have higher removal efficiencies and q_e compared to those for chloride. The maximum removal efficiencies for chloride, iodide, and bromide at their optimal dosages approached to 80.88%, 98.79%, and 98.89% after 20 min, respectively (Figure *3-3*a). In addition, the q_e of chloride, iodide, and bromide at the optimal dosage were 80.88 mg/g, 148.20 mg/g, and 148.33 mg/g, respectively (Figure *3-3*b).
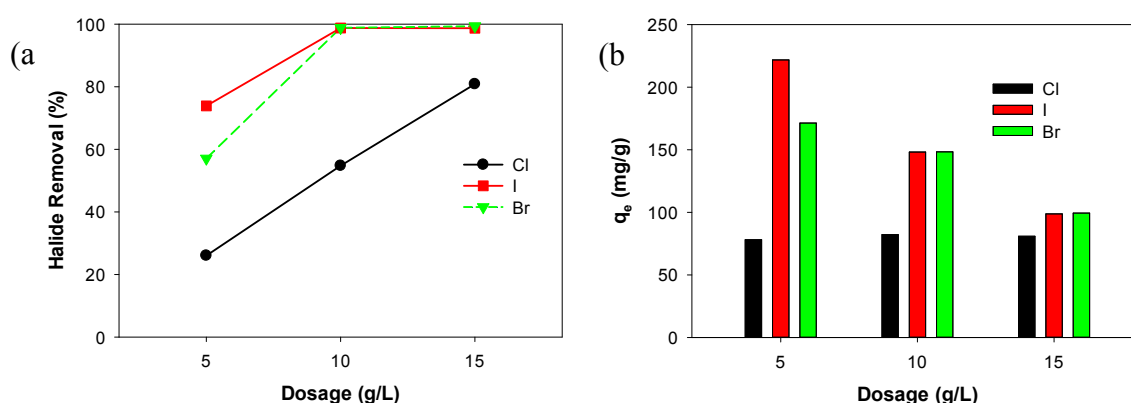
Figure 3-3. Effect of various bismuth hydroxide sulphate dosages on (a) halide removal and (b) maximum adsorption capacity.

3.4.2.2.Effect of pH on halide removal

For evaluating the effect of pH on the halides' adsorption capacity with bismuth hydroxide sulphate, the initial pH of solution was set to 2-12. It was observed that chloride would have a lower adsorption capacity at pH≥8, while the pH variations would not have any effect on the adsorption capacities of iodide and bromide. The q_e of chloride decreased from 81 to 24.28 mg/g when the pH increased from 2 to 12 (Figure *3-4*). At higher pH values, OH$^-$ would be in competition with halide to be attached to the bismuth material. However, iodide and bromide have stronger affinity than that for chloride and

would not be affected by increasing OH$^-$ concentration in the solution. This is because iodide and bromide have bigger size than chloride and hydroxide, therefore, would be attached to the bismuth hydroxide sulphate stronger.
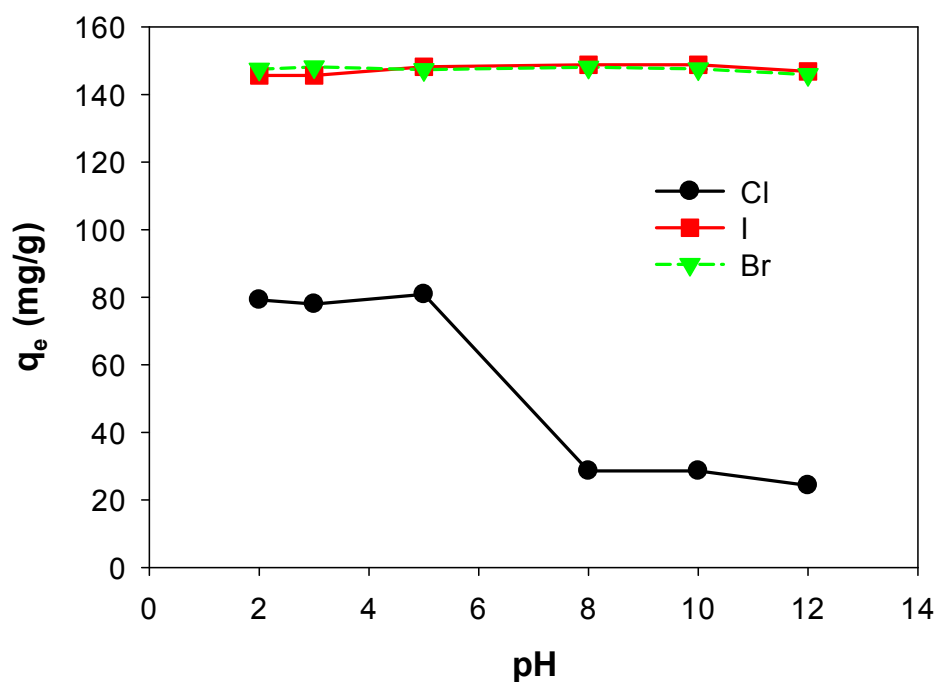
Figure 3-4. The effect of solution pH on the halide adsorption capacity at optimal dosage of bismuth hydroxide sulphate (chloride: 15 g/L, iodide and bromide: 10 g/L).

3.4.2.3. Effect of initial halide concentration

For investigating the effect of halide concentration on the adsorption capacity, various concentrations (1500-4000 mg/L) of halides (Cl$^-$, I$^-$, Br$^-$) were tested. It was observed that increasing initial concentrations would have different effects in halides removal. With increasing chloride concentration, the removal would be decreased more considerably than iodide and bromide and q$_e$ with increasing initial concentration has been increased, more considerably for iodide and bromide than chloride (Figure *3-5*). On the other hand, with converting the concentrations from mg/L to mol/L, it observed that although iodide would be least influenced by increasing initial concentration, it has the least mol/L. For example, 4000 mg/L of chloride equivalent to 0.11 mol/L, while this would be 0.03 and 0.05 mol/L for iodide and bromide, respectively.
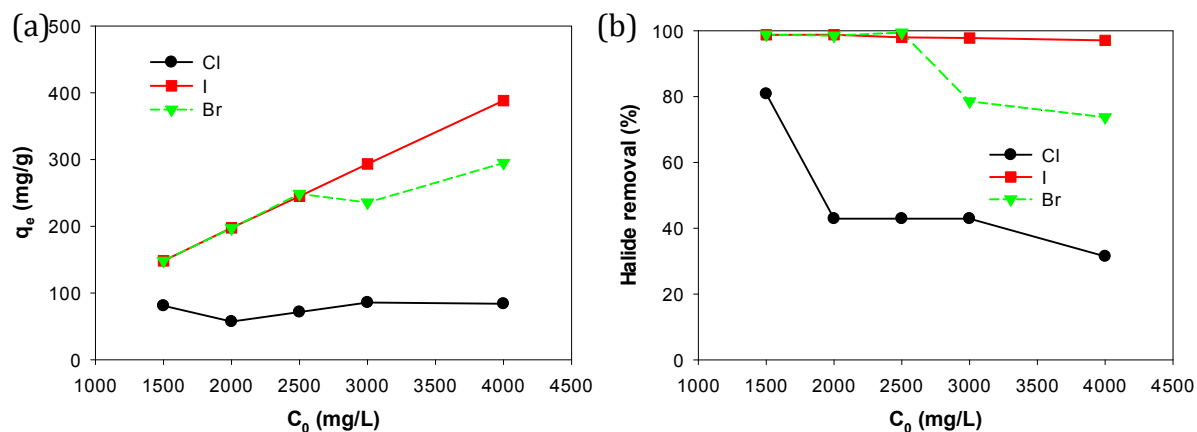
Figure 3-5. Effect of initial halide concentration on (a) halide adsorption capacity removal and (b) removal efficiency at optimal dosage of bismuth hydroxide sulphate (chloride: 15 g/L, iodide and bromide: 10 g/L).

3.4.2.4. Effect of presence of other anions on halide removal

To investigate   the effect of other anions present on the removal efficiency of halide with the bismuth material, a synthetic mining water was made from the specific concentrations of various anions and pH 7.5 (Table *3-1*). It was shown that adsorption capacity would not be affected by the presence of these anions in water (Figure *3-6*).

Table 3-1. Synthetic alkaline mine water various parameters.

ions	halide (Cl⁻, I⁻, Br⁻)	NO_3^-	HCO_3^-	SO_4^{2-}	pH
Concentration (mg/L)	1500 each	56	389	987	7.5
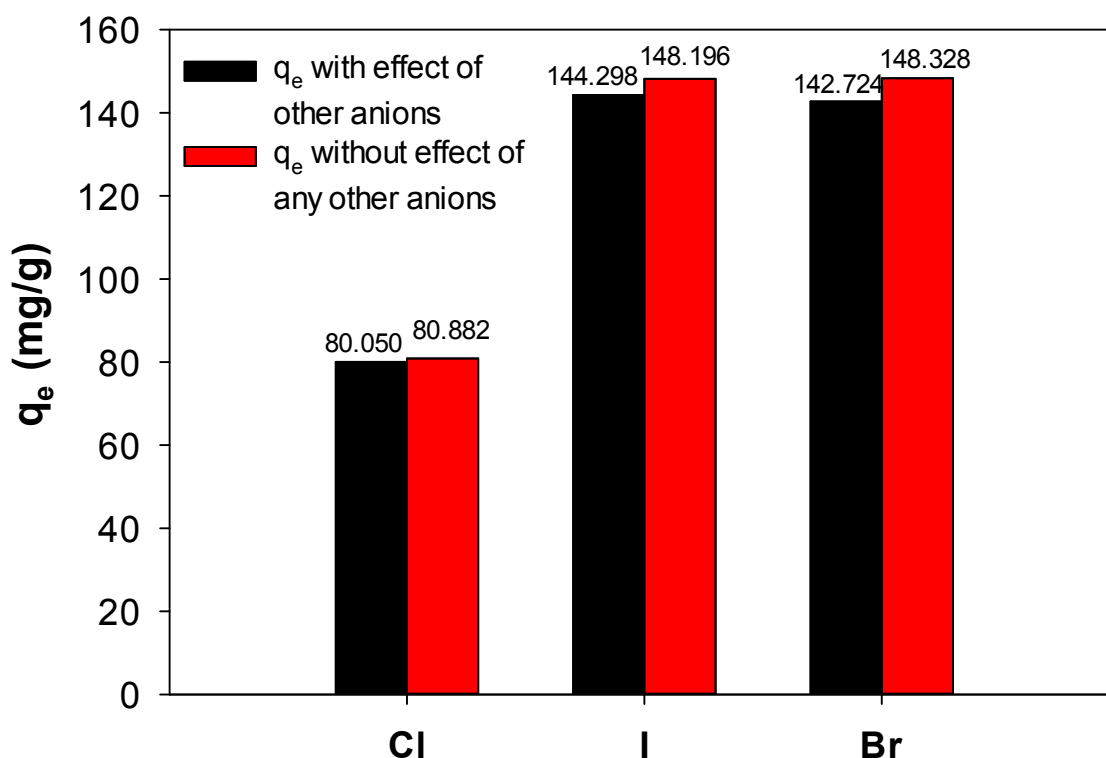
Figure 3-6. Effects of other anions present (halide concentration (Cl⁻, I⁻, Br⁻): 1500 mg/each, NO_3^-: 56 mg/L, HCO_3^- 389 mg/L, SO_4^{2-}: 987 mg/L, pH: 7.5) on adsorption capacity and comparison with adsorption capacity without presence of those anions

3.4.2.5. Effect of temperature on halide removal

Initial halide concentration of 1500 and 4000 mg/L was selected for these experiments. This selection was because 1500 mg/L was the lowest and 4000 mg/L was highest halide concentrations that were tested in previous experiments. Optimal dosage of bismuth hydroxide sulphate was used for the experiments. Reaction time was set 20 min as previous experiments.

Q_e was decreased in case of chloride with increasing temperature, while it did not decrease for iodide and bromide. One of the reasons lies in the conversion of mg/L to molar. For example, 1500 mg/L of chloride is 42.31 µmol/L, but 1500 mg/L of iodide is 11.82 µmol/L and will be 18.77 µmol/L for bromide (Figure 3-7a).

While when halide concentration increases to 4000 mg/L, the effect of temperature on bismuth hydroxide sulphate efficiency on halide removal would be more visible (Figure 3-7b).

It can be concluded that increasing temperature would have a negative effect. This might because the reaction of bismuth hydroxide sulphate with halides are exothermic and increasing temperature would lead to the left part of reaction (Equation 3-3).

Table 3-2. Q_e effects by temperature on Qe with initial halide concentrations of 1500 mg/L and 4000 mg/L.

Temperature (°C)	Chloride		Bromide		Iodide	
	1500 mg/L	4000 mg/L	1500 mg/L	4000 mg/L	1500 mg/L	4000 mg/L
	Q_e (mg/g)		Q_e (mg/g)		Q_e (mg/g)	
20	80.88	83.87	146.35	388.36	148.20	295.00
30	76.13	33.78	149.17	384.00	148.30	195.56
40	50.015	3.74	149.13	304.35	148.60	103.23
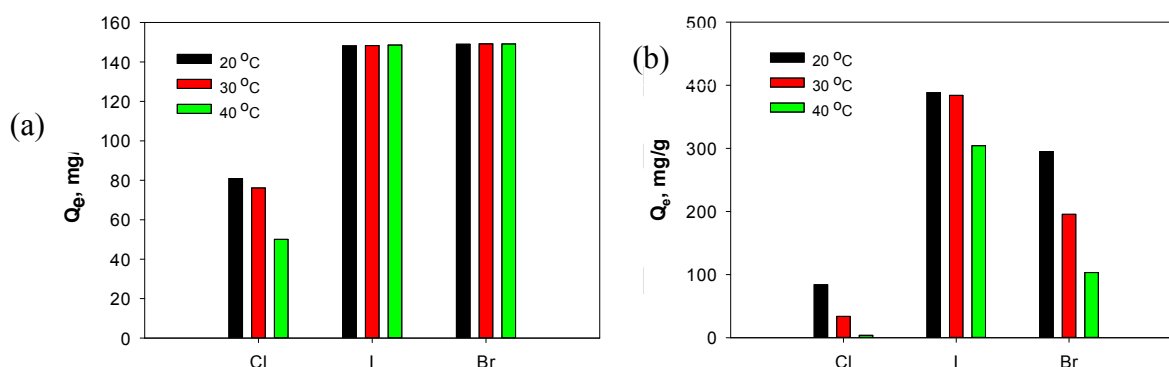
Figure 3-7. Effect of the temperature on the halide removal (a): effect of temperature on Qe for 1500 mg/L of halides, (b): effect of temperature on 4000 mg/L of halides (after 20 min, and with optimal dosage for halides [chloride =15 g/L, iodide and bromide=10 g/L]).

3.4.3. Mechanism of halide removal with bismuth hydroxide sulphate

We propose the chemical formula of the material is $Bi(OH)SO_4.H_2O$, due to its matching with XRD patterns with Riomarinaite mineral, as was shown in Figure 3-12S, and we name it bismuth hydroxide sulphate. Furthermore, the possible reaction between halides with the bismuth hydroxide sulphate is as shown in Equation 3-3. For supporting this reaction equation, sulphate concentrations after reaction with halides (1500 and 3000 mg/L), has been measured and shown. As can be seen in Figure *3-8*a the amount of halides being

removed, were similar to the amount of sulphate released into the solution. Furthermore, hydrogen ion (H$^+$) concentrations were measured by pH meter. The pH of solution decreased after the reaction and the amount of hydrogen ion (H$^+$) released in solution is also reported here (Figure *3-8*a). However, the amount of H$^+$ released might not be the same as sulphate or halide adsorbed. This might be due to the fact that HSO$_4^-$ might not dissociate completely in water in some cases (Figure *3-8* a and Equation 3-3).

$$Bi(OH)SO_4.H_2O + X^- \rightarrow BiOX.H_2O + HSO_4^- \leftrightarrow BiOX.H_2O + H^+ + SO_4^{2-}$$ Equation 3-3

In addition, the XRD patterns of the remaining material after reaction with (3000 mg/L of halides) was showing that the initial material (bismuth hydroxide sulphate) has been turned into BiOX (BiOCl, BiOI, and BiOBr). Specifically, bismuth hydroxide sulphate after reaction with 3000 mg/L chloride has shown same XRD peaks with BiOCl (JCPDS card No. 85-0861), and the resultant BiOCl crystal tend to grow at the orientation of (102) after reaction with bismuth hydroxide sulphate, due to the highest peak (Figure *3-8* b) [60]. Bismuth hydroxide sulphate after reaction with 3000 mg/L of iodide also has been changed to BiOI (JCPDS No. 10-0445) that was matched (Figure *3-8* c) [61]. Samples can be indexed as the tetragonal BiOI phase with cell parameters of a = 3.9940 Å, b = 3.9940 Å and c = 9.1490 Å (JCPDS No. 10-0445) . The last but not least, bromide after reaction with 3000 mg/L of bromide has been shown changed to BiOBr, too. The XRD of bismuth hydroxide sulphate after reaction with bromide which is in agreement with the BiOBr (JCPDS 09-0393). BiOBr has the strongest peak at (110) which indicates that it is growing in this orientation (Figure *3-8* d) [62, 63]. Eventually, it can be said that bismuth hydroxide sulphate would be transformed into the BiOCl, BiOI, BiOBr based on the XRD analysis.

Also, the SEM images indicated that the material morphology would transform into different ones (from plain rod into rod formed from the small plates), indicating the chemical transformation (Figure 3-2). Therefore, the proposed reaction of bismuth hydroxide sulphate with halides has been supported by the aforementioned results (Eqaution 3-3).

(a)
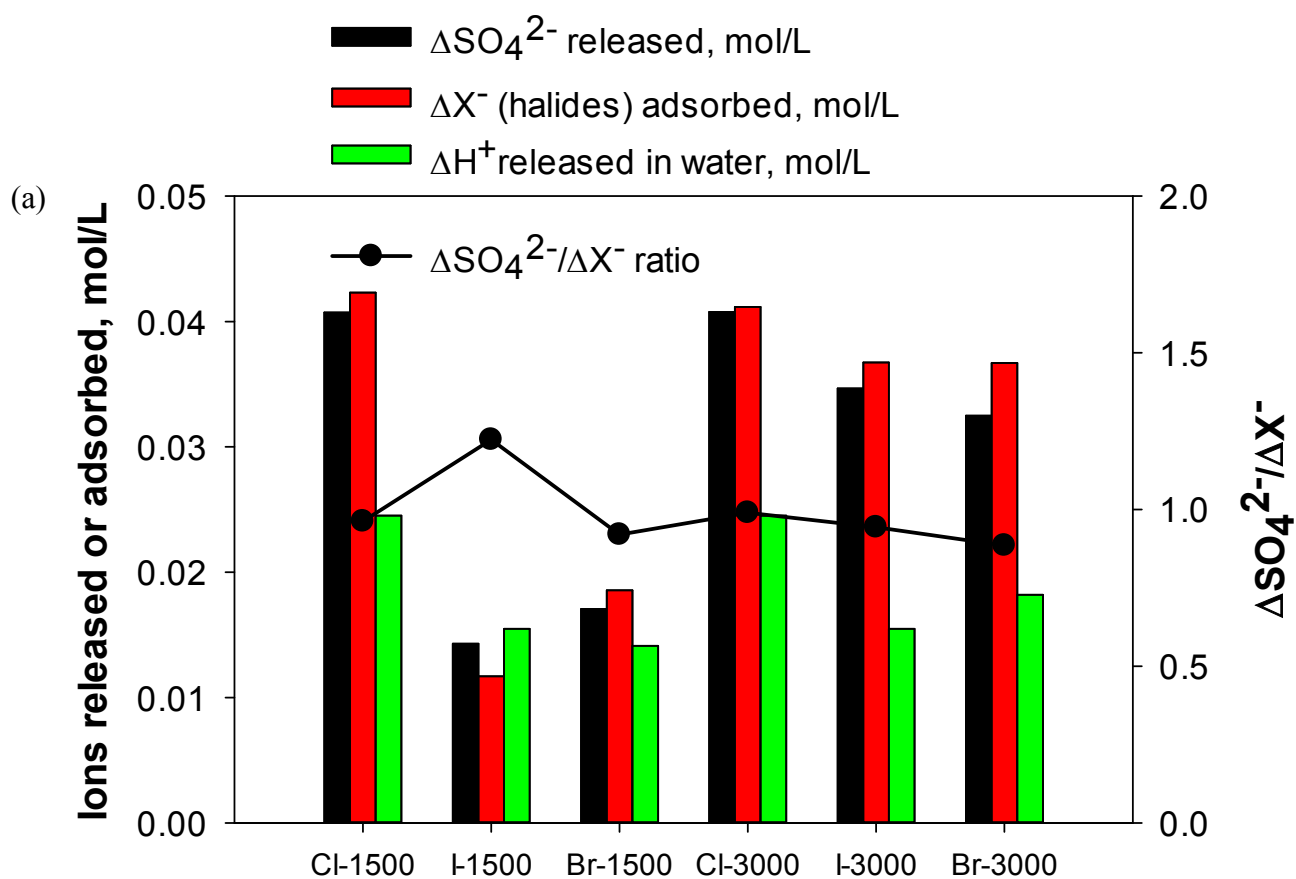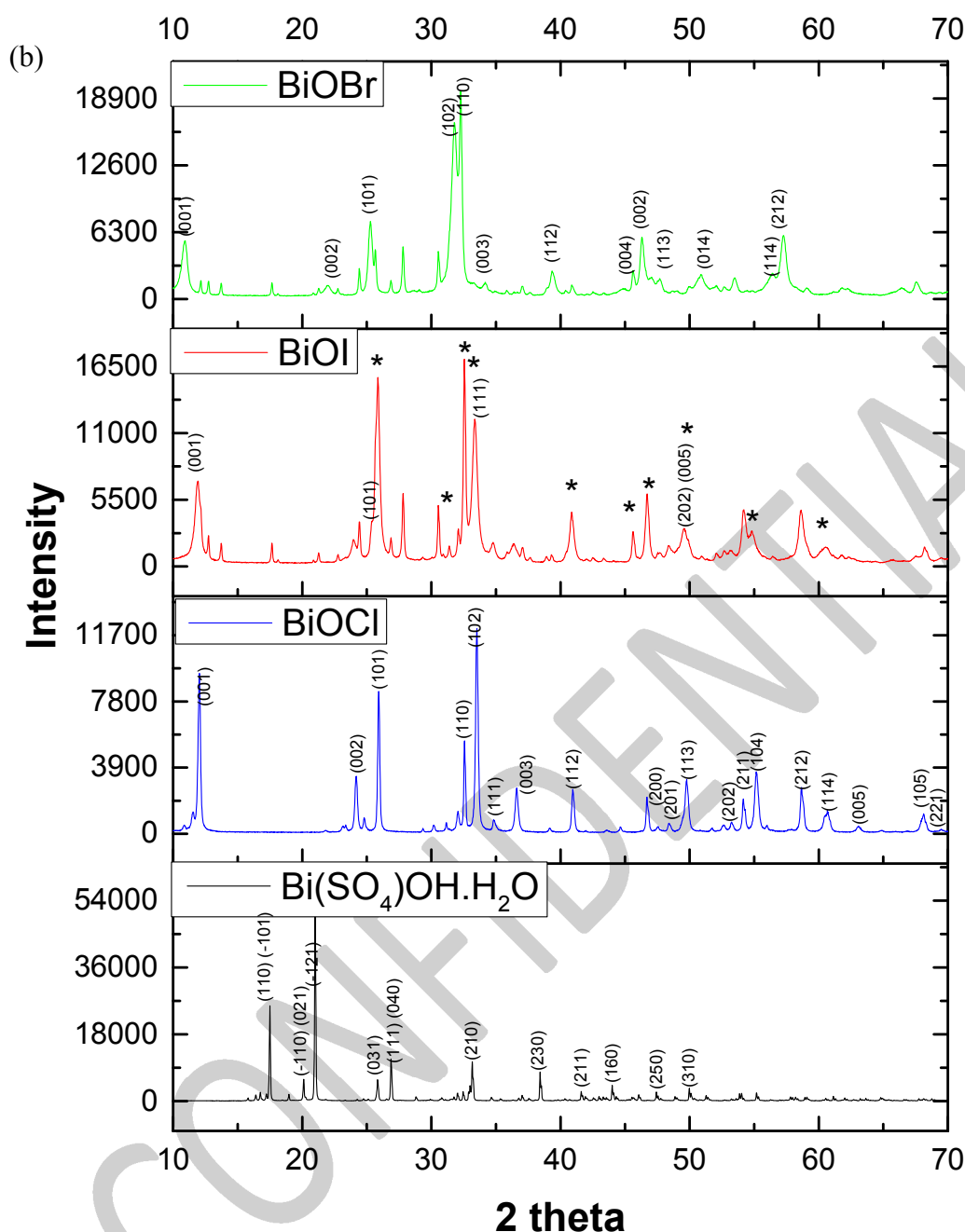
Figure 3-8. (a) The amount of sulphate release, halide adsorption and H$^+$ release in water (mol/L) after adsorption with halides (X$^-$ (Cl$^-$,I$^-$, Br$^-$): at concentration of 1500 and 3000 mg/L and optimal dosage (chloride: 15 g/L, iodide and bromide: 10 g/L of bismuth hydroxide sulphate), (b) XRD spectrum of bismuth hydroxide sulphate before and after adsorption with 3000 mg/L of halides and formation of BiOX (X=Cl,I,Br).

Sulphate released into water after reaction, which does not have adverse effect on human health [64]. Sulphate removal is a well-established process by adding the lime or calcium oxide. Other process is application of aluminium and calcium salts to precipitate sulphate

as ettringite mineral [65, 66]. Also barium carbonate or other barium salts precipitation is available [67].

The predominance area for sulphate was made by Medusa-Hydra software. The graph shows that the sulphate is precipitating as $CaSO_4$ in presence of calcium in various pH values (Figure 3-14S).

3.4.4. Isotherms

Various equations (Langmuir and Freundlich) were applied to find out the dominant isotherm and mechanism of the halide removal and simulation of experimental data. In Langmuir isotherm q_e and C_e are the amount of adsorbed halide at equilibrium (mg/g), equilibrium concentration of adsorbate in solution (mg/L). In addition, b and q_m represent the Langmuir constant related to the binding energy (L/mg) and maximum amount of halide adsorbed on the bismuth hydroxide sulphate (mg/g) (Equation 3-4 and its linear form Equation 3-5) [68]. The data were fitted with the following equation (showed best-fitting regression) and are shown in Figure 3-15S.

$$q_e = \frac{q_m b C_e}{1 + b C_e} \qquad \text{Equation 3-4}$$

$$\frac{C_e}{q_e} = \frac{1}{b q_m} + \frac{C_e}{q_m} \qquad \text{Equation 3-5}$$

Freundlich isotherm K_F and $1/n$ are representing the Freundlich constants related to the adsorption capacity of adsorbent and tendency of adsorbate to the adsorbed, respectively (Equation 3-6) [68, 69].

$$q_e = K_F C_e^{\frac{1}{n}} \qquad \text{Equation 3-6}$$

As can be seen, the high R^2 for this equation fitting shows that Langmuir isotherm is the best fitted isotherm in the halide removal (Table 3-3S), and the fitted isotherms are presented (Figure 3-15S).

3.4.5. Kinetics

The pseudo-first-order kinetics and pseudo-second-order kinetics models were used for the kinetic studies and their formula is presented here.

$$q_t = q_e(1 - e^{-k_1 t})$$

Equation 3-7

$$\frac{t}{q_t} = \frac{1}{k_2 q_e^2} + \frac{t}{q_e}$$

Equation 3-8

The applicability of the kinetics models was validated by normalized standard deviation (Δq_e), which is defined as Δq_e (Equation 3-9). In which N id the number of data points, $q_{e,cal}$ and $q_{e,exp}$ (mg/g) are the calculated and experimental sorption capacity values, respectively [70].

$$\Delta q_e(\%) = 100 \sqrt{\frac{\Sigma \left[\frac{q_{e,exp} - q_{e,cal}}{q_{e,exp}}\right]^2}{N-1}}$$

Equation 3-9

For investigating which kinetic model is fitting better, the two parameters of R^2 and $\Delta Q_e(\%)$ were considered, simultaneously.

Based on the calculations it was found that all halides follow first-order kinetics, as they have higher R^2 and lower $\Delta Q_e(\%)$ (Figure 3-16 S and Table 3-4S). Also, generally k_1 decreased with increasing halide concentrations, except for iodide in which k_1 did not follow any trend in relation to initial concentrations, which can be a case sometimes [71]. In addition, k_1 for iodide, then bromide is relatively higher than chloride. Pseudo- first-order kinetics indicates that a surface reaction-controlled process is the controlling kinetics [71]. The calculations related to pseudo-second-order kinetics and the related figure are shown in Table 3-5S and Figure 3-16S.

3.4.6.   Regeneration experiment

The BiOI after reaction with 4000 mg/L of iodide was used. The precipitates were washed with water and then was dried at 100 °C. Then precipitates calcined at 600 °C with temperature rate of 10 °C/min. It was kept at 600 °C for 20 min to obtain $Bi_2O_{2.3}$ [72]. Subsequently, the bismuth oxide was be reacted with H_2SO_4 (70 g/L) at 60 °C for one hour. The final product would be washed off with water and dried. Subsequently, it was tested for iodide removal (4000 mg/L). Iodide removal efficiency after 20 min reaction with 10 g/L of regenerated bismuth hydroxide sulphate is shown below (Figure *3-9*).

Figure below depicts the removal efficacy of bismuth hydroxide material after each time of regeneration. This shows that regenerated material is keeping its high efficiency for iodide removal with a slight decrease at the 4th times regeneration. This decline in removal is as a result of not complete conversion of BiOI to $Bi_2O_{2.3}$. The FTIR shows that at the end of procedure, there are Bi-O and S=O groups bonds. Therefore, the $Bi_2O_{2.3}$ active sites would be less than the pure Bi_2O_3 to react with H_2SO_4 in the next step.
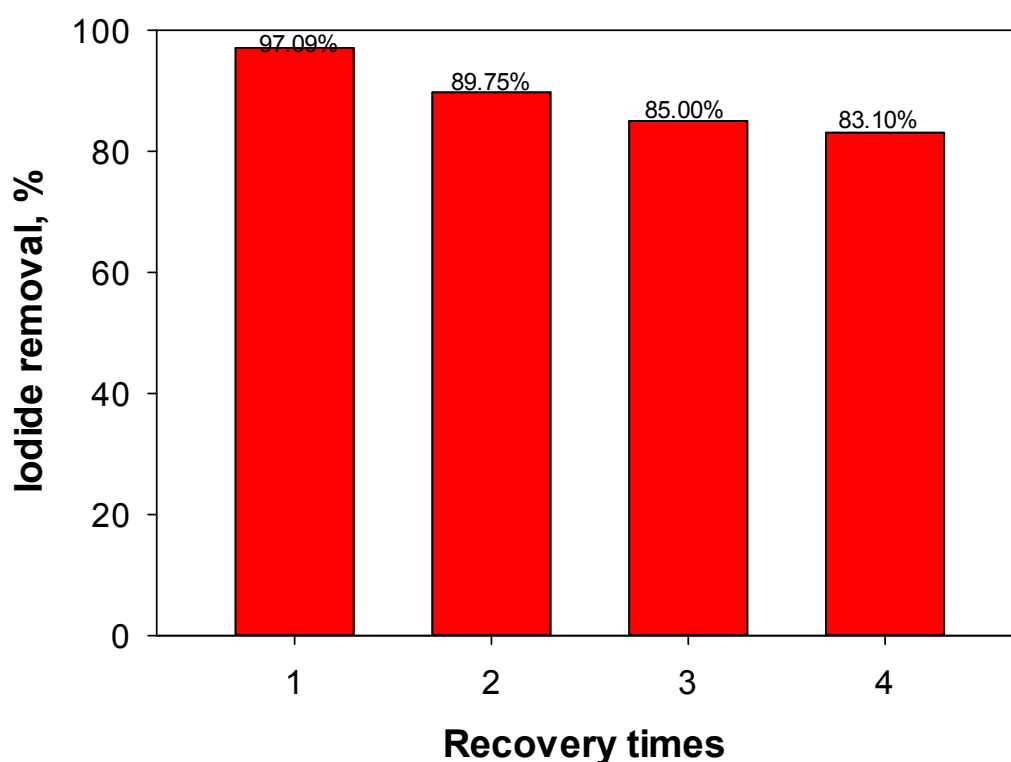
Figure 3-9. Effect of regeneration of bismuth hydroxide sulphate on the iodide removal [initial concentration=4000 mg/L, dosage of material=10 g/L, reaction time=20 min, no pH adjustment].

As it can be seen the final regenerated material has same FTIR as the bismuth hydroxide sulphate which was synthesized initially. Therefore, it shows that the recycling of material was successful (Figure 3-10 a and b).

$Bi_2O_{2.3}$ which was gained from the calcination of BiOI at 600 °C was shown still has S=O groups at 1056 cm^{-1}. S=O groups remained in the material shows the active sites of $Bi_2O_{2.3}$ would be less to react with acid sulfuric (70 g/L) compared to pure Bi_2O_3, therefore, the final material would have less removal efficiency from the first experiments. Other peaks

for $Bi_2O_{2.3}$ are 593 and 461 cm^{-1} that are related to Bi-O. The spectrum from 200-800 cm^{-1} are related to Bi-O (Figure 3-10 c) [45].

The final product (after final regeneration and reaction with iodide) shows Bi-O peaks at 481.6, 619.3 cm^{-1}, which is related to BiOI [45]. The peaks at 1154, 1090, 959.5 and 619.3 cm^{-1} are related to S=O groups [73]. The peak at 1600 cm^{-1} which is related to the stretching and bending water molecules [73].
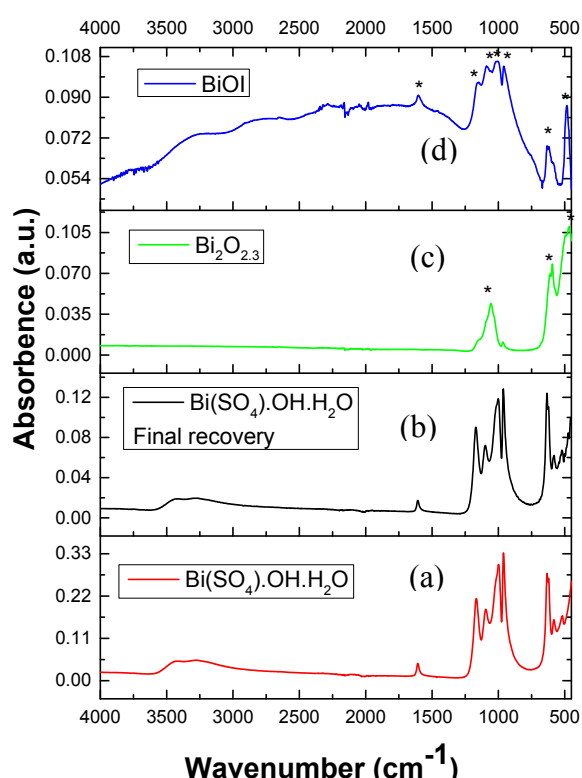
Figure 3-10. FTIR spectrum of (a) initial bismuth hydroxide sulphate, (b) after final regeneration (4 times reaction with iodide and regeneration from the explained procedure), (c) $Bi_2O_{2.3}$ (regeneration of bismuth oxide from BiOI after 4 time reaction with iodide), (d) BiOI (the product that obtained from iodide and bismuth hydroxide sulphate at the final regeneration experiment).

It is notable that iodide was used for these tests due to the safety. Because the calcination of BiOI can produce iodine gas. If BiOCl, BiOBr was tested for regeneration, it might produce chlorine and bromine gas which are more toxic than iodine gas. The halogen gas toxicity would be less with increasing their molecular weight. This procedure also can be used for regeneration of bismuth hydroxide sulphate from BiOCl and BiOBr but needs

more precautions. The algorithm for the regeneration procedure and decision making presented (Figure 3-11).
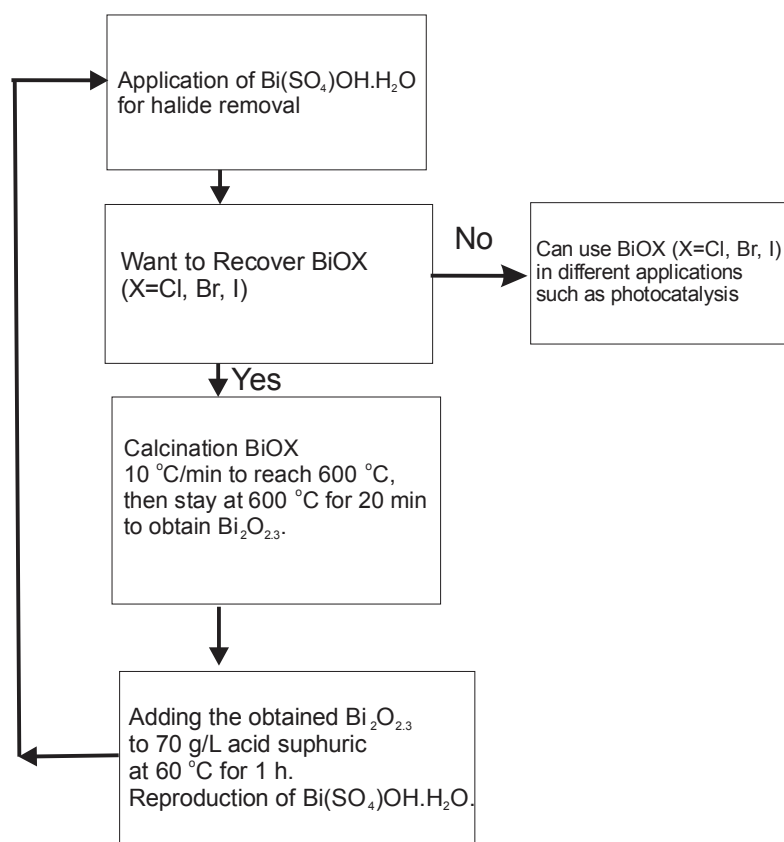
Figure 3-11. The algorithm for BiOX regeneration or not regeneration.

3.5. Conclusions

A novel bismuth hydroxide sulphate adsorption material was synthesized. The material showed a fast adsorption kinetics and high capacities for removing halides (Cl^-, I^-, Br^-). The adsorption capacities are 81, 148 and 146 mg/g for Cl^-, I^-, and Br^- at 1500 mg/L of halides within 20 min, respectively. From the experiments, it was found out that pH did not affect the removal efficiency of material, except for chloride which had a lower removal efficiency at pH≥8. With increased initial concentration of halides, the removal efficiency decreased. This decrease was more significant for chloride compared to the other halides. Overall, the as-synthesized bismuth hydroxide sulphate is very effective in removing the high halide concentrations in the presence of other tested anions. The mechanism of the adsorption/ion exchange reaction with halides was presented and supported by XRD, SEM and stoichiometry measurement of sulphate and hydrogen ions

released into the solution sulphate. The final material after the ion exchange is in the form of BiOX (X=Cl, I, Br), which may be used in other applications such as photocatalysis, for sludge management after reaction [74-76].

3.6. Supplementary information
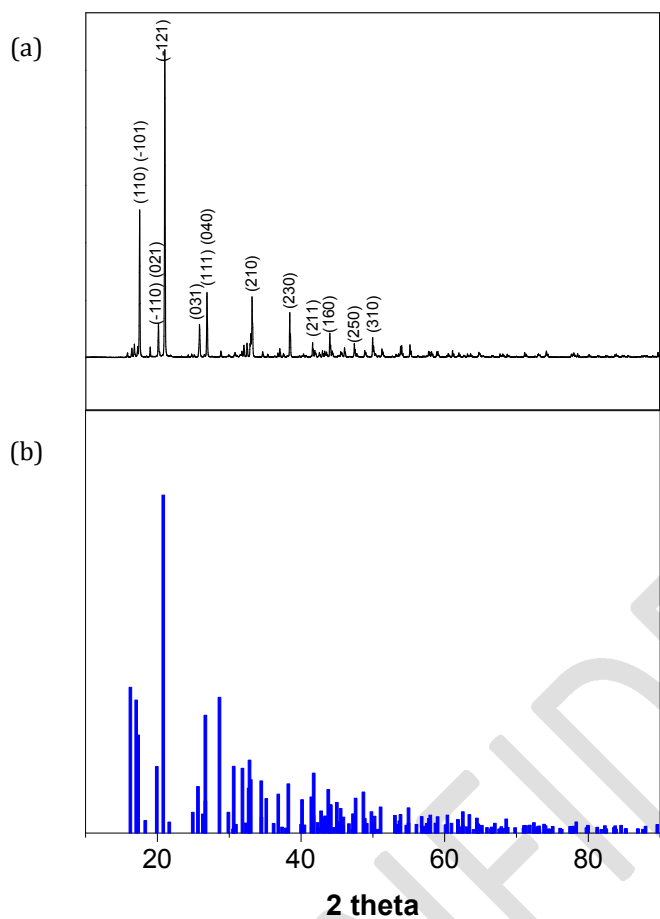
Figure 3-12S. XRD patterns of (a) synthesized bismuth hydroxide sulphate, and (b) XRD pattern of Riomarinaite mineral with a chemical formula of $Bi(OH)SO_4.H_2O$
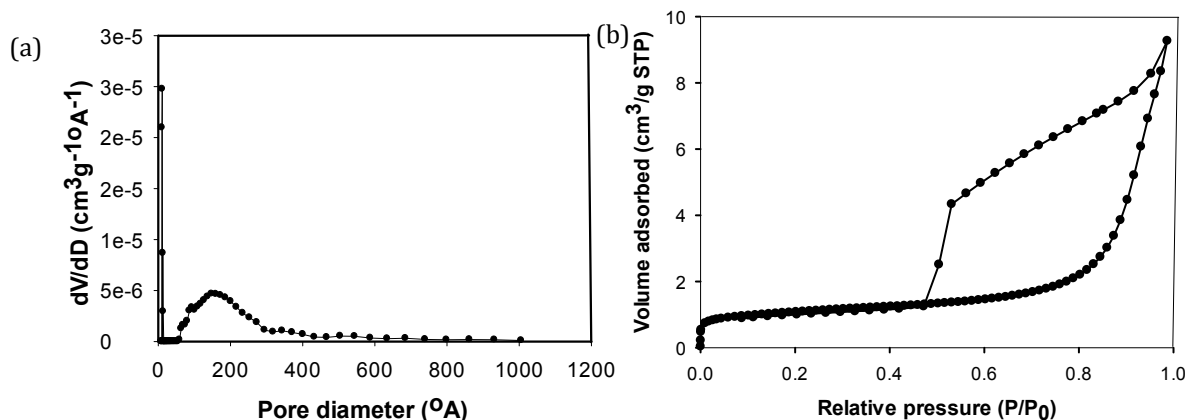
Figure 3-13S. N₂ adsorption and desorption isotherms and pore size distribution for bismuth hydroxide sulphate.
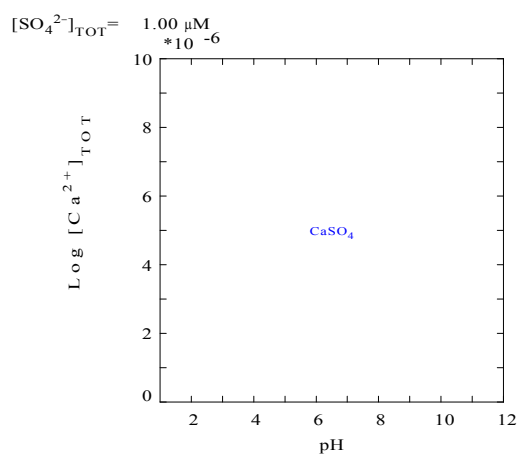
Figure 3-14S. Predominance area for sulphate in presence of calcium at various pH values (sulphate concentration was considered 1 μM. The graph is made by Hydra-Medusa software from KTH University.
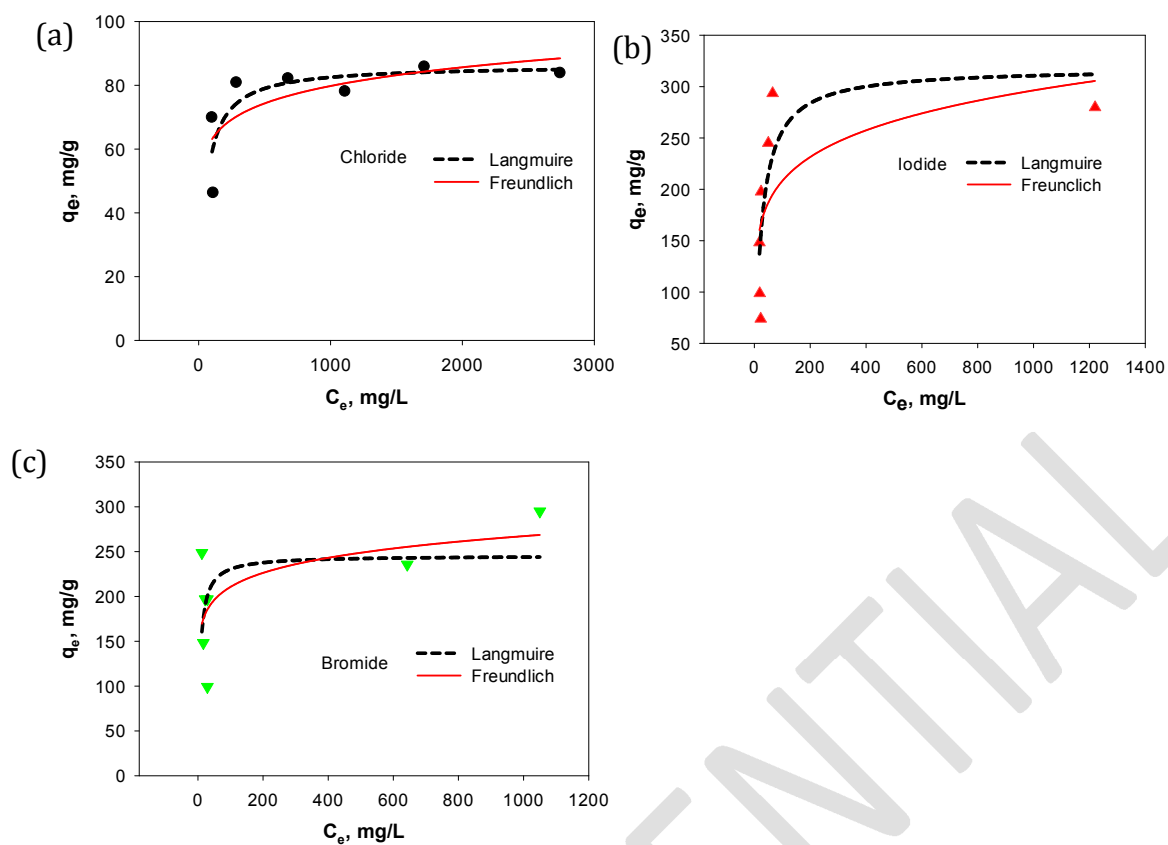
Figure 3-15S. Langmuir and Freundlich isotherms of (a) chloride, (b) iodide and (c) bromide. Solid dashed lines represent theoretical values calculated from isotherm equations.

Table 3-3S. Calculated parameters of Langmuir and Freundlich isotherms.

Isotherms	Langmuir			Freundlich		
Parameters	b	q_m	R^2	K_F	1/n	R^2
Chloride	0.021	85.67	0.9982	39.37	0.1023	0.5417
Iodide	0.044	285.28	0.9976	102.6	0.1535	0.4018
bromide	0.037	284.53	0.9838	130.9	0.1034	0.3751
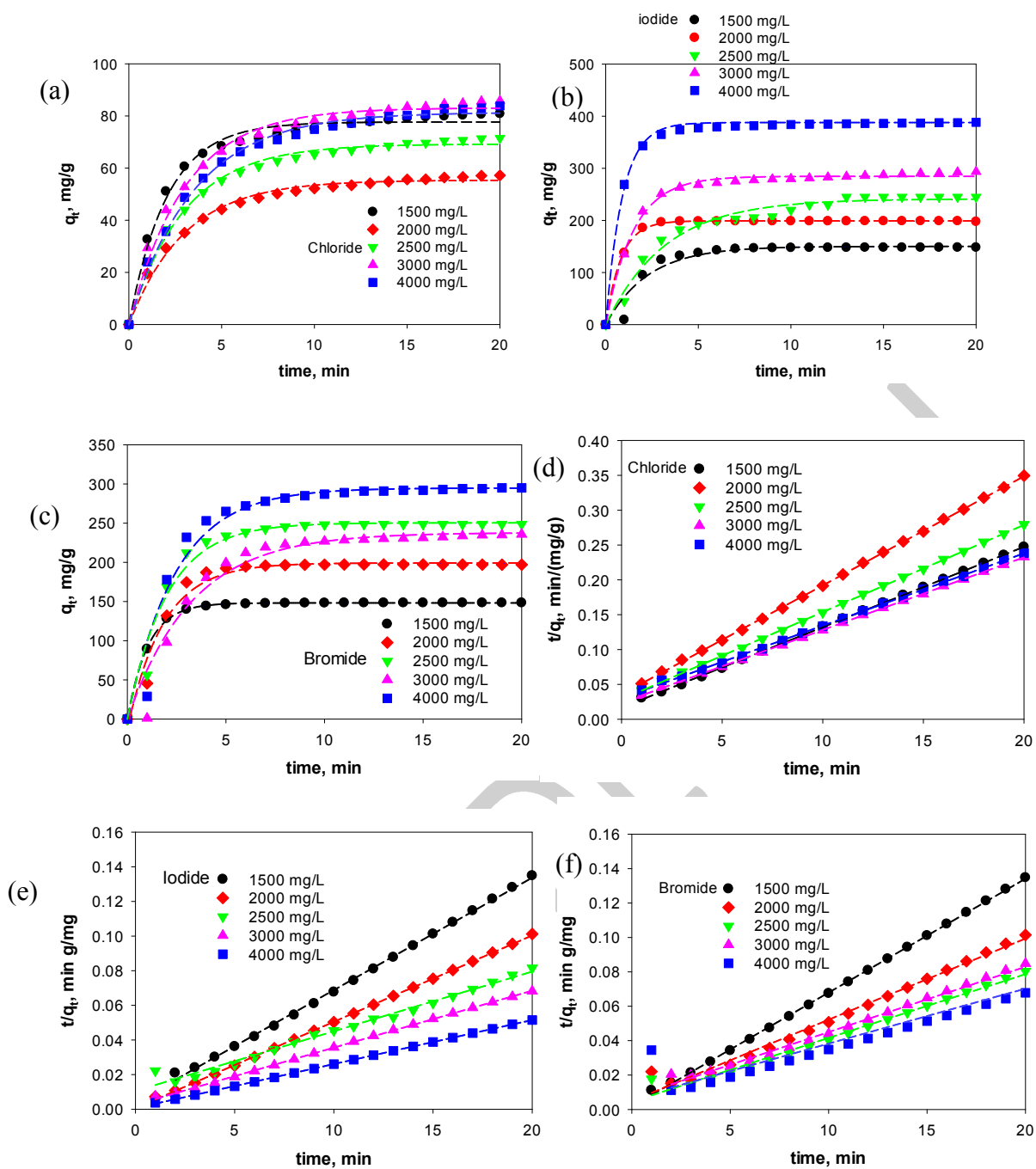
Figure 3-16S. Fitted pseudo-first-order kinetic models for (a): chloride, (b): iodide, (c): bromide, and pseudo-second-order kinetic model (d): chloride, (e): iodide, (f): bromide) with experimental data.

Table 3-4S. Pseudo-first-order kinetic calculations based on different initial halide concentrations.

Concentration, mg/L	Chloride					Iodide					Bromide				
	q_e (cal) mg g^{-1}	$q_{e(exp)}$ mg g^{-1}	Δq_e (%)	K_1 g mg^{-1} min^{-1}	R^2	q_e (cal) mg g^{-1}	$q_{e(exp)}$ mg g^{-1}	Δq_e (%)	K_1 g mg^{-1} min^{-1}	R^2	q_e (cal) mg g^{-1}	$q_{e(exp)}$ mg g^{-1}	Δq_e (%)	K_1 g mg^{-1} min^{-1}	R^2
1500	77.72	80.88	3.6895	0.4856	0.9860	150.07	148.17	1.7481	0.4395	0.9373	148.162	148.33	0.7957	0.9514	0.9996
2000	55.40	57.23		0.3348	0.9901	199.09	197.6		1.2330	0.9992	199.25	197.09		0.5529	0.9711
2500	69.26	71.53		0.3348	0.99017	241.35	245		0.3105	0.9762	250.4	248.77		0.50131	0.9725
3000	83.11	85.84		0.3348	0.9901	284.71	293.45		0.6719	0.9940	237.91	235.71		0.3061	0.9553
4000	81.40	83.87		0.2860	0.9939	388	388.36		1.1218	0.9961	294.87	295		0.4120	0.9573

Table 3-5S. Pseudo-second-order kinetic calculations based on different initial halide concentrations

Concentration, mg/L	Chloride					Iodide					Bromide				
	q_e (cal) mg g^{-1}	$q_{e(exp)}$ mg g^{-1}	ΔQ_e (%)	K_2 g. mg^{-1}.min^{-1}	R^2	q_e (cal) mg g^{-1}	$q_{e(exp)}$ mg g^{-1}	Δq_e (%)	K_2 g. mg^{-1}.min^{-1}	R^2	q_e (cal) mg g^{-1}	$q_{e(exp)}$ mg g^{-1}	Δq_e (%)	K_2 g. mg^{-1}.min^{-1}	R^2
1500	86.58	80.88	12.9576	0.0081	0.9998	154.09	148.17	9.5536	0.0106	0.9988	151.01	148.33	8.6299	0.0249	0.9996
2000	63.86	57.23		0.0069	0.9999	200.26	197.6		0.0447	0.9998	211.76	197.09		0.0045	0.9866
2500	79.87	71.53		0.0055	0.9999	289.68	245		0.0011	0.9865	269.37	248.77		0.0031	0.9871
3000	95.79	85.84		0.0046	0.9999	304.05	293.48		0.0041	0.9995	263.16	235.71		0.0021	0.9930
4000	96.25	83.87		0.0037	0.9993	393.65	388.36		0.0094	0.9999	312.50	295		0.0016	0.9992

References

1. Rogora, M., et al., *Recent trends in chloride and sodium concentrations in the deep subalpine lakes (Northern Italy).* Environ. Sci. Pollut. Res. Int., 2015. **22**(23): p. 19013-26.

2. Wu, X., Z. Liu, and X. Liu, *Chloride ion removal from Zinc sulfate aqueous solution by electrochemical method.* Hydrometallurgy, 2013. **134–135**: p. 62-65.

3. Tuchman, M.L., E.F. Stoermer, and H.J. Carney, *Effects of increased salinity on the diatom assemblage in Fonda Lake, Michigan.* Hydrobiologia, 1984. **109**(2): p. 179-188.

4. Karraker, N.E., J.P. Gibbs, and J.R. Vonesh, *Impacts of road deicing salt on the demography of vernal pool-breeding amphibians.* Ecol. Appl., 2008. **18**(3): p. 724-734.

5. Lito, P.F., J.P.S. Aniceto, and C.M. Silva, *Removal of anionic pollutants from waters and wastewaters and materials perspective for their selective sorption.* Water Air Soil Pollut., 2012. **223**(9): p. 6133-6155.

6. Mercuri, A.M., J.A. Duggin, and C.D. Grant, *The use of saline mine water and municipal wastes to establish plantations on rehabilitated open-cut coal mines, Upper Hunter Valley NSW, Australia.* Forest Ecol. Manag., 2005. **204**(2): p. 195-207.

7. Silva, T.L.S., et al., *An overview on exploration and environmental impact of unconventional gas sources and treatment options for produced water.* J. Environ. Manage., 2017. **200**: p. 511-529.

8. Rapp, H.-J. and P.H. Pfromm, *Electrodialysis for chloride removal in low effluent Kraft pulp production.* Membr. Technol., 1997. **1997**(89): p. 7-11.

9. Kim, H.I., et al., *A process to recover high purity iodine in wastewater from liquid crystal display (LCD) manufacturing industry.* Hydrometallurgy, 2018. **181**: p. 91-96.

10. Majidnia, Z. and A. Idris, *Photocatalytic reduction of iodine in radioactive waste water using maghemite and titania nanoparticles in PVA-alginate beads.* J. Taiwan Inst. Chem. E., 2015. **54**: p. 137-144.

11. Madrakian, T., et al., *Application of Modified Silica Coated Magnetite Nanoparticles for Removal of Iodine from Water Samples.* Nano-Micro Lett., 2012. **4**(1): p. 57-63.

12.   LENNTECH. *Iodine and water: reaction mechanisms, environmental impact and health effects*. Available from: https://www.lenntech.com/periodic/water/iodine/iodine-and-water.htm.

13.   Fruit, J.T., et al., *Recovery of Iodine from Produced Water Through Anion Resin Exchange*, in *2011 Research Experiences for Undergraduates posters and presentations.* 2011, Advanced Water Technology Center (AQWATEC) Colorado School of Mines, 1500 Illinois street, Golden, CO 80401.

14.   Ordóñez, J.I., et al., *Use of discharged brine from reverse osmosis plant in heap leaching: Opportunity for caliche mining industry.* Hydrometallurgy, 2015. **155**: p. 61-68.

15.   Ikari, M., et al., *Removal of iodide from water by chlorination and subsequent adsorption on powdered activated carbon.* Water Res., 2015. **68**: p. 227-37.

16.   Tauanov, Z. and V.J. Inglezakis, *Removal of iodide from water using silver nanoparticles-impregnated synthetic zeolites.* Sci. Total Environ., 2019. **682**: p. 259-270.

17.   Yu, F., et al., *Enhanced removal of iodide from aqueous solution by ozonation and subsequent adsorption on Ag-Ag$_2$O modified on Carbon Spheres.* Appl. Surf. Sci., 2018. **427**: p. 753-762.

18.   NHMRC and NRMMC, *Australian Drinking Water Guidelines Paper 6 National Water Quality Management Strategy*. 2011: National Health and Medical Research Council, National Resource Management Ministerial Council, Commonwealth of Australia, Canberra.

19.   Wang, Y., M.J. Small, and J.M. VanBriesen, *Assessing the Risk Associated with Increasing Bromide in Drinking Water Sources in the Monongahela River, Pennsylvania.* J. Environ. Eng., 2017. **143**(3): p. 04016089.

20.   Landis, M.S., et al., *The impact of commercially treated oil and gas produced water discharges on bromide concentrations and modeled brominated trihalomethane disinfection byproducts at two downstream municipal drinking water plants in the upper Allegheny River, Pennsylvania, USA.* Sci. Total Environ., 2016. **542**: p. 505-520.

21.   Salameh, E., A. Tarawneh, and M. Al-Raggad, *Origin of high bromide concentration in the water sources in Jordan and in the Dead Sea water.* Arab. J. Geosci., 2016. **9**(5): p. 414.

22.   Ateia, M., et al., *Selective removal of bromide and iodide from natural waters using a novel AgCl-SPAC composite at environmentally relevant conditions.* Water Res., 2019. **156**: p. 168-178.

23.   Gruchlik, Y., et al., *Impact of bromide and iodide during drinking water disinfection and potential treatment processes for their removal or mitigation.* Water, 2014. **41**(8): p. 38-43.

24.   Jang, E., S. Jeong, and E. Chung, *Application of three different water treatment technologies to shale gas produced water.* Geosyst. Eng., 2017. **20**(2): p. 104-110.

25.   Bonyadi, S., T.S. Chung, and R. Rajagopalan, *A novel approach to fabricate macrovoid-free and highly permeable PVDF hollow fiber membranes for membrane distillation.* AIChE J., 2009. **55**(3): p. 828-833.

26.   Bellona, C., *Nanofiltration – theory and application*, in *Desalination*, J. Kucera, Editor. 2014, John Wiley & Sons, Inc. p. 205-253.

27.   Abdel-Wahab, A.I.A., *The ultra-high lime with aluminum process for removing chloride from recirculating cooling water*, in *Civil engineering*. 2003, Texas A&M University.

28.   Abdel-Wahab, A. and B. Batchelor, *Effects of pH, temperature, and water quality on chloride removal with ultra-high lime with aluminum process.* Water Environ. Res., 2006. **78**(9): p. 930-937.

29.   Iakovleva, E., et al., *Industrial products and wastes as adsorbents for sulphate and chloride removal from synthetic alkaline solution and mine process water.* Chem. Eng. J., 2015. **259**: p. 364-371.

30.   Carmona, M., et al., *Removal of chloride ions from an industrial polyethylenimine flocculant shifting it into an adhesive promoter using the anion exchange resin Amberlite IRA-420.* React. Funct. Polym., 2008. **68**(8): p. 1218-1224.

31.   Carmona, M., et al., *Purification of glycerol/water solutions from biodiesel synthesis by ion exchange: sodium and chloride removal. Part II.* J. Chem. Technol. Biotechnol., 2009. **84**(8): p. 1130-1135.

32.   Abu-Arabi, M.K., S. Emeish, and B.I. Hudaib, *Chloride removal from Eshidiya phosphate mining wastewater.* Desalin. Water Treat., 2013. **51**(7-9): p. 1634-1640.

33. Watson, K., M.J. Farré, and N. Knight, *Strategies for the removal of halides from drinking water sources, and their applicability in disinfection by-product minimisation: A critical review.* J. Environ. Manage., 2012. **110**: p. 276-298.

34. Strathmann, H., *Electrodialytic membrane processes and their practical application.* Stud. Environ. Sci., 1994. **59**: p. 495-533.

35. Kumar, E., et al., *Interaction of inorganic anions with iron-mineral adsorbents in aqueous media--a review.* Adv. Colloid Interface Sci., 2014. **203**: p. 11-21.

36. Al-Rawajfeh, A.E., et al., *Adsorption desalination of chloride ions on composite natural–synthetic materials: An approach for the reduction of chlorine corrosion in electrodeionization units.* J. Ind. Eng. Chem., 2013. **19**(6): p. 1895-1902.

37. Yun, G., *Colour and chloride removal from pulp mill effluent using ion-exchange*, in *Civil and Environmental Engineering*. 2001, University of Alberta (Canada): Edmonton, Alberta. p. 100.

38. Lv, L., et al., *Removal of chloride ion from aqueous solution by ZnAl-NO$_3$ layered double hydroxides as anion-exchanger.* J. Hazard. Mater., 2009. **161**(2–3): p. 1444-1449.

39. Gondal, M.A.X., Chang; Dastageer, Md. Abdulkader *Novel Bismuth-Oxyhalide-Based Materials and their Application*, ed. S.Q. Andreas Öchsner, Australia, P. Lucas F.M. da Silva, Portugal, and M. Holm Altenbach, Germany. Vol. 76. 2017: Springer.

40. Cheng, H., B. Huang, and Y. Dai, *Engineering BiOX (X = Cl, Br, I) nanostructures for highly efficient photocatalytic applications.* Nanoscale, 2014. **6**(4): p. 2009.

41. Fu, Y., Y. Zhang, and Z. Xu, *Synthesis and structural characterization of four new organically-directed bismuth sulfates.* Dalton Trans., 2008(35): p. 4792-8.

42. Dong, R., et al., *Visible-Light-Driven BiOI-Based Janus Micromotor in Pure Water.* J. Am. Chem. Soc., 2017. **139**(5): p. 1722-1725.

43. Crumpton, T.E. and C. Greaves, *The structural chemistry and oxide ion conducting properties of the new bismuth oxide sulfate, Bi$_8$O$_{11}$(SO$_4$).* J. Mater. Chem., 2004. **14**(15): p. 2433.

44. Srivastav, A.L., P.K. Singh, and Y.C. Sharma, *Synthesis of a novel adsorbent, hydrous bismuth oxide (HBO$_2$) for the removal of fluoride from aqueous solutions.* Desalin. Water Treat., 2015. **55**(3): p. 604-614.

45.   Srivastav, A.L., et al., *Application of a new adsorbent for fluoride removal from aqueous solutions.* J. Hazard. Mater., 2013. **263, Part 2**: p. 342-352.

46.   Singh, P.K., et al., *Kinetic and equilibrium modeling for removal of nitrate from aqueous solutions and drinking water by a potential adsorbent, hydrous bismuth oxide.* RSC Adv.   , 2015. **5**(45): p. 35365-35376.

47.   Singh, P.K., et al., *Preparation and properties of hydrous bismuth oxides for nitrate removal from aqueous solutions.* Desalin. Water Treat., 2012. **40**(1-3): p. 144-152.

48.   L. Pavia, D., et al., *Introduction to Spectroscopy.* 4th ed. 2015/08/09, Bellingham, Washington: Department of Chemistry Western Washington University 656.

49.   Hallam, H.E., *Infrared and Raman spectra of inorganic compounds.* R. Inst. Chem. Rev., 1968. **1**(1): p. 39-61.

50.   Beattie, D.A., et al., *In Situ ATR FTIR Studies of SO4 Adsorption on Goethite in the Presence of Copper Ions.* Environ. Sci. Technol., 2008. **42**(24): p. 9191-9196.

51.   Maria, S.F., et al., *FTIR measurements of functional groups and organic mass in aerosol samples over the Caribbean.* Atmos. Environ., 2002. **36**(33): p. 5185-5196.

52.   Song, J.-M., et al., *Hierarchical structured bismuth oxychlorides: self-assembly from nanoplates to nanoflowers via a solvothermal route and their photocatalytic properties.* CrystEngComm, 2010. **12**(11): p. 3875.

53.   Trivedi, M.K., et al., *Evaluation of Atomic, Physical, and Thermal Properties of Bismuth Oxide Powder An Impact of Biofield Energy Treatment.* American Journal of Nano Research and Applications, 2015. **3**(6): p. 94-98.

54.   Murphy, T.D., *Bismuth in the supergene environment.* 2015, University of Western Sydney University of Western Sydney

55.   Murphy, T., et al., *Mineral Analyses & Implications on the Dispersion of Bismuth in the Supergene Environment of Eastern Australia.* Microsc. Microanal., 2014. **20**(S3): p. 644-645.

56.   Downs, R.T.B., K. L.; Gibbs, G. V.; Boisen, M. B., *Interactive software for calculating and displaying X-ray or neutron powder diffractometer patterns of crystalline materials.* Am. Mineral., 1993. **78**(9-10): p. 1104-1107.

57.   Mindat. *Riomarinaite.* Available from: https://www.mindat.org/min-27210.html.

58.   Anthony, J.W., et al., *Handbook of Mineralogy, Mineralogical Society of America.* 2014, Chantilly, VA 20151-1110, USA.

59.   Moulder, J.F., et al., *Handbook of X-Ray Photoelectron Spectroscopy (perkin elmer)*. 1992: Perkin-Elmer Corporation.

60.   Tripathi, G.K., K.K. Saini, and R. Kurchania, *Synthesis of nanoplate bismuth oxychloride—a visible light active material.* Opt. Spectrosc., 2015. **119**(4): p. 656-663.

61.   FU Dawei, X.R., ZHANG Linping, XU Hong, ZHONG Yi, SUI Xiaofeng, MAO Zhiping, *Preparation of Hollow Spherical Bismuth Oxyiodide and Its Adsorption and Photocatalytic Degradation of Dyes.* Chin. J. Appl. Chem., 2017. **34**(5): p. 590-596.

62.   Xing, H., et al., *Preparation of BiOBr by solvothermal routes with different solvents and their photocatalytic activity.* J. Renew. Sustain. Ener., 2015. **7**(6): p. 063120.

63.   Cao, F., et al., *An in situ Bi-decorated BiOBr photocatalyst for synchronously treating multiple antibiotics in water.* Nanoscale Advances, 2019. **1**(3): p. 1124-1129.

64.   WHO, *Sulfate in Drinking-water Background document for development of WHO Guidelines for Drinking-water Quality*. 2004.

65.   Kabdaşlı, I., A. Bilgin, and O. Tünay, *Sulphate control by ettringite precipitation in textile industry wastewaters.* Environmen. Technol., 2016. **37**(4): p. 446-451.

66.   Silva, R., L. Cadorin, and J. Rubio, *Sulphate ions removal from an aqueous solution: I. Co-precipitation with hydrolysed aluminum-bearing salts.* Miner. Eng., 2010. **23**(15): p. 1220-1226.

67.   Trusler, G.E., et al. *The chemical removal of sulphates*. in *5th National Meeting of the S.A. Institution of Chemical Engineers*. 1988. Pretoria.

68.   Chen, Z., et al., *Kinetic and isotherm studies on the electrosorption of NaCl from aqueous solutions by activated carbon electrodes.* Desalination, 2011. **267**(2-3): p. 239-243.

69.   Foo, K.Y. and B.H. Hameed, *Insights into the modeling of adsorption isotherm systems.* Chem. Eng. J., 2010. **156**(1): p. 2-10.

70.   Wei, C., et al., *Sorption kinetics, isotherms and mechanisms of PFOS on soils with different physicochemical properties.* Ecotox. Environ.Safe., 2017. **142**: p. 40-50.

71.   Tan, K.L. and B.H. Hameed, *Insight into the adsorption kinetics models for the removal of contaminants from aqueous solutions.* J. Taiwan Inst. Chem. E., 2017. **74**: p. 25-48.

72. Ma, Y., et al., *Z-scheme Bi$_2$O$_{2.33}$/Bi$_2$S$_3$ heterojunction nanostructures for photocatalytic overall water splitting.* Chem. Eng. J., 2020. **382**: p. 123020.

73. Pavia, D.L., et al., *Introduction to Spectroscopy 4e by Pavia.* 4 ed. 2008, Department of Chemistry Western Washington University Bellingham,Washington: Cengage Learning.

74. Pu, F., et al., *Preparation of Surface-Sulfurized Nanoflake-Like BiOCl Layered Semiconductor Films with Interbedded S^{2-} for Enhanced Photoelectrochemical Performances.* J. Electrochem. Soc., 2014. **161**(5): p. H269-H275.

75. Intaphong, P., et al., *Sonochemical synthesis and characterization of BiOI nanoplates for using as visible-light-driven photocatalyst.* Materi. Lett., 2018. **213**: p. 88-91.

76. Wei, X.-X., et al., *Tuning the physico-chemical properties of BiOBr via solvent adjustment: towards an efficient photocatalyst for water treatment.* CrystEngComm, 2019. **21**(11): p. 1750-1757.

4. Template synthesis of nano-micro sized bismuth composites: effect of templates and temperature

4.1. Abstract

Synthesis of the materials (nano and micro) are influenced by the sacrificial templates' chemical active groups, morphology and surface area. Here we have made different templates and then removed partially and fully at different calcination temperatures (450 °C and 600 °C). It was found that hydrothermal sucrose templates which were heated at the same temperature (200 °C), but different duration (2h and 4 h) have slightly different active groups. CNS template which is completely different from the hydrothermal sucrose template and hydrothermal sucrose treated for longer time (4h) are making same product of Bi_2O_3 at 450 °C and 600 °C calcination. However, hydrothermally treated sucrose at 200 °C and shorter time (2h) produced a composite $Bi_2(SO_4)_3$-Bi_2O_3 at 450 °C, and Bi_2S_3-Bi_2O_3 at 600 °C calcination. Further experiments revealed that Bi_2O_3-Bi_2S_3, which was synthesized on CNS template made from sucrose at 200 °C for 2h showed the best performance for iodide removal.

4.2. Introduction

Bismuth materials, specifically Bi_2O_3 and Bi-SO_4, have been synthesized differently by various studies. Any variations in the synthesis procedure could result in a difference in the chemical composition, morphology, and size. Application of surfactant/alcohols (like ethylene glycol, ethylene, ethanol)/urea and their ratio to water, type and concentration of precursors and template, sulphate concentration, temperature and time of thermal treatment are all factors which would affect morphology, size and porosity of bismuth materials such as $Bi_6S_2O_5$, $Bi_2O(OH)_2SO_4$, and Bi_2O_3 [1-6]. For example, $Bi_2(SO_4)_3$ at higher temperatures would convert to α-Bi_2O_3, however, existence of small amount of sulphate (0.05%) could affect the final product [7].

Templates-facilitated synthesis provides a means to control the shape, chemical structure and size of the produced material. The functional groups on the template would control and facilitate the bismuth coating on it [6]. The synthesis of template itself could be a tedious procedure; it is important to select and design the template material for attaining

the good compatibility, good bonding with the target material, and appropriate porosity. Another criteria is whether the template can be easily removed [8]. For this reason, carbonaceous template is a good option as they can be easily removed at high temperature of calcination.

One of the processes that could give cheap and easy access to the carbonaceous porous materials as synthesis template is hydrothermal processes. Hydrothermal synthesis takes place at high temperature (150-250 °C) and under pressure. This is an efficient and inexpensive carbonization process with wide precursor selection, such as cellulose, sucrose and agricultural wastes, and with consistent carbonaceous product possessing a uniform morphology and high oxygen containing functional groups [9]. One of cheap carbonaceous precursors is sugar (e.g. sucrose) which would dissolve in water and after hydrothermal reaction would form furfural or Hydroxymethyl furfural (HMF), then would go for further reactions of polymerization and condensations and form carbonaceous materials with the functional groups of OH and C=O [10]. Agglomeration of carbonaceous materials and de-oxygenating is more plausible at temperature higher than 200 °C and aromatization of carbonaceous material would happen at higher residence time. At temperatures higher than 180 °C, the intramolecular condensation, dehydration and de-carboxylation reactions would happen, which would result in various particle sizes. The more aromatization happens the bigger size particles with less carboxyl and carbonyl groups on it would be produced [11]. Other carbonaceous material is carbonaceous nanosheet (CNS), that is known for high porosity and therefore high capability of adsorption. This material has high nitrogen compound on it [12].

Bi_2O_3-Bi_2S_3 composite showed is a good sodium capacitor, because of n-p type heterojunction. Bi_2O_3 (E_g 2.8 eV) and Bi_2S_3 (E_g 1.3 eV) which could lead an electric field between them and electrons would transfer to Bi_2S_3, which would result in positive charge Bi_2O_3 [13]. In addition, Bi_2O_3 has been shown to be able to adsorb iodide [2].

This chapter will describe the effect of various parameters on the synthesized material. In addition, it will show the characterization of different materials which were obtained at different stages. Various products were made based on various templates, based on the functional groups. Here, we use sucrose to see the effect of oxygen containing functional groups and CNS to see the effect of nitrogen containing groups on the yield of production

(how much attach the precursor to the template) and the final products (chemistry of the functional groups).

The products at different stages were characterized by BET, SEM, DLS, XPS and XRD. The micro-nano bismuth composites were then tested on their efficiency for removing trace amount of iodide. Later the best one would have been chosen for the iodide and bromide removal at trace concentrations.

4.3. Materials and methods

All chemicals were used were analytical reagents and did not being processed further. Bismuth nitrate ($Bi(NO_3)_3$ with 99% purity), sodium sulphate, sodium iodide, sucrose, and glacial acid were purchased from Chem-Supply Australia. Glassware and plasticware were cleaned before each usage.

4.3.1. Methods of chemical analysis and characterization

Iodide was measured by iodide ion-selective electrodes (TPS) and were connected to the smartCHEM-Ion3, measured automatically and recorded every second. The iodide ion-selective electrode was calibrated each time.

The surface chemistry of synthesized materials was characterized with a Kratos Axis ULTRA Xray Photoelectron Spectrometer incorporating a 165 mm hemispherical electron energy analyzer. The XPS was equipped with a monochromated Al-Kα (1486.6 eV). X-ray source operated at 150 W (15 kV, 10 mA) with a base pressure 1.0×10^{-9} torr and pressure during analysis of 1.0×10^{-8} torr, to detect the element compositions. Atomic concentrations were calculated using the CasaXPS version 2.3.14 software and a Shirley baseline with Kratos library Relative Sensitivity Factors (RSFs). Peak fitting of the high-resolution data was also carried out using the CasaXPS software. A Fourier transform infrared spectroscopy (Perkin Elmer 'Spectrum Two FT-IR Spectrometer' with an ATR accessory) was used for characterization of samples. The vacuum-dried samples were pressed into a pellet. The structural properties of samples were evaluated through X-ray diffraction (Powder X-ray diffractometer, X'pert Pro) with Cu-Kα radiation, 40 kV anodic voltage and a 50 mA current. A scanning electron microscope (SEM, JEOL 7001) operated at 15 kV, was employed to examine the morphologies of samples. The samples for SEM observation were prepared by coating onto a silicon wafer. The nitrogen adsorption and desorption isotherms were measured at the liquid nitrogen temperature (77 K) using a TriStar II 3020 automated surface area analyzer.

4.3.2. Synthesis procedure

For synthesis of nano sized bismuth materials, different factors were considered. One of them is the template and the other one is the temperature of the calcination. Because different templates could have different functional groups and different porosity which could lead to formation of different bismuth materials. For this aim, different templates of hydrothermal sucrose at 200 °C for 2h, and hydrothermal sucrose at 200 °C for 4h, and CNS were used. Their synthesis procedure would be explained in the related sections. Furthermore, they are being characterized with a various method of BET, SEM, and XPS. The second parameter which could affect on the final product is the calcination temperature which is selected 450 °C and 600 °C, and the steps of calcination in all were kept constant of 5 °C/min. It is notable that the materials which were made from the mixing of template with the formed particles in solution were also characterized with various methods of SEM and XPS, to find out the functional groups and what has been formed. The next step is the products which has been formed at different calcination temperature were also characterized by SEM, DLS, XRD, and XPS. Various templates and calcination temperatures have led to different final materials.

4.3.3. Experimental

4.3.3.1.Sucrose templates synthesis

For obtaining carbonaceous templates from sucrose, 130 g of sucrose were mixed in 250 mL deionized water and then were hydrothermally heated by 200 °C in autoclave for 2h and 4h. Then, the obtained material was washed with de-ionized water and 100% ethanol.

Different hydrothermal time was being used, because various hydrothermal time would effect on the functional groups of hydrothermally carbonaceous material that would obtain [11]. As one molecules sucrose is made from one molecule glucose and one molecule fructose, therefore, the glucose part would have the below reactions in the hydrothermal reactions and might form poly furan (Figure *4-1*) [11]. Different hydrothermal reaction time would affect the amount of oxygen containing molecules such as C-O and carboxylic groups (COOH).

Polyfuranic intermediate is stable and does not further react if T ≤180 °C, which would lead to Aromatic network composed HTC Carbon
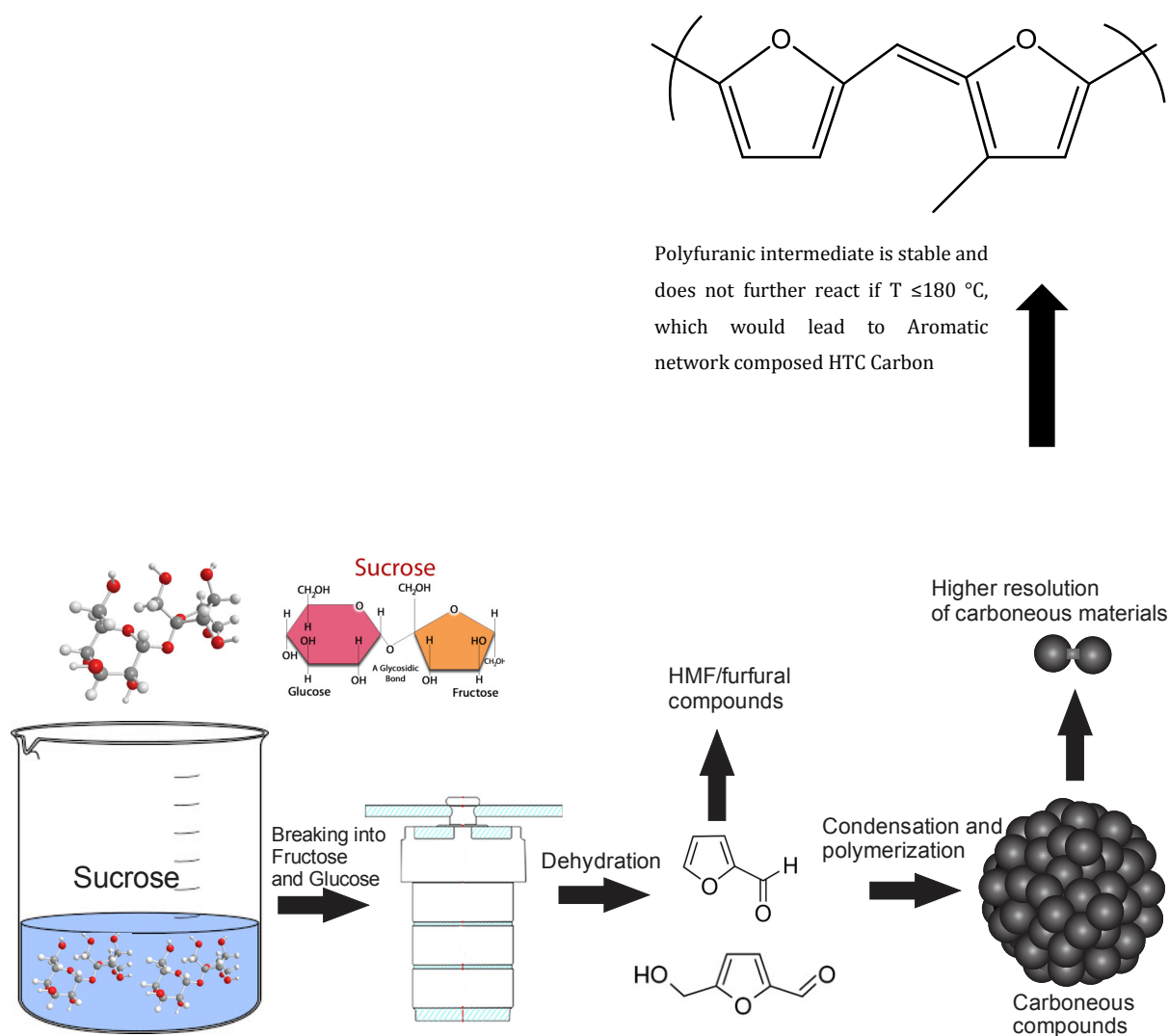
Figure 4-1. The process of carbonaceous material production from sucrose at 180-280 °C, explained by [9, 11].

4.3.3.2. CNS synthesis

CNS synthesis has been followed by the previous studies [12], which is dissolving of 0.5 g of melamine in the 10 mL of glycerol, then following adding 10 mL acid sulfuric (98%) and stirring. The final solution would be led to an autoclave vessel and would be heated for 4h at the temperature of 180 °C. The polymerized product would be washed with Milli-Q water and ethanol three times for the impurity removals [12]. Melamine can react with acid sulfuric and forms the following product (Figure 4-2) [14], however, our synthesis is under autoclave pressure and glycerol has been used, therefore, CNS might be different from the below product or might have this product partially.
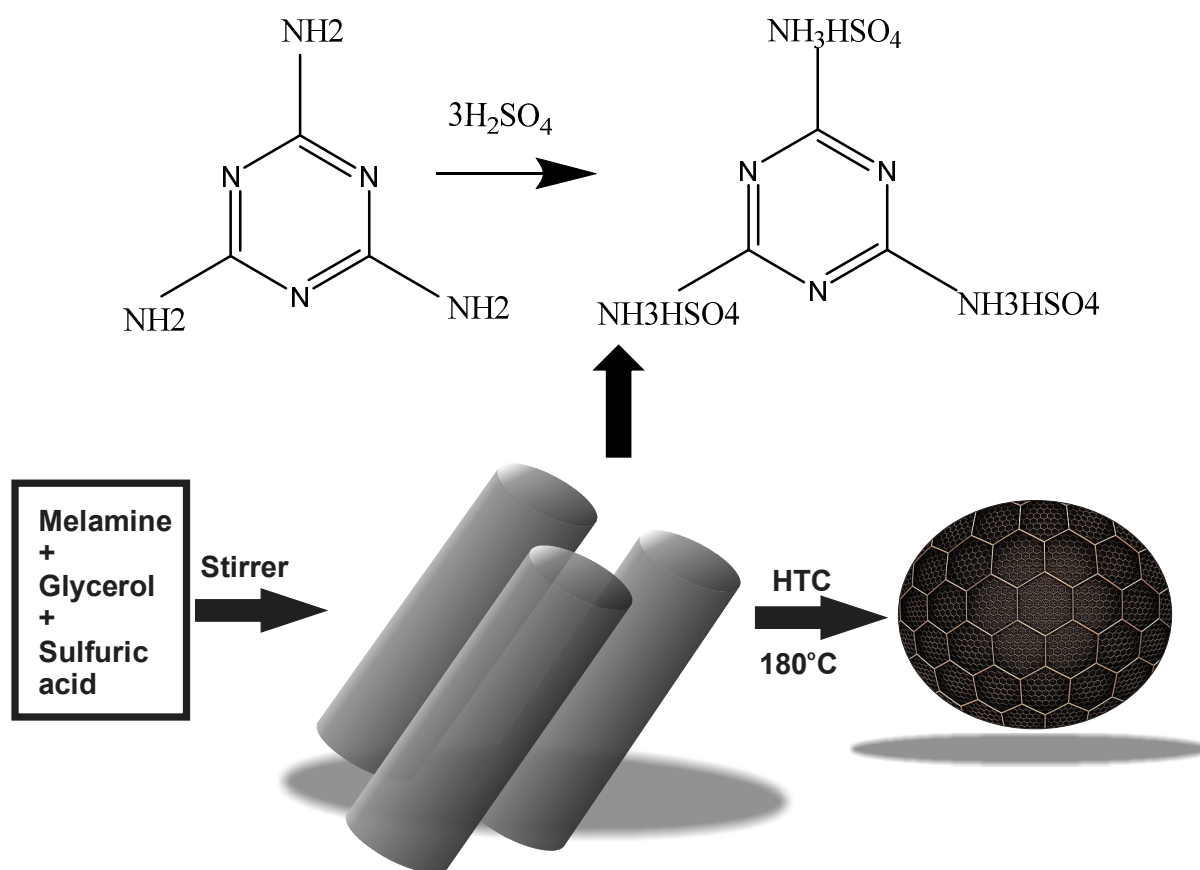
Figure 4-2. CNS production procedure modified image from [14, 15].

4.3.3.3.Synthesis of bismuth composites and final bismuth products

1mmol of $Bi(NO_3)_3$ was dissolved in 150 mL of 10% acetic acid, then 1 mmol of Na_2SO_4 was added to the solution. At this stage, small white particles would be formed, and the white emulsion would be seen in the solution. Subsequently, 0.6 g of carbonaceous template would be added to the solution and would be stirred for 6-8 h. Finally, the suspension would be collected and washed several times with deionized water and ethanol, finally would be air dried at 80 °C. The final products from various templates mixture with the obtained white emulsion would be calcined by 450 °C and 600 °C with the rate of 5 °C/min. The schematic of synthesis has been shown in Figure 4-3.
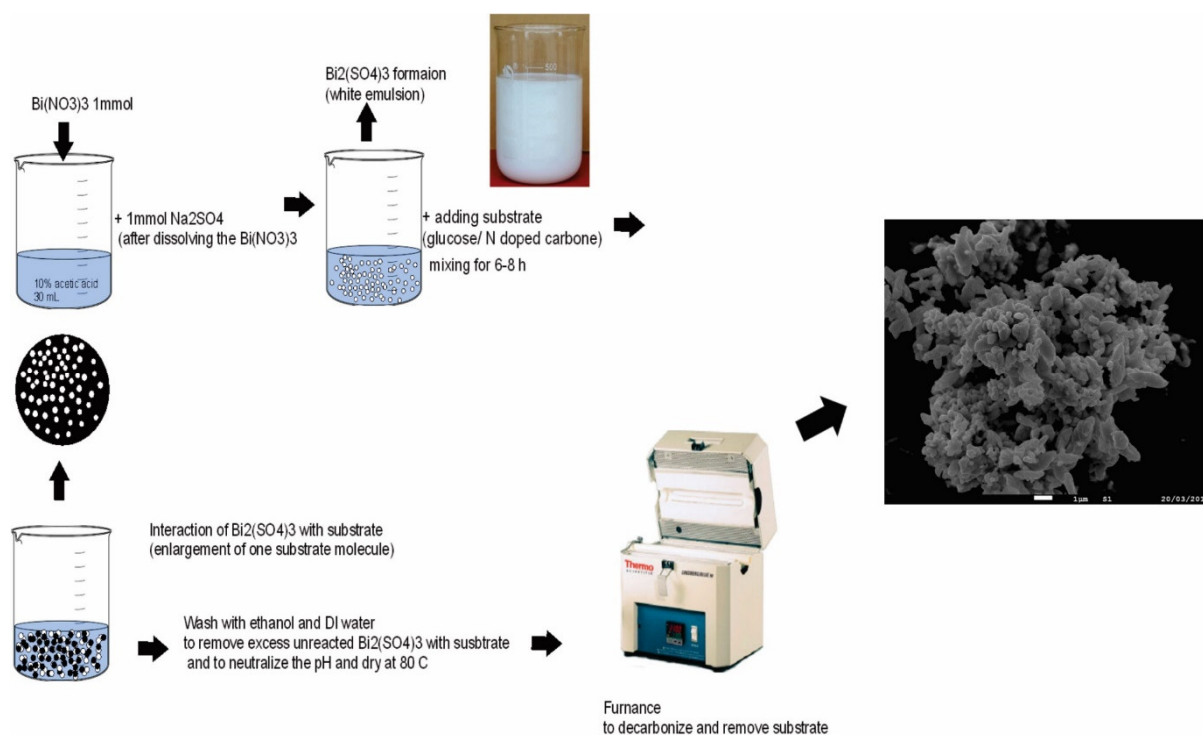
Figure 4-3. Schematic of the experiment procedures for synthesis of bismuth composites.

Table 4-1. Products, composites and template gotten from the templates.

Final products sample name	Composite products	Sample name (template)	Time of hydrothermal Reaction for template (h)	Calcination heating rate (°C/min)	Template
BS-2-200-450	BS-2-200	S-2-200	2	5	sucrose
BS-2-200-600				5	
BS-4-200-450	BS-4-200	S-4-200	4	5	sucrose
BS-4-200-600				5	
BCNS-450	BCNS	CNS	4	5	Melamine
BCNS-600				5	

4.3.3.4. Iodide removal experiments

Iodide solutions were made from sodium iodide with concentration (5 mg/L), then 20 mL of the solution were transferred into the beakers and were constantly agitated with a stirrer and magnet (500 rpm). For understanding which sample a better candidate for the halide removal is (iodide and bromide in the next stage), 5 g/L of the adsorbents (samples synthesized) were added to 20 mL iodide solution with initial concentration of 5 mg/L. Subsequently, the concentration of the iodide was monitored and recorded continuously at every second by iodide ion-selective electrodes, and experiments were carried out within 180 min.

The removal efficiency of synthesized adsorbents was calculated by Equation 4-1, where C_i and C_e are the initial and equilibrium concentrations of iodide (mg/L).

$$Halide\ removal, \% = \left(\frac{C_i - C_e}{C_i} \right) \times 100\% \qquad \text{Equation 4-1}$$

4.4. Results and discussion

4.4.1. Morphology

4.4.1.1. Templates

Templates were characterized by SEM to see their morphology. The SEM images S-2-200 has been shown (Figure 4-4a). The morphology is circular/ball shapes (attached together) with the size of few μm.

The morphology of S-4-200 shows same morphology of S-2-200. This shows that the time of reaction from 2-4 h (treating hydrothermally) would not affect the morphology of HTC-sucrose (Figure 4-4b).

Another template which was being used is CNS. The morphology of this material has been shown to be small patches of small particles, which when it is magnified is showing like a honeycomb. In addition, each small honeycomb rooms have a diameter, which is shown in the SEM images (Figure 4-4c).
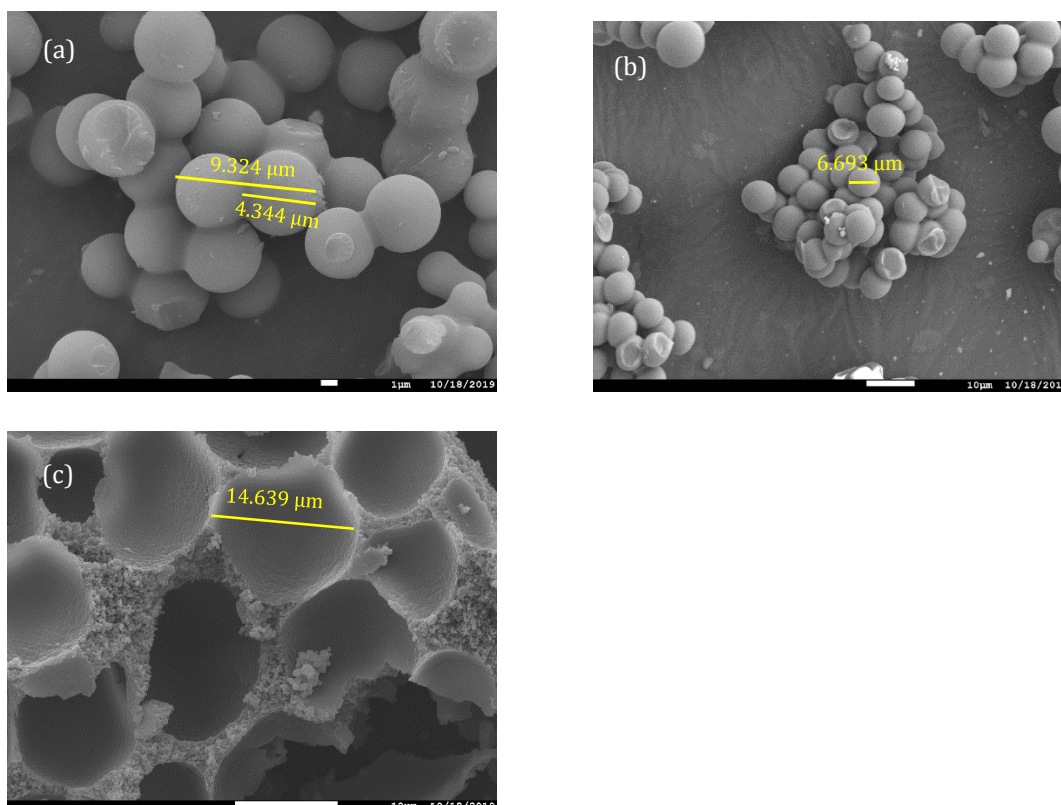
Figure 4-4. SEM images of different synthesized templates: (a) S-2-200 (b) S-4-200, (c) CNS.

The BET measurements showed that S-2-200 and S-4-200 templates were under detection limit of the BET instrument. It is obvious after SEM images of glucose samples that they are not porous as they are big ball shapes with the diameter of few μm. That's is because that sucrose hydrochars without any carbonization would not show any porosity, but after carbonization under nitrogen gas would have a higher porosity [16]. However, BET for CNS template showed quite good results with BET surface area of 1096.1588 m^2/g (Figure 4-5).
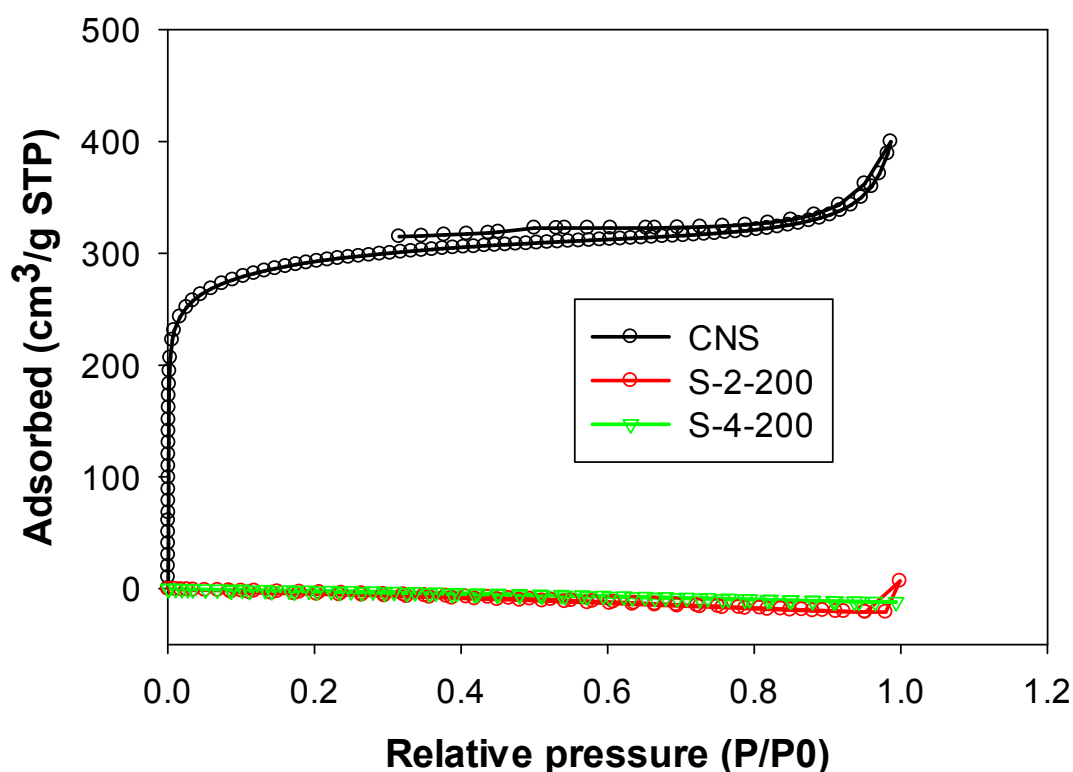
Figure 4-5. N$_2$ adsorption and desorption isotherms for various templates of S-2-200, S-4-200 and CNS.

4.4.1.2. Composites

SEM images of samples after mixing with the bismuth particles (Bi-O and Bi-SO$_4$ species) in the solution with different templates are shown (Figure 4-6). As can be seen, the bismuth particles were deposited on the templates. S-2-200 and S-4-200 with bismuth particles composites are showing similar morphologies. The circular shapes of hydrothermal sucrose are observable in both BS-2-200 and BS-4-200. However, CNS-bismuth particles composite is showing different morphology, and that is because of different templates have different morphology. Bismuth particles deposited on different templates are having similar morphologies, which is a rough layered morphology.
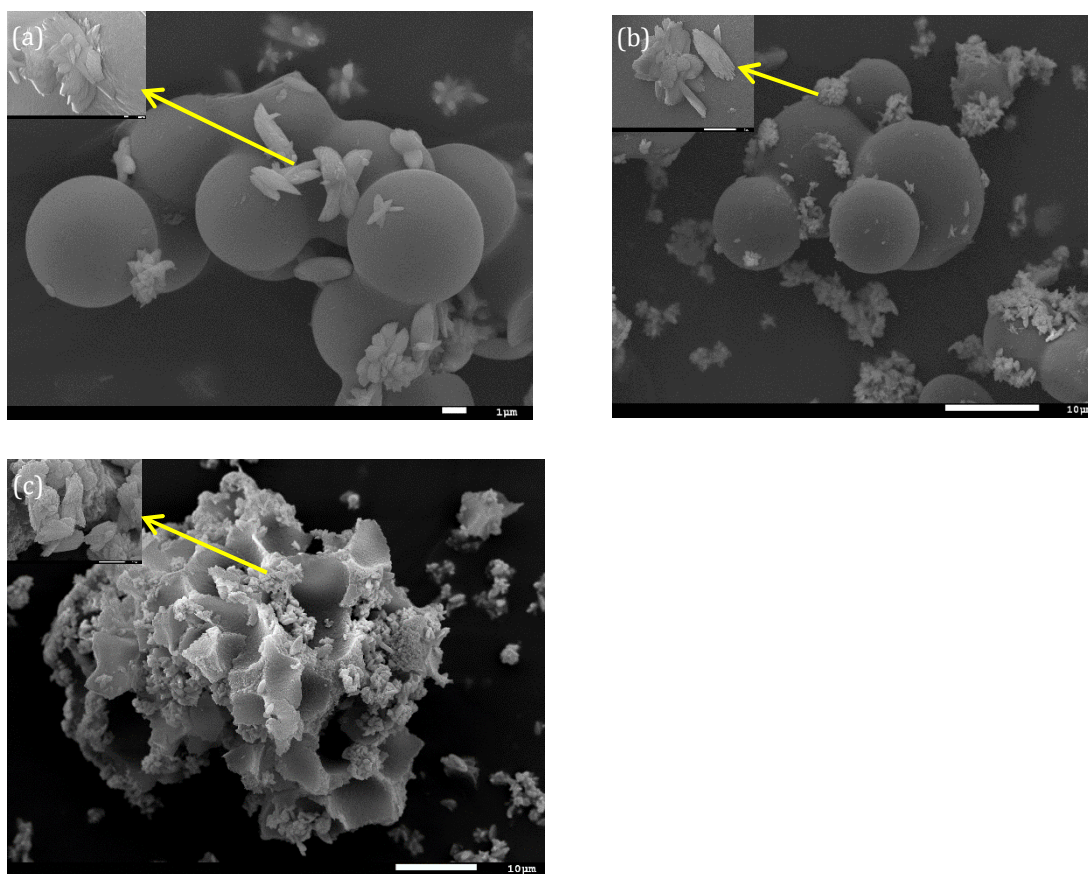
Figure 4-6. SEM images of (a) BS-2-200 (b) BS-4-200, and (c) BCNS [bismuth products on the templates are magnified and shown on top of each image].

4.4.1.3. Bismuth micro nano particles

Morphology of final products which were calcined at 450 °C are shown in Figure 4-7. As can be seen de-carbonization did not happen fully and the hydrothermally sucrose are observable. However, the structure of CNS is hardly observable because is covered by the bismuth particles. However, by the visual observation still CNS was in the sample after 450 °C, the sample was grey, which indicating of carbonaceous material exist in the sample. The magnified of the bismuth particles which was formed on the top of the templates (S-2-200, S-4-200and CNS). As can be seen, bismuth particles have a rough surface with scallop shape.
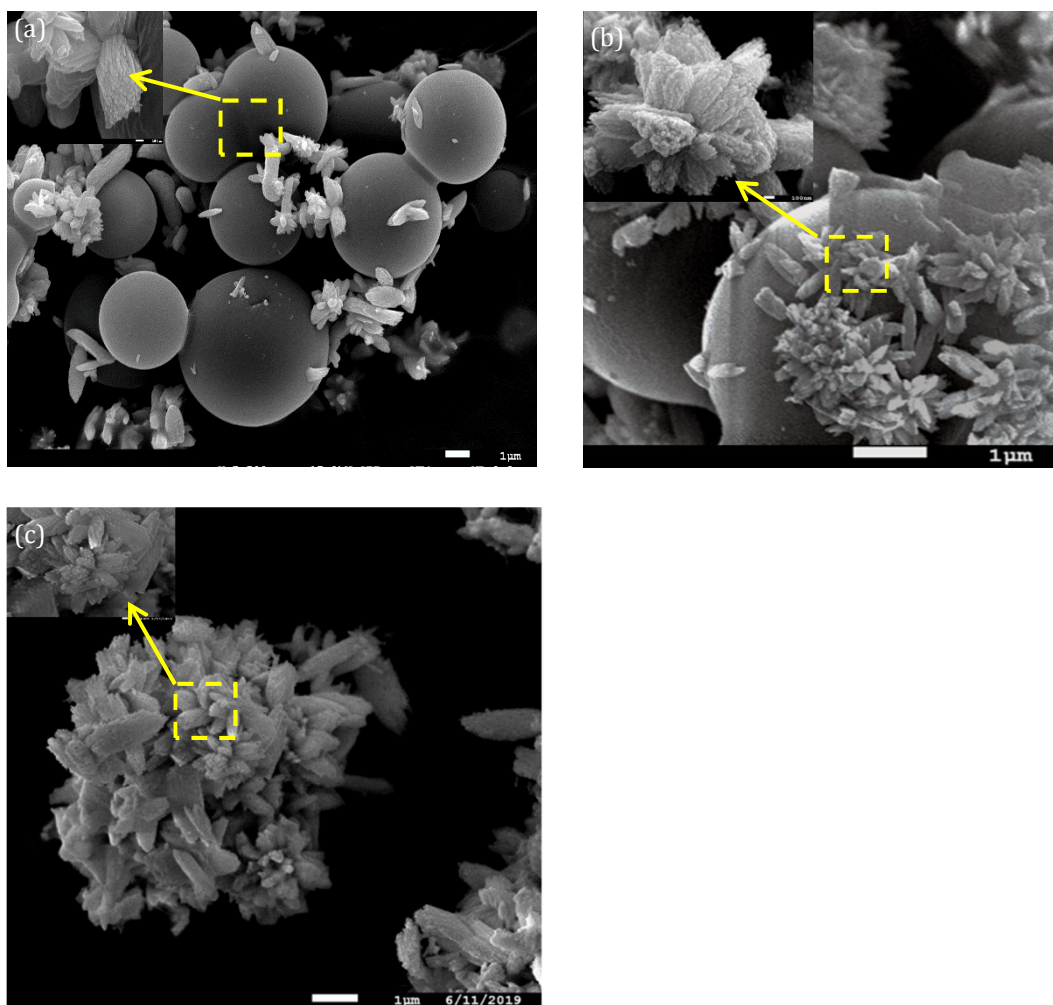
Figure 4-7. SEM images of samples after calcination with various magnification at 450 °C (a) BS-2-200-450 (b) BS-4-200-450, (c) BCNS-450 [bismuth particles on the templates are magnified and shown on top of each image].

Morphology of final products which were calcined at 600 °C are shown in (Figure 4-8). Samples after calcination at higher temperature (600 °C) showed to get smaller because of removing the templates and would be consisted of nano and micro particles. The below image it is showing the population of smaller sizes are more than bigger ones (Figure 4-8a). The particles of all products (calcined at 600 °C) are agglomerated together (Figure 4-8). Furthermore, the calcination at higher temperature of 600 °C shows that has removed the carbonaceous templates, completely.
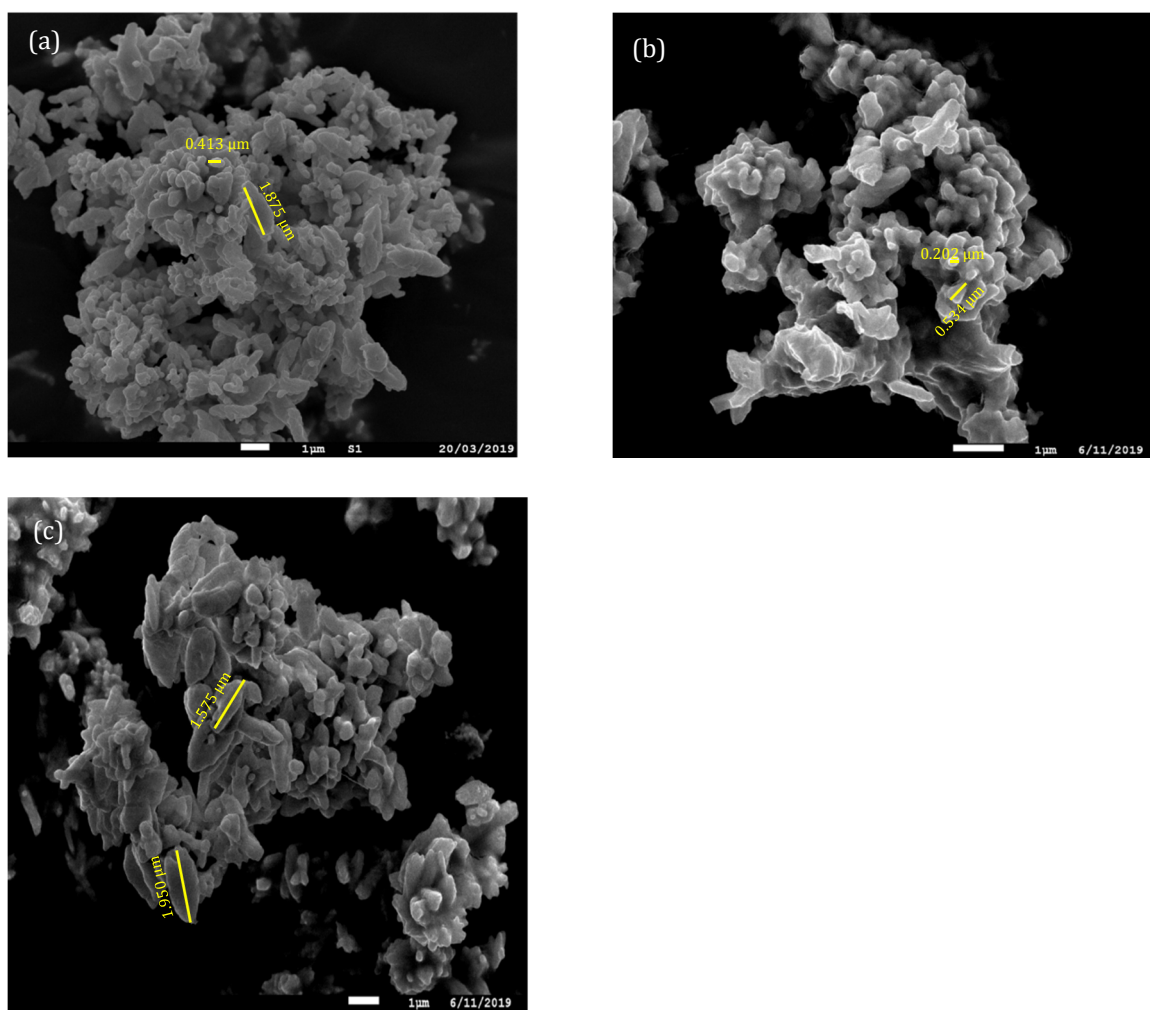
Figure 4-8. SEM images of samples after calcination at 600 °C with different magnifications: (a) BS-2-200-600 (b) BS-4-200-600 at different perspectives, (c) BCNS-600.

Generally speaking, calcination at 450 °C will make the surface of material scallop shape and rough, however, at the 600 °C the roughness of the surface would be removed and will turn into a softer surface shape. Also, templates of S-2-200 and S-4-200 at 450 °C is observable (round shape balls) and CNs is not probably is the same shape as the material. This depicts that the calcination at 450 °C was not enough to de-carbonize material, which is also observable the material at 450 °C calcined would be in grey colour indicating of carbon existence and in 600 °C is white and yellow mixtures.

DLS was used for measuring the final products sizes and the measurements were done 3 times. The results show that all products are mixture of nano and micro sized particles at 450 °C and 600 °C (Figure *4-9*). In addition, the synthesized materials after calcination

at 600 °C would have smaller size compared to the 450 °C. This trend also has been seen in other samples, too. This is due to the more removing of carbonaceous templates with big size at higher temperature 600 °C. This data obtained from DLS are in agreement with SEM images too and shows that products are mixtures of nano and micro particles.
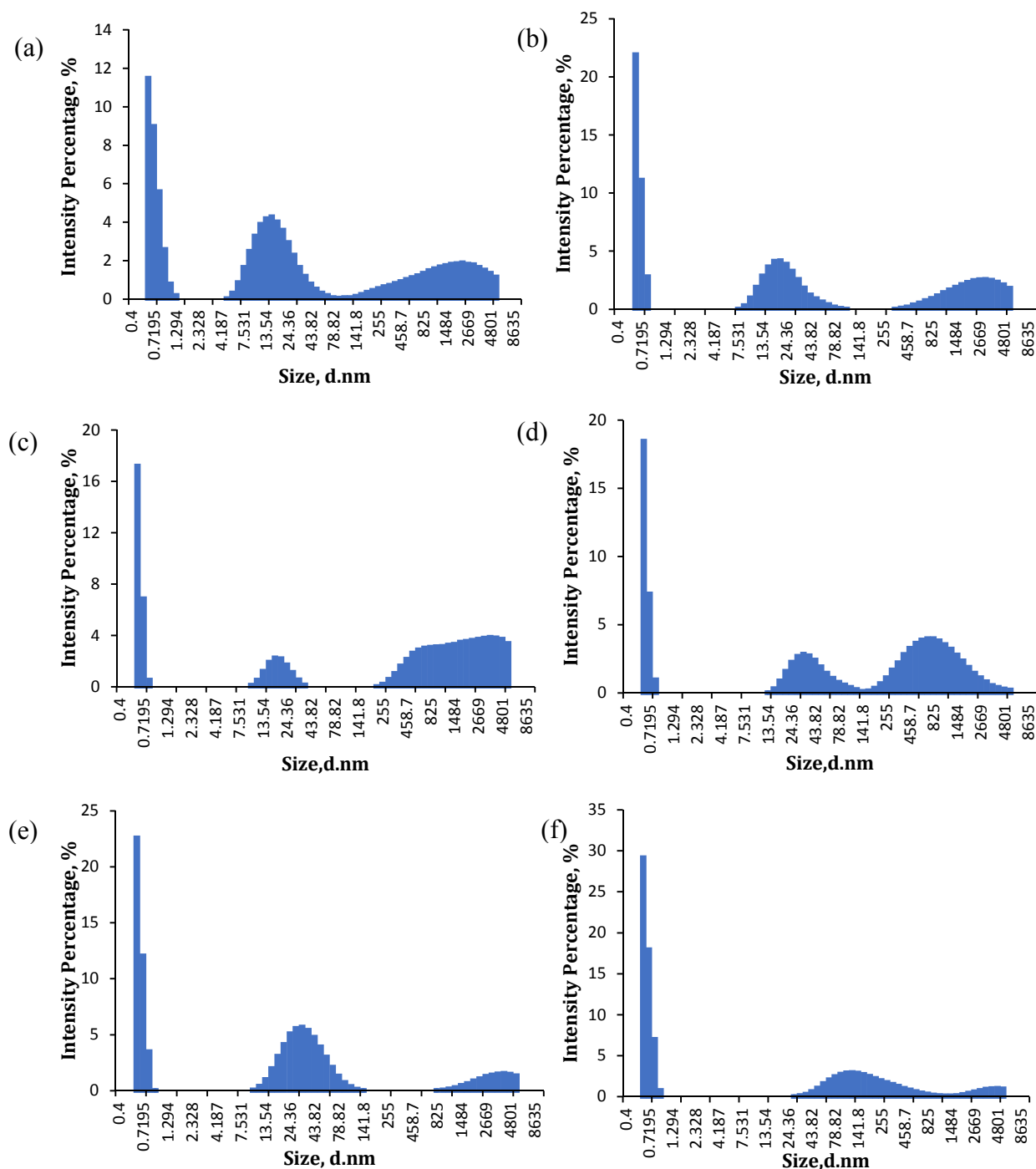
Figure 4-9. Sizes of materials after calcination at 450 and 600 C with 5°/min. (a): BS-2-200-450 (b): BS-2-200-600, (c): BS-4-200-450, (d): BS-4-200-600, (e): BCNS-450, (f): BCNS-600.

4.4.2. Chemical composition

4.4.2.1.Templates

The XPS survey related to the S-2-200 template shows in Figure 4-10. It shows that the carbon is mostly C-C within the structure of O_2-C—CH_3 or is within reaction with oxygen. The oxygenated carbons are in the form of C-O or C=O. Furthermore, with analysis and deconvolution of oxygen region in the survey it was observed that the C-O is binding with an aromatic structure in the form of O_2C-aromatic partially and some other parts are in the form of O_2C=O or –(C=O)-O*-(C=O)-, and C=O is binding with an aliphatic structure in the form of O-C=O-C.

This shows that this structure has readily active oxygen to bind with bismuth, because C=O is in the aliphatic form and although C-O is mostly binding with aromatic structure but needs less energy to bind with bismuth than C=O (the energy to split the C=O is more than splitting C-O structure normally).

Figure 4-10. Survey XPS spectrum of S-2-200 sample (a): whole spectrum, (b) C1s, (c) O 1s.

Template S-4-200 is also is showing carbon and oxygen regions (Figure 4-11). The carbon region in the survey shows that carbon is in the form of C-O or C=O. However, with deconvolution of oxygen region it is revealing more information. Almost half of oxygen is in the form of C=O which is in the structure of aromatic (O—C—Ar with double bond O). The rest of oxygen (almost half) are in the form of C-O in O-C=O aliphatic or C-OH (Figure 4-11).

The difference of S-2-200 and S-4-200 templates are: 1) in oxygen region; C=O in the S-2-200 is in the structure of aliphatic and C-O in the aromatic structure. However, in S-4-200, it gets vice versa. Specifically, C-O is in the aliphatic form and C=O is in the aromatic forms.

This means that C=O combined with aromatic structure is harder to react with bismuth particles in S-4-200 sample, compared to C-O binding with aromatic S-2-200 samples.
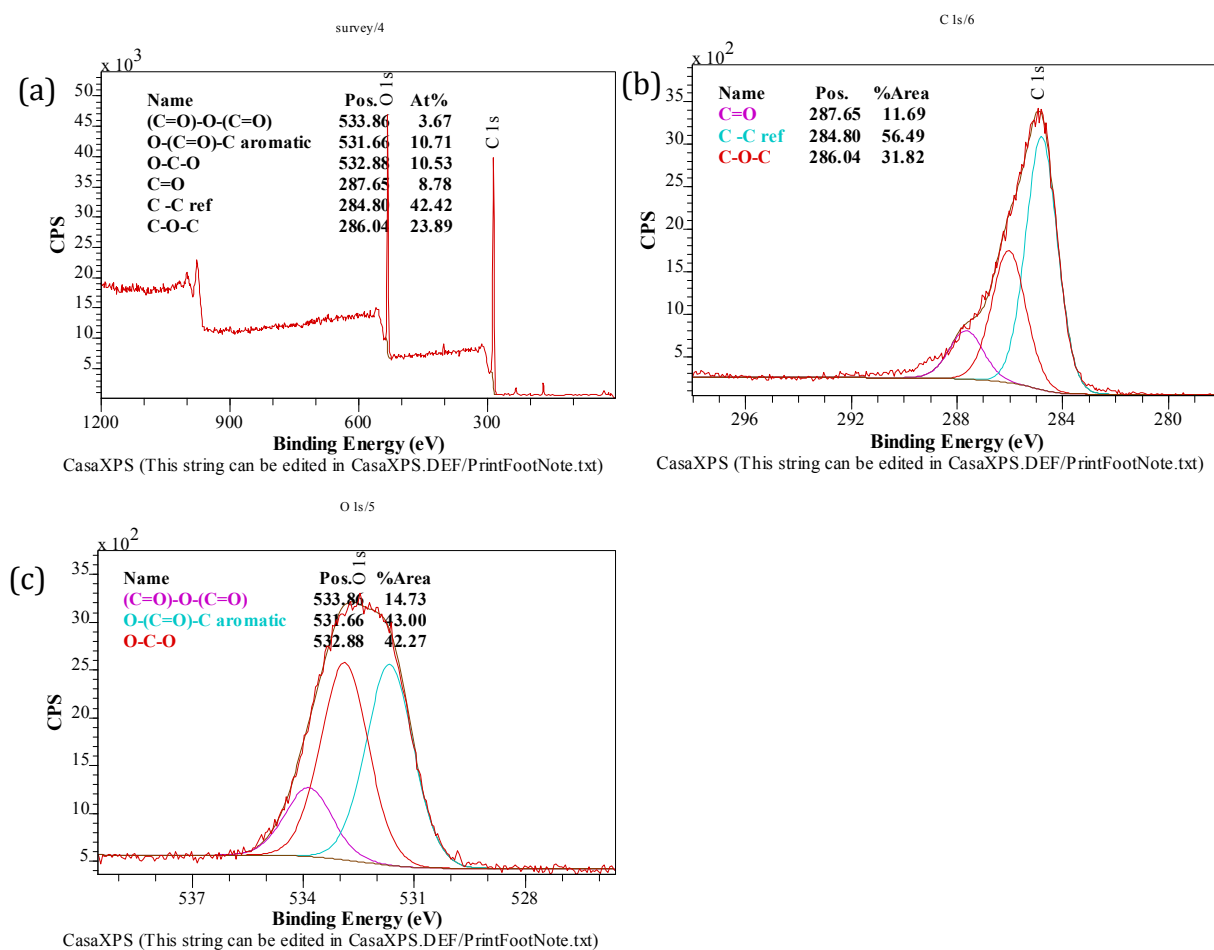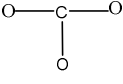
Figure 4-11. Survey XPS spectrum of S-4-200 sample (a): whole spectrum, (b) C1s, (c) O 1s.

XPS of CNS has been shown in Figure 4-12. As in the synthesis of CNS acid sulfuric was being used the peaks of sulfate has been showed and are dominant in the S2p region. Also, some of sulfate has been bind to the melamine ring as sulfinyl R_2-SO was being observed in the XPS. However, the percentage is very small and most of sulfur in the material is in the form of S2p.

In the carbon region, C-O has been found in the region, which it can be in the form of C-O-C, -C-OH, or C-O-C=O. Furthermore, C=OOH or C-O in O-CO_2 ( ) has been found in the carbon region. C with N (-C-N species) has been found in the XPS regions of carbon which is related to melamine ring [12, 17]. Finally, pi-pi interaction in the carbon region has been found which is indicating of carbon-carbon pi-pi interactions as a result of rings pi-pi interactions. C=C was found in the survey of C1s, which is indicating the C=C in the polypyrole or it can be between the rings.

In nitrogen region, the pyloric N species (NH in pentagon ring/pyrrole) exhibits an N1s BE peak at 400.3 ± 0.3 eV [18, 19]. Moreover, ammonium salt has been found in the nitrogen region [19]. This shows that melamine has been degraded under pressure and temperature and has formed pyyrole and the rest is in the form of -NH_4^+.

By the investigating, the oxygen region we found that most of oxygen is in the form of SO_4. Also, some of oxygen is possibly in the form of SO_2 connected to the ring (PES), or O=C-N. It is plausible that some of oxygen be in the form of O-C=O connected to an aromatic ring. Only 9.08% of oxygens are in simple single bonds with carbon (C-O) (Figure 4-12). Therefore, this will depict that most of oxygens in the CNS material is very strongly connected and need high energy to overcome and therefore bismuth cannot connect to it, properly. Eventually, the possibility of bismuth connection to oxygen would be less with CNS. This will explain why CNS interaction with bismuth particles (Bi-O and Bi-SO_4 species) was low, specifically, after the mixing and washing off the extra and non-reacted bismuth compound to CNS, most of bismuth compound was washed off, and the yield of production was low.
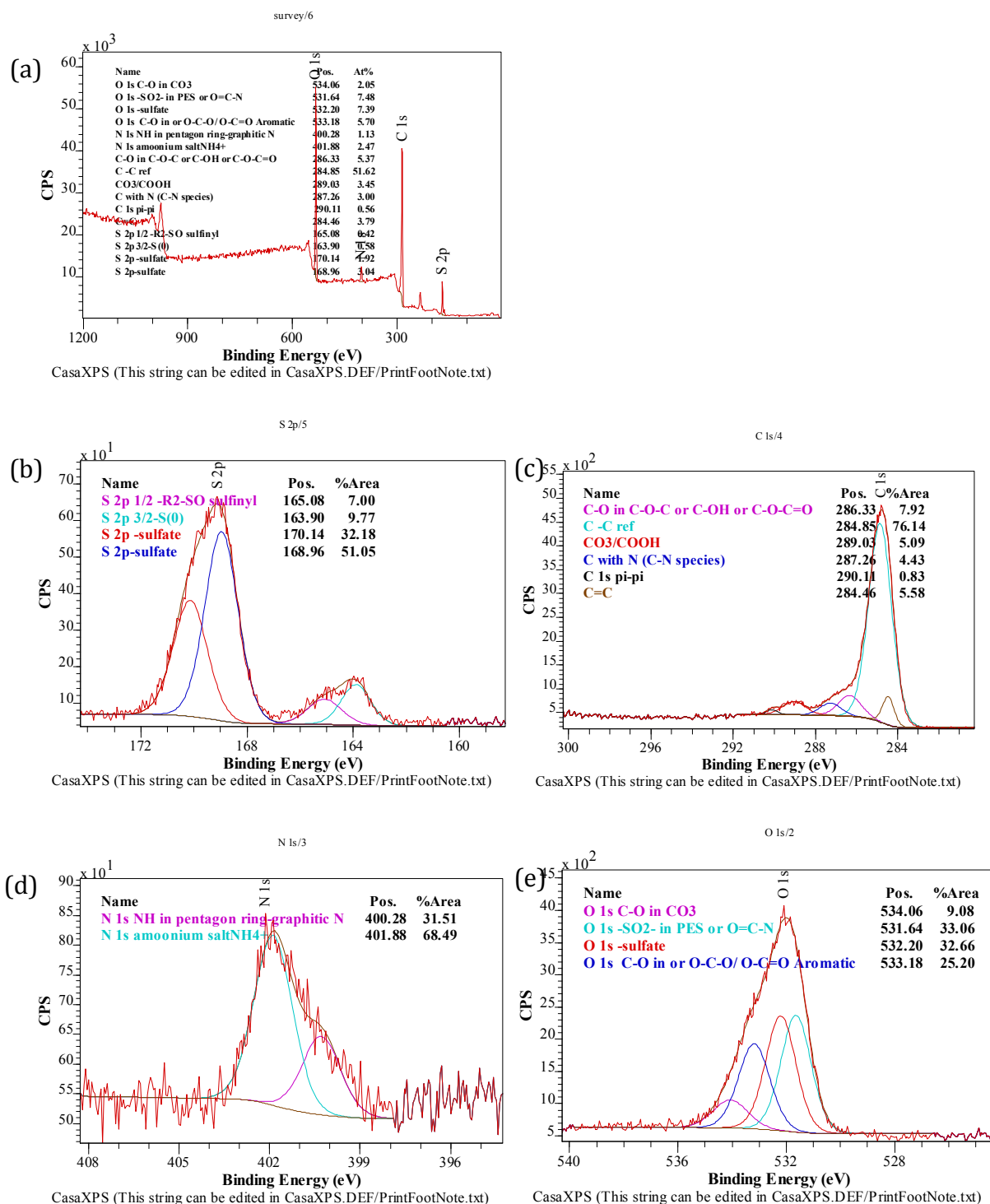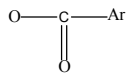
Figure 4-12. Survey XPS spectrum of CNS sample: (a) whole spectrum, (b) S2p, (c) C1s, (d) N 1s, (e) O 1s.

4.4.2.2.Composites

XPS of BS-2-200 has been shown in Figure 4-13. This sample has gotten from the template S-2-200 mixture with the bismuth species precipitates (Bi-O and Bi-SO$_4$ species) and collecting then washing after 8 hours mixing. It will show that some part of precipitate is Bi$_2$O$_3$ and some would be in the form of Bi$_2$(SO$_4$)$_3$. Also, some sulphate also was being

detected in XPS regions of Bi 4f and S 2p, which can be as free sulphate which did not react.

By investigating of C 1s XPS survey, it can be seen that most of carbons are C-O in the context of *C-O-C=O. Then, C=O in the context of ketone/aldehyde are positioned at 287.21 eV [17]. Also, C=O was detected from C-O-*C=O. The percentage of C-O binding is most in the C1S. O1s deconvolution survey depicts that most of oxygens are C=O in the context of *O=C-O-C=O* or SO_4 in the 532.59 eV. C=O (*O=C-O, $\overset{O-C-Ar}{\underset{O}{|}}$) and C-O (*O-C-C=O) have been detected at 531.63 and 533.79 eV, respectively. Furthermore, Bi_2O_3 was detected at 530.52 eV (Figure 4-13).

Figure 4-13. Survey XPS spectrum of BS-2-200 sample: (a) whole spectrum, (b) Bi4f and S2p, (c) C1s, (d) O 1s.

XPS of BS-4-200 has been shown in Figure 4-14. This sample has gotten from the template S-4-200 mixture with the bismuth species precipitates and collecting then washing after 8 hours mixing. This sample is composed of Bi_2O_3 and $Bi_2(SO_4)_3$ (come from the Bi-O and

Bi-SO$_4$ species in the emulsion), which might attach to the template physically or chemically. Also, SO$_4$ was found in which is related to Bi$_2$(SO$_4$)$_3$. C1s showed that most of carbon are in the form of C-O-C, followed by C=O in the complex of (-CH2CH2C=O-)$_n$ [17].

$$O\text{---}C\text{---}O$$
$$|$$
$$O$$
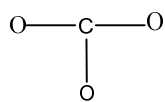
And some of carbon is in form of C-O in   .

O1s has deconvoluted and showed that SO$_4$ and Bi$_2$O$_3$. Also, it has showed C-O binding in *O-C-C=O aliphatic and *C-O-C. This depicts that only aliphatic forms of O-C were detected in the precursor indicating only the aliphatic forms are available for the Bi$_2$(SO$_4$)$_3$ and Bi$_2$O$_3$ energy available to attach. While C=O aromatic was found in the S-2-200 which showing the other forms of oxygen there was also energetically available for the oxygen reaction (in Bi$_2$O$_3$/Bi$_2$(SO$_4$)$_3$) with carbon. Therefore, our theory of glucose 2h is has more active sites to bind with bismuth oxide and bismuth sulphate is confirmed (Figure 4-14).

(a)

Name	Pos.	At%
O 1s C-O aliphatic in O-CC=O	533.69	4.50
O 1s - Bi2O3	530.25	3.22
O 1s sulfate	531.55	15.63
O 1s C-O-C aliphatic	532.48	12.38
C 1s C-O in -CO3	289.14	3.59
C-C ref	284.80	28.02
C 1s C-O-C	285.97	14.43
C with O in poly (-CH2CH2C=O-)n	287.4	7.38
Bi 4f 7/2 Bi2(SO4)3.H2O	161.06	0.94
Bi 4f 5/2 Bi2(SO4)3.H2O	166.37	0.70
S 2p- sulfate	169.36	3.61
Bi 4f 7/2 Bi2O3	160.00	3.20
Bi 4f 5/2 Bi2O3	165.31	2.40

CasaXPS (This string can be edited in CasaXPS.DEF/PrintFootNote.txt)

(b)

Name	Pos.	%Area
Bi 4f 7/2 Bi2(SO4)3.H2O	161.06	8.65
Bi 4f 5/2 Bi2(SO4)3.H2O	166.37	6.48
S2p- sulfate	169.36	33.26
Bi 4f 7/2 Bi2O3	160.00	29.50
Bi 4f 5/2 Bi2O3	165.31	22.11

CasaXPS (This string can be edited in CasaXPS.DEF/PrintFootNote.txt)

C 1s/19

(c)

Name	Pos.	%Area
C 1s C-O in -CO3	289.14	6.71
C-C ref	284.80	52.47
C 1s C-O-C	285.97	27.01
C with O in poly (-CH2CH2C=O-)n	287.41	13.81

Binding Energy (eV)

CasaXPS (This string can be edited in CasaXPS.DEF/PrintFootNote.txt)

(d)

O 1s/18

Name	Pos.	%Area
O 1s C-O aliphatic in O-CC=O	533.69	12.58
O 1s - Bi_2O_3	530.25	9.02
O 1s sulfate	531.53	43.75
O 1s C-O-C aliphatic	532.48	34.64

Binding Energy (eV)

CasaXPS (This string can be edited in CasaXPS.DEF/PrintFootNote.txt)

Figure 4-14. Survey XPS spectrum of BS-4-200 sample: (a) whole spectrum, (b) Bi4f and S2p, (c) C1s, (d) O 1s.

BCNS which is from the mixing of the CNS and precipitates of bismuth particles (Bi-O and Bi-SO_4 species) is shown in Figure 4-15. Nitrogen is not being detected by XPS, because we have ground the CNS mechanically to make it powder and then mixed with the bismuth particles for 6-8 hours. Mechanically grinding of powder resulted in surface contamination and as a result N peak was not found in XPS.

Second understanding of this mixture is that it is also mixture of Bi_2O_3-$Bi_2(SO_4)_3$, which is the precipitate formed in the reaction. Also, the sulphate was detected in the region of Bi 4f + S 2p. Also, C 1s has been shown some of C 1s peaks which was detected in the XPS of CNS, except C-N species peak which is as a result of surface contamination as mentioned before. C-O in aliphatic form (C-O-C/C-O-C=O) was the maximum carbon form detected, which is indicating that aliphatic form was more readily available to react with oxygen of bismuth compound (Bi_2O_3 and $Bi_2(SO_4)_3$). O 1s shows most of oxygen are associated with the sulphate group, then C-O aliphatic and C=O in aromatic ring (Figure 4-15).

CNS mixing at room temperature with bismuth particles and washing after 8 h showed that most of the bismuth particles would be washed off from the template as is not attached to the CNS (white precipitates were washed off from the filter).

From the mixing of hydrothermally sucrose and bismuth composite and washing the residues and filtering them, shows that the yield of S-2-200 binding with bismuth

particles (Bi-O and Bi-SO₄ species) was more compared to the other templates as follow:
S-2-200> S-4-200>> CNS.
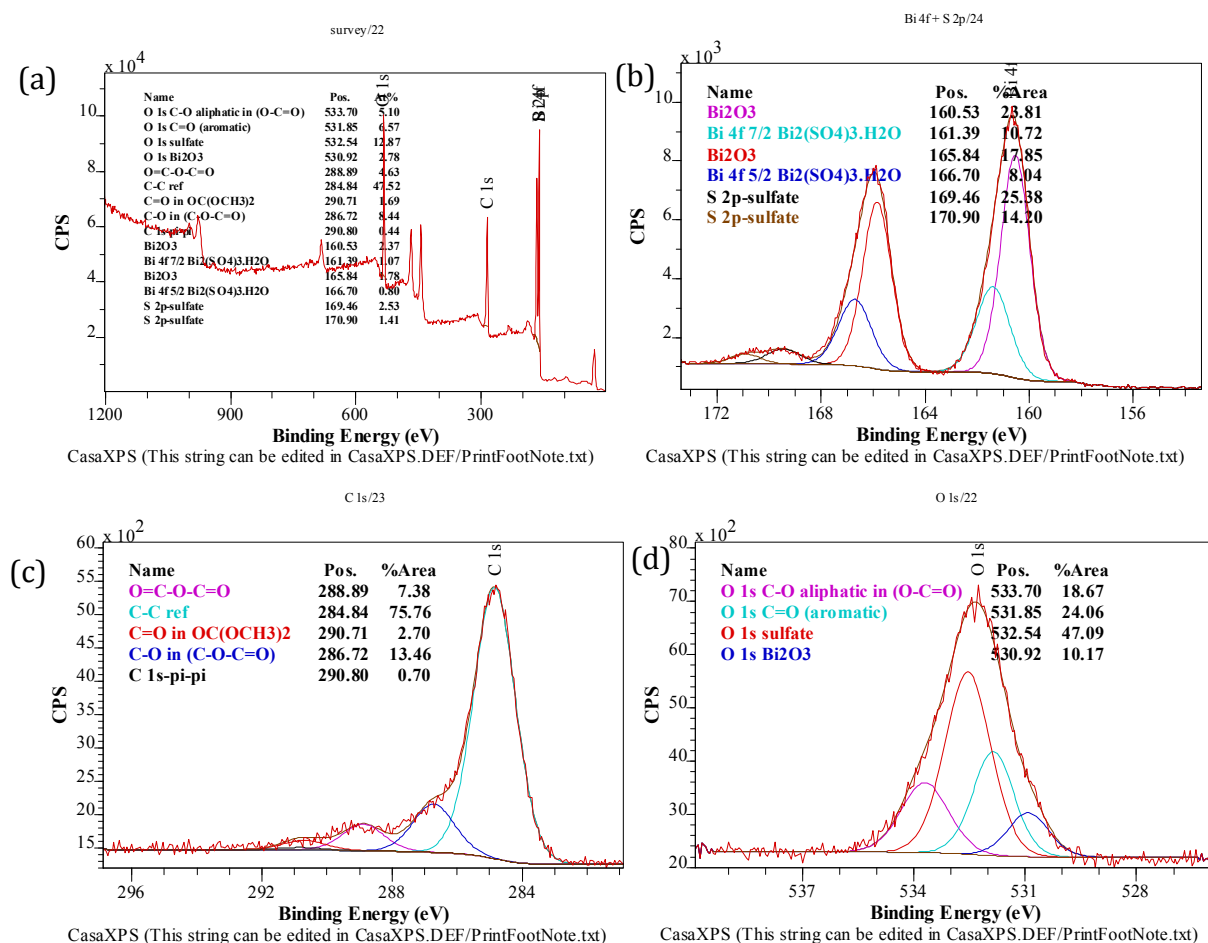
Figure 4-15. Survey XPS spectrum of BCNS sample: (a) whole spectrum, (b) Bi4f and S2p, (c) C1s, (d) O 1s.

4.4.2.3. Bismuth micro nano particles

XPS of BS-2-200-450 is shown in Figure 4-16. BS-2-200-450 showed that after calcination of 450 °C, $Bi_2(SO_4)_3$ was increased and Bi_2O_3 was decreased, which would increase at higher calcination temperature of 600 °C. This is showing that $Bi_2(SO_4)_3$ in S-2-200 grows with increasing temperature by 450 °C and therefore it has more potential to form Bi_2S_3 at 600 °C. In addition, it shows that S-2-200 has more potential sites that sulphate can bind with it. After increasing calcination temperature, the active sites for reacting with sulphate would increase. Specifically, $Bi_2(SO_4)_3$ was 3.78% and Bi_2O_3 64.12%, then after calcination at 450 °C; $Bi_2(SO_4)_3$ was 14.44% and Bi_2O_3 58.04%.

After calcination by 450 °C, the ratio of Bi_2O_3 and SO_4 would be more in the O1s spectrum. However, before calcination the ratio of C=O in O=C-O and SO_4/C=O in O=C-O-C=O were the highest. This is as a result of calcination as well which was removing carbonaceous template partially from the material and therefore, the ratio of SO_4 and Bi_2O_3 would increase in the O1s. Also, the calcined material shows that C-O-C aromatic was detected, and this shows that the composite also has been attached to the aromatic ring, as mentioned before the carbon-oxygen groups (in S-2-200) are more readily and active for the attachment with the bismuth sulphate-bismuth oxide mixed particles in the solution. Last but not least, the carbon C1s had simpler peaks (less peaks) after calcination (Figure 4-16).
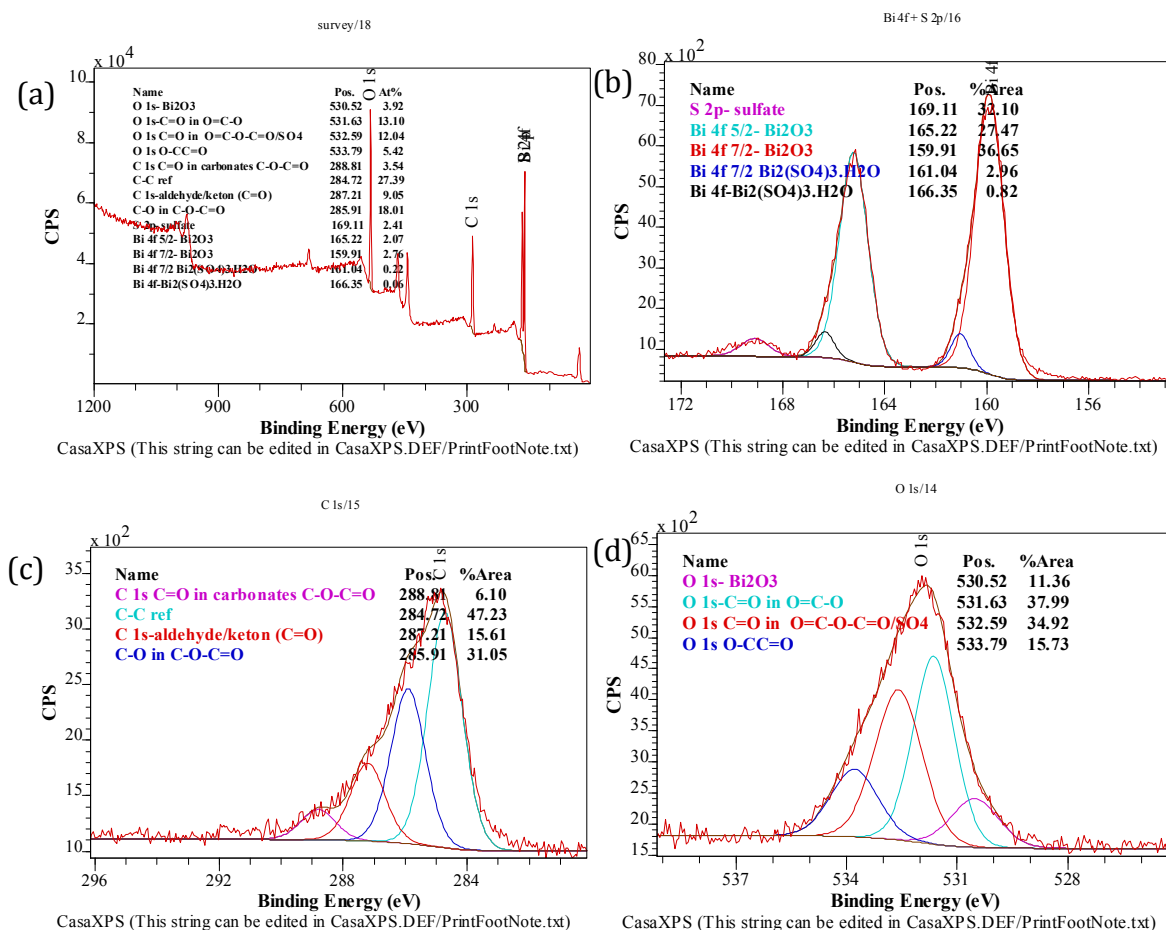

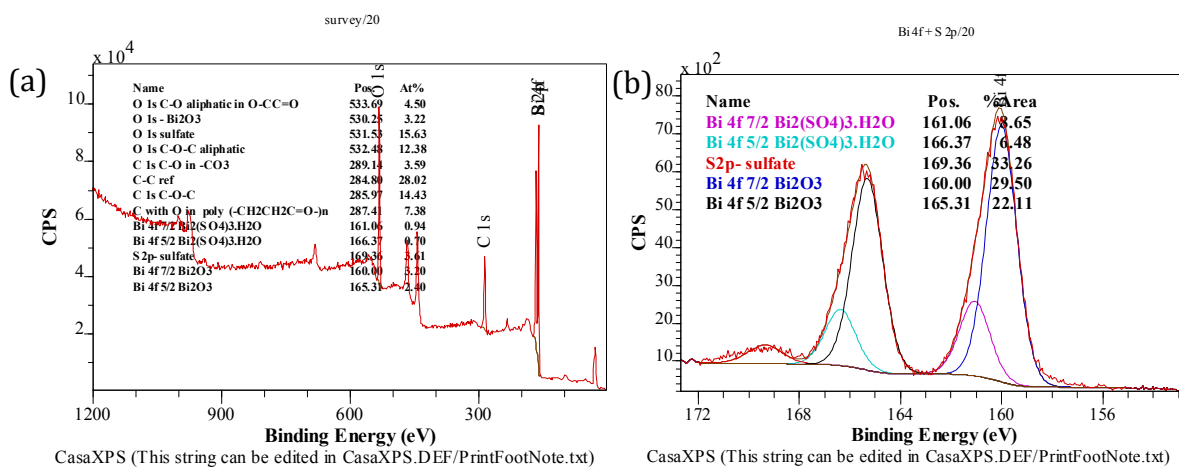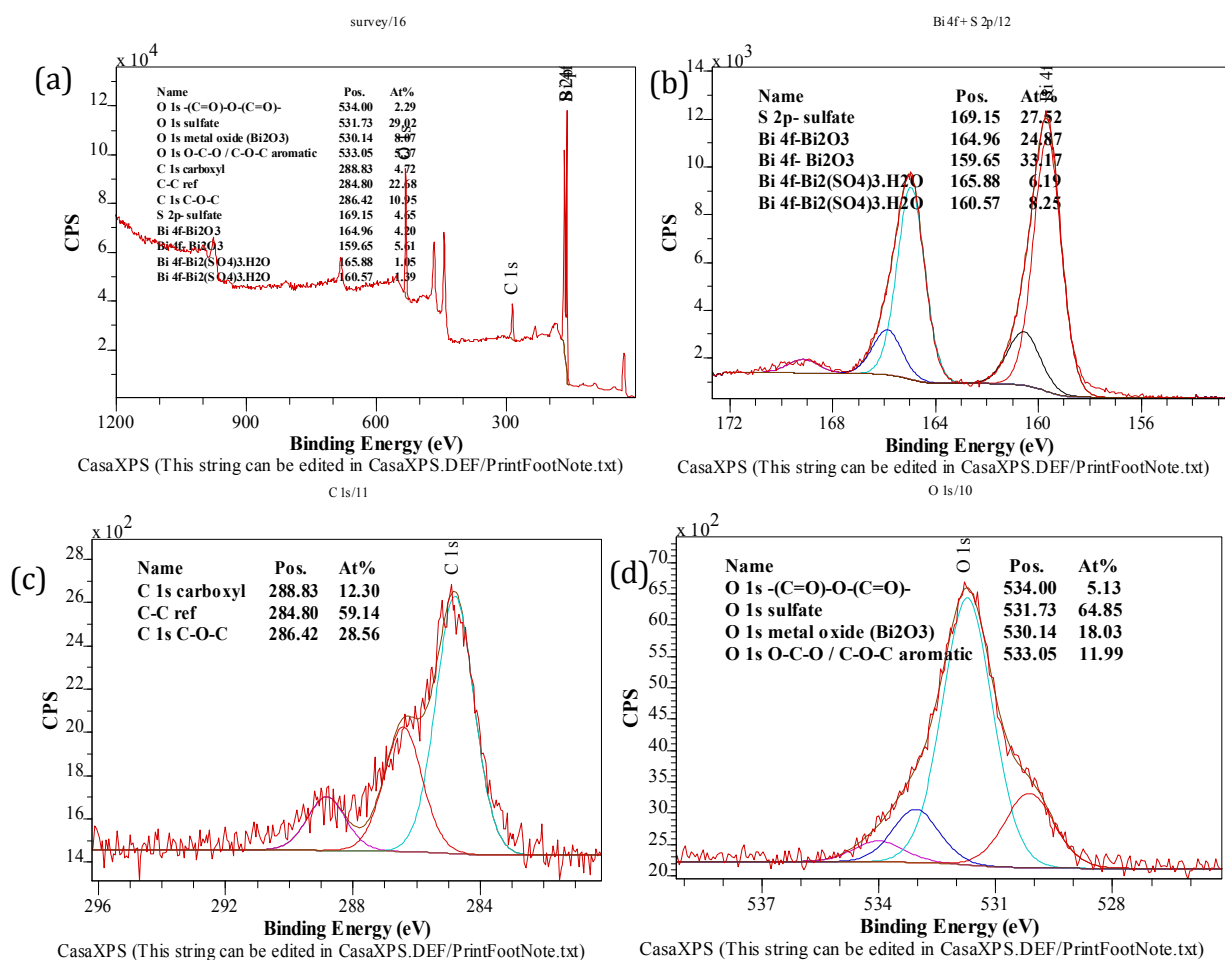Figure 4-16. Survey XPS spectrum of BS-2-200-450 sample: (a) whole spectrum, (b) Bi4f and S2p, (c) C1s, (d) O 1s.

XRD pattern of BS-2-200-450 is shown in Figure 4-17 a, and for fitting the XRD data we used Treor program. As can be seen, XRD pattern for the sample BS-2-200-450 is matching with hexanedioic acid and carbon (graphite) which are indicating the products

of hydrothermal sucrose after de-carbonization at 450 °C. As mentioned before, decarbonization at 450 °C did not take place completely and SEM images also depicted the hydrothermal sucrose still was in the samples. Furthermore, Bi_2O_3 and $Bi_2(SO_4)_3$ was found in the sample (Figure 4-17) [20].

Also, we have analysis the XRD pattern of the sample with sucrose and $Bi_2(SO_4)_3$ and Bi_2O_3, and it was indexed (Figure 4-18) [16].

(e)
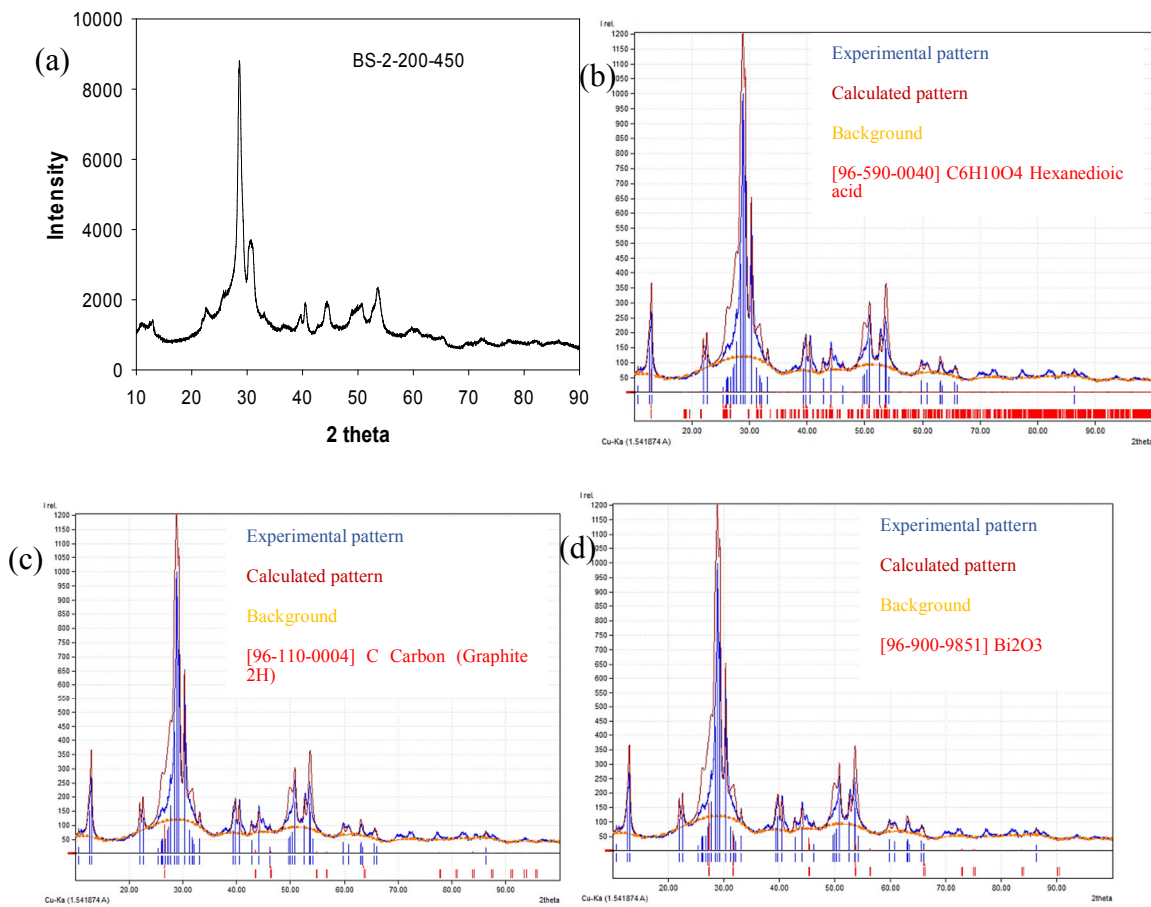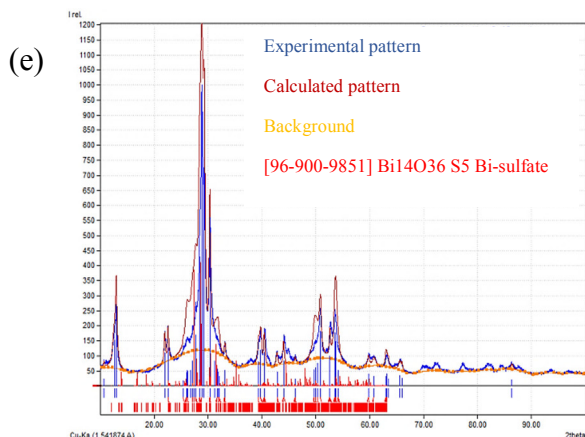
Figure 4-17. XRD pattern of: (a) BS-2-200-450; (b-e) matching of XRD BS-2-200- with TREOR program [(b) sample's XRD matched with hexanedioic acid, (c) carbon graphite, (d) Bi_2O_3, (e) Bi-sulfate.
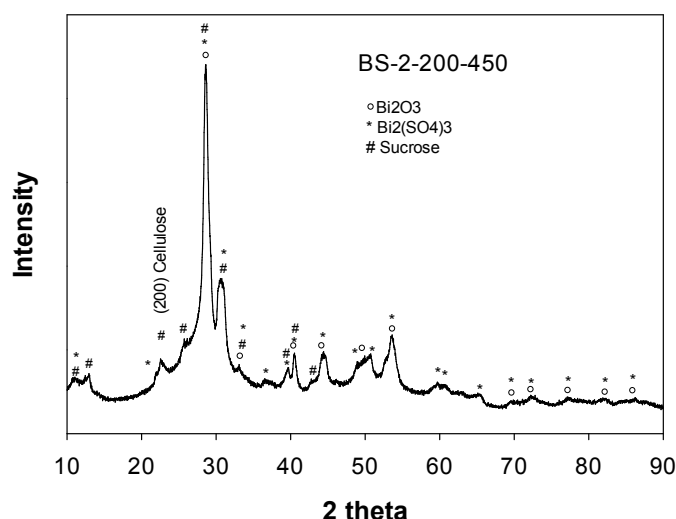
Figure 4-18. XRD pattern of BS-2-200-450 and matching with $Bi_2(SO_4)_3$ and Bi_2O_3 and sucrose.

XPS of BS-4-200-450 has been shown in Figure 4-19. This material is being calcined at 450 °C and therefore, there is still some degree of carbon in the material but is way less than the sample without any calcination. Also, this material is Bi_2O_3 and $Bi_2(SO_4)_3$ did not form in the material. There is some SO_4 in the S2p region, which is a non-reacted SO_4 from Na_2SO_4. Because the SO_4 peaks are also shown as Na_2SO_4 at higher calcination temperatures (600 °C) [refer XPS of BS-4-200-600].

Also, in the oxygen part most of oxygen are attributed to the Bi_2O_3 and SO_4 after calcination (non-reacted SO_4), while before calcination most of oxygen were in the form of SO_4 and C-O-C. This is also is as a result of high temperature calcination, which removed

partially carbonaceous template and therefore, the ratio of Bi_2O_3 and SO_4 would be dominant compared to the carbon oxygen species in the O1s (Figure 4-19).
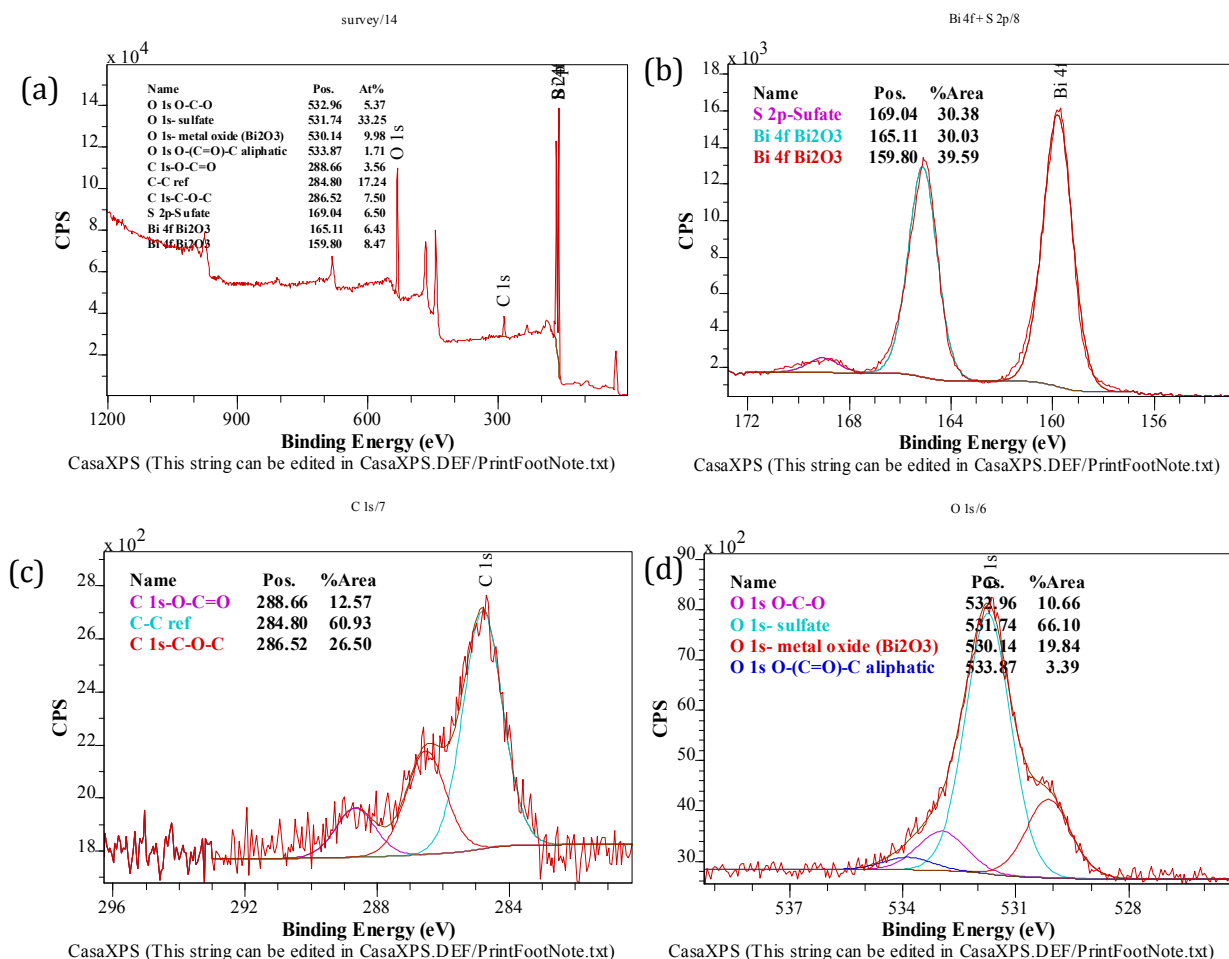
Figure 4-19. Survey XPS spectrum of BS-4-200-450 sample: (a) whole spectrum, (b) Bi4f and S2p, (c) C1s, (d) O 1s.

Due to the XRD analysis of BS-4-200-450, no Bi-sulfate was found in the compound, but the Bi_2O_3 and graphite was found in the compound. Graphite is the product of the sucrose hydrothermally heated and partially de-carbonized. Also, no hexanedioic acid was found in the XRD analysis with Treor program, which indicates that the products would have different by-products from calcination of hydrothermally treated sucrose at same temperature. This data matches with the XPS analysis which will be presented in Figure 4-20.
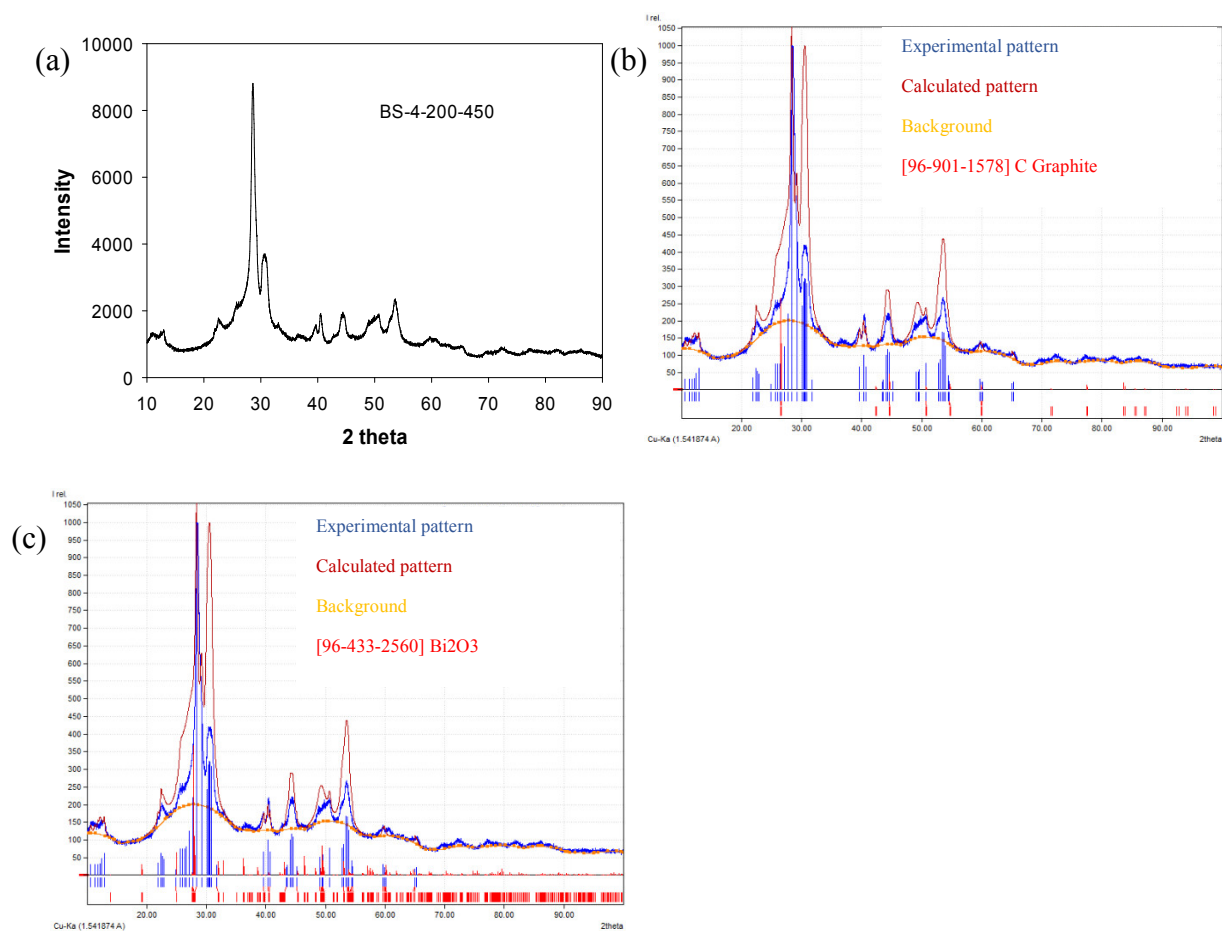
Figure 4-20. XRD pattern of: (a) BS-4-200-450; and (b-c) matching of XRD BS-4-200-450 with Teror program [(b) sample's XRD matched with graphite and (c) matched with Bi_2O_3.

With comparing the sample before and after calcination at 450 °C, it is found that the it was converted to Bi_2O_3 and $Bi_2(SO_4)_3$ was removed from the sample. There was no nitrogen found in the sample, despite there was CNS in the sample and it was not completely removed at 450 °C. The reason could be that the sample was ground mechanically and hence the surface contamination did not allow nitrogen get detected by the XPS . However, XRD patterns are showing the changes of nitrogen and opening melamine ring after calcination at 450 °C.

Also, from the C1s comparison would be found that after calcination, the carbon would be removing in different forms and just C-O would be remaining. The other forms of C=O and carbonate is removed after calcination. Furthermore, O1s comparison shows that Bi_2O_3 ratio has been increased in the oxygen region after calcination, which is because of the carbon-oxygen ratio has been decreased after calcination.

Finally, it can be said that the Bi_2O_3 was just found in the sample after the calcination like the BS-4-200-450 sample. Sample has some small amount of SO_4 which is a residual SO_4 (from Na_2SO_4) non reacted to the sample, as it was detected as Na_2SO_4 in BCNS-600 sample (Figure 4-21).
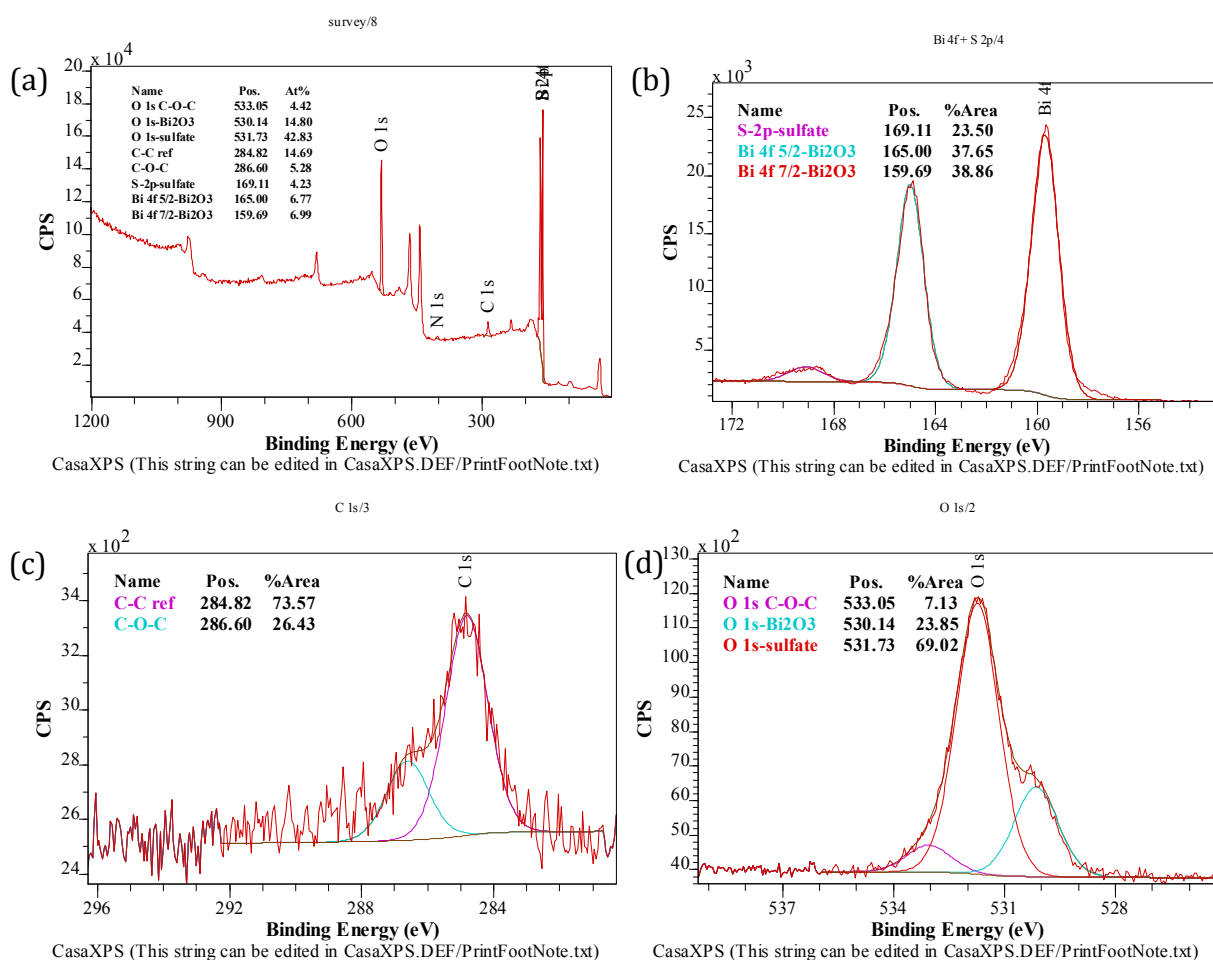
Figure 4-21. Survey XPS spectrum of BCNS-450 sample: (a) whole spectrum, (b) Bi4f and S2p, (c) C1s, (d) O 1s.

After analysing XRD of this sample with Treor program, it was found that it matches with carbonyl diazide and with C_6N_6 (2,4,6 tricyano-1,3,5 triazine), and $C_8N_{12}O_{10}$, C_2N_2, CN_6O, C_3N which is indication of nitrogen in the compound after decarbonization at 450 °C. These compounds show the nitrogen carbonaceous material after calcination, which unfortunately because of grinding material mechanically the nitrogen related peaks were not detected in the XPS of related sample, because of surface contamination. Also, Bi_2O_3 was found in the XRD of sample which is with alignment of the XPS of sample. The nitrogen containing groups in the XRD of sample depict that melamine compound would

be open up its ring by calcination at 450 °C (Figure 4-22). Also, we have indexed the sample after comparison with Bi_2O_3 and C_3N_4 (Figure 4-23).
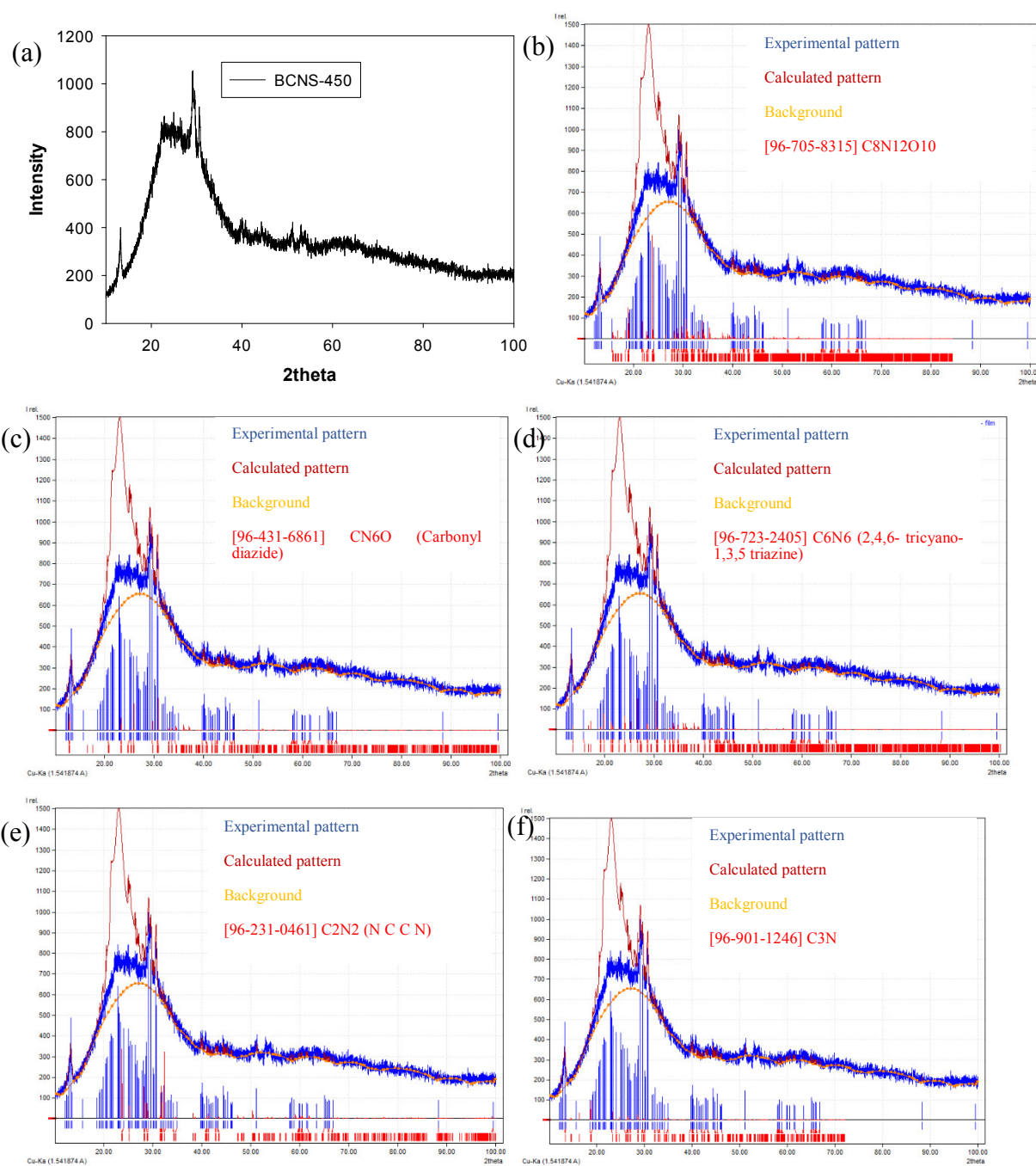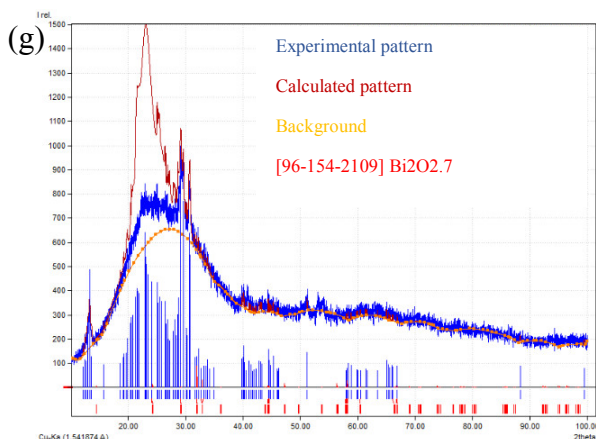
Figure 4-22. XRD pattern of: (a) BCNS-450; and (b-g) matching of XRD BCNS-450 with TREOR program [(b): sample XRD matching with $C_8N_{12}O_{10}$, (c) CN_6O, (d) C_6N_6, (e)C_2N_2, (f) C_3N, (g) $Bi_2O_{2.7}$.
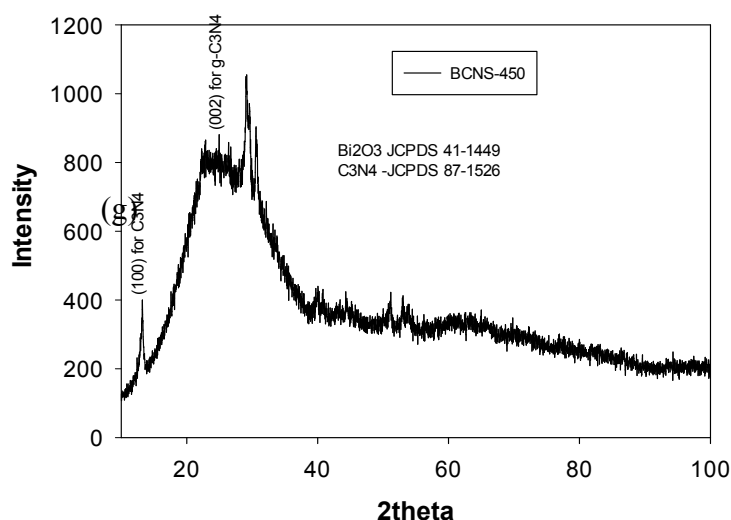
Figure 4-23. XRD pattern of a) BCNS-450 matched and indexed with Bi_2O_3 and C_3N_4.

XPS of BS-2-200-600 has been shown in Figure 4-24. It is shown that after calcination at high temperature of 600 °C has resulted in $Bi_2(SO_4)_3$ conversion to Bi_2S_3, there would not be any SO_4 in this sample ($Bi4f$). Bi_2S_3 was 19.93% and 80.08% is Bi_2O_3 in the $Bi4f$ region. Also, de-carbonization at higher temperature resulted in more carbon removal and leading to the more oxygen percentage allocating to Bi_2O_3. Specifically, O1s shows that Bi_2O_3 in BS-2-200-450 sample was 18.03% and after 600 °C calcination the Bi_2O_3 in O1s was 27.16%. Furthermore, with higher temperature calcination leaded to remove carboxyl removal. Therefore, the final material is a composite of Bi_2O_3 and Bi_2S_3 which is

111

different from other synthesised materials at this temperature calcined or at lower temperature calcined. The allocated peaks for this sample has been shown in Table 4-2 and Figure 4-24 [17].
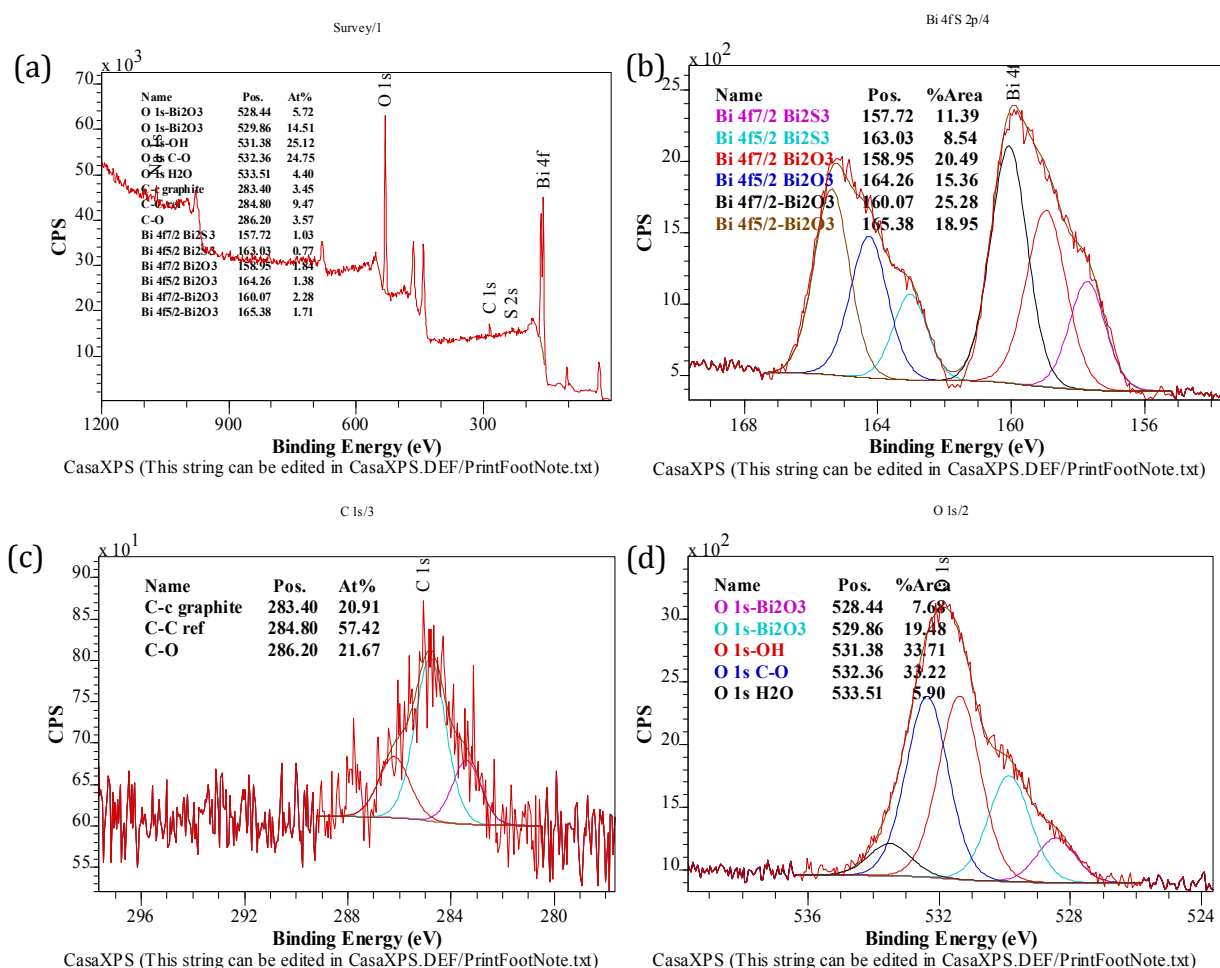
Figure 4-24. Survey XPS spectrum of BS-2-200-600 sample: (a) whole spectrum, (b) Bi4f and S2p, (c) C1s, (d) O 1s.

Table 4-2. XPS peaks and the allocate compounds for BS-2-200-600 extracted by [17].

Elements	Peaks	Compound
O 1s	528.44	Metal oxide
O 1s	529.86	Metal oxide
O 1s	531.38	hydroxide
O 1s	532.37	C-O
O 1s	533.5	H_2O
C 1 s	283.40	C-C graphite

C 1 s	284.80	C-C ref
C 1 s	286.20	C-O
Bi 4f 7/2	157.72	Bi_2S_3
Bi 4f 5/2	163.03	Bi_2S_3
Bi 4f 7/2	158.95	Bi_2O_3
Bi 4f 5/2	164.26	Bi_2O_3
Bi 4f 7/2	160.07	Bi_2O_3
Bi 4f 5/2	165.38	Bi_2O_3

The XRD was analysed with Treor program and the results shows it is mixture of Bi_2O_3 and Bi_2S_3 (Figure 4-25) [20].

Also we index the XRD pattern with Bi_2S_3 (JCPDS Card No. 17-0320) [21] and Bi_2O_3 XRD (JCPDS 76-1730) (Figure 4-26) [22]. Some of the XRD patterns will overlap each other (Bi_2S_3 and Bi_2O_3). Material orientation is more inclined towards (211), due to its highest peak (Figure 4-26). The orthorhombic phase Bi_2S_3 (JCPDS 17-0320) [23] and α-Bi2O3 (monoclinic phase) with a = 5.8405 (6) Å, b = 8.254 (1) Å, c = 7.330 (1) Å and cell volume = 328.57 (6) (Å)^3 [24].

The crystal size was determined by Scherrer formula for the peak with highest intensity at the 2θ of 28.432 and it was found that it is 0.59 nm.

$$D = \frac{k\lambda}{\beta cos\theta} = \frac{0.9 \times 0.15406}{0.24171 \times cos(0.248)} = 0.59 \, nm$$

β=FWHM calculated via origin software with R^2_{adj} 0.94 with the value of 0.24171.
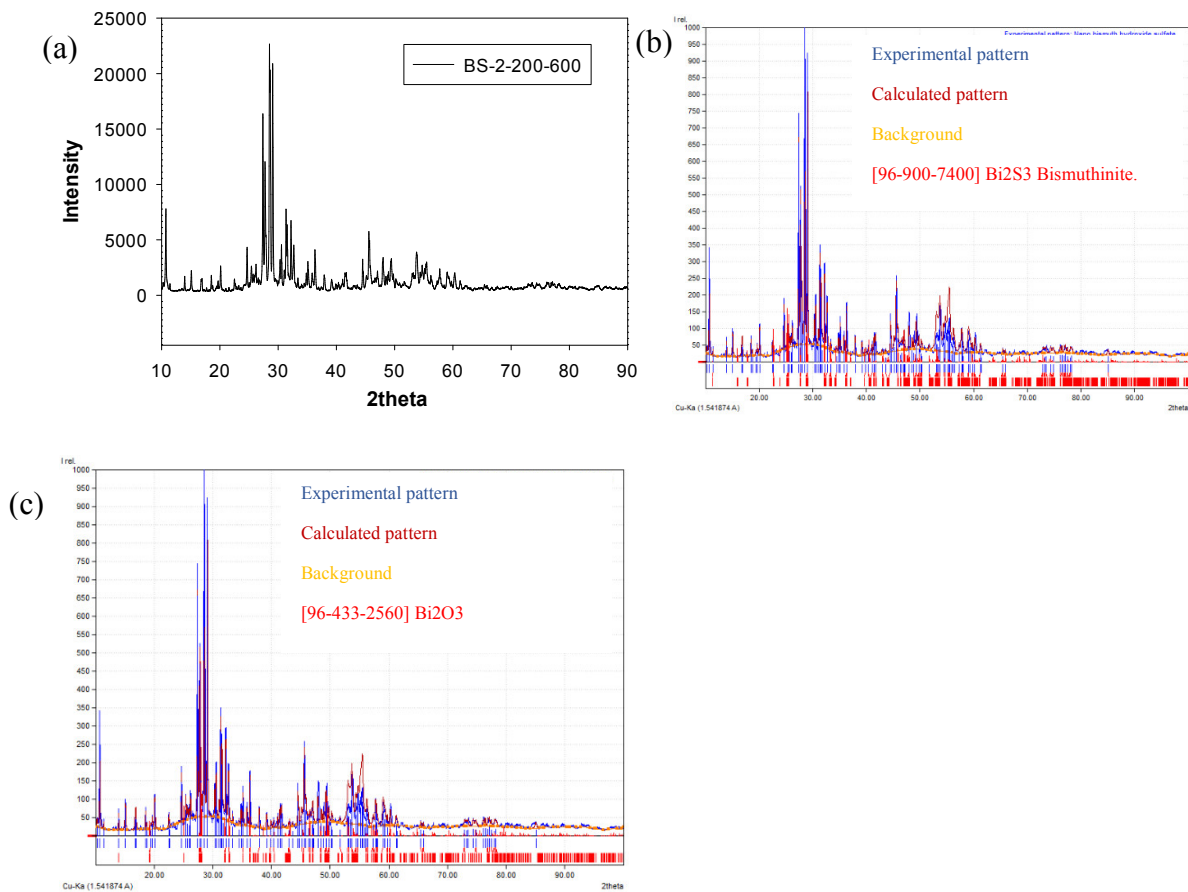
Figure 4-25. XRD pattern of: (a) BS-2-200-600; (b) matching XRD pattern of BS-2-200-600 with Bi_2S_3, and (C) matching of XRD pattern with Bi_2O_3 with Treor program.
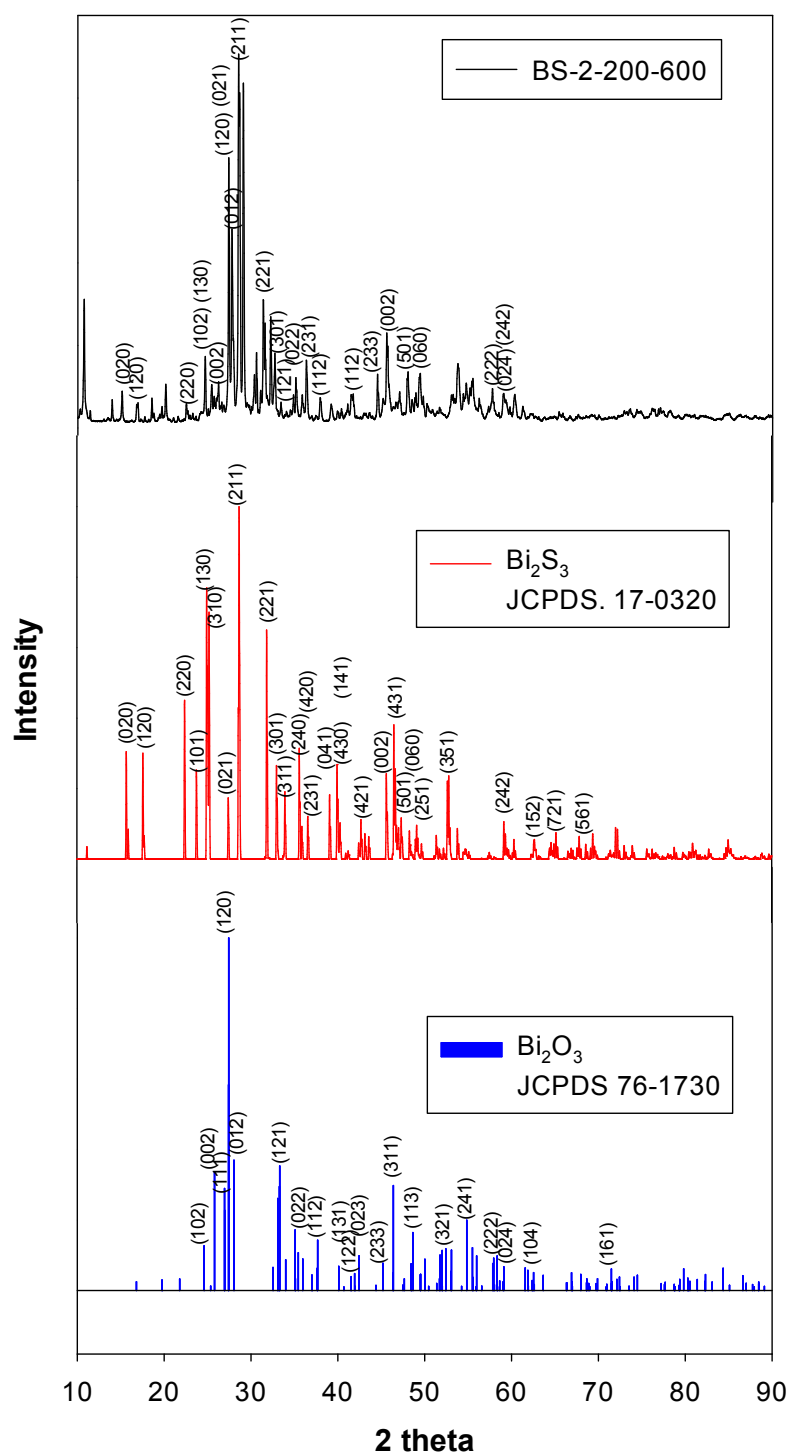
Figure 4-26. XRD pattern of BS-2-200-600 and indexing and matching with Bi_2S_3 and Bi_2O_3.

XPS of BS-4-200-450 has been depicted in Figure 4-27. After calcination at higher temperature 600 °C, the sample is still Bi_2O_3 and the carbon content has been decreased. There would be some small amount of SO_4 which is from Na_2SO_4 which was not reacted

to the sample, almost same amount of SO₄ found in this sample was found in BS-4-200-450 in S2p. This is confirming that SO₄ in the BS-4-200-450 sample is from Na₂SO₄ (Figure 4-27).
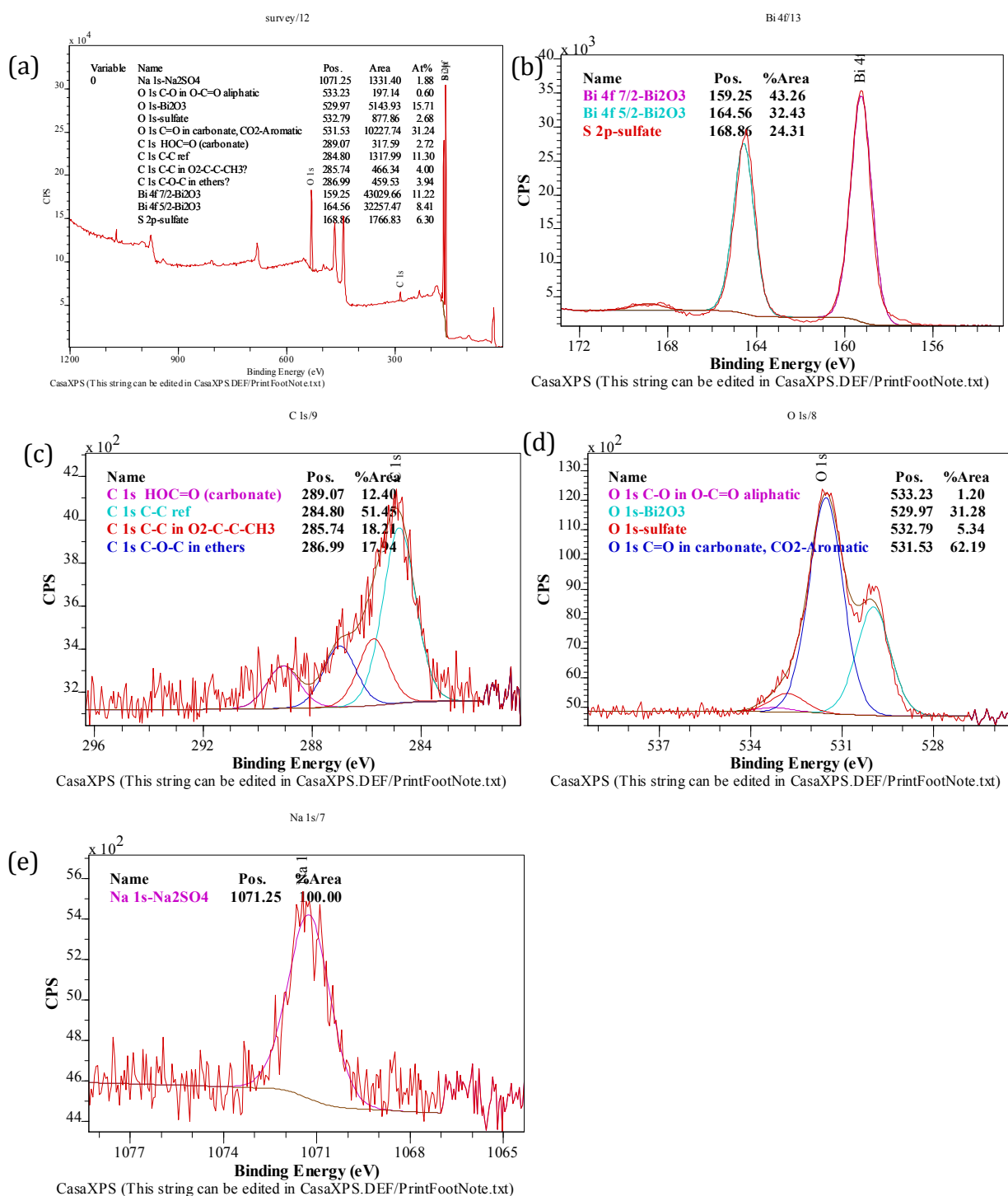
Figure 4-27. Survey XPS spectrum of BS-4-200-600 sample: (a) whole spectrum, (b) Bi4f and S2p, (c) C1s, (d) O 1s, (e) Na 1s.

XRD pattern analysis of BS-4-200-600, has been shown here (Figure 4-28). XRD of this material has been matched with Treor program, and it was showed that this material is Bi_2O_3 [20].
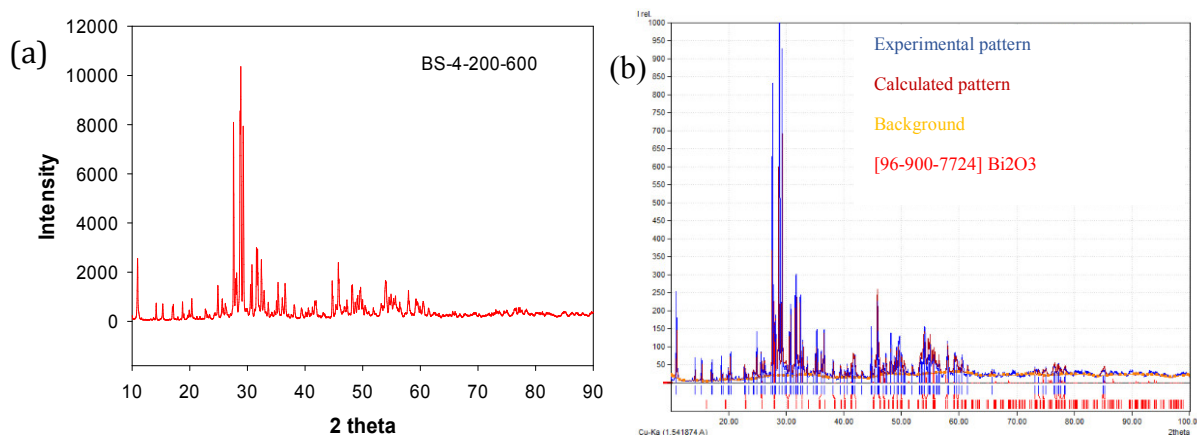
Figure 4-28. XRD pattern of a) BS-4-200-600; and b) sample XRD matching with Bi_2O_3 with Treor program.

XPS of BCNS-600 has been shown in Figure 4-29. After calcination at temperature 600°C, it showed that at higher temperature material would be still in the form of Bi_2O_3.

Also, from the O1s it can be found that oxygen in Bi_2O_3 has increased more when it is calcined at higher temperature, which is as a result of removing carbon would increase the ratio of Bi_2O_3 in the oxygen region (O1s). SO_4 in this sample is allocated for the Na_2SO_4, and the SO_4 in S2p amount is almost same amount with the sample of BCNS-450. Therefore, the SO_4 in BCNS-450 is also allocated for Na_2SO_4 as was mentioned before (Figure 4-29).
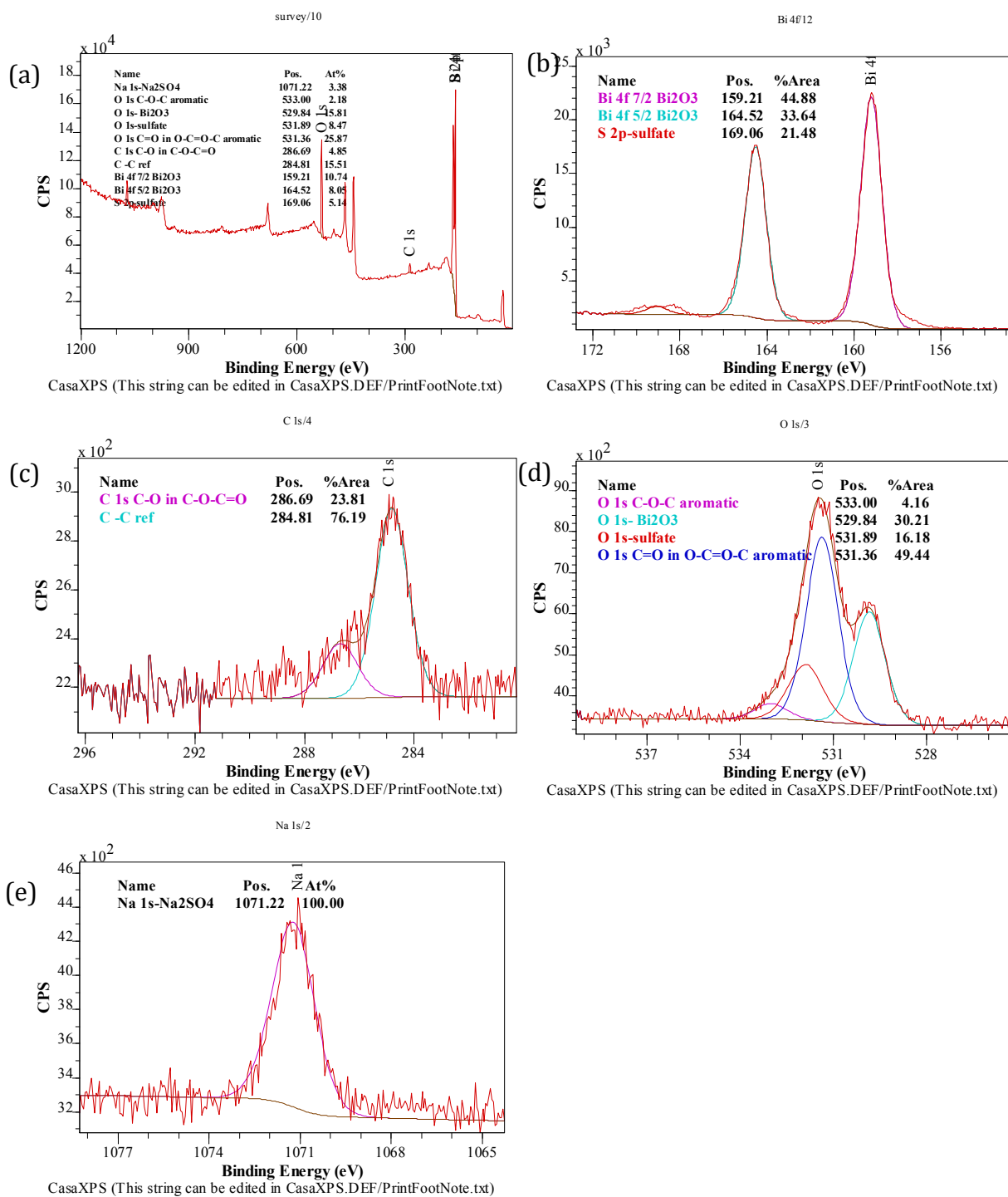
Figure 4-29. Survey XPS spectrum of BCNS-600 sample: (a) whole spectrum, (b) Bi4f and S2p, (c) C1s, (d) O 1s, (e) N 1s.

XRD pattern of BCNS-600 after matching with Treor program, it shows that is Bi_2O_3 crystals (Figure 4-30).
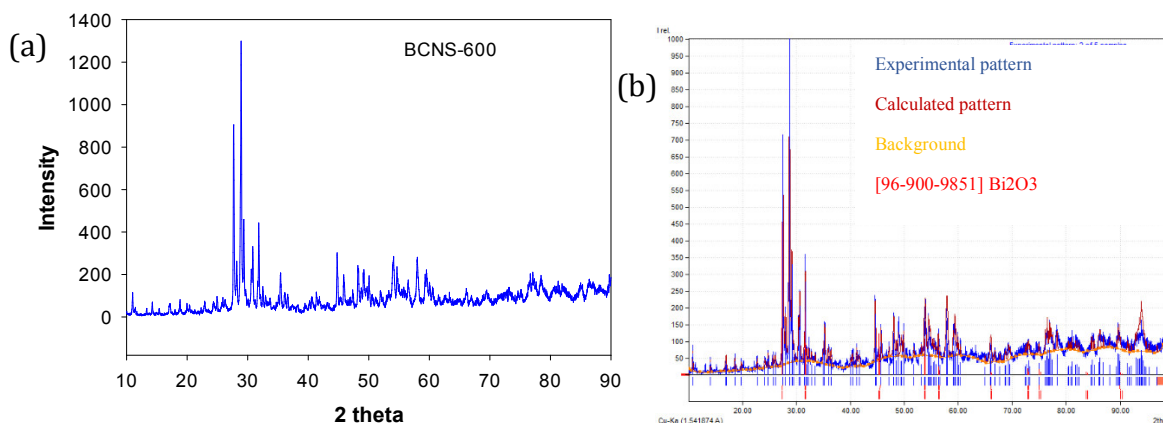
Figure 4-30. XRD pattern of: (a) BCNS-600; and (b) sample XRD matched with Bi_2O_3 with Treor program.

4.4.3. Halide removal test

From the experiments (Figure 4-32) it is clear that S-2-200 template has the highest efficiency compared to the other templates because it has the highest amount of oxygen as C-O and C=OOH (carboxylic group) rather than the glucose treated in more resident time. It is also will be more clear when bismuth tend to react and be attached to the oxygen in the polyfuran [11]. Also, this template has produced Bi_2O_3-Bi_2S_3 at 600 °C, which is a different product from others. Specifically, it was found that Bi_2O_3-Bi_2S_3 is a n-p heterojunction would induce an electric field with the direction from Bi_2O_3 to Bi_2S_3 (Figure 4-31) [13]. It can be said that Bi_2S_3 is a Na capacitor and can adsorb it, therefore, for maintaining the charge balance in the composite to neutral, Bi_2O_3 can shift some of its electrons towards Bi_2S_3 and would be more positively charged and more readily active to bind to iodide (halides) [13]. As a result, the best template would be S-2-200 and the best sample for removing of halide is BS-2-200-600.
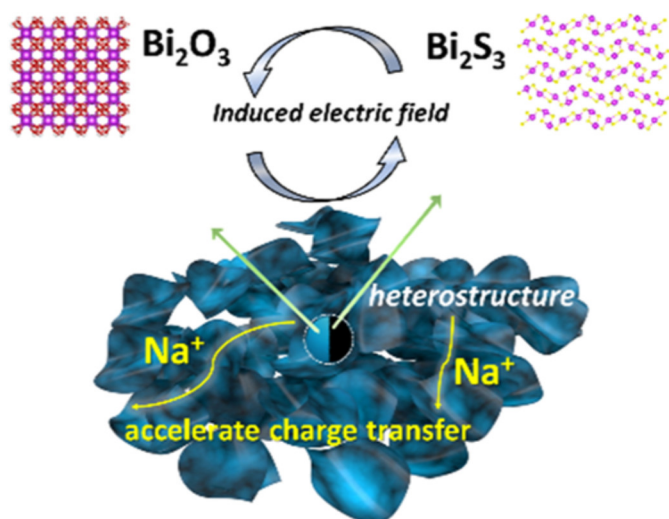
Figure 4-31.Sodium sorption due to the induced electric field in the composite of Bi_2O_3-Bi_2S_3 gotten from [13].
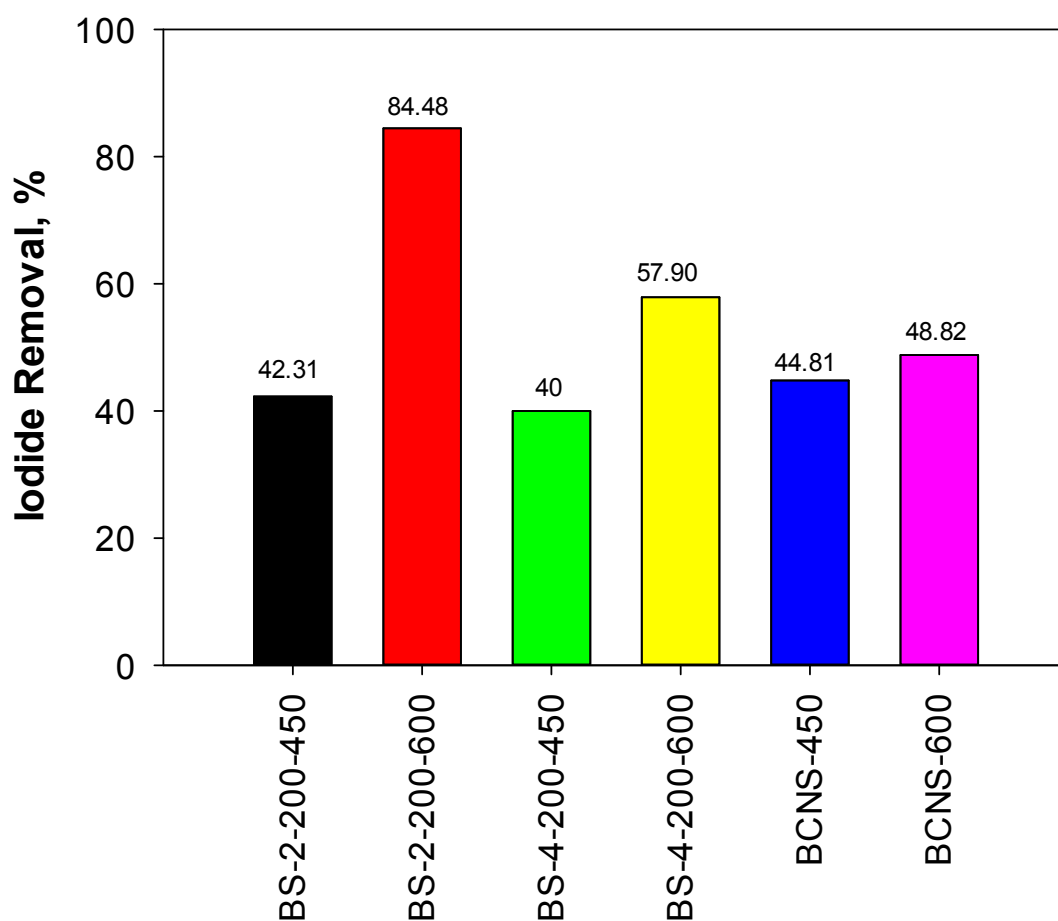
Figure 4-32. Removal efficiency of 5 mg/L of iodide after 3h reaction with 5 g/L dosages of various synthesized materials by various templates and de-carbonization temperatures (450 and 600 °C).

Other products (BS-4-200-450, BS-4-200-600, BCNS-450, BCNS-600) have more or less same iodide removal, as they are making same product of Bi_2O_3. A slight increase for iodide removal has obtained via these products which were calcined at higher temperatures (BS-4-200-600, and BCNS-600). That is as a result of removal of template, therefore decreasing the particle sizes (related DLS and SEM images), and eventually increasing more surface area contacting with pollutant (pollutant).

4.5. Conclusion

Based on the reactions we have a proposed chemical reaction which probably happens and explains the samples products. First of all, $Bi(NO_3)_3$ has been dissociate and dissolved in acetic acid glacial. The dissolving of $Bi(NO_3)_3$ in 10% of acetic acid glacial is due to the below reactions, and based on fully or partially hydrolysing and reaction with acetic acid glacial could produce $Bi(CH_3COO)_3$, $Bi(CH_3COO)_2^+$, $Bi(CH_3COO)^{2+}$, Bi^{3+}, BiO^+. Following with adding Na_2SO_4 in water can produce $Bi_2(SO_4)_3$, $BiSO_4^+$, $Bi_2SO_4^{2+}$. These products are depending on the hydrolysed products, the reactions are shown below (Equation *4-2-* Equation 4-7).

Eventually it can be said that in the mixed solution (formed white precipitates emulsion), there are various products of $Bi_2(SO_4)_3$, $BiSO^+$, $Bi_2SO_4^{2+}$, Bi^{3+}, BiO^+.

Reactions with CH_3COO^- from acetic acid:

$Bi(NO_3)_3 + CH_3COOH \rightleftarrows Bi(CH_3COO)_3 + 3H^+ + 3NO_3^-$ (fully hydrolysing) $\xrightarrow{+Na2SO4} Bi_2(SO_4)_3$ *Equation 4-2*

$Bi(NO_3)_3 + CH_3COOH \rightleftarrows Bi(CH_3COO)_2^+ + 3H^+ + 3NO_3^-$ (partially hydrolysing) $\xrightarrow{+Na2SO4} BiSO4^+$ *Equation 4-3*

$Bi(NO_3)_3 + CH_3COOH \rightleftarrows Bi(CH_3COO)^{2+} + 3H^+ + 3NO_3^-$ (partially hydrolysing) $\xrightarrow{+Na2SO4} Bi_2SO_4^{2+}$ Equation 4-4

Reactions with H^+ from acetic acid:

$Bi(NO_3)_3 + 3H^+ \rightarrow Bi^{3+} + 3HNO_3$ Equation 4-5 $\Big]$ $\xrightarrow{+H_2O} Bi^{3+} + H_2O = BiO^+ + 2H^+$ Equation 4-6 $\xrightarrow{+Na_2SO_4} Bi_2(SO_4)_3$ Equation 4-7

$\xrightarrow{+Na_2SO_4} BiSO_4^+$ Equation 4-8
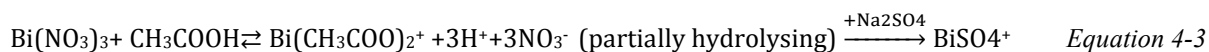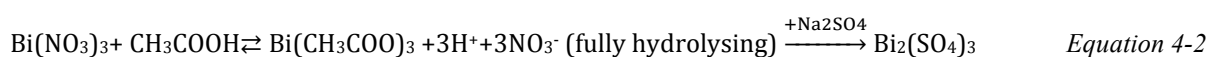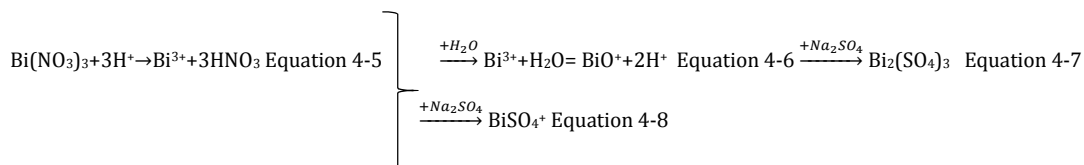
Therefore, the products are:

Based on the template surface active areas, Bi^{3+}, BiO^+, $Bi_2(SO_4)_3$, $BiSO_4^+$, $Bi_2SO_4^{2+}$ can interact and attach to template chemically or physically. Some of templates (S-4-200 and CNS) did not show the affinity to react with Bi-sulfate species and just the sodium sulfate has been detected on these templates after mixing and de-carbonization at different temperatures (450 °C and 600 °C), which is probably from the residues of Na_2SO_4 was not washed-off properly. However, all templates have shown to be able to react with the BiO^+ and Bi^{3+} and produce Bi_2O_3. Specifically, we speculate that Bi^{3+} has the possibility to react with oxygen containing carbonaceous material and produce Bi_2O_3 (Figure 4-33).

De-carbonization @ 450 °C

will bind to the negative charge of oxygen covalently and would form Bi_2O_3 or Bi_2O_3-$Bi_2(SO_4)_3$ composite depends on the

Sucrose HTC (C=O,C−O groups) or CNS(C−O,C=O,C with N groups)

Bi^{3+},BiO^+, $Bi_2(SO_4)_3$, $BiSO_4^+$, $Bi_2SO_4^{2+}$

De-carbonization @ 600 °C

Formation of Bi_2O_3 or Bi_2O_3-Bi_2S_3
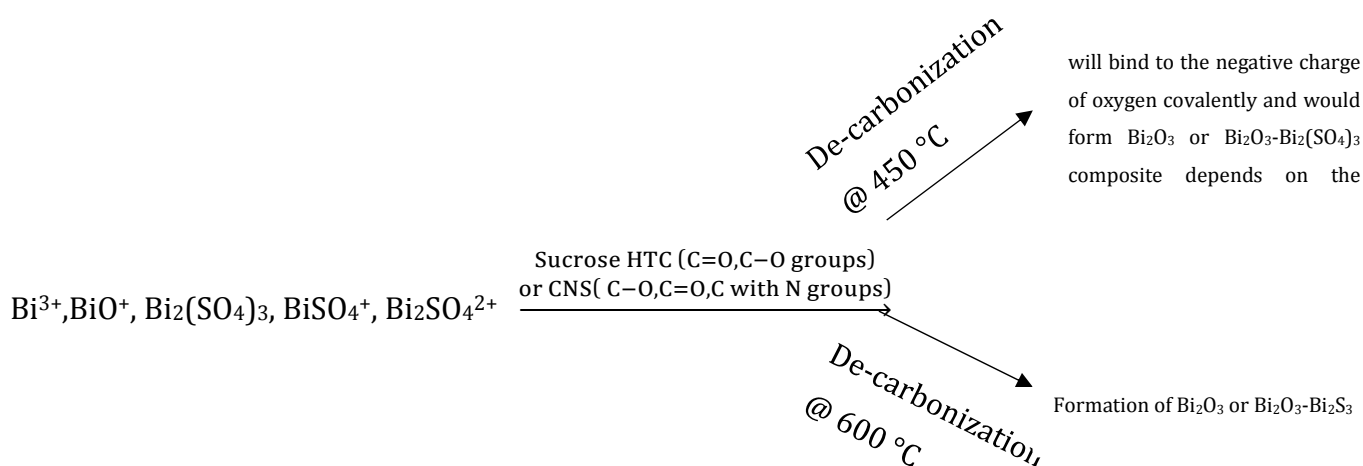
Figure 4-33. Proposed reaction of Bismuth products and formation of Bi_2O_3 or Bi_2O_3/Bi_2S_3 composite after calcination at different temperatures.

Also, visually analysis of the mixtures of the Bismuth compounds mixed templates (S-2-200, S-4-200 and CNS), showed that more bismuth species in water were attached to S-2-200, followed by S-4-200 and CNS had least attached bismuth-compound attached to it after washing off. Specifically, after washing off CNS-Bismuth compounds with ethanol and water, the white unreacted residues were mostly washing off after filtering. because CNS structure has N in the rings and therefore, bismuth has not that much tendency to react to it and if it reacted would be weak Van der Waals forces. Specifically, electronegativity of oxygen is more than nitrogen. This means bismuth compounds with positive charges can attach to oxygenated groups better than nitrogen-containing

compounds. Furthermore, nitrogen in CNS is in the ring (pentagon ring due to XPS) and is hardly available to be reacted to bismuth-compounds in the aqueous solutions.

Products of CNS and S-4-200 would be same at 450 and 600 °C. Product of BS-4-200-450 and BCNS-450 is Bi_2O_3 (XPS results). And at higher temperature of calcination of 600 °C, their product would be still Bi_2O_3. This explains why their removal efficiency for iodide are same. On the other hand, the product of bismuth species mixed with S-2-200 (BS-2-200-450 and BS-2-200-600) are different at various temperatures of calcination. The product (BS-2-200-450) at 450 °C calcination is Bi_2O_3-$Bi_2(SO_4)_3$ and its product at 600 °C calcination (BS-2-200-600) is Bi_2O_3-Bi_2S_3. Interestingly, after calcination at 450 °C, the amount of Bi-sulfate has been increased in the S-2-200 -Bismuth compounds (BS-2-200-450), compared to without calcination (BS-2-200). Also, with increasing the temperature of calcination temperature to 600 °C, this sample would form and grow Bi_2S_3.

XPS results showed that calcination at 600 °C the best results for de-carbonization is for the S-2-200-600, however, for the BS-4-200-600 still the C=O would be observed and on the BCNS-600 C=O also is observable which showed that the calcination at high temperature still could not remove these parts.

The removal efficiency of halide was highest with the BS-2-200-600 sample. This sample was obtained from hydrothermally treated sucrose at 200 °C as template mixing with bismuth particles for 8h, then calcined at 600 °C. It shows that hydrothermally treated sucrose at 200 °C was the best template for this recipe and 600 °C calcination resulted in the desirable result for halide removal. That may be as a result of composite of Bi_2O_3-Bi_2S_3 made from this method shows different crystal structures which is different from other ones. Templates of S-4-200 and CNS are making Bi_2O_3 at different calcination temperatures of 450 °C and 600 °C, while S-2-200 is making Bi_2O_3-$Bi_2(SO_4)_3$ and Bi_2O_3-Bi_2S_3 when is calcined at 450 °C and 600 °C. It seems that the impact of Bi_2S_3 on the composite and eventually enhancement in halide removal.

Reference

1.   Zhang, J., et al., *Large-scale synthesis of self-assembled ultralong cannonite nanobelt film as a visible-light photocatalyst.* RSC Adv., 2015. **5**(12): p. 8537-8543.

2.   Liu, L., et al., *Selective Capture of Iodide from Solutions by Microrosette-like δ-Bi$_2$O$_3$.* ACS Appl. Mater. Inter., 2014. **6**(18): p. 16082-16090.

3.   Xu, J., et al., *Understanding the contribution of hydroxyl to the energy band of a semiconductor: Bi$_2$O(OH)$_2$SO$_4$vs. Bi$_6$S$_2$O$_{15}$.* Dalton Trans., 2016. **45**(16): p. 6866-77.

4.   Wang, X., et al., *Low crystallized BiOCl$_{0.75}$I$_{0.25}$ synthesized in mixed solvent and its photocatalytic properties under simulated solar irradiation.* Mater. Lett., 2014. **136**: p. 30-33.

5.   Liu, Y., et al., *Preparation, electronic structure, and photocatalytic properties of Bi$_2$O$_2$CO$_3$ nanosheet.* Appl. Surf. Sci., 2010. **257**(1): p. 172-175.

6.   Cui, P., et al., *Bismuth oxychloride hollow microspheres with high visible light photocatalytic activity.* Nano Res., 2016. **9**(3): p. 593-601.

7.   Ryoko, M., M. Hagio, and S. Yuzo, *The Phase Transition of Bismuth(III) Oxide Prepared by the Thermal Decomposition of Bismuth Sulfate.* B. Chem. Soc. JPN, 1975. **48**(11): p. 3397-3398.

8.   Dong, F., et al., *Template-free fabrication and growth mechanism of uniform (BiO)$_2$CO$_3$ hierarchical hollow microspheres with outstanding photocatalytic activities under both UV and visible light irradiation.* J. Mater. Chem., 2011. **21**(33): p. 12428-12436.

9.   Bai, C.-X., F. Shen, and X.-H. Qi, *Preparation of porous carbon directly from hydrothermal carbonization of fructose and phloroglucinol for adsorption of tetracycline.* Chinese Chem. Lett., 2017. **28**(5): p. 960-962.

10.   Yao, C., et al., *Hydrothermal Dehydration of Aqueous Fructose Solutions in a Closed System.* J. Phys. Chem. C, 2007. **111**(42): p. 15141-15145.

11.   Falco, C., N. Baccile, and M.-M. Titirici, *Morphological and structural differences between glucose, cellulose and lignocellulosic biomass derived hydrothermal carbons.* Green Chem., 2011. **13**(11): p. 3273.

12.   Wang, W., et al., *A novel bottom-up solvothermal synthesis of carbon nanosheets.* J. Mater. Chem. A, 2014. **2**(7).

13.   Luo, W., et al., *Heterostructured Bi$_2$S$_3$-Bi$_2$O$_3$ Nanosheets with a Built-In Electric Field for Improved Sodium Storage.* ACS Appl. Mater. Interfaces, 2018. **10**(8): p. 7201-7207.

14. Chehardoli, G. and M.A. Zolfigol, *Melamine-(H_2SO_4)$_3$/melamine-(HNO_3)$_3$ instead of H_2SO_4/HNO_3: a safe system for the fast oxidation of thiols and sulfides under solvent-free conditions.* J. Sulfur Chem., 2015. **36**(6): p. 606-612.

15. Tahir, M., et al., *One Dimensional Graphitic Carbon Nitrides as Effective Metal-Free Oxygen Reduction Catalysts.* Sci. Rep., 2015. **5**: p. 12389.

16. Zhao, H., et al., *Effects of additives on sucrose-derived activated carbon microspheres synthesized by hydrothermal carbonization.* J. Mater. Sci., 2017. **52**(18): p. 10787-10799.

17. Moulder, J.F., et al., *Handbook of X-Ray Photoelectron Spectroscopy (perkin elmer).* 1992: Perkin-Elmer Corporation.

18. Kondo, T., et al., *Observation of Landau levels on nitrogen-doped flat graphite surfaces without external magnetic fields.* Sci. Rep., 2015. **5**(1): p. 16412.

19. Pels, J.R., et al., *Evolution of nitrogen functionalities in carbonaceous materials during pyrolysis.* Carbon, 1995. **33**(11): p. 1641-1653.

20. Werner, P.-E., L. Eriksson, and M. Westdahl, *TREOR, a semi-exhaustive trial-and-error powder indexing program for all symmetries.* J. Appl. Crystallogr., 1985. **18**(5): p. 367-370.

21. Li, Y., et al., *Selected-Control Hydrothermal Synthesis and Photoresponse Properties of Bi_2S_3 Micro/Nanocrystals.* CrystEngComm, 2013. **15**(33): p. 6611-6616

22. M. J, J.F., N. C. V, and S. S, *α-Bi_2O_3 photoanode in DSSC and study of the electrode–electrolyte interface.* RSC Adv., 2015. **5**(95): p. 78299-78305.

23. Lu, F., et al., *Synthesis of Bi_2S_3–Bi_2O_3 composites and their enhanced photosensitive properties.* RSC Adv., 2014. **4**(11): p. 5666-5670.

24. M, M. and P. Padiyan, *Role of pH in the hydrothermal synthesis of phase pure alpha Bi_2O_3 nanoparticles and its structural characterization.* Adv. Mater. Proc., 2016. **2**: p. 51-55.

5. Removal of iodide and bromide at low/trace concentrations with novel bismuth composite material

Elham Nariyan[1,2], Nikhil Aravindakshan [1,2], Qiming Jimmy Yu[2] and Qin Li[1,2]*

1. Queensland Micro- and Nanotechnology Centre, Griffith University, Nathan, QLD 4111, Australia
2. School of Engineering and Built Environment, Griffith University, Nathan, QLD 4111, Australia

5.1. Abstract

Iodide and bromide in natural and ground waters (typically less than 0.05 mg/L for iodide and 0.5 mg/L for bromide) could react with the natural organic matters in the water treatment plants and produce toxic disinfectant by-products (DBPs).

We have synthesized a micro-nano Bi_2O_3-Bi_2S_3 composite through a carbogenic-sphere-supported synthesis strategy. A hydrothermal processing of sucrose resulted in uniform spherical carbogenic micro-spheres, which served as an excellent substrate for reaction between $Bi(NO_3)_3$ an Na_2SO_4 in emulsion, forming abundant precipitates on substrate. Based on XPS results, the mixture of precipitates in emulsion reacting with template would be Bi_2O_3-$Bi_2(SO_4)_3$ compositions, which after de-carbonization at 600 °C would produce Bi_2O_3-Bi_2S_3.

Subsequently, this material (Bi_2O_3-Bi_2S_3) was being used for iodide and bromide removal at trace concentrations. With 8 g/L of this material, 87.69% of iodide with initial concentration of 0.05 mg/L was removed after 3 hours, and 86.38% of bromide with initial concentration of 0.5 mg/L was removed after 14 hours. This material (Bi_2O_3-Bi_2S_3) was tested for artificial ground water treatment and the existence of other anions did not have any effect on the removal efficiency. pH does not have any effect on the adsorption

capacity of bromide, while acidic pH values could have an impact on the adsorption capacity of iodide. Overall, this study has proposed a new method to produce Bi_2O_3-Bi_2S_3 composite in high yield, and the as-synthesized Bi_2O_3-Bi_2S_3 composites exhibit extraordinary removal efficiency towards I^- and Br^- through adsorption mechanism.

Keywords: iodide, bromide, water treatment, nano-micro particles, bismuth composite, DBPs

5.2. Introduction

Iodide/iodine exists in nature such as waters and rocks, 50% in the form of iodide in surface waters [1]. Weathering of rocks such as caliche could release iodide into water [1]. Anthropogenic activities such as mining and gas production (produced water) are other source of this halide release into the water [2-5].

Furthermore, iodide and iodine are released in water because of the nuclear fission reactions [6-9]. Some of iodide/iodine has released as a result of nuclear disasters were seen in Chernobyl and Fukushima disasters [10]. Also, liquid crystal display (LCD) polarizing films industry would release a significant amount (1-1.5 wt%) of iodine /iodide into the water [4, 9, 11]. Finally, iodine can enter into waters by industries such as chemical wastes of x-ray, disinfection, and medical (nuclear medicine) dumps [12, 13].

Similar to iodide/iodine, bromide can end up in waterways because weathering of rocks naturally, or by human activities such as mining and gas production industries [2-5].

Iodide/iodine are radioactive and some of the isotopes have long half-life, and they can enter human and animal organs, environment (water and air), and plants [6, 8, 9, 14]. Iodide /iodine related health problems are often shown as thyroid problems such as hyperthyroidism, hypothyroidism, and goiter [15]. Other problem of iodide/iodine is iodinated disinfection by-products (DBPs) formation which are 10^5 times more cyto/geno-toxic than chlorinated DBPs [16].

Bromide compare to iodide/iodine is less toxic, but will change the taste and odour of water [17]. Similar to iodide/iodine, bromide can react and produce brominated DBPs, which are very toxic 10^4 times more than chlorinated DBPs [16, 18]. Increasing bromide concentration would lead to increasing the concentration of brominated trihalomethanes (THMs) and brominated haloacetic acids (HAAs) [19].

Iodine exists in the natural waters, and its average concentration in seawater, rivers and fresh waters are 60 μg/L, almost 5 μg/L and 2 μg/L , respectively [8]. Bromide concentration in seawater is in the range of 65-80 mg/L [20, 21], whilst about 0.1-3 mg/L in groundwater and rivers [16]. In fresh and in desalinated waters bromide concentration is about 0.5 and 1 mg/L, respectively [20]. Brackish water has higher bromide concentration of 1-10 mg/L [22]. In some cases, due to geological nature, groundwater could have high bromide and iodide concentrations. For example, the North-West Coastal groundwater in Perth, Western Australia showed high bromide and iodide concentrations of 8455 and 594 μg/L, respectively [17].

USA has more restrict guidelines for iodide concentrations than Australian guidelines. The safe drinking water guidelines in Australia has set the safe limit for iodide at 0.5 mg/L, while in the U.S. it is set at 4-18 μg/L [23, 24]. So far there is not any regulations set for bromide concentration, however, the Australian guidelines suggests to keep bromide concentration below 0.1 mg/L to decrease the formation of bromate in water [24]. Specifically, they suggested that if bromide is less than 0.1 mg/L in water, then the water would contain less than 0.02 mg/L bromate which is within Australian regulation alignment. Furthermore, when bromide is less than 60 μg/L is considered as low risk, in 60-500 μg/L it has moderate risk and more than 500 μg/L it has very high risk to form DBPs [18].

The best strategy for avoiding DBPs formation and other negative impacts of iodide and bromide on environments is to remove them before disinfection. Technologies such as RO, NF, ED/EDR, electrolysis, CDI, resins are used for iodide and bromide removal. They are relatively expensive technologies for low halide concentrations removal, especially membrane assisted technologies with considering their CAPEX and OPEX [16, 18, 25]. Therefore, for trace concentration bromide and iodide removal, adsorption is a suitable

technology. However, not many adsorbents have been tested for both bromide and iodide removal. Their capabilities for removing both are questionable.

Adsorption with silver ions is not very economical [16, 25]. The removal efficiencies of silver doped carbon for halides are affected by the ion species in water and percentage of silver doped. With increasing chloride concentration or NOM in water the removal efficiency would decrease significantly [26]. Silver nanoparticles have good adsorption capabilities at high pH values. However, H_2O_2 is used to increase the removal efficiency. The use of H_2O_2 would result in higher risks of DBPs formation [27]. Silver impregnated activated carbon are also good adsorbents except that silver will leach out at acidic conditions and silver is expensive [18]. In addition, NOM with sulphur and nitrogen function groups can result in silver leaching. Because nitrogen and sulfur compounds can interact and adsorb onto the silver and reduce the number of the silver active sites to interact with bromide and iodide. Using some conditions such as using perchlorate and high pH values would reduce silver leaching [18]. However, perchlorate is not be a good option due to possibility of DBPs formation.

Some resins for iodine removal are Amberlite 400 and DOW 21K XLT, however, they are expensive [3, 11, 28, 29]. LDHs has capabilities to remove halides from water. Their disadvantage is the release of anions into water. For example Mg-Al-(NO₃) will release NO_3^- into water [28].

Coagulation with aluminium can have low removal of 30.4% for bromide [30, 31]. Therefore, coagulation disadvantage is that it cannot be applied for iodide removal and its bromide removal is limited.

Minerals and sediments were tested for halide removal such as bentonite, zeolite and S- Cinnabar [13, 32-37]. S- Cinnabar has absorbability towards iodide with 32% removal [35]. Some natural zeolites are not good options for iodide removal, however, iodide removal efficiency increases with their modifications [34]. Some soils also showed iodide removal their removal range was from 11-99% [38, 39]. Soils for bromide removal has not been tested.

Iodide adsorption with activated carbon is only 13-46% [38]. Coals such as sub-bituminous coals have been used for iodide removal [26]. But these coals have bromine in their content which could be released into water [40]. Activated carbon has been used for the iodide removal by the oxidation of iodide [40]. However, the application of oxidation for iodide removal under the presence of NOM and bromide in water could result in DBPs formation. Activated carbon impregnated with silver is effective for halide removals but NOM can block the active sites of adsorbate and resin for iodide/bromide removal [18, 41]. Also, silver can leach and is expensive.

Bismuth-based compounds have shown affinity towards iodide such as bismuth hydroxide [8, 42, 43]. However, there are only few studies which were focused on iodide removal with bismuth materials [44, 45], and no study has been tested for bismuth materials/composites for bromide removal. Bi_2O_3-Bi_2S_3 is known for its photocatalytic properties and it has p-n junction [46, 47]. It is also being used for sodium capacitator [48].

Here we synthesised a novel bismuth composite material that can remove both iodide and bromide. Bismuth is a much cheaper material than silver. In addition, this adsorbent was not affected by solution pH except at very acidic conditions for iodide. This material does not need the use of H_2O_2 and it will not release anions into water.

The new bismuth composite material (Bi_2O_3-Bi_2S_3) is highly effective for iodide and bromide removal at trace concentrations that are typically found in fresh water and groundwater. We have characterized and tested this composite for iodide and bromide removal at different conditions of different dosage of synthesized material, pH variations, and various halide concentrations to examine the effects of these parameters on the performance of this composite on the iodide and bromide removal. Finally, different isotherms and kinetics of this material were fitted with the experimental data to understand the mechanism of this material for removing iodide and bromide.

5.3. Materials, methods and experimental procedures

5.3.1. Materials

All chemicals used were of analytical reagents and were not processed further. Bismuth nitrate ($Bi(NO_3)_3$ with 99% purity), sodium sulphate, sodium iodide, sucrose, and glacial acid were purchased from Chem-Supply Australia. Glassware and plasticware were cleaned before each usage.

5.3.2. Methods of chemical analysis and characterization

The surface chemistry of synthesized materials was characterized with a Kratos Axis ULTRA Xray Photoelectron Spectrometer incorporating a 165 mm hemispherical electron energy analyser. The XPS was equipped with a monochromated Al-Kα (1486.6 eV). X-ray source operated at 150 W (15 kV, 10 mA) with a base pressure 1.0×10^{-9} torr and pressure during analysis of 1.0×10^{-8} torr, to detect the element compositions. Atomic concentrations were calculated using the CasaXPS version 2.3.14 software and a Shirley baseline with Kratos library Relative Sensitivity Factors (RSFs). Peak fitting of the high-resolution data was also carried out using the CasaXPS software. The structural properties of samples were evaluated through X-ray diffraction (Powder X-ray diffractometer, X'pert Pro) with Cu-Kα radiation, 40 kV anodic voltage and a 50 mA current. A scanning electron microscope (SEM, JEOL 7001) operated at 15 kV, was employed to examine the morphologies of samples. The samples for SEM observation were prepared by coating onto a silicon wafer. The nitrogen adsorption and desorption isotherms were measured at the liquid nitrogen temperature (77 K) using a TriStar II 3020 automated surface area analyser.

Iodide and bromide were measured by iodide and bromide ion-selective electrodes (TPS) that were connected to the smartCHEM-Ion3. The data were measured and recorded, automatically. The ion-selective electrodes were calibrated each time.

5.3.3. Experiments

5.3.3.1. Synthesis of sucrose-derived carbogenic spheres

For obtaining templates from sucrose, 130 g of sucrose were mixed in 250 mL deionized water and then were hydrothermally heated by 200 °C in autoclave for 2h. Then, the obtained material was washed with de-ionized water and 100% ethanol.

5.3.3.2. Synthesis of bismuth composites and final bismuth products

1mmol of $Bi(NO_3)_3$ was dissolved in 150 mL of 10% acetic acid, then 1 mmol of Na_2SO_4 was added to the solution. At this stage, small white particles were formed, and the white emulsion was observed in the solution. Subsequently, 0.6 g of synthesized sucrose-derived carbogenic substrate was be added to the solution and stirred for 6-8 h. Finally, the suspension was collected and washed several times with deionized water and ethanol, finally was air dried at 80 °C. The final product from template mixture with the obtained white emulsion was calcinated at 600 °C in the air with the rate of 5 °C/min. The schematic of synthesis has been shown in Figure 5-1.
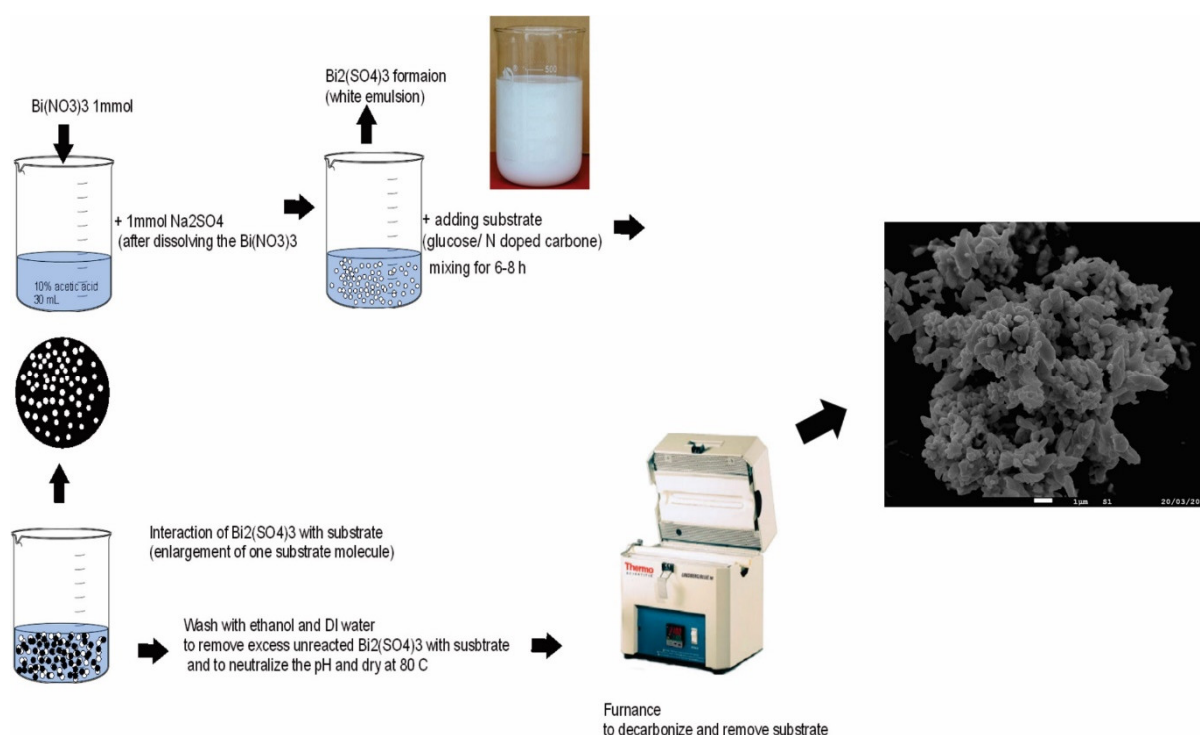
Figure 5-1.Schematic of the experiment procedures for synthesis of bismuth composites.

5.3.4. Halide removal experiments

Halide solution was made from sodium halide (sodium iodide, and sodium bromide). The stirring speed was 500 rpm, while the concentration of the halide was monitored and recorded continuously at every 1 min intervals by halide ion selective electrodes, and experiments were carried out till it reaches equilibrium. Equilibrium time for iodide was 3 hours and for bromide was 14 hours, based on observations.

Removal efficiency and adsorption capacity, q_e (mg g^{-1}) of as-synthesized bismuth composite (Bi_2O_3-Bi_2S_3) were calculated by Equation 5-1 and Equation 5-2, respectively. In which C_i and C_e are the initial and equilibrium concentration of halides (mg/L), m is the mass of bismuth composite which was added to each experiment, and V is the volume of the solution (L).

$$Halide\ removal, \% = \left(\frac{C_i - C_e}{C_i}\right) \times 100 \qquad\qquad \text{Equation 5-1}$$

$$q_e = \frac{(C_i - C_e) \times V}{m} \qquad\qquad \text{Equation 5-2}$$

Bromide concentrations were tested at 0.5, 1, 2, 5, 8 mg/L, based on the Western Australian water with high bromide concentrations [17]. Since the concentration ratio of bromide to iodide (Br$^-$:I$^-$) in the natural waters is typically 10:1 [16], we have selected the iodide concentrations of 0.05, 0.1, 0.2 and 0.5 (simulation of salt lake) [49]. For checking the material's capability for iodide removal, higher concentrations of 5 mg/L and 8 mg/L were also tested. It is notable that 0.05 mg/L and 0.5 mg/L were set as initial concentrations for iodide and bromide, respectively, except in the experiments of concentration variations and artificial ground water (AGW).

5.4. Results and discussion

5.4.1. Morphology

The morphology of the carbon template derived from sucrose was characterized by SEM. The SEM images show it is circular/ball shaped with the size of few μm (*Figure 5-2*a).

The surface area of the template was under detection limit of BET instrument (Figure 5-9S). Its SEM images showed that it is mixture of big balls with sizes of few μm. The SEM images shows it is not porous because the sucrose hydrochars without any carbonization would not show any porosity. But they will show porosity after carbonization under nitrogen gas would have a higher porosity [50].

SEM images of samples after mixing with the bismuth particles (Bi-O and Bi-SO$_4$ species) in the solution with the template is shown (Figure *5-2*b). As can be seen, the bismuth particles with rough layered morphology are attached on the template spherical particles.

Figure 5-2c displays the SEM of final product which was calcined at 600 °C in air, showing exposed irregular-shaped fine particles ranging from nanometers to μms after the removal of carbonaceous spheres. It is showing the population of smaller sizes are more than bigger ones because DLS measurements showed 84.4% of particle sizes are below 1000 nm (Figure 5-2d). The particles of all products (calcined at 600 °C) are agglomerated together (Figure 5-2c). Furthermore, the calcination at 600 °C shows that template has been removed, completely.

DLS was used for measuring the final products sizes and the measurements were done 6 times. The results show that final product (calcined at 600 °C) is the mixture of nano and micro sized particles (Figure 5-2d). This data obtained from DLS are in agreement with SEM image of the final product and shows that final product is mixtures of nano and micro particles. The distinct multimodal size distribution could be attributed to the angular shape of the as-synthesized particles.
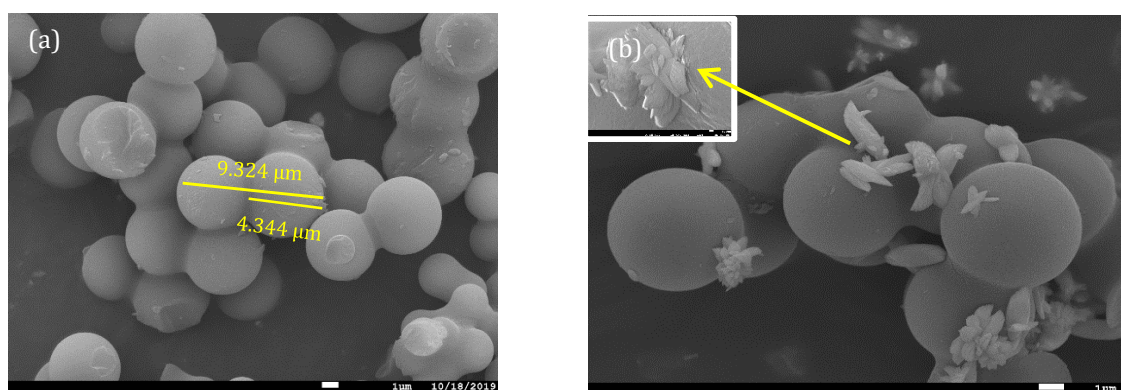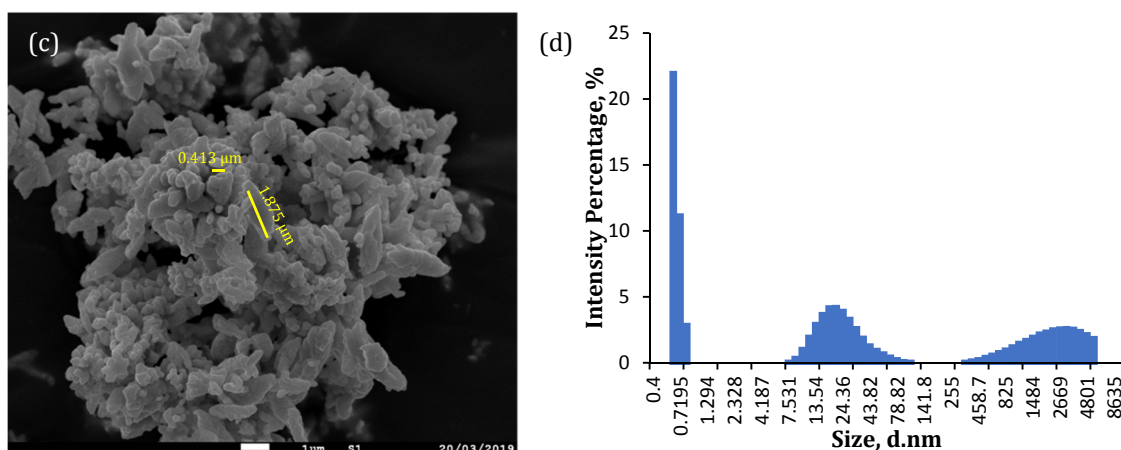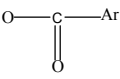
Figure 5-2. SEM images of (a) synthesized templates, (b) composite of bismuth particles with template after mixing 6-8h and washing, (c) bismuth particles after calcination at 600 °C, and (d) size measurement of final product after calcination at 600 °C with 5°/min.

5.4.2. Chemical composition

The XPS survey related to template shows in Figure 5-3a and b and Figure 5-10Sa. It shows that the carbon is mostly C-C within the structure of O_2-C—CH_3 or is within reaction with oxygen. The oxygenated carbons are in the form of C-O or C=O. Furthermore, with analysis and deconvolution of oxygen region in the survey it was observed that the C-O is binding with an aromatic structure in the form of O_2C-aromatic partially and some other parts are in the form of O_2C=O or –(C=O)-O*-(C=O)-, and C=O is binding with an aliphatic structure in the form of O-C=O-C. This shows that this structure has readily active oxygen to bind with bismuth, because C=O is in the aliphatic form and although C-O is mostly binding with aromatic structure but needs less energy to bind with bismuth than C=O (the energy to split the C=O is more than splitting C-O structure normally).

XPS of composite of bismuth particles and template after mixture has been shown in Figure 5-10S b-e. It will show that some part of precipitates (white emulsion) is Bi_2O_3 and some would be in the form of $Bi_2(SO_4)_3$. Also, some sulphate also was being detected in XPS regions of Bi 4f and S 2p, which can be as free sulphate which did not react. By investigating of C 1s XPS survey, it can be seen that most of carbons are C-O in the context of *C-O-C=O. Then, C=O in the context of ketone/aldehyde are positioned at 287.21 eV [51]. Also, C=O was detected from C-O-*C=O. The percentage of C-O binding is most in

135

the C1S. O1s deconvolution survey depicts that most of oxygens are C=O in the context of

O=C-O-C=O or SO_4 in the 532.59 eV. C=O (*O=C-O, [structure: O—C—Ar with =O]) and C-O (*O-C-C=O) have been detected at 531.63 and 533.79 eV, respectively. Furthermore, Bi_2O_3 was detected at 530.52 eV (Figure 5-10S b-e).

XPS of final bismuth product after calcination has been shown in Figure 5-3c-f. It is shown that after calcination at high temperature of 600 °C has resulted in $Bi_2(SO_4)_3$ conversion to Bi_2S_3, there would not be any SO_4 in this sample (Bi4f). Bi_2S_3 was 19.93% and 80.08% is Bi_2O_3 in the Bi4f region. Also, de-carbonization at higher temperature resulted in more carbon removal and leading to the more oxygen percentage allocating to Bi_2O_3. Furthermore, with higher temperature calcination leaded to remove carboxyl removal. Therefore, the final material is a composite of Bi_2O_3 and Bi_2S_3. The allocated peaks for this sample (final product) has been shown in Table 5-6S [51].

(a) C 1s/3

Name	Pos.	%Area
C-C Ref	284.80	46.00
C-C in O2C-C-CH3	285.68	24.49
C-O in C-O-C=O	286.47	16.40
C=O	287.61	10.37
-COOH	289.09	2.73

(b) O 1s/2

Name	Pos.	%Area
C=O aliphatic in O-C=O-C	531.86	49.20
O-C in O-C=O aromatic	533.11	47.00
O-C in O=CO2	533.93	2.48
O-C in -(C=O)-O-(C=O)-	534.51	1.32

(c) Survey/1

Name	Pos.	At%
O 1s-Bi2O3	528.44	5.72
O 1s-Bi2O3	529.86	14.51
O 1s-OH	531.38	25.12
O 1s C-O	532.36	24.75
O 1s H2O	533.51	4.40
C-c graphite	283.40	3.45
C-C ref	284.80	9.47
C-O	286.20	3.57
Bi 4f7/2 Bi2S3	157.72	1.03
Bi 4f5/2 Bi2S3	163.03	0.77
Bi 4f7/2 Bi2O3	158.95	
Bi 4f5/2 Bi2O3	164.26	1.38
Bi 4f7/2-Bi2O3	160.07	2.28
Bi 4f5/2-Bi2O3	165.38	1.71

(d) Bi 4f S 2p/4

Name	Pos.	%Area
Bi 4f7/2 Bi2S3	157.72	11.39
Bi 4f5/2 Bi2S3	163.03	8.54
Bi 4f7/2 Bi2O3	158.95	20.49
Bi 4f5/2 Bi2O3	164.26	15.36
Bi 4f7/2-Bi2O3	160.07	25.28
Bi 4f5/2-Bi2O3	165.38	18.95

(e) C 1s/3

Name	Pos.	At%
C-c graphite	283.40	20.91
C-C ref	284.80	57.42
C-O	286.20	21.67

(f) O 1s/2

Name	Pos.	%Area
O 1s-Bi2O3	528.44	7.68
O 1s-Bi2O3	529.86	19.48
O 1s-OH	531.38	33.71
O 1s C-O	532.36	33.22
O 1s H2O	533.51	5.90

Figure 5-3. Survey XPS spectrum of template (a and b): (a) C1s, (b) O 1s; and survey XPS spectrum of bismuth particles after calcination at 600 °C (c-f): (c) whole spectrum, (d) Bi4f and S2p, (e) C1s, (f) O 1s.

XRD of the final product has is shown below. XRD pattern were with alignment of Bi_2S_3 (JCPDS Card No. 17-0320) [52] and Bi_2O_3 XRD (JCPDS 76-1730) (Figure 5-4) [53]. Some of the XRD patterns will overlap each other (Bi_2S_3 and Bi_2O_3). Material orientation is more inclined towards (211), due to its highest peak (Figure 5-4). The orthorhombic phase Bi_2S_3 (JCPDS 17-0320) [47] and α-Bi_2O_3 (monoclinic phase) with a = 5.8405 (6) Å, b = 8.254 (1) Å, c = 7.330 (1) Å and cell volume = 328.57 (6) (Å)^3 [54].
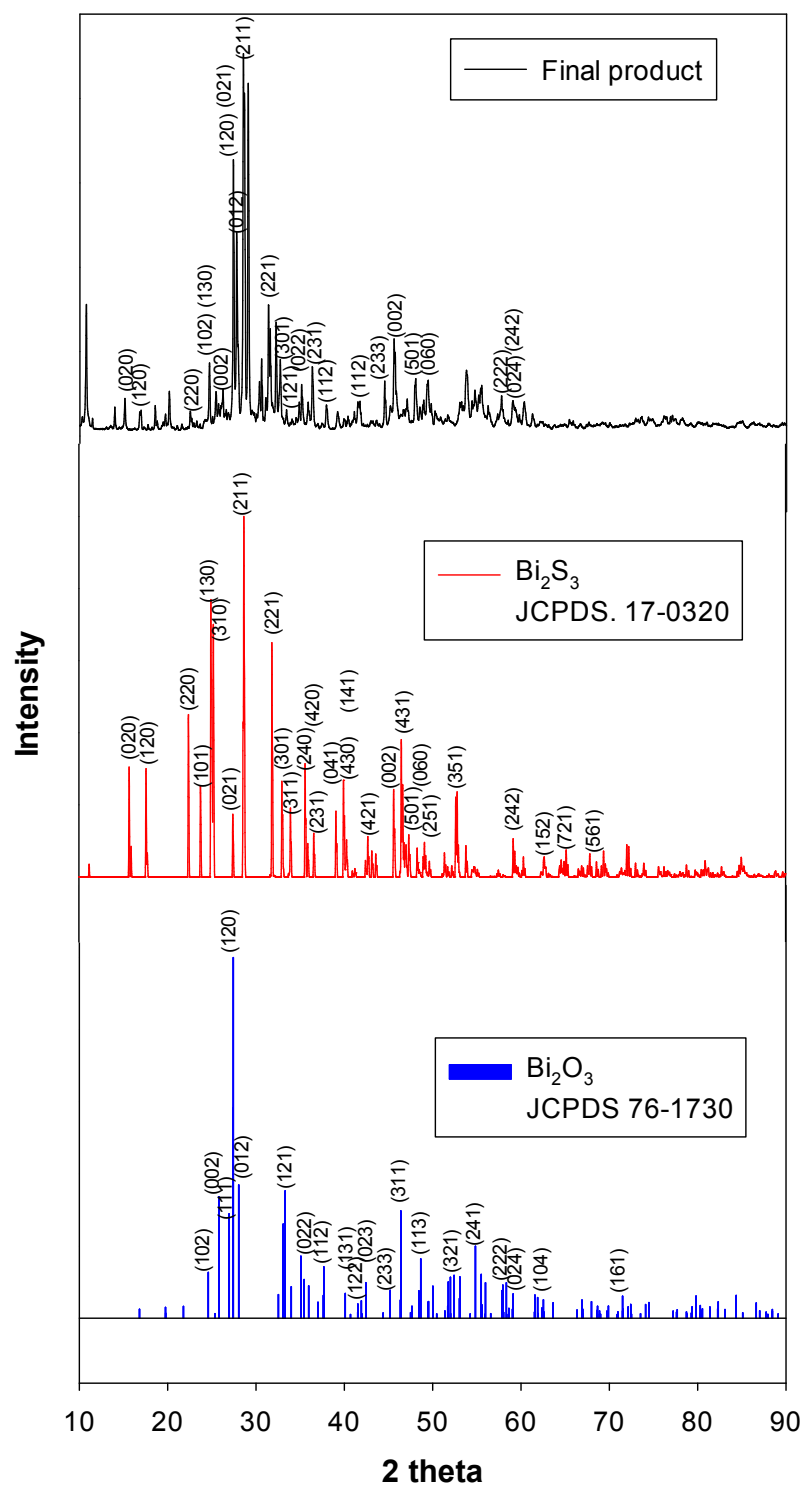
Figure 5-4. XRD pattern of final product after 600 °C calcination and indexing and matching with Bi_2S_3 and Bi_2O_3 XRD patterns.

5.4.3. Proposed mechanism of reactions

5.4.3.1. Template

The mechanism of template formation is being shown in Figure 5-5. As one molecule of sucrose is comprised of one molecule glucose and one molecule fructose, therefore, the glucose part would have the below reactions in the hydrothermal reactions and might form furfural and polyfuranic compounds (Figure 5-5) [55]. However, furfural compounds are not stable above 180 °C. They would form an carbonaceous aromatic network [55]. Hydrothermal reaction would produce oxygen containing molecules such as C-O and carboxylic groups (COOH).
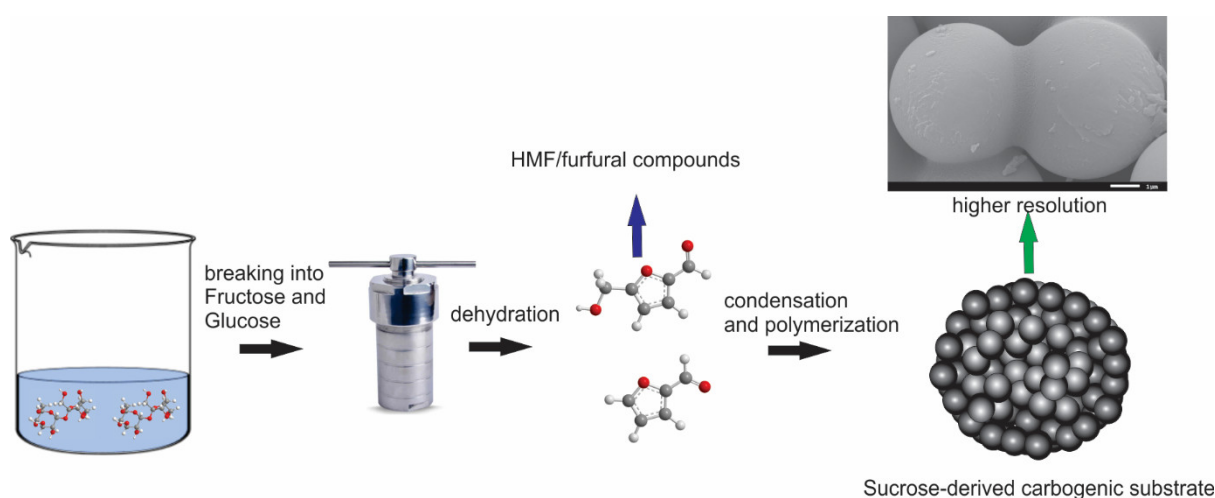
Figure 5-5. The process of carbonaceous material production from sucrose at 200°C.

5.4.3.2. Particles formation and their reaction with template

The next step is formation of bismuth particles in the solution (white emulsion). First of all, $Bi(NO_3)_3$ has been dissociate and dissolved in acetic acid glacial. The dissolving of $Bi(NO_3)_3$ in 10% of acetic acid glacial is due to the below reactions, and based on fully or partially hydrolysing and reaction with acetic acid glacial could produce $Bi(CH_3COO)_3$, $Bi(CH_3COO)_2^+$, $Bi(CH_3COO)^{2+}$, Bi^{3+}, BiO^+. Following with adding Na_2SO_4 in water can produce $Bi_2(SO_4)_3$, $BiSO_4^+$, $Bi_2(SO_4)_2^{2+}$. These products are depending on the hydrolysed products, the reactions are shown below (Equation 5-3-Equation 5-9).

Eventually it can be said that in the mixed solution (formed white precipitates emulsion), there are various products of $Bi_2(SO_4)_3$, $BiSO^+$, $Bi_2SO_4^{2+}$, Bi^{3+}, BiO^+.

Reactions with CH_3COO^- from acetic acid

$Bi(NO_3)_3 + CH_3COOH \rightleftarrows Bi(CH_3COO)_3 + 3H^+ + 3NO_3^-$ (fully hydrolysing) $\xrightarrow{+Na_2SO_4} Bi_2(SO_4)_3$ Equation 5-3

$Bi(NO_3)_3 + CH_3COOH \rightleftarrows Bi(CH_3COO)_2^+ + 3H^+ + 3NO_3^-$ (partially hydrolysing) $\xrightarrow{+Na_2SO_4} BiSO_4^+$ Equation 5-4

$Bi(NO_3)_3 + CH_3COOH \rightleftarrows Bi(CH3COO)^{2+} + 3H^+ + 3NO_3^-$ (partially hydrolysing) $\xrightarrow{+Na_2SO_4} Bi_2(SO_4)_2^{2+}$ Equation 5-5

Reactions with H^+ from acetic acid

$Bi(NO_3)_3 + 3H^+ \rightarrow Bi^{3+} + 3HNO_3$ *Equation 5-6* $\begin{cases} \xrightarrow{+H_2O} Bi^{3+} + H_2O = BiO^+ + 2H^+ \text{ } \textit{Equation 5-7} \xrightarrow{+Na_2SO_4} Bi_2(SO_4)_3 \text{ } \textit{Equation 5-8} \\ \xrightarrow{+Na_2SO_4} BiSO_4^+ \text{ } \textit{Equation 5-9} \end{cases}$
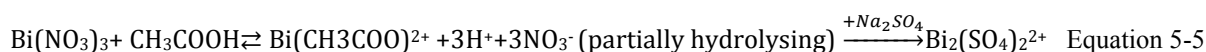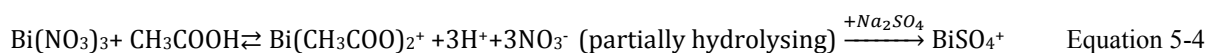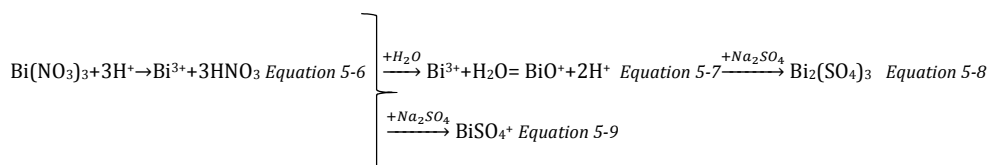
Based on the template surface active areas, Bi^{3+}, BiO^+, $Bi_2(SO_4)_3$, $BiSO_4^+$, $Bi_2SO_4^{2+}$ can interact and attach to template based on electrostatic attractions (Equation 5-10).

Bi^{3+}, BiO^+, $Bi_2(SO_4)_3$, $BiSO_4^+$, $Bi_2(SO_4)_2^{2+}$ $\xrightarrow[\text{Burns off at 600 °C}]{\text{Hydrothermallyed treated Sucrose (C=O,C−O groups)}}$

Formation of Bi_2O_3-Bi_2S_3 Equation 5-10
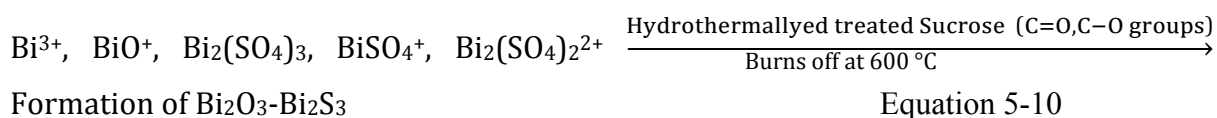
The carbogenic sphere template in this synthesis is important. White precipitates formed in the emulsion have been collected, washed with water and ethanol and measured. In comparison, production yield of the white precipitates was low without template.

This is because various species formed in the solution are $Bi_2(SO_4)_3$, $BiSO^+$, $Bi_2SO_4^{2+}$, Bi^{3+}, BiO^+. Washing the white precipitates with water and ethanol will remove the species. Only $Bi_2(SO_4)_3$ would be in the final precipitates after washing. The white precipitates was

used for halide removal test and the removal was negligible. Hence the material is $Bi_2(SO_4)_3$ and is different from Bi_2O_3-Bi_2S_3 formed in the subsequent template-supported synthesis.

When we applied carbogenic template and stirred it with the white emulsion, the final yield production of bismuth particles was higher than not using the template. Because the active sites (oxygen groups) on the template are ready to absorb the bismuth species in the solution. All of the species of $Bi_2(SO_4)_3$, $BiSO^+$, $Bi_2SO_4^{2+}$, Bi^{3+}, BiO^+ can react to the template and attach to it which would increase the production yield.

5.4.4. Halide removal test

5.4.4.1. Dosage of bismuth composite

The initial iodide and bromide concentration for this experiment was set at 0.05 and 0.5 mg/L, respectively. Various dosages of synthesized bismuth composite (as adsorbent) were used for finding out which dosage is the most efficient for their removal. Adsorption capacity and adsorption removal efficiency were used as parameters for evaluating these experiments. The results shown in Figure 5-6 (a and b) depict that with increasing dosage the removal capacity would be decreasing, which is explained by its formula (Equation5-2). However, with increasing dosage of adsorbent, the removal efficiency was increased. When denominator (m) increases the Q_e decreases. When adsorbent dosage (m) increases, the removal percentage increases, but the Q_e would decrease due to the aforementioned reason (Equation 5-2) [56].

The removal efficiencies for iodide at the equilibrium reached 16.64%, 50.12%, 87.69% with 1, 5 and 8 g/L of bismuth composite, respectively. In addition, the adsorption capacities were 0.0083 mg/g, 0.0050 mg/g and 0.0055 mg/g for 1, 5 and 8 g/L dosages, respectively. The removal efficiencies for bromide at the equilibrium reached 44.17%, 71.74%, 86.38% with 1, 5 and 8 g/L of bismuth composite, respectively, and the corresponding removal capacities were 0.22 mg/g, 0.071 mg/g and 0.054 mg/g for 1, 5 and 8 g/L dosages, respectively. Based on these observations, 8 g/L of bismuth composite was chosen as optimal dosage for iodide and bromide removal and was being used for other experiments. It is notable that iodide removal capacity was lower than bromide

because the initial concentration of bromide was 10 times as high as that of iodide based on a typical water chemical composition (Figure 5-6 a and b).

5.4.4.2.pH

For understanding the pH effect on the removal capacity of iodide and bromide with the bismuth composite, various pH was set in these experiments (2-10). The iodide and bromide concentrations were set 0.05 and 0.5 mg/L, respectively, and the optimal dosage of nano bismuth composite was used (8 g/L), as discussed above.

It was found that with increasing pH, removal capacity of iodide increases. Substantial increase was found when the pH increases from 2 to 6. pH increase from 6 to 10 would result in slight increase in the removal capacity of iodide (Figure 5-6c). The removal would be enhancing after pH 4, probably can be explained by the E_h-pH diagram of iodide (Figure 5-11Sa). At lower pH values, iodide could be in the other forms of $I_{2(aq)}$ and $I_2OH^-_{(aq)}$, which is explaining why at lower pH values the adsorption capacity is lower than higher pH values for iodide (Figure 5-11Sa). Also Decamp and Happel mentioned that iodide in very acidic and very oxidizing condition would be transformed into other species of iodate (IO_3^-) and a small quantity of iodine (I_2). Other than that it is very stable and occurs in the form of iodide (I^-) [29]. These forms (I_2, IO_3^-, HIO) might not have affinity towards bismuth compound. The adsorption capacity for iodide at equilibrium were reached at 0.0023, 0.0046, 0.0055, 0.0052, 0.006 mg/g for pH values of 2, 4, 6, 8 and 10, respectively (Figure 5-6c).

Unlike iodide, bromide removal was not as affected by pH variations. With pH increase, a slight increase in the removal capacity was observed (Figure 5-6c). Basically, bromide is very stable at different pH values dues to the E_h-pH diagram (Figure 5-11Sb). Adsorption capacities were reached to 0.05 mg/g with negligible variations in the broad range of pH values. These results depict that bismuth composite is capable to remove bromide at different pH values with negligible changes in its capacity.

5.4.4.3.Effect of initial concentrations

With increasing initial concentration of the halides ions, the removal capacity was increased (Figure 5-6 d and e), because in its formula initial concentration matters (Equation 5-2). With same initial concentrations such as 0.5, 5 and 8 mg/L of halides, the nano bismuth composite has shown to have almost similar adsorption capacity. For illustration, with 8 mg/L of the removal capacity was reached to 0.94 mg/g and 0.93 mg/L for iodide and bromide, respectively (Figure 5-6 d and e).

Furthermore, the highest tested iodide concentrations (8 mg/L) after 3 hours reaction the iodide concentration was reduced to 0.49 mg/L, which meets the Australian guidelines (0.5 mg/L), nevertheless still too high to meet the other guidelines [24]. This depicts that this material would be a potent adsorbent for iodide to meet the guidelines.

5.4.4.4.Effect of other anions

An artificial ground water (AGW) was made in order to examine the effect of the other anions on the halide removal with nano bismuth composite material. AGW analytic compounds specifications are presented here (Table 5-1) [13]. As can been seen, the removal capacity for both halides at the same condition would be reaching to the same point after 14 hours reaction time and reaching to the equilibrium. However, bromide would have slightly higher adsorption capacity than iodide (Figure 5-6 f).

Therefore, the presence of these anions in water would not have any effect on the removal capacity of iodide and bromide. The final concentration of iodide and bromide would be reached 0.16 mg/L and 0.0091 mg/L, respectively (Figure 5-6 f).

These anions and chloride would not have any effect on the removal, because iodide and bromide have natural tendency/affinity towards bismuth (in case of sulphate). In the case of chloride, iodide and bromide have larger ionic radius and would not allow the replacement of smaller ions/ligands such as chloride. This happens in the soil, and the iodide would not let other smaller anions to be exchanged such as fluoride and hydroxide [8]. Also, when iodide or bromide with same concentrations and same reaction time and water quality being used, their adsorption capacity would be same (Figure 5-6 f).

143

Table 5-1. Analytical compound specifications of AGW.

Ions	Halide (I⁻/Br⁻)	SO₄²⁻	Cl⁻	Na⁺	pH
mg/L	5	0.73	5.51	4.66	6
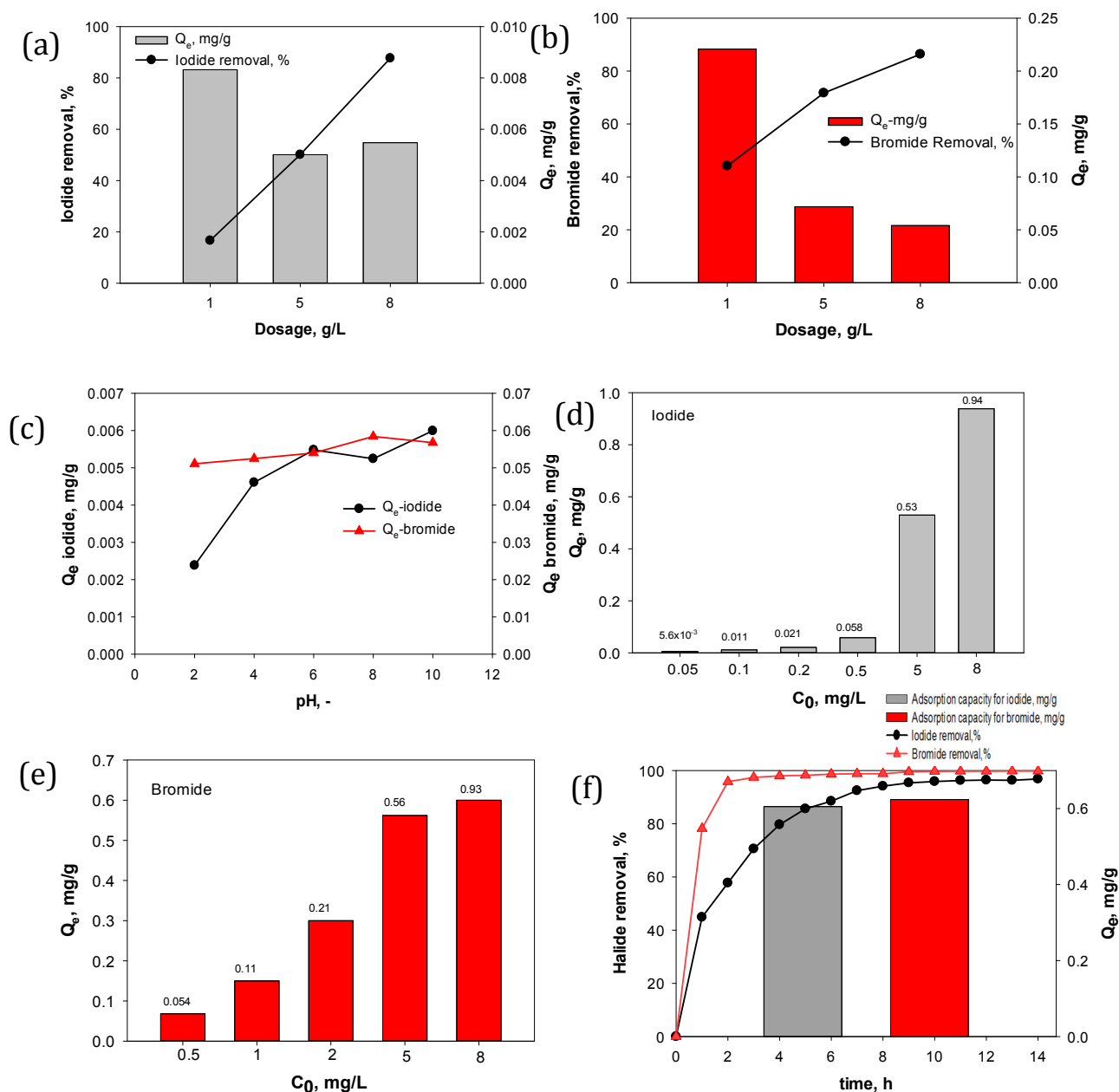
Figure 5-6. Halide removal experiments (a and b) dosage of bismuth compound effect on adsorption capacity and halide removal (c) Effect of pH on iodide and bromide adsorption capacity, (d and e) effect of initial concentrations of iodide and bromide on their adsorption capacity with bismuth composite after equilibrium time, (f) removal

efficiency and adsorption capacity of the bismuth material for iodide and bromide in the artificial ground (AGW): [C_0 iodide=0.05 mg/L and C_0 bromide=0.5 mg/L and without pH adjustment (a,b and c); the initial chemical composition of AGW is C_0 (iodide/bromide)=5 mg/L, C_0 (sulphate)=0.73 mg/L, C_0 (chloride)=5.51 mg/L, C_0 (sodium)=4.66 mg/L, pH=6 (f); and 8 g/L of material being used as optimal dosage for (c, d, e and f); equilibrium time for equilibrium time for (a,b,c,d, and e) iodide:3 hours and for bromide: 14 hours, and equilibrium time for iodide and bromide for f: 14 hours; AGW contained 5 mg/L iodide/bromide (f)].

5.4.4.5.Stability of material during reaction with halides

It has been reported that Bi_2S_3 [57] and Bi_2O_3 [58] are both very stable. For checking the material's stability within the halide removal experiments, the predominance areas of Bi_2O_3 and Bi_2S_3 was checked within various pH and halide concentrations. We used the software Hydra and Medusa that is provided by KTH University-Sweden for checking the predominance areas. The concentration of Bi_2O_3 and Bi_2S_3 were assumed to be 10 mM. The below figure shows that halide would not affect the stability of Bi_2O_3 and Bi_2S_3. At low pH values Bi_2O_3 would be in the form of $Bi_6(OH)_{12}^{6+}$ that can be beneficial for attraction of halide anions, while Bi_2S_3 would be stable (Figure 5-7).

(c)

Log [I⁻]ₜₒₜ ... Bi₂S₃(s) ... pH

(d)

Log [Br⁻]ₜₒₜ ... Bi₂S₃(s) ... pH
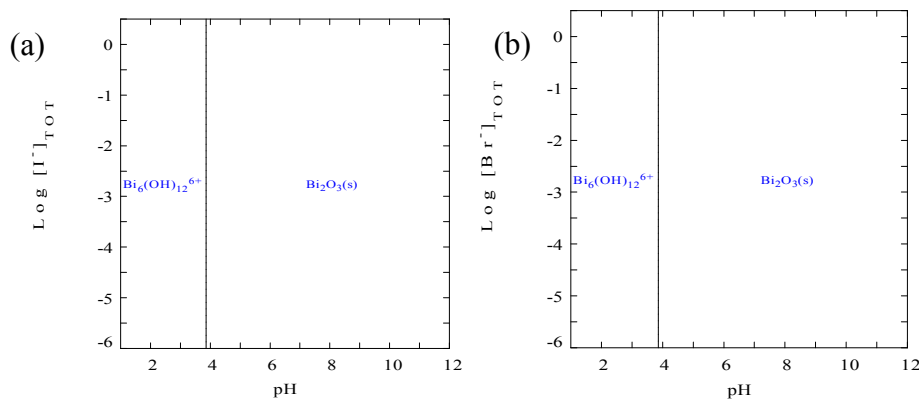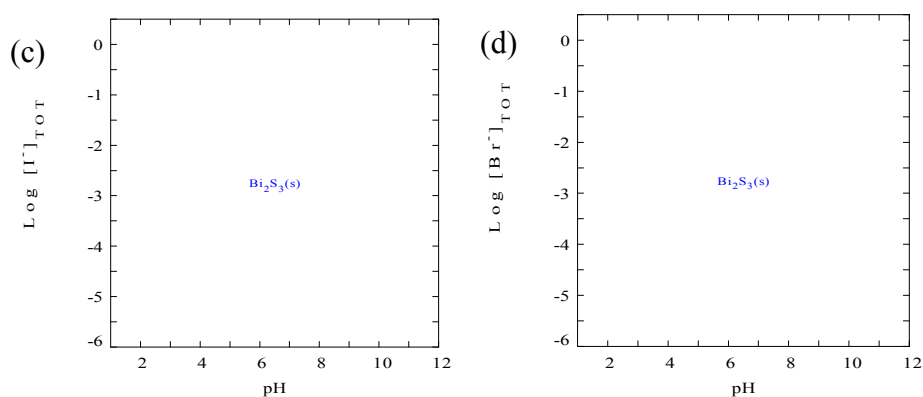
Figure 5-7. Predominance area of Bi₂O₃ and Bi₂S₃ in presence of iodide and bromide at various pH values. Bi₂O₃ in presence of (a) iodide (b) bromide, Bi₂S₃ in presence of (c) iodide, (d) bromide.

Also, Table 5-2 shows that Bi₂S₃ and Bi₂O₃ have very low solubility unless in very concentrated acids [59].

Table 5-2. The reported solubility constant, with other physical properties, and solubility in various solutions for Bi₂O3 and Bi₂S₃ [59].

Name	ksp	Melting point	Boiling point	Solubility in 100 parts solvent
Bi_2O_3	-	817	1890	Insoluble in aqueous; soluble in HCl, HNO_3
Bi_2S_3	1×10^{-97}	850	-	Insoluble in aqueous and ethyl acetate; soluble in HNO_3, HCl

5.4.4.6. Isotherm

Isotherms were used to understand the mechanism of iodide and bromide adsorption on the bismuth composite (Bi₂O₃-Bi₂S₃). The most common used isotherms of Freundlich and Langmuir, and two 3 parameters isotherms of Hill and Langmuir-Freundlich isotherms were used here.

Langmuir isotherm (Equation 5-11) and Freundlich isotherm equations are shown below (Equation 5-12). Where C_e and q_e are the amount of equilibrium concentration of

adsorbate in solution (mg/L), and the amount of equilibrium adsorbed halide at equilibrium (mg/g). In addition, in Freundlich isotherm equation (Equation 5-12), K_F and $1/n$ are representing the Freundlich constants related to the adsorption capacity of adsorbent and tendency of adsorbate to the adsorbed, respectively [60, 61].

$$q_e = \frac{q_m b C_e}{1 + b C_e} \qquad \text{Equation 5-11}$$

$$q_e = K_F C_e^{\frac{1}{n}} \qquad \text{Equation 5-12}$$

The Hill isotherm equation is presented (Equation 5-13) and it describes the different species binding towards the homogenous substrate would influence based on different binding sites [61]. In Equation 5-13, q_{SH} refers to the Hill isotherm uptake saturation (mg/g), and K_D and n_H are constants [62].

$$q_e = \frac{q_{s_H} C_e^{n_H}}{K_D + C_e^{n_H}} \qquad \text{Equation 5-13}$$

Langmuir-Freundlich isotherm equation is as below (Equation 5-14), where q_m is the adsorption capacity of the system (mg of sorbate/g adsorbent), C_{eq} is the equilibrium concentration (mg/L), K_a is the affinity of adsorption (L/mg) and n is the index of heterogeneity [63].

$$q = \frac{q_m (K_a C_{eq})^n}{(K_a C_{eq})^n + 1} \qquad \text{Equation 5-14}$$

Iodide would obey all isotherms specially; it has showed high R^2 values for all isotherms. On the other hand, bromide has highest R^2 value towards Langmuir isotherm, but it is not physically possible because of negative value obtained from the fitting from Langmuir isotherm. Also, if we put $b > 0$ as the condition of fitting, R^2 value would be 0.8662 which is lower than other fitted isotherms. Bromide is obeying all the fitted isotherms (Freundlich isotherm, Hill), except Langmuir isotherm and Langmuir-Freundlich isotherms (Figure 5-8a and Table 5-3).

In Hill isotherm, q_{SH} refers to the hill isotherm uptake saturation (mg/g) and n_H and K_D are constants [62, 64]. In Hill isotherm, n_H for both iodide and bromide are more than 1 which means positive cooperativity in binding. Specifically, n_H is bigger than 1 which shows that adsorbing one molecule iodide or bromide on bismuth composite would enhance the binding of other iodide or bromide molecules [64]. This can be explained by the van der Waals forces between iodide-iodide and bromide-bromide molecules. When one halide (iodide/bromide) molecule attaches to an absorbent, then next molecule (iodide/bromide) has more affinity to also attach due to the van der Waals interactions.

Iodide adsorbed on the homogenous and heterogenous active sites on the adsorbent. Hence it is obeying both Langmuir and Freundlich isotherm. Also, it obeys hill isotherm that shows the sorbate-sorbate interactions also play a role in the adsorption of the next molecule [61]. First, the adsorption of iodide is the monolayer on the homogenous surfaces of adsorbent. Iodide would attach to the first to the sites with stronger binding sites and then the rest would be adsorbing to the rest of the sites till get into the equilibrium. Then the non-homogenous sites would get occupied by iodide in multilayers. Also based on the Hill isotherm it is showing that the iodide which already adsorbed on the adsorbent, the next iodide can attach to the next iodide or the iodide already attached to the adsorbent have cooperative interactions which helps to adsorb more iodide to the adsorbent. Finally, iodide follows Langmuir-Freundlich isotherm, and this isotherm is converting to Langmuir isotherm hence n is 1. Iodide can have more attraction to the homogenous surfaces than non-homogenous surfaces. Because the q_m in Langmuir isotherm is bigger than K_F in Freundlich isotherm, K_F shows the adsorption capacity in L/mg [65].

However, bromide cannot bind onto the monolayer and homogenous active sites of the adsorbent. As it was mentioned was not obeying the Langmuir isotherm. This might be because bromide is a smaller ion than iodide and the Van der Waals forces related to iodide (bigger molecule) is bigger than bromide. Non homogenous active sites of adsorbent play a key role in the adsorption in the case of bromide. Hence Freundlich isotherm is obeyed and the next bromide molecules are added in multilayers. Bromide-

148

bromide interactions also have a cooperative effect on the bromide adsorption. K_F for bromide is higher than iodide, which shows the capacity of adsorption of bromide on the non-heterogenous surface is higher for bromide than iodide. But iodide has higher adsorption capacity on the homogenous surfaces based on q_m in Langmuir isotherm. Bromide does not follow Langmuir -Freundlich isotherm because the low R^2 value.

In nutshell, non-homogenous active sites are playing a key role for adsorption of both iodide and bromide. Also, the sorbate-sorbet interactions are playing a positive role in adsorption.

Table 5-3. Various calculated parameters of Langmuir, Freundlich, and Hill isotherms.

Isotherms	Langmuir isotherm			Freundlich isotherm			Hill isotherm				Langmuir-Freundlich isotherm			
Parameters	q_m	b	R^2	K_F	1/n	R^2	q_{SH}	K_D	n_H	R^2	q_m	k_a	n	R^2
Iodide	3.025	0.28	0.9978	0.6212	0.8289	0.9954	2.2138	2.339	1.129	0.9981	3.025	2.760×10^{-1}	1	0.9978
bromide	-0.3470	-1.2	0.9602	1.854	1.676	0.9359	5598×10^4	3019×10^4	1.676	0.9359	6.997×10^6	1.623×10^{-7}	1	0.8662

5.4.4.7.Kinetic

Two different kinetics of pseudo first order (PFO) and pseudo second order (PSO) were used for kinetic studies. Based on the calculations (R^2), it can be concluded that best PSO for iodide and bromide (Figure 5-8b-c and Table 5-4). PFO fitted graphs are shown in Figure 5-12S. PSO is a better fit for both iodide and bromide. It is because PSO is a better model when C_0 is low. Other than that, PSO depicts that adsorbent is abundant with active sites, and adsorption is in the final stage. PSO also shows adsorption on active sites is the kinetic controlling rather than internal diffusion and external diffusion [66, 67].

Furthermore, with increasing initial concentrations of halides (iodide and bromide), k_2 values which is representing of reaction rates, has been decreased [67].

Also, iodide has a faster kinetic rate compared to bromide. For example, k_2 value was 0.502641 g mg^{-1} min^{-1} for 0.5 mg/L of iodide, while this value would be 6.271429 g mg^{-1} h^{-1} for 0.5 mg/L of bromide.

Table 5-4. Pseudo-first- order and Pseudo-second- order kinetics calculation based on different initial halides concentration.

	Pseudo-first order-kinetic					Pseudo-second order-kinetic			
	Concentration, mg/L	$Q_{e\,(exp)}$ mg g^{-1}	$Q_{e(cal)}$ mg g^{-1}	K_1 1/ min	R^2	$Q_{e\,(exp)}$ mg g^{-1}	$Q_{e\,(cal)}$ mg g^{-1}	K_2 g mg^{-1} min^{-1}	R^2
Iodide	0.05	5.631×10^{-3}	5.371×10^{-3}	0.02459	0.9602	0.005631	0.006655	3.969	0.9903
	0.1	0.01126	0.01074	0.02459	0.9602	0.01126	0.01331	1.987	0.9904
	0.2	0.02101	0.02049	0.02002	0.9011	0.02101	0.02587	0.8063	0.9567
	0.5	0.05816	0.05498	0.03134	0.9099	0.05816	0.06704	0.5026	0.9864
	5	0.5298	0.6904	8.032×10^{-3}	0.9836	0.5298	0.8951	0.008467	0.9040
	8	0.9383	0.9771	0.01430	0.9247	0.9383	0.9658	0.1748	0.9998
	Pseudo-first order-kinetic					Pseudo-second order-kinetic			
	Concentration, mg/L	$Q_{e\,(cal)}$ mg g^{-1}	$Q_{e(exp)}$ mg g^{-1}	K_1 1/h	R^2	$Q_{e\,(cal)}$ mg/g	$Q_{e(exp)}$ mg g^{-1}	K_2 g mg^{-1} h^{-1}	R^2
Bromide	0.5	0.05331	0.05399	0.3443	0.9894	0.06409	0.05399	6.271	0.9987
	1	0.1263	0.1063	0.1565	0.9617	0.1587	0.1063	1.047	0.9727
	2	0.3148	0.2125	0.07265	0.9886	0.3695	0.2125	0.2081	0.9430
	5	0.5691	0.5548	0.2602	0.9979	0.7285	0.5548	0.3442	0.9945
	8	0.8437	0.9250	0.7581	0.8799	1.016	0.9250	0.6386	0.9905

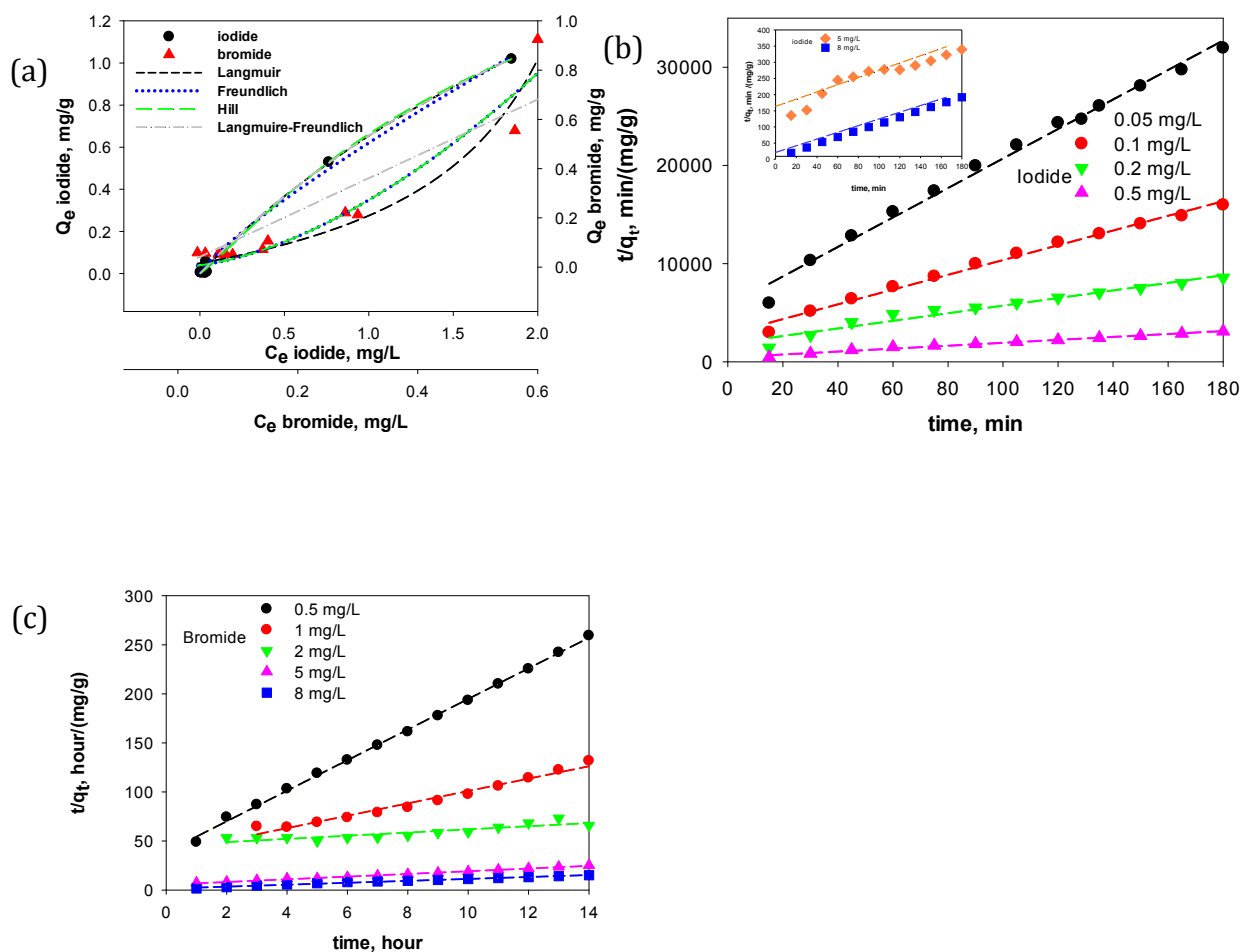Figure 5-8. Isotherms and kinetics fitting; (a) fitted isotherms of Langmuir, Freundlich, hill and Langmuir-Freundlich for iodide and bromide; (b) fitted PSO model for iodide and, (d) and fitted PSO model for bromide.

The following table is representing some methods for iodide and bromide removal compared to current method (Table *5-5*). This illustrates the potential of this adsorbent for removing iodide and bromide from water.

Table 5-5. Comparison of different methods and their capacity for iodide and bromide removal with current study.

Removal type	Adsorbent name	I⁻ removal capacity (µmol/g)/removal %	Br⁻ removal capacity (µmol/g)/removal%	Water type	Ref
Adsorption	Activated Ag-aerogel (A-C)	3.71	4.68 µmol/g	Lake Zürich (switzerland)	[68]
	Activated Ag-aerogel (A-A)	5.03	5.78 µmol/g	Lake Zürich (switzerland)	
	Ag aerogel (A)	1.98	3.01 µmol/g	Lake Zürich (switzerland)	
	Sub-bituminous coal	-	46%	Synthetic water	[69]
	Udic Ferrisols	57.5%	-	Synthetic water	[39]
	Silver impregnated activated carbon (20 wt % of Ag)	98%	-	Synthetic water	[70]
	Bismuth composite	4.770 µmol/g (96.846%)	7.808 µmol/g (99.818%)	Artificial ground water	(current study)
Resin	MIEX®	-	0-94%	synthetic water, Natural water	[71, 72]
Coagulation	Aluminium coagulation		30.4-98.8%	Synthetic water and natural water	[30, 31]
Coagulation and resin	EC/GAC	65%-85%	14.9%-34%	Water treatment plant at Capalaba, Mt Crosby, and Molendinar - Qld	[41]
	EC/SIAC	65-87%	79.4-94.5%		
	EC/MIEX	>65%	46.1-89.2%		

5.5. Conclusion

In this work, we first demonstrated a novel carbogenic sphere-supporting method for synthesizing Bi_2O_3-Bi_2S_3 submicron particles in high yield. Carbogenic microspheres were synthesized by a hydrothermal treatment of sucrose solution at 200 °C for 2 hrs. Due to the rich C-O and C=O groups on surface on the carbogenic microspheres, as revealed by XPS analysis, mixing with a mixture of $Bi(NO_3)_3$ and Na_2SO_4 solution resulted in high yield precipitation. The high electronegativity of C-O and C=O sites appear to initiate or catalyse the $Bi_2(SO_4)_3$ and Bi_2O_3 precipitation on the carbogenic spheres. The solid phase of the mixture was then collected, washed, dried and calcinated at 600 °C in air. The resultant mixture of white -yellow powder was characterised to be Bi_2O_3-Bi_2S_3 composite in semi-rod to irregular shape of submicro- to micrometer size. The carbogenic spheres appear to have functioned as space separators that prevent aggregation during calcination.

The resultant Bi_2O_3-Bi_2S_3 composite showed extraordinary removal efficiency towards iodide and bromide at concentrations that are typical to fresh water sources (0.05 mg/L for I⁻ and 0.5 mg/L for Br⁻). The optimum dosage of bismuth composite for the tested ranges of iodide and bromide, based on Q_e and removal efficiency was 8 g/L. pH variations would have effect on the iodide but not on the bromide removal. Furthermore, this material was effective for higher concentrations of iodide and bromide up to 8 mg/L. Iodide and bromide were effectively removed from an artificial groundwater, almost with almost same adsorption capacity of 0.61 and 0.62 mg/g, respectively, showing no interference on the adsorption by other ions. Isotherm studies depict that iodide obeys all fitted isotherms, and bromide obeys all isotherms except Langmuir isotherm and Langmuir- Freundlich isotherm. n_H values for both iodide and bromide were higher than 1 that shows with attaching one iodide or bromide molecule to the bismuth composite the next iodide or bromide molecule would have more affinity to attach to the bismuth composite.

5.6. Supplementary information

Removal of iodide and bromide at low/trace concentrations with novel bismuth composite material

Elham Nariyan[1,2], Nikhil Aravindakshan [1,2], Qiming Jimmy Yu[2] and Qin Li[1,2]*

1. Queensland Micro- and Nanotechnology Centre, Griffith University, Nathan, QLD 4111, Australia
2. School of Engineering and Built Environment, Griffith University, Nathan, QLD 4111, Australia

Surface area of template synthesized from hydrothermal treated of sucrose at 200 °C for 2hrs (Figure 5-9S). Template surface area was not detected by the BET instrument. This is because of big carbonaceous spheres (few μm) formed from hydrothermal process.
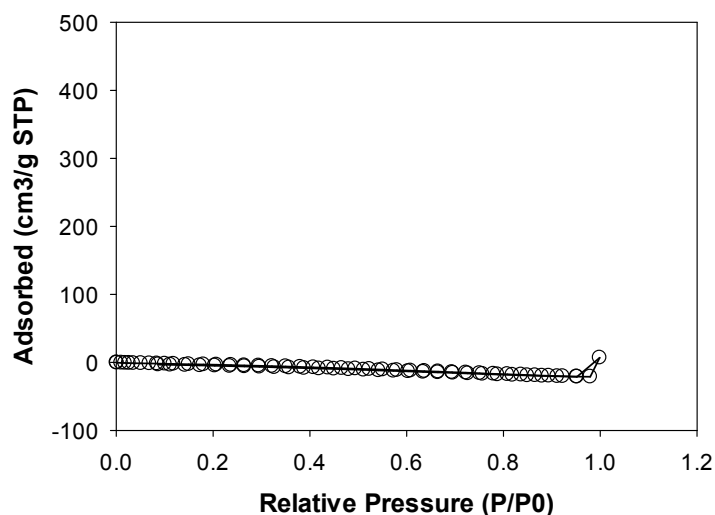
Figure 5-9S. N$_2$ adsorption and desorption isotherms for various template.

The chemical composition of template (the whole spectrum) has been shown in Figure 5-10Sa. This shows that the carbonaceous spheres have functional groups of C-O and C=O in different matrixes.

The XPS survey of matrix bismuth particles with template is shown in Figure 5-10S (b-e). The results show the particles formed on the template are Bi$_2$O$_3$ and Bi$_2$(SO$_4$)$_3$.

(a)

survey/2

Name	Pos.	At%
C=O aliphatic in O-C=O-C	531.86	11.31
O-C in O-C=O aromatic	533.11	10.81
O-C in O=CO2	533.93	0.57
O-C in -(C=O)-O-(C=O)-	534.51	0.30
C-C Ref	284.80	35.43
C-C in O2C-C-CH3	285.68	18.86
C-O in C-O-C=O	286.47	12.63
C=O	287.61	7.99
-COOH	289.09	2.10

CasaXPS (This string can be edited in CasaXPS.DEF/PrintFootNote.txt)
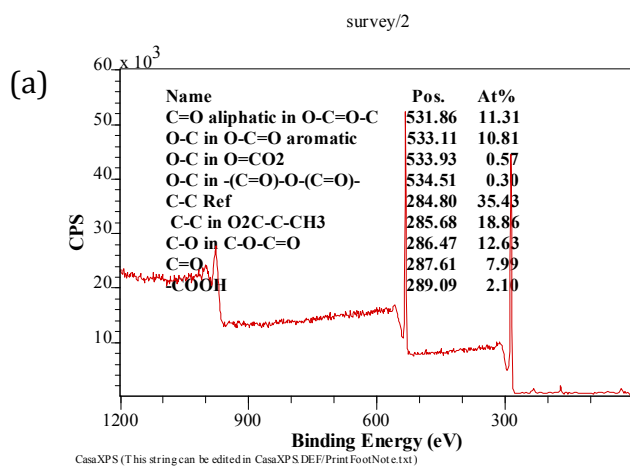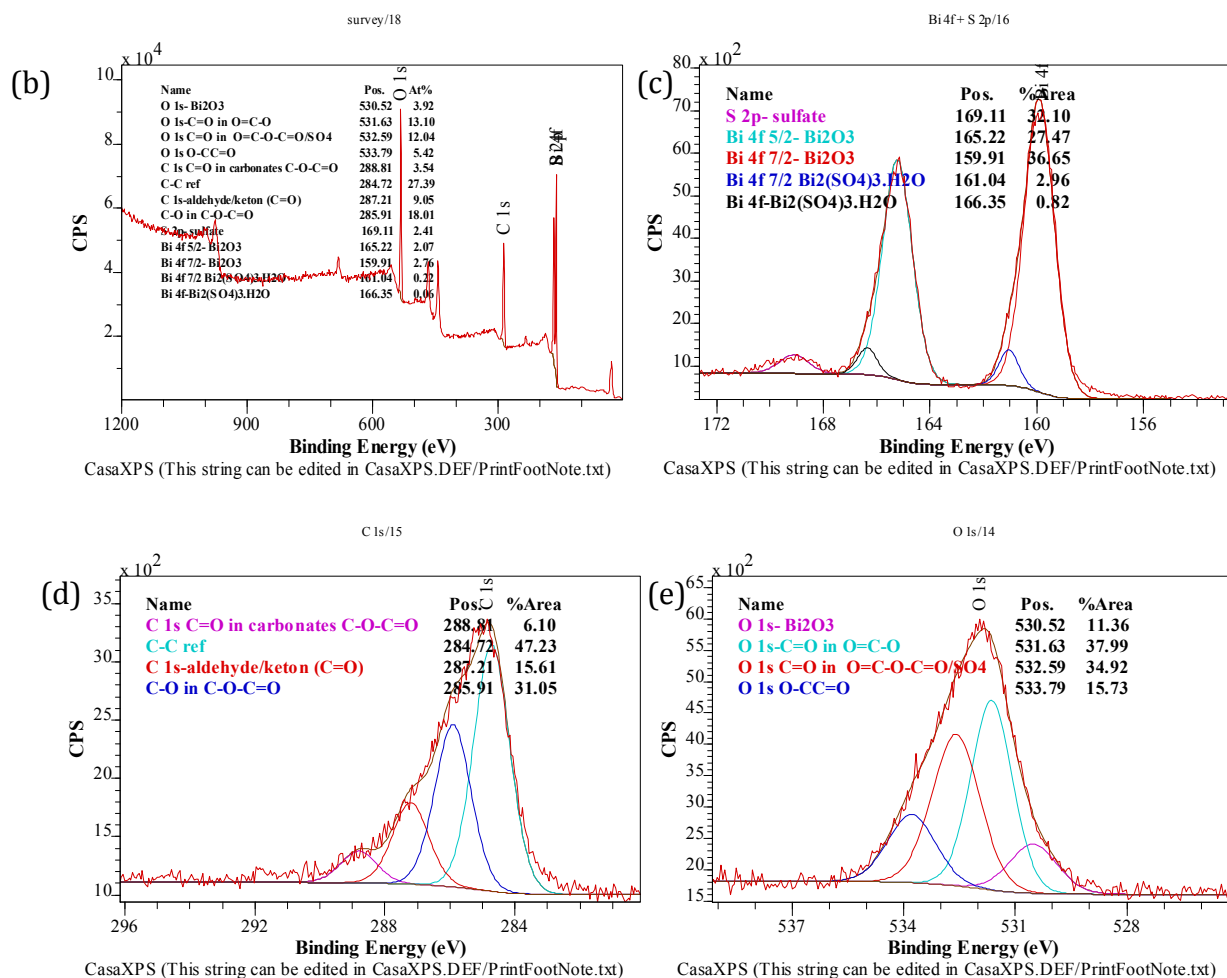
Figure 5-10S. Survey XPS spectrum of: (a) the whole spectrum of template; survey XPS spectrum of composite after mixing within 6-8h (b-e): (b) whole spectrum, (c) Bi4f and S2p, (d) C1s, (e) O 1s. .

After calcination at 600 °C, XPS results showed that the material is transformed from Bi_2O_3-$Bi_2(SO_4)_3$ to Bi_2O_3-Bi_2S_3. The allocated peaks are extracted and are shown in Table 5-6S [51].

Table 5-6S. XPS peaks and the allocate to final product calcined at 600 °C extracted [51].

Element	Peaks	Compound
O 1s	528.44	Metal oxide
O 1s	529.86	Metal oxide
O 1s	531.38	hydroxide

O 1s	532.37	C-O
O 1s	533.5	H_2O
C 1 s	283.40	C-C graphite
C 1 s	284.80	C-C ref
C 1 s	286.20	C-O
Bi 4f 7/2	157.72	Bi_2S_3
Bi 4f 5/2	163.03	Bi_2S_3
Bi 4f 7/2	158.95	Bi_2O_3
Bi 4f 5/2	164.26	Bi_2O_3
Bi 4f 7/2	160.07	Bi_2O_3
Bi 4f 5/2	165.38	Bi_2O_3

In E_h-pH diagrams, FACT database was used which is available and released by GTT-Technologies [73]. It shows that at very acidic condition iodide would transform into I_2OH^- (Figure 5-11Sa). This explains why at low pH values iodide removal would be lower. However, bromide is stable at whole pH range shown (Figure 5-11Sb).
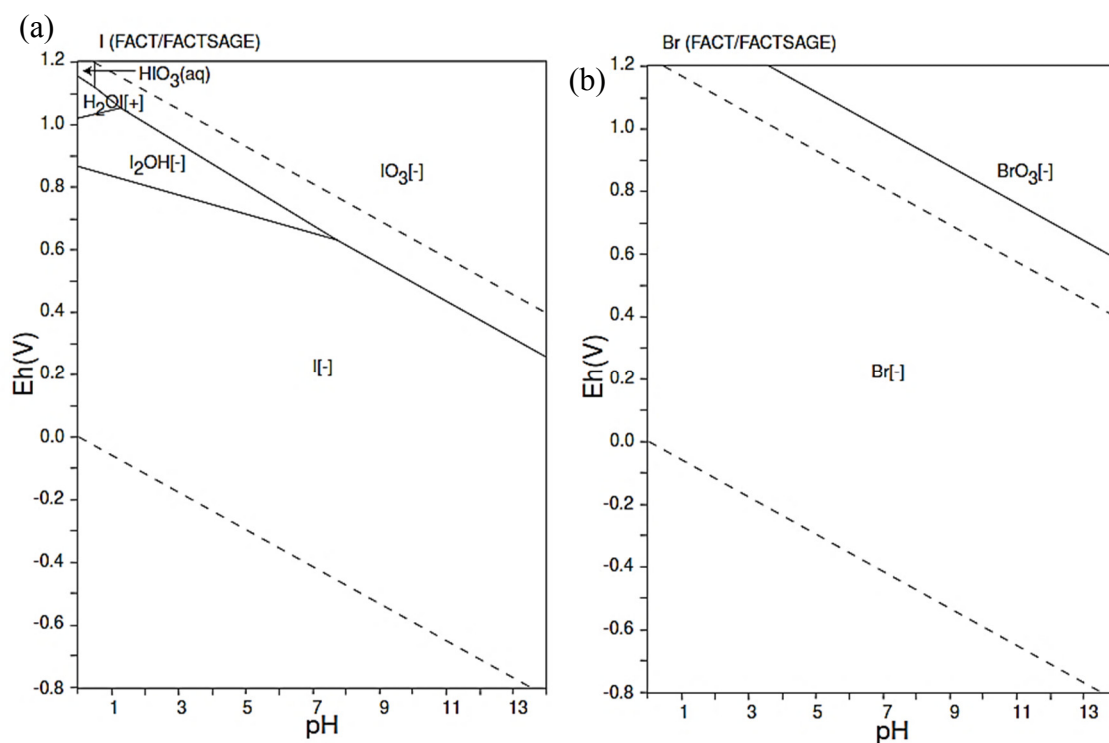
Figure 5-11S. E_h-pH diagrams of (a): I-O-H and (b): Br-O-H with various data base and considerations of activity I= 10^{-10} and Br= 10^{-10} and within 10^5 Pa and T= 298.15 K [73].

Pseudo first order (PFO) kinetics was used for iodide and bromide removal studies (Figure 5-12S). R^2 values show that the PFO is fitted well for halides, but not as good as PSO (Table 5-4). Generally, with increasing initial concentration k_1 values decreased for both iodide and bromide. However, there are some exceptions such as 5 mg/L and 8 mg/L for bromide, k_1 value increased [67].
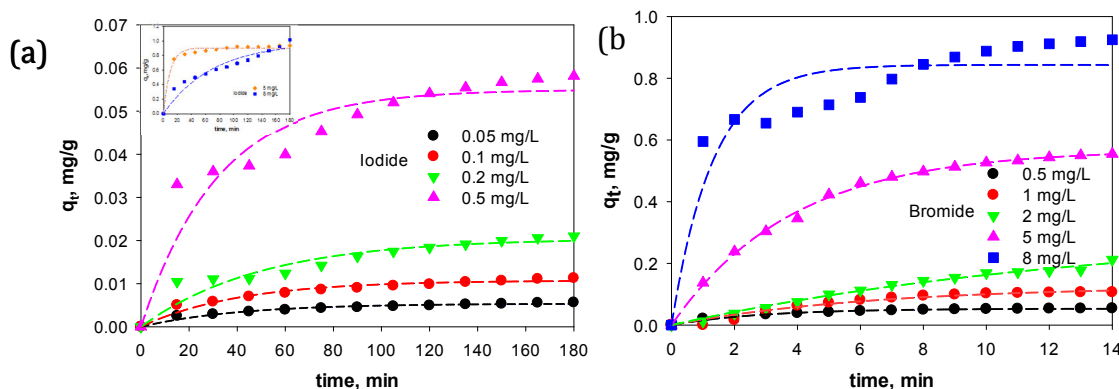
Figure 5-12S. Fitted PFO model (a,): iodide and (b) bromide.

References

1. Álvarez, F., et al., *Iodine budget in surface waters from Atacama: Natural and anthropogenic iodine sources revealed by halogen geochemistry and iodine-129 isotopes.* Appl. Geochem., 2016. **68**: p. 53-63.

2. Northey, S.A., et al., *Water footprinting and mining: Where are the limitations and opportunities?* J. Cleaner Prod., 2016. **135**: p. 1098-1116.

3. Fruit, J.T., et al., *Recovery of Iodine from Produced Water Through Anion Resin Exchange*, in *2011 Research Experiences for Undergraduates posters and presentations*. 2011, Advanced Water Technology Center (AQWATEC) Colorado School of Mines, 1500 Illinois street, Golden, CO 80401.

4. Kim, H.I., et al., *A process to recover high purity iodine in wastewater from liquid crystal display (LCD) manufacturing industry.* Hydrometallurgy, 2018. **181**: p. 91-96.

5. Ordóñez, J.I., et al., *Use of discharged brine from reverse osmosis plant in heap leaching: Opportunity for caliche mining industry.* Hydrometallurgy, 2015. **155**: p. 61-68.

6. Rong, J., et al., *High-specific surface area hierarchical Al$_2$O$_3$ carbon fiber based on a waste paper fiber template: preparation and adsorption for iodide ions.* J. Wood Chem. Technol., 2017. **37**(6): p. 485-492.

7. Liu, Y., et al., *An investigation into the use of cuprous chloride for the removal of radioactive iodide from aqueous solutions.* J. Hazard. Mater., 2016. **302**: p. 82-89.

8. Liu, Y. and H.R.v. Guten, *migration chemistry and behaviour of iodine relevant to geological disposal of radioactive wastes-a literature review with a compilation of sorption data*, in *Technischer Bericht 88-29*. 1998. p. 183.

9. Majidnia, Z. and A. Idris, *Photocatalytic reduction of iodine in radioactive waste water using maghemite and titania nanoparticles in PVA-alginate beads.* J. Taiwan Inst. Chem. E., 2015. **54**: p. 137-144.

10. Foreman, M.R.S.J., *An introduction to serious nuclear accident chemistry.* Cogent Chem., 2015. **1**(1): p. 1049111.

11. Madrakian, T., et al., *Application of Modified Silica Coated Magnetite Nanoparticles for Removal of Iodine from Water Samples.* Nano-Micro Lett., 2012. **4**(1): p. 57-63.

12. Theiss, F.L., G.A. Ayoko, and R.L. Frost, *Iodide removal using LDH technology.* Chem. Eng. J., 2016. **296**: p. 300-309.

13. Li, D., et al., *Removal capacity and chemical speciation of groundwater iodide (I$^-$) and iodate (IO$_3^-$) sequestered by organoclays and granular activated carbon.* J. Environmen. Radioactiv., 2018. **192**: p. 505-512.

14. Hu, Q., J.E. Moran, and V. Blackwood, *Geochemical Cycling of Iodine Species in Soils*. 2007: The Comprehensive Handbook on Iodine, Geochemical Cycling of Iodine Species in Soils, Academic Press, New York, NY 2009, pp. 95-107; Lawrence Livermore National Lab. (LLNL), Livermore, CA (United States). Medium: ED; Size: PDF-file: 41 pages; size: 0.2 Mbytes.

15. Liu, H., Y. Cui, and B. Zhang, *Effects of Iodine and Fluorine in Drinking Water on Human Health*, in *Encyclopedia of Environmental Health (Second Edition)*, J. Nriagu, Editor. 2019, Elsevier: Oxford. p. 256-263.

16. Ateia, M., et al., *Selective removal of bromide and iodide from natural waters using a novel AgCl-SPAC composite at environmentally relevant conditions.* Water Res., 2019. **156**: p. 168-178.

17.   Gruchlik, Y., et al., *Impact of bromide and iodide during drinking water disinfection and potential treatment processes for their removal or mitigation.* Water, 2014. **41**(8): p. 38-43.

18.   Rajaeian, B., *Removal of Bromide from Drinking Water Sources using Silver impregnated activated carbon (SIAC) understanding Br-SIAC interactions*, in *Department of Civil Engineering*. 2017, Curtin University: Curtin University.

19.   Ates, N., U. Yetis, and M. Kitis, *Effects of Bromide Ion and Natural Organic Matter Fractions on the Formation and Speciation of Chlorination By-Products.* J. Environ. Eng., 2007. **133**(10): p. 947-954.

20.   WHO, *Bromide in drinking-water. Background document for development of WHO Guidelines for Drinking-water Quality*. 2009.

21.   Al-Mutaz, I., *Water desalination in the Arabian Gulf region.* Water Purification, 2000. **2**: p. 245-265.

22.   Dorji, P., et al., *Membrane capacitive deionisation as an alternative to the 2nd pass for seawater reverse osmosis desalination plant for bromide removal.* Desalination, 2018. **433**: p. 113-119.

23.   Yu, F., et al., *Enhanced removal of iodide from aqueous solution by ozonation and subsequent adsorption on Ag-Ag$_2$O modified on Carbon Spheres.* Appl. Surf. Sci., 2018. **427**: p. 753-762.

24.   NHMRC and NRMMC, *Australian Drinking Water Guidelines Paper 6 National Water Quality Management Strategy*. 2011: National Health and Medical Research Council, National Resource Management Ministerial Council, Commonwealth of Australia, Canberra.

25.   A.M.S, P., et al., *Halide removal from aqueous solution by novel silver-polymeric materials.* Sci. Total Environ., 2016. **573**: p. 1125-1131.

26.   Rivera-Utrilla, J., et al., *New Technologies to Remove Halides from Water: An Overview*, in *Advanced Research in Nanosciences for Water Technology*, R. Prasad and T. Karchiyappan, Editors. 2019, Springer International Publishing: Cham. p. 147-180.

27.   Polo, A.M.S., et al., *Halide removal from waters by silver nanoparticles and hydrogen peroxide.* Sci. Total Environ., 2017. **607-608**: p. 649-657.

28. Kentjono, L., et al., *Removal of boron and iodine from optoelectronic wastewater using Mg–Al (NO$_3$) layered double hydroxide.* Desalination, 2010. **262**(1): p. 280-283.

29. Decamp, C. and S. Happel, *Utilization of a mixed-bed column for the removal of iodine from radioactive process waste solutions.* J. Radioanal. Nucl. Chem., 2013. **298**(2): p. 763-767.

30. Ge, F. and L. Zhu, *Effects of coexisting anions on removal of bromide in drinking water by coagulation.* J. Hazard. Mater., 2008. **151**(2): p. 676-681.

31. Ge, F., H. Shu, and Y. Dai, *Removal of bromide by aluminium chloride coagulant in the presence of humic acid.* J. Hazard. Mater., 2007. **147**(1-2): p. 457-62.

32. Choung, S., et al., *Effects of radiation and temperature on iodide sorption by surfactant-modified bentonite.* Environ. Sci. Technol., 2014. **48**(16): p. 9684-91.

33. Warchoł, J., et al., *Preparation and application of organo-modified zeolitic material in the removal of chromates and iodides.* J. Hazard. Mater., 2006. **137**(3): p. 1410-1416.

34. Faghihian, H., M. Ghannadi Maragheh, and A. Malekpour, *Adsorption of radioactive iodide by natural zeolites.* J. Radioanal. Nucl. Ch., 2002. **254**(3): p. 545-550.

35. Ikeda, Y., et al., *Adsorption of I$^-$ Ions on Cinnabar for ^{129}I Waste Management.* Radiochim. Acta, 1994. **65**(3): p. 195-198.

36. Bors, J., S. Dultz, and A. Gorny, *Sorption of Iodide, Cesium and Strontium on Organophilic Bentonite.* Radiochim. Acta, 1998. **82**(1): p. 269-274.

37. Sadasivam, S. and S.M. Rao, *Characterization of silver–kaolinite (AgK): an adsorbent for long-lived 129I species.* SpringerPlus, 2016. **5**(1): p. 142.

38. Watson, K., M.J. Farré, and N. Knight, *Strategies for the removal of halides from drinking water sources, and their applicability in disinfection by-product minimisation: A critical review.* J. Environ. Manage., 2012. **110**: p. 276-298.

39. Dai, J.L., et al., *Adsorption and desorption of iodine by various Chinese soils: II. Iodide and iodate.* Geoderma, 2009. **153**(1): p. 130-135.

40. Peng, B.-x. and D.-s. Wu, *Distribution and content of bromine in Chinese coals.* J. Fuel Chem. Technol., 2014. **42**(7): p. 769-773.

41.   José Farré, M., et al., *Assessment of Regulated and Emerging Disinfection By-Products in South East Queensland Drinking Water*. 2012: Urban Water Security Research Alliance.

42.   Nenoff, T., J.L. Krumhansl, and A. Rajan, *In-situ Formation of Bismuth-Based Iodine Waste Forms.* MRS Proceedings, 2007. **1043**: p. 1043-T12-05.

43.   Krumhansl, J.L. and T.M. Nenoff, *Hydrotalcite-like layered bismuth–iodine–oxides as waste forms.* Appl. Geochem., 2011. **26**(1): p. 57-64.

44.   Liu, L., et al., *Selective Capture of Iodide from Solutions by Microrosette-like δ-Bi_2O_3.* ACS Appl. Mater. Inter., 2014. **6**(18): p. 16082-16090.

45.   Xu, W., et al., *Facile synthesis of mesoporous Fe-based MOFs loading bismuth with high speed adsorption of iodide from solution.* J. Solid State Chem., 2019. **269**: p. 558-565.

46.   Sang, Y., et al., *Facile one-pot synthesis of novel hierarchical Bi_2O_3/Bi_2S_3 nanoflower photocatalyst with intrinsic p-n junction for efficient photocatalytic removals of RhB and Cr(VI).* J. Hazard. Mater., 2020. **381**: p. 120942.

47.   Lu, F., et al., *Synthesis of Bi_2S_3–Bi_2O_3 composites and their enhanced photosensitive properties.* RSC Adv., 2014. **4**(11): p. 5666-5670.

48.   Luo, W., et al., *Heterostructured Bi_2S_3-Bi_2O_3 Nanosheets with a Built-In Electric Field for Improved Sodium Storage.* ACS Appl. Mater. Interfaces, 2018. **10**(8): p. 7201-7207.

49.   Liu, S., et al., *Efficient removal of radioactive iodide ions from water by three-dimensional Ag_2O–Ag/TiO_2 composites under visible light irradiation.* J. Hazard. Mater., 2015. **284**: p. 171-181.

50.   Zhao, H., et al., *Effects of additives on sucrose-derived activated carbon microspheres synthesized by hydrothermal carbonization.* J. Mater. Sci., 2017. **52**(18): p. 10787-10799.

51.   Moulder, J.F., et al., *Handbook of X-Ray Photoelectron Spectroscopy (perkin elmer).* 1992: Perkin-Elmer Corporation.

52.   Li, Y., et al., *Selected-Control Hydrothermal Synthesis and Photoresponse Properties of Bi_2S_3 Micro/Nanocrystals.* CrystEngComm, 2013. **15**(33): p. 6611-6616

53. M. J, J.F., N. C. V, and S. S, *α-Bi₂O₃ photoanode in DSSC and study of the electrode–electrolyte interface.* RSC Adv., 2015. **5**(95): p. 78299-78305.

54. M, M. and P. Padiyan, *Role of pH in the hydrothermal synthesis of phase pure alpha Bi₂O₃ nanoparticles and its structural characterization.* Adv. Mater. Proc., 2016. **2**: p. 51-55.

55. Falco, C., N. Baccile, and M.-M. Titirici, *Morphological and structural differences between glucose, cellulose and lignocellulosic biomass derived hydrothermal carbons.* Green Chem., 2011. **13**(11): p. 3273.

56. Silva, C.E.d.F., et al., *Basic-dye adsorption in albedo residue: Effect of pH, contact time, temperature, dye concentration, biomass dosage, rotation and ionic strength.* J. King Saud Univ. Eng. Sci., 2020. **32**(6): p. 351-359.

57. Bernechea, M., Y. Cao, and G. Konstantatos, *Size and bandgap tunability in Bi₂S₃ colloidal nanocrystals and its effect in solution processed solar cells.* J. Mater. Chem. A, 2015. **3**(41): p. 20642-20648.

58. Muruganandham, M., et al., *Facile Fabrication of Tunable Bi₂O₃ Self-Assembly and Its Visible Light Photocatalytic Activity.* J. Phys. Chem. C, 2012. **116**(23): p. 12906-12915.

59. Dean, J.A. and N.A. Lange, *Lange's handbook of chemistry*. 15 ed. Vol. 15. 1985, McGRAW-Hill.

60. Chen, Z., et al., *Kinetic and isotherm studies on the electrosorption of NaCl from aqueous solutions by activated carbon electrodes.* Desalination, 2011. **267**(2-3): p. 239-243.

61. Foo, K.Y. and B.H. Hameed, *Insights into the modeling of adsorption isotherm systems.* Chem. Eng. J., 2010. **156**(1): p. 2-10.

62. Wathukarage, A., et al., *Mechanistic understanding of crystal violet dye sorption by woody biochar: implications for wastewater treatment.* Environ. Geochem. Health, 2019. **41**(4): p. 1647-1661.

63. Jeppu, G.P. and T.P. Clement, *A modified Langmuir-Freundlich isotherm model for simulating pH-dependent adsorption effects.* J. Contam. Hydrol., 2012. **129-130**: p. 46-53.

64.   Tanzifi, M., et al., *Artificial neural network optimization for methyl orange adsorption onto polyaniline nano-adsorbent: Kinetic, isotherm and thermodynamic studies.* J. Mol. Liq., 2017. **244**: p. 189-200.

65.   Al-Ghouti, M.A. and D.A. Da'ana, *Guidelines for the use and interpretation of adsorption isotherm models: A review.* J. Hazard. Mater., 2020. **393**: p. 122383.

66.   Wang, J. and X. Guo, *Adsorption kinetic models: Physical meanings, applications, and solving methods.* J. Hazard. Mater., 2020. **390**: p. 122156.

67.   Tan, K.L. and B.H. Hameed, *Insight into the adsorption kinetics models for the removal of contaminants from aqueous solutions.* J. Taiwan Inst. Chem. E., 2017. **74**: p. 25-48.

68.   Sánchez-Polo, M., et al., *Removal of bromide and iodide anions from drinking water by silver-activated carbon aerogels.* J. Colloid Interface Sci., 2006. **300**(1): p. 437-441.

69.   Balsley, S.D., et al., *Anion Scavengers for Low-Level Radioactive Waste Repository Backfills.* J. of Soil Contam., 1998. **7**(2): p. 125-141.

70.   Ho, P.C. and K.A. Kraus, *Adsorption on inorganic materials—VIII: Adsorption of iodide on AgCl-filled carbon.* J. inorg, nucl. Chem., 1981. **43**(3): p. 583-587.

71.   Boyer, T.H. and P.C. Singer, *Bench-scale testing of a magnetic ion exchange resin for removal of disinfection by-product precursors.* Water Research, 2005. **39**(7): p. 1265-1276.

72.   Singer, P.C. and K. Bilyk, *Enhanced coagulation using a magnetic ion exchange resin.* Water Res., 2002. **36**(16): p. 4009-4022.

73.   Takeno, N., *Atlas Eh-pH Diagrams Intercomparison of thermodynamic databases Geological Survey of Japan Open File Report No.419*. 2005, National Institute of Advanced Industrial Science and Technology, Research Centerfor Deep Geological Environments: Geological Survey of Japan, AIST. p. 285.

6. Conclusion

In summary, this thesis has made following contributions:

- Systematically collected and synthesized the information and knowledge on the environmental impact of the halide ionic species (Cl$^-$, Br$^-$ and I$^-$) and the pros and cons of the current technologies for halide ions removal;
- Synthesized a novel, affordable and effective bismuth material as an ion exchanger for removing halides at high concentrations.
- Synthesized a novel nano-micro bismuth composite using hard templating method and optimized the synthesis protocols;
- Evaluated the novel nano-micro bismuth composite for removing halides at lower concentrations for dealing with DBPs issue in water purification.

In detail, the conclusion that can be summarized from the different studies presented in the thesis:

Chapter 2:

The review of the effect of halide existing on living creatures and environment was presented. Moreover, the importance of halide removal and how they would leach into the environment was revealed. The technologies that are being used conventionally for halide removal and their pros and cons were presented. The knowledge gaps and the research opportunity in this field were identified.

Chapter 3:

Bismuth hydroxide sulfate is a novel material which can remove halides (chloride, iodide and bromide) with fast kinetics and high capacity. Halides removed with the optimal conditions effectively. pH does not affect iodide and bromide removals, while chloride removal efficiency at alkaline conditions was declined, considerably. With increasing halide concentration, bismuth hydroxide sulfate is still effective for the halide removal up

to 4000 mg/L. It is more effective for iodide than bromide removal. Chloride removal efficacy was affected the most compared to other halides. This lies in the conversion of the molecular mass of halides to mole. For example, 4000 mg/L chloride is not as same amount as 4000 mg/L iodide; their molar concentrations are 0.112 mole/L and 0.0315 mole/L, respectively. Therefore, there are more available active sites on material per mole for iodide than chloride. This material has very high affinity and selectivity towards halides than other tested anions such as NO_3^-, HCO_3^- and SO_4^{2-}. After the removal, the material would be converted to the BiOX (X=Cl, I, Br). A procedure to regenerate BiOX (X=Cl, I, Br) was provided If regeneration is not demanded BiOX can be used in other applications such as photocatalytic applications and in beauty products in case of BiOCl. The removal of halides with this material is hardly affected by pH and other anions existing in the water. Also, it is very effective at very high concentrations for few thousands mg/L.

The performance of material at high temperatures are limited. This might be a result of exothermic reaction of bismuth hydroxide sulphate with halides. The other drawback of this material is releasing sulphate into water. Sulphate removal is a well-established technology. It can be removed easily with the lime or with alum and calcium salts to form ettringite.

Chapter 4:

Sucrose was hydrothermally treated at 200 °C and shorter time (2h), which resulted an excellent substrate for the following bismuth compound synthesis, because the sucrose-derived carbon particles have more oxygenated sites. The oxygenated sites on the carbon template provide binding sites for bismuth compounds which are formed in the solution as a white emulsion. Also, at 450 °C, $Bi_2(SO_4)_3$-Bi_2O_3 particles synthesized through the wet-chemistry step. While with increasing calcination temperature to 600 C it would be converted to Bi_2S_3-Bi_2O_3. However, other substrates will produce only Bi_2O_3. This will show the effect of sacrificial substrates' functional groups on the composite reaction with the substrate and final product.

Chapter 5:

The product which was a mixture of Bi_2O_3-Bi_2S_3 was the best for halide removal at ppm concentration. The removal efficacy for trace concentrations of iodide and bromide was more than 80%. In addition, pH>4 would also hardly affect halide removal, and interestingly existing of other anions in water would hardly impact the removal of halides. The last but not least is that this material could be applied till 8 mg/L of bromide and iodide. Bi_2S_3-Bi_2O_3 could induce an electric field which could enhance the halide removal. This would reveal that the potential of bismuth composite material for halide removal. The advantage of this material is its relative cheap cost compare to silver-impregnated adsorbents. Hence, bismuth is available and cheaper material compared to silver. Therefore, this material could be a better option for halide removal at trace concentrations. While the adsorption capacity of this material in presence of NOM is not known and should be tested.

6.1. Perspective and future works

This thesis work can be expanded in several other directions for both real-world applications and fundamental investigations

- The materials halide extraction capacity in more complex waters, such as sea water and real mining tailing water, in which Cl^-, Br^- and I^- may co-exist in large quantities.

- Bismuth hydroxide sulphate to be tested for other iodine species removal such as iodate.

- Bismuth hydroxide sulphate was not effective for low concentrations of halide and that is why we have synthesized another material with a smaller particle size for dealing with trace concentrations of halides. However, with the design of a properly fixed bed batch reactor which provides high contact with the halide might provide the removal efficiency for the low concentrations.

- Bi_2O_3-Bi_2S_3 composite was being used for halide removal in this study, however, it could have photocatalytic activity. Therefore, the tests regarding its bandgap and

its test for Methylene Orange as an organic pollutant removal can be tested in future.

- Testing of Bi_2O_3-Bi_2S_3 for halide removal from other waters such as tap water.

- Testing of temperature on the removal efficiency of Bi_2O_3-Bi_2S_3.

- Computational studies for understanding the underlying mechanisms for the extraordinary abilities of bismuth hydroxy sulphate and Bi_2O_3-Bi_2S_3 composite for selective halide ions removal.

- Application of Bi_2S_3-Bi_2O_3 with other quantum dots (such as ZnS quantum dots) for enhancing the photocatalytic activity and charge separation.

- Application of other templates with oxygenated groups such as silicates, silica (SBA-15), surfactants, alumina to make a mesoporous material. Then, check mesoporous size and performance of material on halide removal.

- Last but not the least, these synthesized materials (bismuth hydroxide sulphate and Bi_2O_3-Bi_2S_3 composite) could be applied in the membrane systems (such as graphene oxide) to increase their selectivity towards halides compared to the other anions and increase their selectivity and halide removal capability.